



EUROPA STUDY 2012 REPORT

EUROPA MULTIPLE FLYBY MISSION

Europa Study Team, 1 May 2012, JPL D-71990
Task Order NMO711062 Outer Planets Flagship Mission

Cover art Michael Carroll

Europa Study Final Report—Multiple-Flyby

Contents

C.	Multiple-Flyby Mission.....	2
C.1	Science of the Multiple-Flyby Mission	5
	C.1.1 Flyby Science	5
	C.1.2 Flyby Traceability Matrix	17
	C.1.3 Science Instrument Complement.....	36
C.2	Multiple-Flyby Mission Concept	39
	C.2.1 Mission Overview.....	39
	C.2.2 Model Payload	42
	C.2.3 Mission Design	54
	C.2.4 Flight System Design and Development.....	72
	C.2.5 Mission Operations Concepts	120
	C.2.6 Systems Engineering.....	126
C.3	Multiple-Flyby Programmatic.....	139
	C.3.1 Management Approach	139
	C.3.2 WBS	140
	C.3.3 Schedule.....	143
	C.3.4 Risk and Mitigation Plan	145
	C.3.5 Cost	147
C.4	Multiple-Flyby Mission Appendices	154
	C.4.1 References	154
	C.4.2 Acronyms and Abbreviations	163
	C.4.3 Master Equipment List.....	168
	C.4.4 Aerospace Corporation Independent Cost Estimate.....	169
	C.4.5 NASA Review Board Report.....	201

This research was carried out at the Jet Propulsion Laboratory, California Institute of Technology, under a contract with the National Aeronautics and Space Administration, with contributions from the Applied Physics Laboratory, Johns Hopkins University.

The cost information contained in this document is of budgetary and planning nature and is intended for informational purposes only. It does not constitute a commitment on the part of JPL and/or Caltech.

C. MULTIPLE-FLYBY MISSION

The Flyby Mission would explore Europa to investigate its habitability, delivering cost-effective, low-risk science.

Executive Summary

Background

The 2011 Planetary Science Decadal Survey recommended an immediate effort to find major cost reductions for the Jupiter Europa Orbiter (JEO) concept. To that end, NASA Headquarters appointed a Science Definition Team (SDT) and directed the Europa Study Team, guided by the SDT, to redefine a set of minimal science missions to Europa. The cost target was \$2.25B (\$FY15, excluding launch vehicle) and additional guidelines were levied, as described in Section A. Independent cost and technical review was to be performed on all study results. These studies, independent reviews, and all deliverables were delivered to NASA Headquarters on May 1, 2012.

One of these mission concepts, a Europa Multiple-Flyby Mission, is well suited to addressing the chemistry and energy themes of Europa exploration. It would involve a spacecraft in wide orbit around Jupiter that makes many close passes by Europa, each flying over a different region for broad coverage (see Fold-out C-2 [FO C-2]). This concept, as detailed below, represents the combined effort since April 2011 of the SDT and a technical team from the Jet Propulsion Laboratory (JPL) and Johns Hopkins University's Applied Physics Laboratory (APL).

Science Objectives

Europa is a potentially habitable world and is likely to be geologically and chemically active today. Many well-defined and focused science questions regarding past and present habitability may be addressed by exploring Europa.

The 2003 Planetary Decadal Survey, "New Horizons in the Solar System" (Space Studies Board 2003) and 2011 Planetary Decadal Survey, "Vision and Voyages" (Space Studies

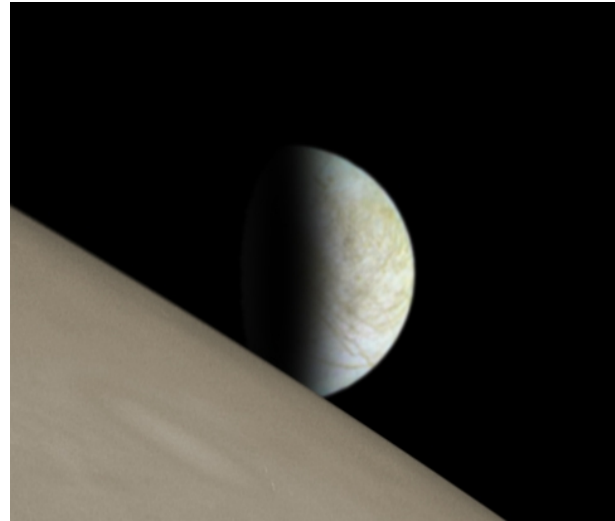


Figure C-1. Europa over the horizon of its parent planet, Jupiter.

Board 2011) both emphasize the importance of Europa exploration as "the first step in understanding the potential of the outer solar system as an abode for life" (Space Studies Board 2011, p. 1). The 2011 Decadal Survey discusses the likelihood of contemporary habitats with the necessary conditions for life, stressing the inherent motivation for "a Europa mission with the goal of confirming the presence of an interior ocean, characterizing the satellite's ice shell, and understanding its geological history" (Space Studies Board 2011, pp. 1–2). Thus, the goal adopted for the current Europa studies is to "Explore Europa to investigate its habitability", which recognizes the significance of Europa's astrobiological potential. "Habitability" includes characterizing any water within and beneath Europa's ice shell, investigating the chemistry of the surface and ocean, and evaluating geological processes that may permit Europa's ocean to possess the chemical energy necessary for life. Understanding Europa's habitability is intimately tied to understanding the three "ingredients" for life: water, chemistry, and energy.

Rationale for Multiple-Flyby Science

Science observations that address chemistry and energy themes can be accomplished via a spacecraft that orbits Jupiter and focuses on

remote measurements accomplished via multiple close flybys of Europa. Such a mission—investigating subsurface dielectric horizons, surface constituents, atmospheric constituents, and targeted landforms—would be directly responsive to the Decadal Survey’s recommendation for reduced Europa science, and would be an excellent platform from which to investigate Europa’s potential as a habitable environment. Comprehensive remote sensing campaigns capable of addressing regional and global investigations tend to produce considerable data. The short-flyby, long-orbit periodicity of a flyby mission design is well suited to this type of campaign.

Complete traceability of chemistry and energy science to a plausible Flyby Mission implementation is compiled and contained in this report. This is summarized in a Traceability Matrix (FO C-1), which provides specific prioritized objectives, investigations, and example measurements, each directed toward the overarching goal to “Explore Europa to investigate its habitability.” These are described further in the narrative.

In addition, notional instruments are provided as a proof of concept to demonstrate that these investigations, objectives, and goals could be realistically addressed. The model payload contains an Ice-Penetrating Radar (IPR), Shortwave Infrared Spectrometer (SWIRS), Ion and Neutral Mass Spectrometer (INMS), and Topographical Imager (TI). However, these examples are not meant to be exclusive of other measurements and instruments that might be able to meet the scientific objectives in other ways. NASA will ultimately select the payload through a formal Announcement of Opportunity (AO) process.

Architecture Implementation

The Multiple-Flyby Mission architecture described here is well suited to satisfying the science objectives in a cost-effective, lowest-risk manner. A trajectory has been identified that provides globally distributed regional coverage

of the European surface through a series of flybys. Once the flyby campaign begins, Europa is encountered every 7 to 21 days. This approach allows for high-data-rate science collection followed by days of playback time, while greater mass margins afforded by foregoing Europa orbit insertion enable shielding to a lower radiation dose. This mission architecture is well suited to Europa Multiple-Flyby Mission instruments, which are heavy, require significant operating power, and generate considerable data. On each flyby, science data is collected for approximately one hour, leaving the remainder of the 7 to 21 days between Europa encounters for science data return and battery recharging. Science operations for the flybys are repetitive, which leads to lower cost mission operations.

The conceptual flight system (Figure C-2) uses a modular architecture, which facilitates the implementation, assembly, and testing of the system. This is facilitated further by the approach to Europa planetary protection requirements, which are met through system-level dry-heat microbial reduction in a thermal-vacuum chamber late in the integration process at the launch site. The chosen instru-

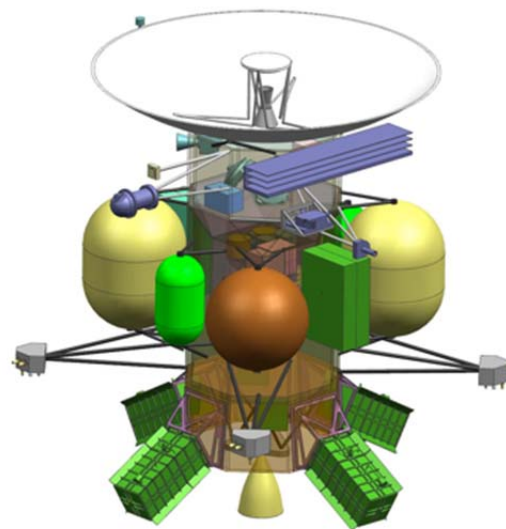


Figure C-2. The Europa Multiple-Flyby Mission flight system provides a robust platform to collect, store, and transmit a high volume of science data.

ment interfaces and other accommodations also allow for delivery late into the system level integration and tests, providing program flexibility.

The flight system is 3-axis-stabilized for precise instrument pointing, and avoids solar pointing constraints by using four Advanced Stirling Radioisotope Generators (ASRGs) for power. An innovative propulsion system accommodation for an internal, Juno-style electronics vault and a nested shielding strategy provides significant protection from the radiation environment, allowing the use of 300-krad-tolerant parts.

Technical margins for the mission design concept are robust, with 48% mass margin, and 40% power margin and 80% downlink margin during science operations.

Schedule and Cost

A top-level development schedule is shown in Figure C-3. Phase durations draw on experience from previous outer planets missions and are conservative. This schedule would facilitate front-loading of requirements development, provide significant time during instrument development to understand the actual design implications for radiation and planetary protection, and offer a flatter than typical mission funding profile.

The Flyby Mission study applied a hybrid costing methodology that includes institutional cost models, the NASA Instrument Cost Model (NICM), percentage wrap factors, expert-based opinion, and JPL's Team X cost estimates. An S-curve analysis performed on the

study cost estimates resulted in a \$2.0B (\$FY15, excluding launch vehicle) 70th-percentile cost estimate. In addition, the Aerospace Corporation performed an Independent Cost Estimate (ICE) and a Cost And Technical Evaluation (CATE) and found no cost or schedule threats, as opposed to the 2011 Decadal Survey conclusion.

Summary

A Multiple-Flyby Mission concept meets the challenge from NASA and the Decadal Survey for a reduced scope Europa mission relative to JEO, yet still has exceptional science merit. Study results are in compliance with NASA Headquarters' direction and guidelines. The mission design concept is conservative, has large margins, and meets the NASA cost target of ~\$2.25B (\$FY15, excluding launch vehicle). The Europa Multiple-Flyby Mission was presented to the Outer Planets Assessment Group (OPAG) in October 2011, and the feedback from the community was extremely positive. An independent technical review of the Europa Multiple-Flyby Mission concept was conducted, chaired by Scott Hubbard. The key findings were:

- The overall approach to modularity and radiation shielding was universally lauded as a creative approach to reducing technical risk and cost;
- No engineering “showstoppers” were identified;
- The Flyby concept satisfied the “existence proof” test as a mission that met Europa

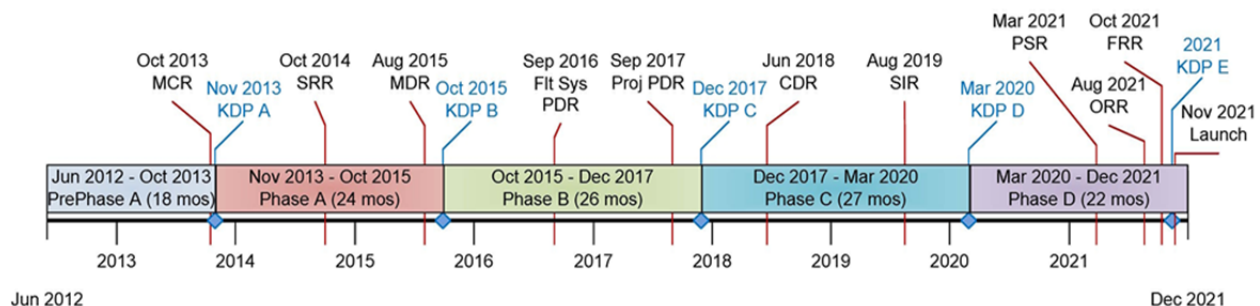


Figure C-3. Top-level development schedule with conservative durations provides appropriate time to address radiation and planetary protection challenges.

science requirements, could be conducted within the cost constraints provided and has substantial margins;

- Two technical risks were identified: ASRG and radiation mitigation for instrument detectors.

The detailed findings of this technical review are shown in Section C.4.5.

C.1 Science of the Multiple-Flyby Mission

C.1.1 Flyby Science

Europa is a potentially habitable world that is likely to be geologically and chemically active today. As outlined below, there are many well-defined and focused science questions to be addressed by exploring Europa. The 2003 Planetary Decadal Survey, *New Horizons in the Solar System*, and the 2011 Planetary Decadal Survey, *Vision and Voyages*, both emphasize the importance of Europa exploration (Space Studies Board 2003, 2011). These Decadal Surveys discuss Europa's relevance to understanding issues of habitability in the solar system, stressing this as the inherent motivation for Europa exploration.

“Because of this ocean’s potential suitability for life, Europa is one of the most important targets in all of planetary science” (Space Studies Board 2011).

Understanding Europa's habitability is intimately tied to understanding the three “ingredients” for life: water, chemistry, and energy (Section A of this report). A Jupiter-orbiting spacecraft that makes many flybys of Europa would be an excellent platform from which to conduct remote sensing measurements to investigate Europa's ice shell, composition, and geology, and thus the three ingredients for life. Remote sensing investigations tend to be resource-intensive, in terms of data volume and data rate drivers, and in the mass and power of necessary instruments. Such needs are readily accommodated by a multiple-flyby mission implementation. In this section, we discuss the

science background of a multiple-flyby mission that concentrates on remote sensing to address Europa's habitability.

C.1.1.1 Ice Shell

To assess Europa's habitability, it is necessary to see how the ingredients for life might be brought together in this environment. This includes unraveling the dynamic processes that connect Europa's underlying ocean to the surface of its ice shell. Therefore, a detailed understanding of the internal structure of the Europa's ice (Figure C.1.1-1) is essential. Probing the third dimension of the shell is key to understanding the distribution of subsurface water both within and beneath the ice shell. Understanding the processes of ice–ocean exchange would indicate whether surface oxidants can be transported to Europa's ocean, providing the chemical nutrients for life. Moreover, if ocean material can be transported back to Europa's surface, then we could confidently understand the chemistry of the ocean by examining the composition of surface and atmospheric materials. Therefore, exploration of Europa's ice shell is pertinent to all three ingredients for life: water, chemistry, and energy.

Remaining questions to be addressed about Europa's ice shell include the following:

- Is Europa's ice shell thin and thermally conductive, or thick and convecting?
- Are surface oxidants transported from the surface into the ocean (providing chemical energy to the ocean) and vice-versa (allowing us to understand ocean chemistry through surface observations), and if so, what are the transport processes?
- What are the three-dimensional characteristics of Europa's geological structures, and do they enable surface–ocean communication?
- Are there liquid water bodies within Europa's ice shell?

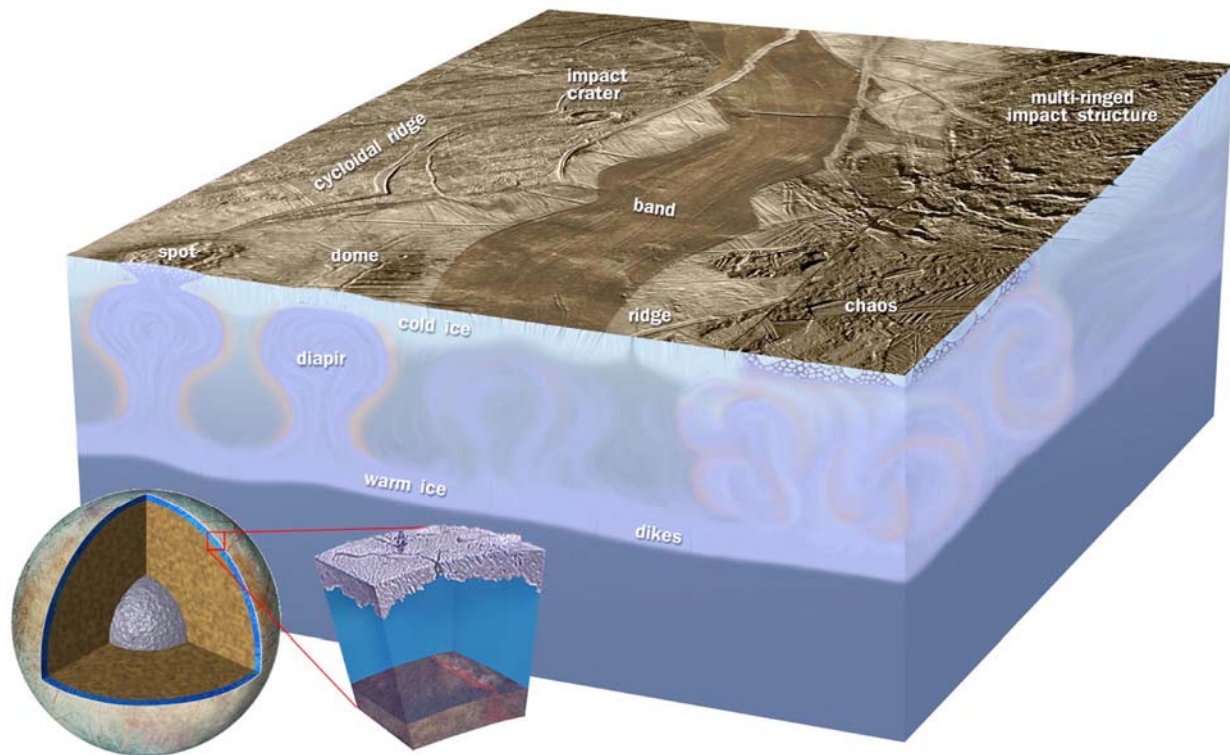


Figure C.1.1-1. Diagram of Europa's ice shell above a global-scale ocean, showing possible ice-shell processes leading to thermal, compositional, and structural horizons. Hypothesized convective diapirs (domed upwellings at the front of the block diagram) could cause thermal perturbations and partial melting in the overlying rigid ice. Tectonic faulting driven by tidal stresses (upper surface) could result in fault damage and frictional heating. Impact structures (back right) are expected to have central refrozen melt pools and to be surrounded by ejecta.

The thickness of Europa's ice shell is an important question left unanswered by the Galileo mission. While the total depth of Europa's H₂O-rich outer shell—ice over liquid water—is believed to be approximately 100 kilometers, the current thickness of the ice shell is unknown, with estimates ranging from relatively thin (a few kilometers) to relatively thick (tens of kilometers) (Billings and Kattenhorn 2005). Depending on thickness and other factors, a number of different processes may be at work shaping this shell and its dynamics. These include episodes of thickening and thinning, thermal and geological processing, and exogenic processes. For instance, geological processes have clearly altered and deformed the surface and transported material horizontally and vertically within the shell, while exogenic processes such as cratering and regolith formation have influenced the surface

and deeper structure. Determining the ice-shell thickness is of fundamental astrobiological significance: It constrains answers to questions about how much tidal heat the satellite is generating; whether the silicate interior exhibits high heat production or not; and to what extent the ocean and near-surface ice are likely to exchange material.

Just as a geologist on Earth uses structural information to understand the dynamics of the Earth's crust, three-dimensional electromagnetic sounding of the ice shell—with the potential to find water within the ice shell, identify the ice-ocean interface of Europa, and measure the ice shell thickness—would reveal the processes connecting the surface to the ocean. Dielectric losses in very cold ice are low, yet highly sensitive to increasing temperature, water, and impurity content; therefore, much could be learned through remote elec-

tromagnetic sounding of the ice shell. This is especially true when subsurface profiling is coupled to observations of the topography and morphology of surface landforms and placed in the context of both surface composition and subsurface density distribution. Because of Jupiter's strong radio emissions and the unknown size of volume scatterers within Europa's ice shell, the range of sounding frequencies must be carefully matched to the science objectives.

C.1.1.1.1 Thermal Processing

Regardless of the properties of the shell or the overall mechanism of heat transport, the uppermost several kilometers of the ice shell are cold and stiff. The thickness of this conductive "lid" is set by the total amount of heat that must be transported. Thus, a measurement of the thickness of the cold and brittle part of the shell is a powerful constraint on the heat production in the interior. The lower, convecting part of the shell (if it exists) is likely to be much cleaner because regions with impurities should have experienced melting at some point during convective circulation, and melt would segregate downward efficiently, extracting impurities (Pappalardo and Barr 2004). Thermal processing might have altered the internal structure of the shell through convection or local melting, potentially creating huge "lakes" within the ice shell (Schmidt et al. 2011).

Convective instabilities can also result in thermal variations in the outer part of the shell, including rising diapirs of warm ice, which might be associated with features at the surface of Europa (lenticulae and chaos), with scales ranging from ~1–100 km. If warm, relatively pure ice diapirs from the interior approach the surface, they might be far from the pure-ice melting point, but above the eutectic point¹ of some material trapped in the shallow portions of the ice shell, potentially creating regions of melting (Schmit et al. 2011). Other

¹ The eutectic point is the reduced melting temperature of substances when they are mixed.

sources of local heating such as friction on faults might also lead to local melting (Gaidos and Nimmo 2000).

The ability to perform electromagnetic sounding through Europa's ice shell is essential to understanding its thermal processing. Detection of water lenses would require a vertical resolution of at least a few tens of meters. High horizontal resolution (a few hundred meters) is required to avoid scale-related biases.

C.1.1.1.2 Ice–Ocean Exchange

Europa's ice shell has likely experienced one or more phases of thickening and thinning over time (Hussmann and Spohn 2004, Moore and Hussmann 2009). This would likely lead to significant structural horizons from contrasts in ice-crystal fabric and composition.

Similarly, melting to form lenticulae and chaos on Europa's surface (Greenberg et al. 1999, Schmidt et al. 2011) implies that ice would accrete beneath the melt feature after it forms. This process would result in a sharp boundary between old ice and deeper accreted ice. The amount of accreted ice would be directly related to the time since melting occurred and could be compared with the amount expected, based on the inferred surface age.

Testing these hypotheses would require measuring the depth of interfaces to a resolution of a few hundred meters and horizontal resolutions of a fraction of any lid thickness, i.e., a kilometer or so.

C.1.1.1.3 Surface and Subsurface Structure

Europa represents a unique tectonic regime in the solar system, and the processes controlling the distribution of strain in Europa's ice shell are uncertain. Tectonic structures could range from low-angle extensional fractures to near-vertical strike-slip features. These would produce structures associated primarily with the faulting process itself through formation of pervasively fractured ice and zones of deformational melt, injection of water, or preferred orientation of crystal fabric. Some faults might

show local alteration of preexisting structure, including fluid inclusions, or by juxtaposition of dissimilar regions through motion on the fault.

There are many outstanding questions regarding tectonic features. A measurement of their depth and association with thermal anomalies or melt inclusions would strongly constrain models of their origins. In particular, correlation of subsurface structure with surface properties (length, position in the stratigraphic sequence, height, and width of the ridges) would test hypotheses for the mechanisms that form the fractures and support the ridges. The observation of melt along ridges could make these features highly desirable targets for future *in situ* missions.

Dilational bands observed on Europa might be particularly important for understanding material-exchange processes. If the analogy with terrestrial spreading centers (Prockter et al. 2002) is accurate, the material in the band is newly supplied from below and might have a distinct structure.

Thus, the origin of band material can be constrained by sounding the subsurface. Bands and ridges typically have widths of several kilometers. Horizontal sounding resolutions of several hundred meters would be required to discriminate processes. The ability to image structures sloping more than a few degrees is also needed. Additionally, tens of meters of vertical resolution would be required to image any near-surface melt inclusions.

The impact process should also represent a profound disturbance of the local structure of the shell, yet few large impact sites are apparent. An outstanding mystery on Europa is the process by which these craters are erased from the surface. It is possible though that Europa's *sub*-surface records events that have penetrated the entire thickness of the shell. Around the impact site, the ice would have been fractured and heated, and some melt generated; the surface directly around the impact would be bur-

ied with a blanket of ejecta; and relaxation of the crater would have created a zone of deformation that could include both radial and circumferential faulting. These processes all create subsurface structures that might be probed by sounding. Thus, it might be possible to find the subsurface signature of impacts that are no longer evident at the surface, which would place constraints on the resurfacing processes that operate at Europa.

Three types of structural horizons are expected to be derived from impact: the former surface buried beneath an ejecta blanket, solidified melts in the impact structure itself, and impact-related fractures. Vertical resolutions on the scales of a few tens to hundreds of meters would be required to identify ejecta blankets and frozen melt pools. Detection of at least the edges of steep interfaces would aid in the identification of radial dikes, buried crater walls, and circumferential fractures.

C.1.1.2 Composition

Characterizing the surface organic and inorganic composition and chemistry provides fundamental information about Europa's history and evolution, the properties and habitability of the subsurface and ocean, its interaction with the surface, and the role of exogenic processes. Surface materials might be ancient, derived through time from the ocean and altered by radiation, or they might be exogenic in origin.

Current understanding of Europa's bulk density and of solar and stellar composition suggests the presence of both water and silicates. It is likely that the differentiation of Europa resulted in mixing of water with the silicates and carbonaceous materials that formed the moon, resulting in chemical alteration and redistribution. Interior transport processes would then have brought a variety of materials from the interior first into the ocean and from there up to the surface.

Much of what is known about Europa's composition comes from spectroscopic observa-

tions in the visible to near-infrared. Earth-based telescopic observations and data from the Voyager and Galileo spacecraft (see reviews by Alexander et al. 2009 and Carlson et al. 2009) show that the surface of Europa is primarily water ice in both crystalline and amorphous forms.

The barrage of high-energy particles from Jupiter's magnetosphere also leaves an imprint on the surface composition that provides clues to this environment, further complicating the formation, evolution, and modification of the surface.

Finally, surface materials could be incorporated into the subsurface and react with the ocean, or could be sputtered from the surface to form Europa's tenuous atmosphere.

C.1.1.2.1 *Icy and Non-Icy Composition*

Compositional information from Earth-based telescopic observations and data from the Voyager and Galileo spacecraft (e.g., Kuiper 1957, Moroz 1965, Clark and McCord 1980, Dalton 2000, McCord 2000, Spencer et al. 2005, Alexander et al. 2009) show that the surface of Europa is composed primarily of water ice in both crystalline and amorphous forms (Pilcher et al. 1972, Clark and McCord 1980, Hansen and McCord 2004).

The dark, non-icy materials that make up much of the rest of Europa's surface are of extreme interest for unraveling Europa's geological history; determining their composition is the key to understanding their origin. The spatial distribution and context of these materials at geologically relevant scales allows the processes that have formed the surface and the connection between the surface and the interior to be understood. This link provides important constraints on the nature of the interior, the potential habitability of subsurface liquid water environments, and the processes and time scales through which interior materials are transported to the surface. Compositional variations in surface materials might reflect age differences indicative of recent activity,

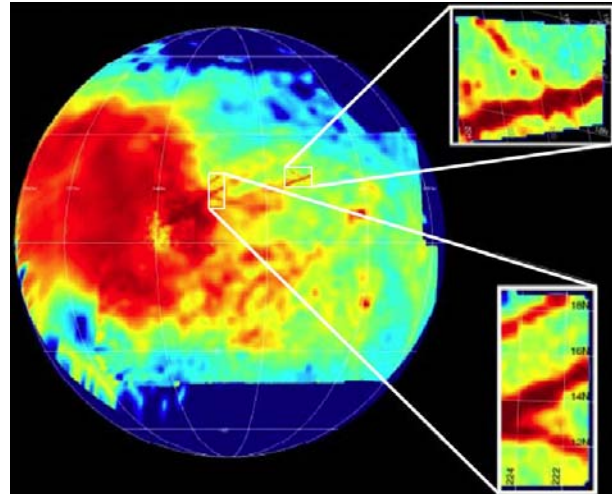


Figure C.1.1-2. The distribution of hydrated materials on Europa (red) reaches its maximum near the apex of the trailing hemisphere, where impinging radiation flux is highest, and is associated with geologically disrupted terrains and triple bands (insets).

and the discovery of active vents or plumes would show current activity.

The non-ice components are known to include carbon dioxide (CO₂), sulfur dioxide (SO₂), hydrogen peroxide (H₂O₂) and molecular oxygen (O₂), based on comparison of measured spectra with laboratory studies of the relevant compounds (Lane et al. 1981; Noll et al. 1995; Smythe et al. 1998; Carlson 1999, 2001; Carlson et al. 1999a, b; Spencer and Calvin 2002; Hansen and McCord 2008). Spectral observations from the Galileo Near-Infrared Mapping Spectrometer (NIMS) reveal disrupted dark and chaotic terrains on Europa with distorted and asymmetric absorption features indicative of water bound in non-ice hydrates. Hydrated materials observed in regions of surface disruption (Figure C.1.1-2) have been suggested to be magnesium and sodium sulfate minerals (Figure C.1.1-3) that originate from subsurface ocean brines (McCord et al. 1998a, 1998b, 1999). Alternatively, these materials might be sulfuric acid hydrates created by 1) radiolysis² of sulfur from Io, 2) processing of endogenic

² Radiolysis is chemical decomposition by ionizing radiation.

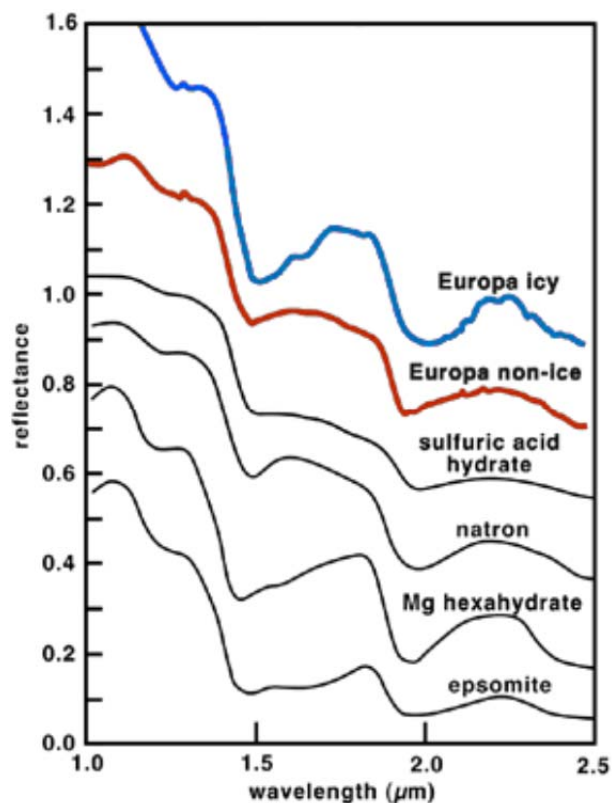


Figure C.1.1-3. Reflectance spectra of hydrated materials on Europa. Candidate materials for Europa's non-ice component include sulfuric acid hydrate ($\text{H}_2\text{SO}_4 \cdot n\text{H}_2\text{O}$) and various hydrated sulfate and carbonate salts (McCord et al. 1999, 2002).

SO_2 , and/or 3) extrusion of ocean-derived sulfates (Carlson et al. 1999b, 2002, 2005). It is also possible that these surfaces are a combination of both hydrated sulfate salts and hydrated sulfuric acid (Dalton 2000; McCord et al. 2001a, b, 2002; Carlson et al. 2005; Orlando et al. 2005; Dalton et al. 2005), as suggested by linear spectral mixture analyses of disrupted terrains (Dalton 2007). An important objective for Europa science is to resolve the compositions and origins of these hydrated materials.

Material in the space surrounding Europa also provides compositional clues. Brown and Hill (1996) first reported a cloud of sodium around Europa, and Brown (2001) detected a cloud of potassium and reported that the Na/K ratio suggested that endogenic sputtering produced these materials.

A broad suite of additional compounds is predicted for Europa based on observations of other icy satellites, as well as from experimental studies of irradiated ices, theoretical simulations, and geochemical and cosmochemical arguments. Organic molecular groups, such as CH and CN, have been found on the other icy Galilean satellites (McCord et al. 1997, 1998b), and their presence or absence on Europa is important to understanding Europa's potential habitability. Other possible compounds that might be embedded in the ice and detectable by high-resolution spectroscopy include H_2S , OCS, O_3 , HCHO, H_2CO_3 , SO_3 , MgSO_4 , H_2SO_4 , H_3O^+ , NaSO_4 , HCOOH, CH_3OH , CH_3COOH , and more complex species (Moore 1984; Delitsky and Lane 1997, 1998; Moore and Hudson 1998; Moore et al. 2003; Brunetto et al. 2005).

As molecules become more complex, however, their radiation cross-section also increases and they are more susceptible to alteration by radiation. Radiolysis and photolysis could alter the original surface materials and produce many highly oxidized species that react with other non-ice materials to form a wide array of compounds. Given the extreme radiation environment of Europa, complex organic molecules are not expected in older deposits or in those exposed to higher levels of irradiation (Johnson and Quickenden 1997, Cooper et al. 2001). However, diagnostic molecular fragments and key carbon, nitrogen, and sulfur products might survive in some locales. Regions of lesser radiation (i.e., the leading hemisphere) and sites of recent or current activity would be the most likely places to seek evidence of organic or derived products.

Improved spectral observations at significantly higher spectral and spatial resolution than is presently available, together with detailed laboratory analyses under the appropriate temperature and radiation environment, are needed to fully understand Europa's surface chemistry. These data would provide major improvements in the identification of original and

derived compounds and of the radiation environment and reaction pathways that create and destroy them.

C.1.1.2.2 *Isotopic Constraints*

The varying degree of preference for lighter isotopes in many physical and chemical processes is expected to lead to mass fractionation effects that should be evident in isotopic ratios. Ratios of D/H, $^{13}\text{C}/^{12}\text{C}$, $^{15}\text{N}/^{14}\text{N}$, $^{18}\text{O}/^{17}\text{O}/^{16}\text{O}$, $^{34}\text{S}/^{32}\text{S}$, and $^{40}\text{Ar}/^{36}\text{Ar}$, and comparison among them, could provide insights into geological, chemical, and possible biological processes, such as planetary formation, interior transport, surface evolution, radiolysis, atmospheric escape, and metabolic pathways.

The determination of isotopic ratios would provide a powerful indicator of several planetary processes. Exchange rates among the Earth's oceans, crust, mantle, and atmosphere are closely linked to ratios of radiogenic noble gas isotopes; these isotope ratios have also been used at Venus and Mars to better understand the evolution of their volatile reservoirs. In satellite systems around large gaseous planets such as Jupiter and Saturn, questions about the presence, extent, and composition of a primordial circumplanetary disk surrounding the host protoplanet could be addressed by comparing isotope ratios measured at different satellites in the system with those measured in the host planet's atmosphere.

Endogenic processes on Europa might have measurable effects on isotope compositions. Moreover, the exogenic processes of sublimation and sputtering should also cause isotopic fractionation. Differences in solubilities and clathrate dissociation pressures would cause materials and isotopes of interest to freeze or become enclathrated into Europa's ice shell in different proportions than found in the aqueous solution of the ocean. Such differences might be evident from comparison of the predominant ice-rich background terrain on Europa's surface with cracks, chaos regions, and other

features rich in non-icy material, which might have been deposited directly from the ocean.

C.1.1.2.3 *Relationship of Composition to Processes*

Galileo's instruments were designed to study surface compositions at regional scales. The association of hydrated and reddish materials with certain geologic terrains, revealed by Galileo, suggests an endogenic source for the emplaced materials, although these might since have been altered by radiolysis. Many surface features with compositionally distinct materials were formed by tectonic processes, suggesting that the associated materials are derived from the subsurface. Major open questions include the links between surface composition and that of the underlying ocean and rocky interior (Fanale et al. 1999, Kargel et al. 2000, McKinnon and Zolensky 2003), and the relative significance of radiolytic processing (Johnson and Quickenden 1997; Cooper et al. 2001; Carlson et al. 2002, 2005; Grundy 2007). For example, compositional variations associated with surface features such as chaos suggest that material might be derived from an ocean source, either directly through melting or eruptions, or indirectly through processes such as diapirism (McCord et al. 1998b, 1999; Fanale et al. 1999; Orlando et al. 2005).

One of the critical limitations of the Galileo NIMS experiment was the low spatial resolution of the high-quality spectra and the limited spatial coverage due to failure of the spacecraft's high-gain antenna. The spectra used to identify hydrated materials were typically averaged from areas ~75 km by 75 km (McCord et al. 1998b, Carlson et al. 1999b) (although a few higher-resolution "postage stamp" data sets were obtained and analyzed). This typical footprint is shown in Figure C.1.1-4, illustrating the tremendous mixing of surface terrain types that occurs within an area of this extent; less than 10% of the NIMS footprint contains materials associated with ridges, bands, or fractures. In order to isolate and identify the young, non-ice materials associated with these

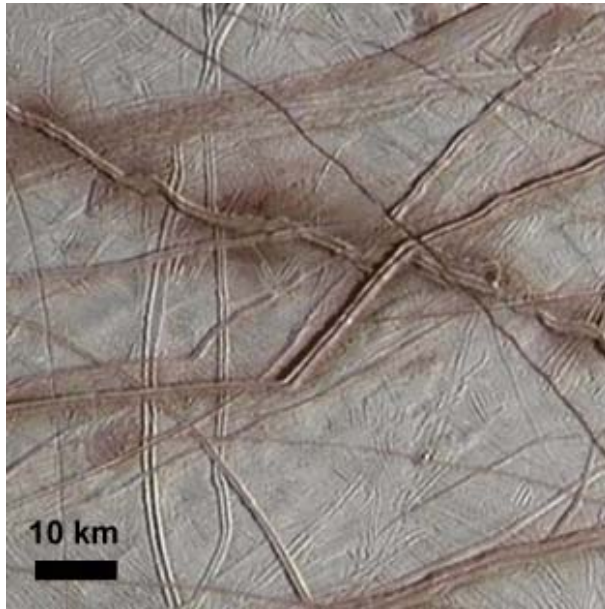


Figure C.1.1-4. This portion of a Galileo image is the size of a typical Galileo NIMS footprint, demonstrating how NIMS sampled multiple terrain types in each spectrum.

structures, and look for spectral variations within geological structures, future observations must be able to resolve the non-ice materials to better than 100-m scales.

In addition to compositional differences associated with recent geological activity, compositional changes related to exposure age also provide evidence for sites of recent or current activity. The composition of even the icy parts of Europa is variable in space and time. Polar fine-grained deposits suggest frosts formed from ice sputtered or sublimated from other areas (Clark et al. 1983, Dalton 2000, Hansen and McCord 2004). Equatorial ice regions are more amorphous than crystalline, perhaps due to radiation damage. Venting or transient gaseous activity on Europa would indicate present-day surface activity.

Exogenic processes are also a key part of Europa's composition story, but much remains unknown about the chemistry and sources of the materials being implanted. Magnetic field measurements by Galileo of ion-cyclotron waves in the wake of Europa provide evidence of sputtered and recently ionized Cl, O₂, SO₂

and Na ions (Volwerk et al. 2001). Medium energy ions (tens to hundreds of keV) deposit energy in the topmost few tens of microns; heavier ions, such as oxygen and sulfur ions, have an even shorter depth of penetration, while MeV electrons could penetrate and affect the ice to a depth of more than 1 m (Paranicas et al. 2002, and references therein, Paranicas et al. 2009). The energy of these particles breaks bonds to sputter water molecules, molecular oxygen, and any impurities within the ice (Cheng et al. 1986), producing the observed atmosphere and contributing to the erosion of surface features.

A major question is the exogenic versus endogenic origin of volatiles, such as CO₂, and their behavior in time and space. CO₂ was reported on the surfaces of Callisto and Ganymede (McCord et al. 1998b), with hints of SO₂ (Smythe et al. 1998) and H₂O₂ (Carlson et al. 1999a). Recent analyses of the NIMS spectra indicate a concentration of CO₂ and other non-ice compounds on the anti-Jovian and trailing sides of Europa (Hansen and McCord 2008), suggesting an endogenic origin. Radiolysis of CO₂ and H₂O ices is expected to produce additional compounds (Moore 1984; Delitsky and Lane 1997, 1998; Brunetto et al. 2005). Determining the presence and source of organic molecular compounds, such as CH and CN groups detected by IR spectroscopy at Callisto and Ganymede (McCord et al. 1997, 1998b) and tentatively identified on Phoebe (Clark et al. 2005), would be important to evaluating the astrobiological potential of Europa, especially if there is demonstrable association with the ocean.

Some surface constituents result directly from exogenic sources. For example, sulfur from Io is transported by the magnetosphere and is implanted into Europa's ice. Once there it could form new molecules and might create some of the dark components on the surface. It is important to separate surface materials formed by implantation from those that are endogenic, and this could be done by quantitative analy-

sis. For example, the detected Na/K ratio is supportive of an endogenic origin—and perhaps an ocean source—for sodium and potassium (Brown 2001, Johnson et al. 2002, McCord et al. 2002, Orlando et al. 2005).

Spatial variations could also help separate exogenic and endogenic processes. For example, comparison of spectra of disrupted terrain on the leading and trailing hemispheres, which encounter far different radiolytic fluxes, would help to isolate the effects of the radiation environment and unravel endogenic and exogenic chemical processes that led Europa to its present state (Shirley et al. 2010).

Regardless of origin, surface composition results from combinations of all these processes, and materials emplaced at the surface are subsequently processed by radiation to produce the observed composition (Dalton 2000). For example, material derived from the ocean could be a mixture of dominantly Mg and Na salts. Na sulfates would be more vulnerable to radiative disassociation, producing sulfuric acid (H₂SO₄) (Dalton 2000, 2007; McCord et al. 2001b, 2002; Orlando et al. 2005). Such a mixture would allow for both indigenous salts and sulfuric acid, and could account for the origin of Na and K around Europa.

Some key outstanding questions to be addressed regarding Europa's composition include the following:

- Are there endogenic organic materials on Europa's surface?
- Is chemical material from depth carried to the surface?
- Is irradiation the principal cause of alteration of Europa's surface materials through time?
- Do materials formed from ion implantation play a major role in Europa's surface chemistry?

C.1.1.2.4 *Geology*

By understanding Europa's varied and complex geology (Figure C.1.1-5), we can deci-

pher the moon's past and present processes, along with implications for habitability. By such understanding we can also gather clues about geological processes on other icy satellites with similar surface features, such as Miranda, Triton, and Enceladus.

The relative youth of Europa's surface (60 million years on average) (Schenk et al., 2004) compared to most other solar system bodies is inherently linked to the ocean and the effects of gravitational tides, which trigger processes that include cracking of the ice shell, resurfacing, and possibly a release of materials from the interior. Clues to these and other processes are provided by spectacular surface features, such as linear fractures and ridges, chaotic terrain, and impact craters.

C.1.1.2.5 *Linear Features*

Europa's unusual surface is dominated by tectonic features in the form of linear ridges, bands, and fractures. The class of linear features includes simple troughs and scarps (e.g., Figure C.1.1-5g), double ridges separated by a trough, and intertwining ridge-complexes. Whether these represent different processes or stages of the same process is unknown. Ridges are the most common feature type on Europa and appear to have formed throughout the satellite's visible history (Figure C.1.1-5j and l). They range from 0.1 to >500 km long, are as wide as 2 km, and could be several hundred meters high. Cycloidal ridges are similar to double ridges, but form chains of linked arcs.

Most models of linear feature formation involve fracturing in response to processes within the ice shell (Greeley et al. 2004, Kattenhorn and Hurford 2009, Prockter and Patterson 2009). Some models suggest that liquid oceanic material or warm mobile subsurface ice squeezes through fractures to form the ridge, while others suggest that ridges form by frictional heating and possibly melting along the fracture shear zone. Thus, ridges might represent regions of material exchange between the surface, ice shell, and ocean, providing a

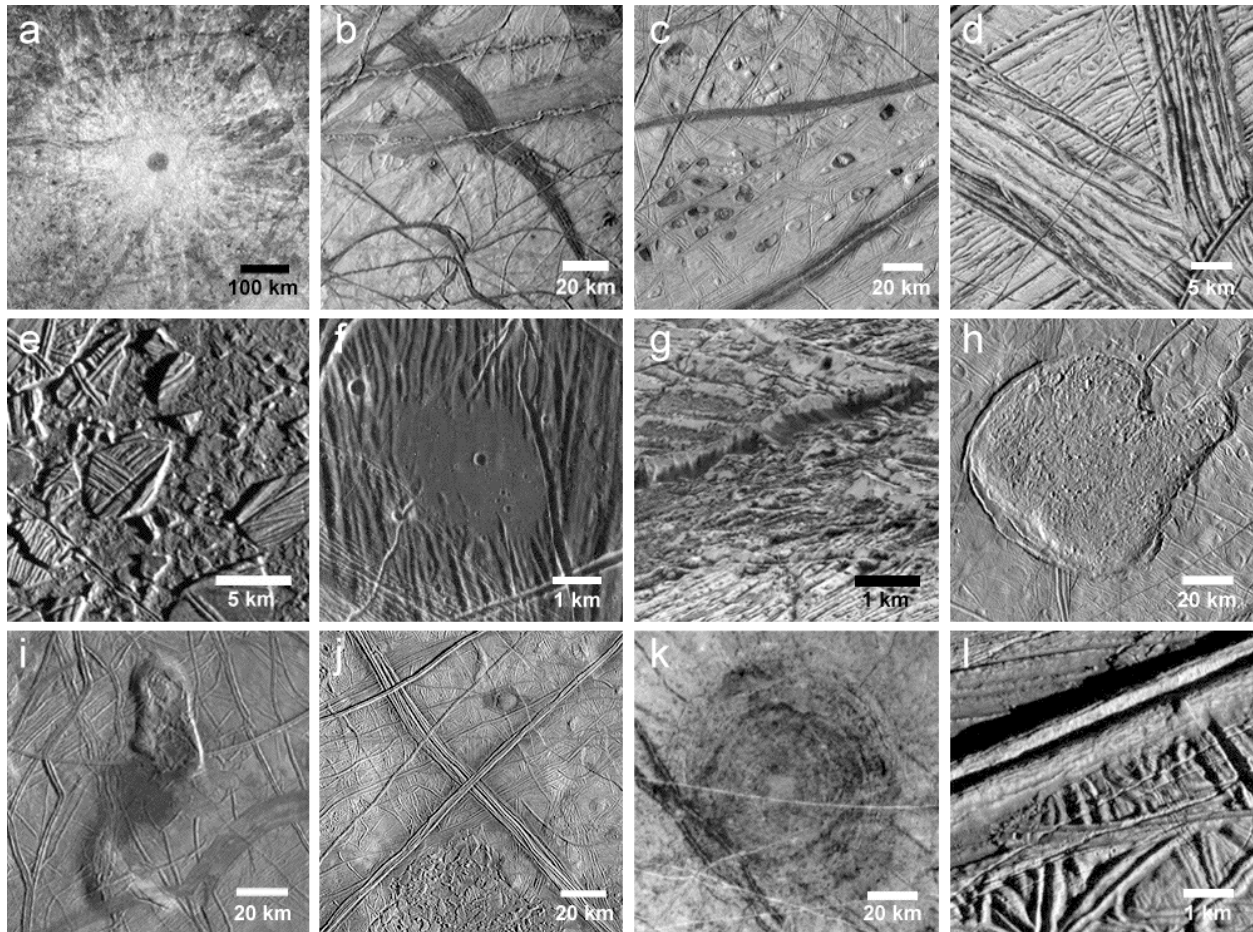


Figure C.1.1-5. Europa is a geological wonderland, with a wide variety of surface features. Many appear to be unique to this icy moon. While much was learned from Galileo, it is still not understood how many of these features form, or their implications for Europa's evolution. Shown here are (a) the impact crater Pwyll, the youngest large crater on Europa; (b) pull-apart bands; (c) lenticulae; (d) pull-apart band at high resolution; (e) Conamara Chaos; (f) dark plains material in a topographic low, (g) very high-resolution image of a cliff, showing evidence of mass wasting; (h) Murias Chaos, a cryovolcanic feature which appears to have flowed a short distance across the surface; (i) The Castalia Macula region, in which the northernmost dome contains chaos and is ~900 m high; (j) regional view of two very large ridge complexes in the Conamara region; (k) Tyre impact feature, showing multiple rings; and (l) one of Europa's ubiquitous ridges, at high resolution.

means for surface oxidants to enter the ocean. Some features, such as cycloidal ridges, appear to arise as a direct result of Europa's tidal cycle (Hoppa et al. 1999).

Bands reflect fracturing and lithospheric separation, much like sea-floor spreading on Earth, and most display bilateral symmetry (e.g., Sullivan et al. 1998) (Figure C.1.1-5b and d). Their surfaces vary from relatively smooth to heavily fractured. The youngest bands tend to be dark, while older bands are bright, suggest-

ing that they brighten with time. Geometric reconstruction of bands suggests that a spreading model is appropriate, indicating extension in these areas and possible contact with the ocean (Tufts et al. 2000, Prockter et al. 2002).

The accommodation of extensional features remains a significant outstanding question regarding Europa's geology. A small number of contractional folds were found on the surface (Prockter and Pappalardo 2000) and some sites of apparent convergence within bands have been suggested (Sarid et al. 2002), but these

are insufficient to accommodate the extension documented across Europa's surface. Some models suggest that ridges and local folds could reflect such contraction, but the present lack of global images, topographic information, and knowledge of subsurface structure precludes testing these ideas.

Fractures are narrow (from hundreds of meters to the ~10 m limit of image resolution) and some exceed 1,000 km in length. Some fractures cut across nearly all surface features, indicating that the ice shell is subject to deformation on the most recent timescales. The youngest ridges and fractures could be active today in response to tidal flexing. Subsurface sounding and surface thermal mapping could help identify zones of warm ice coinciding with current or recent activity. Young ridges might be places where there has been material exchange between the ocean and the surface, and would be prime targets as potentially habitable niches.

C.1.1.2.6 Chaotic Terrain

Europa's surface has been disrupted to form regions of chaotic terrain. Disrupted terrain may appear in the form of irregularly shaped, generally larger (tens to hundreds of kilometers) chaos zones (Figure C.1.1-5j), or smaller terrain (10-15 km) subcircular regions known as lenticulae (Collins and Nimmo 2009). Lenticulae include pits, spots of dark material, and domes where the surface is upwarped and commonly broken (Figure C.1.1-5c and f). Chaos is generally characterized by fractured plates of ice that have been shifted into new positions within a background matrix (Figure C.1.1-5e). Much like a jigsaw puzzle, many plates could be fit back together, and some ice blocks appear to have disaggregated and "foundered" into the surrounding finer-textured matrix (Spaun et al. 1998). Some chaos areas stand higher than the surrounding terrain (Figure C.1.1-5h and i).

Pappalardo et al. (1998, 1999) argued that chaos features are typically ~10 km across and

possibly formed by upwelling of compositionally or thermally buoyant ice diapirs through the ice shell. In such a case, their size distribution would imply an ice shell thickness of at least 10 to 20 km at the time of formation. Models of chaos formation suggest whole or partial melting of the ice shell, perhaps enhanced by local pockets of brine (Head and Pappalardo 1999). Downward and upward doming forms have been interpreted to correlate with recently formed chaos regions, each created through subsurface brine mobilization and subsequent freezing as occurs in Antarctic ice. Based on this model, at least one chaotic region, Thera Macula, might have been actively forming at the time of observations by the Galileo mission (Schmidt et al. 2011).

An alternative model suggests that there is no dominant size distribution and that lenticulae are small members of chaos (Greenberg et al. 1999), formed through either direct material exchange (through melting) or indirect exchange (through convection) between the ocean and surface (e.g., Carr et al. 1998a). Thus, global mapping of the size distribution of these features could address their origin.

Chaos features are stratigraphically young (Figueredo and Greeley 2004), possibly indicating a geologically recent increase in internal heating in Europa. Chaos and lenticulae commonly have associated dark, reddish zones thought to be material derived from the subsurface, possibly from the ocean. However, these and related models are poorly constrained, because the total energy partitioning within Europa is not known, nor are details of the composition of non-ice components. Subsurface sounding, surface imaging, and topographic mapping (e.g., Schenk and Pappalardo 2004) are required to understand the formation of chaotic terrain, and its implications for habitability.

C.1.1.2.7 Impact Features

Only 24 impact craters ≥ 10 km have been identified on Europa (Schenk et al. 2004), re-

flecting the youth of the surface. This is remarkable in comparison to Earth's Moon, which is only slightly larger but far more heavily cratered. The youngest crater on Europa is thought to be the 24 km-diameter Pwyll, (Figure C.1.1-5a) which still retains its bright rays, and likely formed less than 5 million years ago (Zahnle et al. 1998, Bierhaus et al. 2009).

Complete global imaging would provide a full crater inventory, allowing a more comprehensive determination of the age of Europa's surface, and helping to identify the very youngest areas.

Crater morphology and topography provide insight into ice layer thickness at the time of the impact. Morphologies vary from bowl-shaped depressions with crisp rims, to shallow depressions with smaller depth-to-diameter ratios. Craters up to 25–30 km in diameter have morphologies consistent with formation in a warm but solid ice shell, while the two largest impacts (Tyre [Figure C.1.1-5k] and Callanish) might have punched through brittle ice about 20 km deep into a liquid zone (Moore et al. 2001, Schenk et al. 2004, Schenk and E.P. Turtle 2009).

C.1.1.2.8 *Geological History*

Determining the geological histories of planetary surfaces requires identifying and mapping surface units and structures and placing them into a time-sequence. In the absence of absolute ages derived from isotopic measurements of rocks, planetary surface ages are commonly assessed from impact crater distributions, with more heavily cratered regions reflecting greater ages. The paucity of impact craters on Europa limits this technique. Thus, superposition (i.e., younger materials burying older materials) and cross-cutting relations are used to assess sequences of formation (Figueredo and Greeley 2004, Doggett et al. 2009). Unfortunately, only 10% of Europa has been imaged at a resolution sufficient to understand temporal relationships among surface features; for most of Europa, imaging data is both incom-

plete and disconnected from region to region, making the global surface history difficult to decipher.

Where images of sufficient resolution exist (i.e., better than 200 m/pixel), it appears that the style of deformation has evolved through time from ridge and band formation to chaotic terrain (Greeley et al. 2004), although there are areas of the surface where this sequence is less certain (e.g., Riley et al. 2000). The mechanism for the change in geological style is uncertain, but a plausible mechanism for the change is one in which Europa's ocean is slowly cooling and freezing out as the ice above it is thickening. Once the ice shell reaches a critical thickness, solid-state convection might be initiated, allowing diapiric material to be convected toward the surface. A thickening ice shell could be related to a waning intensity of geological activity.

Given the relative youth of Europa's surface, such a fundamental change in style might seem unlikely over the last ~1% of the satellite's history, and its activity over the rest of its ~4.5-billion-year existence could only be speculated. Four possible scenarios have been proposed (Figure C.1.1-6):

- (a) Europa resurfaces itself in a steady-state and relatively constant, but patchy style;
- (b) Europa is at a unique time in its history, having undergone a recent major resurfacing event;
- (c) Global resurfacing is episodic or sporadic;
- (d) Europa's surface is actually much older than current cratering models suggest (Zahnle et al. 2003).

From the standpoint of the dynamical evolution of the Galilean satellite system, there is good reason to believe that Europa's surface evolution could be cyclical. If so, Europa could experience cyclical variations in its orbital characteristics and tidal heating on time-

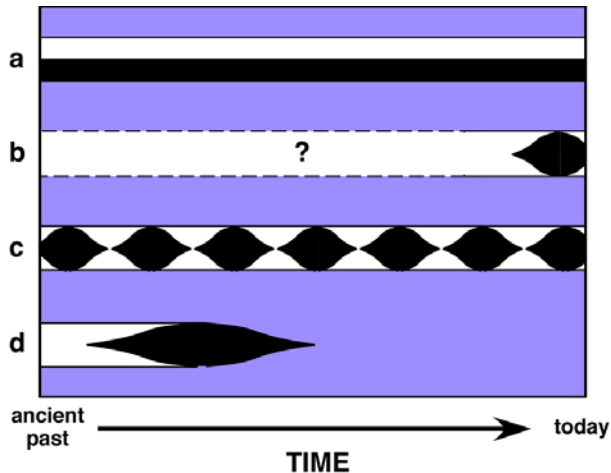


Figure C.1.1-6. Possible evolutionary scenarios for Europa's surface: (a) steady-state, relatively constant resurfacing; (b) unique time in history with recent major resurfacing event; (c) episodic or sporadic global resurfacing; (d) surface older than cratering models suggest. Geological mapping of imaging data would help to distinguish among these models. After Pappalardo et al. (1999).

scales of perhaps 100 million years (Hussman and Spohn 2004).

Global monochrome and color imaging, coupled with topography and subsurface sounding, would enable these evolutionary models to be tested. Europa's surface features generally brighten and become less red through time, so albedo and color could serve as a proxy for age (Geissler et al. 1998, Moore et al. 2009). Quantitative topographic data (Schenk and Pappalardo 2004) could provide information on the origin of geologic features and might show trends with age. Profiles across ridges, bands, and various chaotic terrains would aid in constraining their modes of origin. Moreover, flexural signatures are expected to be indicative of local elastic lithosphere thickness at the time of their formation, and might provide evidence of topographic relaxation (e.g., Nimmo et al. 2003, Billings and Kattenhorn 2005).

Some remaining outstanding questions related to Europa's geology include the following:

- Do Europa's ridges, bands, chaos, and/or multiringed structures require the presence of near-surface liquid water to form?
- Where are Europa's youngest regions?
- Is current geological activity sufficiently intense that heat flow from Europa's interior is measurable at the surface?

C.1.2 Flyby Traceability Matrix

Understanding planetary processes and habitability are key drivers for Europa exploration. Thus, the goal adopted for the Europa Multiple-Flyby Mission concept is to

Explore Europa to investigate its habitability.

The phrase "investigate its habitability" recognizes the significance of Europa's astrobiological potential. As discussed in Section A, "habitability" includes characterizing any water within and beneath Europa's ice shell, investigating the chemistry of the surface and ocean, and evaluating geological processes that might permit Europa's ocean to possess the chemical energy necessary for life.

The Europa Multiple-Flyby Mission objectives flow from the key science issues outlined in Section A.3. These objectives represent a key subset of Europa science best accomplished by a Europa Multiple-Flyby Mission. These objectives are categorized in priority order as

- I. Europa's Ice Shell: Characterize the ice shell and any subsurface water, including their heterogeneity, and the nature of surface-ice-ocean exchange.
- C. Europa's Composition: Understand the habitability of Europa's ocean through composition and chemistry.
- G. Europa's Geology: Understand the formation of surface features, including sites of recent or current activity, and characterize high science interest localities.

The complete traceability from goal to objectives to investigations, and then to example measurements and the notional instruments

that could accomplish them, is compiled in Foldout C-1 (FO C-1). These example measurements and the notional instruments that could accomplish them are provided as a proof of concept, to demonstrate the types of measurements that could address the goal, objectives, and investigations. These measurements and notional instruments are in no way meant to be exclusive of other measurements and instruments that might be able to address the objectives and investigations in other ways.

The traceability matrix (FO C-1), with its overarching goal to “explore Europa to investigate its habitability,” provides specific objectives (listed in priority order), along with specific investigations (listed in priority order within each objective). The example measurements that could address each investigation are also listed in priority order for each investigation. Each objective and its investigations are described in Sections C.1.2.1 through C.1.2.4 below, along with the corresponding example measurements that could address them. The right-hand columns of the traceability matrix provide an assessment regarding which of the three themes (water, chemistry, and energy) each investigation addresses.

C.1.2.1 Europa’s Ice Shell

C.1.2.1.1 *Investigation I.1: Characterize the distribution of any shallow subsurface water and the structure of the icy shell.*

The subsurface signatures from near-global Ice-Penetrating Radar (IPR) surveys at high depth resolution, combined with surface topography of similar vertical resolution, would identify regions of possible ongoing or relatively recent upwelling of liquid water or brines. Orbital subsurface profiling of the top 3 km of Europa’s ice shell should be feasible (Chyba 1998, Moore 2000) and is recommended at frequencies slightly above the upper end of Jupiter’s radio noise spectrum (i.e., about 60 MHz) to establish the geometry of various thermal, compositional, and structural horizons to a depth resolution of about 10 m

(requiring a bandwidth of about 10 MHz). This high-resolution search for shallow water would produce data analogous to that of the Shallow Subsurface Radar (SHARAD) instrument onboard the Mars Reconnaissance Orbiter (Figure C.1.2-1).

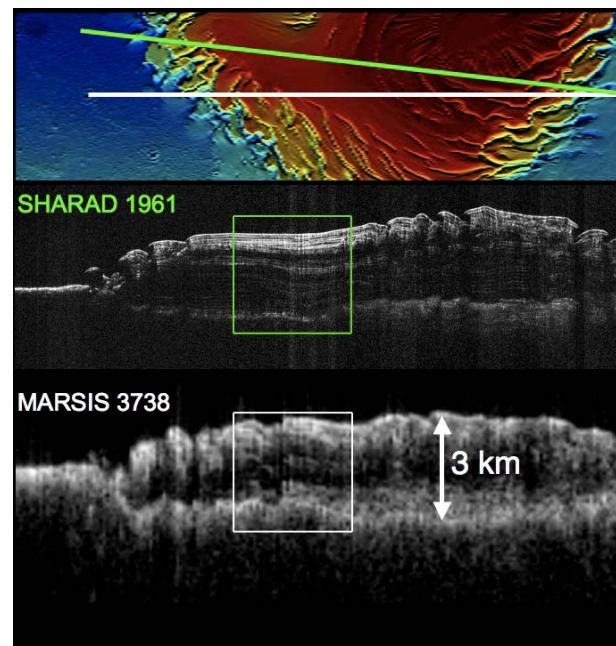


Figure C.1.2-1. Orbital subsurface profiling of Mars north polar cap. These nearly co-linear profiles across the Mars North Polar Cap (Mars Orbiter Laser Altimeter data at top left) demonstrate the value of the complementary perspectives provided by the high-center-frequency and high-bandwidth profiling of the SHARAD instrument (20 MHz and 10 MHz, respectively), and the low-center-frequency and low-bandwidth profiling of the Mars Advanced Radar for Subsurface and Ionosphere Sounding (MARSIS) (5 MHz and 1 MHz, respectively). In particular, note the clarity of shallow horizons revealed by SHARAD (detail at top right) and the prominence of deep interfaces revealed in the MARSIS results (detail at bottom right). The value of a multifrequency approach to subsurface profiling on Europa would be significantly enhanced in the presence of strong volume scattering. (MARSIS data courtesy of Picardi, Plaut, and the MARSIS Team; SHARAD data courtesy of Seu, Phillips, and the SHARAD Team.)

Goal	Objective	Investigation	Measurement	Model Instrument	Mission Constraints/Requirements	Water	Chemistry	Energy
Explore Europa to investigate its habitability	I. Ice Shell	I.1 Characterize the distribution of any shallow subsurface water and the structure of the icy shell.	I.1a Identify and regionally characterize subsurface thermal or compositional horizons and structures related to the current or recent presence of water or brine. Obtain pairs of intersecting profiles of subsurface dielectric horizons and structures at depths of 100 meters to 3 km at 10-meter vertical resolution, with estimations of subsurface dielectric properties and the density of buried scatterers.	Ice-Penetrating Radar (IPR) with altimeter mode	(1) Globally distributed regions: 6 equatorial panels (± 30 deg Lat) and 4 panels at each pole (± 60 deg in Lat); total of 14 panels. (2) Low-altitude flyby along a groundtrack achieving 800-km segments within each panel at altitude <400 km, at <6 km/s, and with 25- to 100-km closest approach. Two 800-km groundtrack segments in each sub-Jovian panel and at least three 800-km groundtracks in anti-Jovian panels. Each groundtrack shall also intersect another groundtrack (intersection may be outside the panel of interest); a single radar pass of sufficient length and geometry may satisfy groundtrack and intersection requirements in adjacent panels. (3) Radar groundtrack begins below ~1000-km altitude. (4) Tracks of 1/12 Europa's circumference in length co-located with a nadir-pointed altimetric profile with absolute height accuracy of 10 m. (5) <u>Floor:</u> (1) & (2) satisfied in 8 of 14 of the panels, including both anti- and sub-Jovian equatorial panels; <u>Baseline:</u> (1) & (2) satisfied in 11 of 14 panels; one groundtrack intersection within each panel, if possible.	✓		✓
			I.1b Topography on the order of 250-m horizontal scale and better than or equal to 20-m vertical resolution and accuracy extending to 50 km on either side of subsurface profiles.	Topographical Imager (TI) and Ice-Penetrating Radar (IPR) with altimeter mode	(1) Globally distributed regions: 6 equatorial panels (± 30 deg Lat) and 4 panels at each pole (± 60 deg in Lat); total of 14 panels. (2) Low-altitude flyby along a groundtrack achieving 800-km segments within each panel at altitude <400 km, at <6 km/s, and with 25- to 100-km closest approach. Two 800-km groundtrack segments in each sub-Jovian panel and at least three 800-km groundtracks in anti-Jovian panels. Each groundtrack shall also intersect another groundtrack (intersection may be outside the panel of interest); a single radar pass of sufficient length and geometry may satisfy groundtrack and intersection requirements in adjacent panels. (3) Radar groundtrack begins below 1000-km altitude with altimetry mode. (4) Tracks of 1/12 Europa's circumference in length, co-located with a nadir-pointed altimetric profile with absolute height accuracy of 10 m. <u>Stereo imaging:</u> (5) The cross-track angular width (FOV) should be sufficient to provide stereo imaging of the radar sounder groundtrack. (6) Acceptable range for stereo imaging is incidence angles of ~20 to 80°. To the extent possible, imaging should be at solar incidence angles greater than 45°. Ideally, the incidence angle would be 70°. <u>Ice-Penetrating Radar:</u> (7) <u>Floor:</u> (1) & (2) satisfied in 8 of 14 of the panels, including both anti- and sub-Jovian equatorial panels; <u>Baseline:</u> (1) & (2) satisfied in 11 of 14 panels; one groundtrack intersection within each panel, if possible.	✓		✓
		I.2 Search for an ice-ocean interface.	I.2a Identify deep thermal, compositional, or structural horizons by obtaining globally distributed regional profiles of subsurface dielectric horizons and structures at depths of 1- to 30-km at 100-m vertical resolution.	Ice-Penetrating Radar (IPR) with altimeter mode	(1) Globally distributed regions: 6 equatorial panels (± 30 deg Lat) and 4 panels at each pole (60 deg in Lat); total of 14 panels. (2) Low-altitude flyby along a groundtrack achieving ~1600-km segments within each panel at altitude <1000 km, at <6 km/s, and with 25- to 100-km closest approach. Each groundtrack shall also intersect another groundtrack (intersection may be outside the panel of interest); a single radar pass of sufficient length and geometry may satisfy groundtrack and intersection requirements in adjacent panels. (3) Radar groundtrack begins below 1000-km altitude with altimetry mode. (4) Tracks of 1/6 of Europa's circumference in length co-located with a nadir-pointed altimetric profile with absolute height accuracy of 10 m. (5) <u>Floor:</u> (1) & (2) satisfied in 8 of 14 of the panels, thus including both anti- and sub-Jovian equatorial panels; <u>Baseline:</u> (1) & (2) satisfied in 11 of 14 of panels, including polar and equatorial anti-Jovian panels.	✓		✓

Floor
 Baseline only

Water: Water in its liquid form as pertaining to habitability as an oxidizer and medium for the transport of chemical constituents.

Energy: Energy that supports and fosters a means for potential metabolism to be established and sustained.

Chemistry: The constituents that foster and sustain the processes and environment for metabolic activity.

Goal	Objective	Investigation	Measurement	Model Instrument	Mission Constraints/Requirements	Water	Chemistry	Energy	
Explore Europa to investigate its habitability	I. Ice Shell	Characterize the ice shell and any subsurface water, including their heterogeneity, and the nature of surface-ice-ocean exchange.	1.2 Search for an ice-ocean interface.	1.2b Topography on the order of 250-m horizontal scale and better than or equal to 20-m vertical resolution and accuracy extending to 50 km on either side of subsurface profiles.	Topographical Imager (TI) and Ice-Penetrating Radar (IPR) with altimeter mode	(1) Globally distributed regions: 6 equatorial panels (± 30 deg Lat) and 4 panels at each pole (± 60 deg in Lat); total of 14 panels. (2) Low-altitude flyby along a groundtrack achieving ~1600-km segments within each panel at altitude <1000 km, at <6 km/s, and with 25- to 100-km closest approach. Each groundtrack shall also intersect another groundtrack (intersection may be outside the panel of interest); a single radar pass of sufficient length and geometry may satisfy groundtrack and intersection requirements in adjacent panels. (3) Radar groundtrack begins below 1000-km altitude with altimetry mode. (4) Tracks of 1/6 of Europa's circumference in length co-located with a nadir-pointed altimetric profile with absolute height accuracy of 10 m. <u>Stereo Imaging:</u> (5) The cross-track angular width (FOV) should be sufficient to provide stereo imaging of the radar sounder groundtrack. (6) Acceptable range for stereo imaging is incidence angles of ~20 to 80°. To the extent possible, imaging should be at solar incidence angles greater than 45°. Ideally, the incidence angle would be 70°. <u>Ice-Penetrating Radar:</u> (7) <u>Floor:</u> (1) & (2) satisfied in 8 of 14 of the panels, thus including both anti- and sub-Jovian equatorial panels; <u>Baseline:</u> (1) & (2) satisfied in 11 of 14 of panels including polar and equatorial anti-Jovian panels.	✓		✓
			1.3 Correlate surface features and sub-surface structure to investigate processes governing material exchange among the surface, ice shell, and ocean.	1.3a Identification and regional characterization of subsurface dielectric horizons and structures, at depths 1- to 30-km at 100-m vertical resolution and depths of 100-m to 3-km at 10-m vertical resolution, by obtaining intersecting subsurface profiles distributed over a variety of surface features.	Ice-Penetrating Radar (IPR) with altimeter mode	(1) Globally distributed regions: 6 equatorial panels (± 30 deg Lat) and 4 panels at each pole (± 60 deg in Lat); total of 14 panels. (2) Low-altitude flyby along a groundtrack achieving 800-km segments within each panel at altitude <400 km, at <6 km/s, and with 25- to 100-km closest approach. Two 800-km groundtrack segments in each sub-Jovian panel and three 800-km groundtracks in anti-Jovian panels. Each groundtrack shall also intersect another groundtrack (intersection may be outside the panel of interest); a single radar pass of sufficient length and geometry may satisfy groundtrack and intersection requirements in adjacent panels. (3) Radar groundtrack begins below ~1000-km altitude. (4) Tracks of 1/12 Europa's circumference in length co-located with a nadir-pointed altimetric profile with absolute height accuracy of 10 m. (5) <u>Floor:</u> (1) & (2) satisfied in 8 of 14 of the panels, including both anti- and sub-Jovian equatorial panels; <u>Baseline:</u> (1) & (2) satisfied in 11 of 14 panels; one groundtrack intersection within each panel, if possible.	✓	✓	✓
			1.3b Measure surface reflectance from 850-5000 nm with 10-nm resolution $n < 2500$ nm and 20 nm from 2500-5000 nm. Targeted observations of ~100 representative landforms at 300-m/pixel sampling over a wide range of latitudes and longitudes.	Shortwave Infrared Spectrometer (SWIRS)	(1) Ability to target specific geologic locations that are globally distributed (6 equatorial panels (± 30 deg Lat) and 4 panels at each pole (± 60 deg in Lat); total of 14 panels). (2) Low-altitude flyby along a groundtrack within each panel at altitude <1000 km, at ≤ 6 km/s, and with 25- to 100-km closest approach. Ability to collect data at different locations along each groundtrack to sample desired landforms. (3) Observations on the leading and trailing hemisphere are required in addition to at least one high-latitude pass. (4) Solar incidence angles at the equator of less than 45° (local true solar time between 9:00 to 15:00) [Note: Illumination requirements for the SWIRS have a higher priority than those for the Topographical Imager]. (5) Ability of spacecraft to smoothly scan over the surface to build up spectral image cube. (6) Spacecraft stability: Less than 1/2 IFOV over the integration time. (7) Regional scale (300 m/pixel) observations: <u>Floor:</u> Sampling in 8 of the 14 panels; <u>Baseline:</u> Sampling in 11 of 14 panels.	✓	✓	✓	

 Floor
 Baseline only

Water: Water in its liquid form as pertaining to habitability as an oxidizer and medium for the transport of chemical constituents.

Energy: Energy that supports and fosters a means for potential metabolism to be established and sustained.

Chemistry: The constituents that foster and sustain the processes and environment for metabolic activity.

Goal	Objective	Investigation	Measurement	Model Instrument	Mission Constraints/Requirements	Water	Chemistry	Energy	
Explore Europa to investigate its habitability	I. Ice Shell	1.3 Correlate surface features and subsurface structure to investigate processes governing material exchange among the surface, ice shell, and ocean.	1.3c Topography on the order of 250-m horizontal scale and better than or equal to 20-m vertical resolution and accuracy extending to 50 km on either side of subsurface profiles.	Topographical Imager (TI) an Ice-Penetrating Radar (IPR) with altimeter mode	(1) Globally distributed regions: 6 equatorial panels (± 30 deg Lat) and 4 panels at each pole (± 60 deg in Lat); total of 14 panels. (2) Low-altitude flyby along a groundtrack achieving 800-km segments within each panel at altitude <400 km, at <6 km/s, and with 25- to 100-km closest approach. Two 800-km groundtrack segments in each sub-Jovian panel and three 800-km groundtracks in anti-Jovian panels. Each groundtrack shall also intersect another groundtrack (intersection may be outside the panel of interest); a single radar pass of sufficient length and geometry may satisfy groundtrack and intersection requirements in adjacent panels. (3) Radar groundtrack begins below 1000-km altitude with altimetry mode. (4) Tracks of 1/12 Europa's circumference in length co-located with a nadir-pointed altimetric profile with absolute height accuracy of 10 m. <u>Stereo Imaging:</u> (5) Stereo imaging: The cross-track angular width (FOV) should be sufficient to provide stereo imaging of the radar sounder groundtrack. (6) Acceptable range for stereo imaging is incidence angles of ~ 20 to 80° . To the extent possible, imaging should be at solar incidence angles greater than 45° . Ideally the incidence angle would be 70° . <u>Ice-Penetrating Radar:</u> (7) <u>Floor:</u> (1) & (2) satisfied in 8 of 14 of the panels including both anti- and sub-Jovian equatorial panels; <u>Baseline:</u> (1) & (2) satisfied in 11 of 14 panels; one groundtrack intersection within each panel if possible.	✓	✓	✓	
		1.4 Characterize regional and global heat flow variations.	1.4a Identify and map subsurface thermal horizons by obtaining profiles of subsurface dielectric horizons at depths of 1- to 30-km at 10- to 100-m vertical resolution.	Ice-Penetrating Radar (IPR)	(1) Globally distributed regions: 6 equatorial panels (± 30 deg Lat) and 4 panels at each pole (± 60 deg in Lat); total of 14 panels. (2) Low-altitude flyby along a groundtrack achieving 800-km segments within each panel at altitude <400 km, at <6 km/s, and with 25- to 100-km closest approach. Two 800-km groundtrack segments in each sub-Jovian panel and three 800-km groundtracks in anti-Jovian panels. Each groundtrack shall also intersect another groundtrack (intersection may be outside the panel of interest); a single radar pass of sufficient length and geometry may satisfy groundtrack and intersection requirements in adjacent panels. (3) Radar groundtrack begins below ~ 1000 -km altitude. (4) Tracks of 1/12 Europa's circumference in length co-located with a nadir-pointed altimetric profile with absolute height accuracy of 10 m. (5) <u>Floor:</u> (1) & (2) satisfied in 8 of 14 of the panels including both anti- and sub-Jovian equatorial panels; <u>Baseline:</u> (1) & (2) satisfied in 11 of 14 of panels with one groundtrack intersection within each panel if possible.	✓		✓	
	C. Composition	Understand the habitability of Europa's ocean through composition and chemistry.	C.1 Characterize the composition and chemistry of the Europa ocean as expressed on the surface and in the atmosphere.	C.1a Measure surface reflectance from 850-5000 nm with 10-nm resolution $n < 2500$ nm and 20 nm from 2500-5000 nm. Targeted observations of ~ 100 representative landforms at regional-scales (300-m/pixel sampling) over a wide range of latitudes and longitudes.	Shortwave Infrared Spectrometer (SWIRS)	(1) Ability to target specific geologic locations that are globally distributed: 6 equatorial panels (± 30 deg Lat) and 4 panels at each pole (± 60 deg in Lat); total of 14 panels. (2) Low-altitude flyby along a groundtrack within each panel at altitude <1000 km, at ≤ 6 km/s, and with 25- to 100-km closest approach. Ability to collect data at different locations along the groundtrack to sample desired landforms. (3) Observations on the leading and trailing hemisphere are required in addition to at least one high-latitude pass. (4) Solar incidence angles at the equator of less than 45° (local true solar time between 9:00 to 15:00) [Note: Illumination requirements for the SWIRS have a higher priority than those for the Topographical Imager]. (5) Ability of spacecraft to smoothly scan over the surface to build up spectral image cube. (6) Spacecraft stability: Less than 1/2 IFOV over the integration time. (7) Regional scale (300 m/pixel) observations: <u>Floor:</u> Sampling in 8 of the 14 panels; <u>Baseline:</u> Sampling in 11 of 14 panels.	✓	✓	
				C.1b Characterize the composition of sputtered surface products over a mass range better than 300 daltons, mass resolution better than 500, with sensitivity of at least 10 particles cm^{-3} .	Ion and Neutral Mass Spectrometer (INMS)	(1) Flyby Velocity of <7 km/s, with slower speeds desirable. (2) Flight altitudes of <200 km, with lower altitude passes desired (as low as 25 km).	✓	✓	

Floor
 Baseline only

Water: Water in its liquid form as pertaining to habitability as an oxidizer and medium for the transport of chemical constituents.

Energy: Energy that supports and fosters a means for potential metabolism to be established and sustained.

Chemistry: The constituents that foster and sustain the processes and environment for metabolic activity.

Goal	Objective	Investigation	Measurement	Model Instrument	Mission Constraints/Requirements	Water	Chemistry	Energy
Explore Europa to investigate its habitability	C. Composition	C.2 Determine the role of Jupiter's radiation environment in processing materials on Europa.	C.2a Measure surface reflectance from 850-5000 nm with 10-nm resolution $n < 2500$ nm and 20 nm from 2500-5000 nm. Targeted observations of ~100 representative landforms at regional-scales (300-m/pixel sampling) over a wide range of latitudes and longitudes.	Shortwave Infrared Spectrometer (SWIRS)	(1) Ability to target specific geologic locations that are globally distributed: 6 equatorial panels (± 30 deg Lat) and 4 panels at each pole (± 60 deg in Lat); total of 14 panels. (2) Low-altitude flyby along a groundtrack within each panel at altitude < 1000 km, at ≤ 6 km/s, and with 25- to 100-km closest approach. Ability to collect data at different locations along the groundtrack to sample desired landforms. (3) Observations on the leading and trailing hemisphere are required in addition to at least one high-latitude pass. (4) Solar incidence angles at the equator of less than 45° (local true solar time between 9:00 to 15:00) [Note: Illumination requirements for the SWIRS have a higher priority than those for the Topographical Imager]. (5) Ability of spacecraft to smoothly scan over the surface to build up spectral image cube. (6) Spacecraft stability: Less than 1/2 IFOV over the integration time. (7) Regional scale (300 m/pixel) observations: <u>Floor</u> : Sampling in 8 of the 14 panels; <u>Baseline</u> : Sampling in 11 of 14 panels.		✓	✓
			C.2b Characterize the composition of sputtered surface products over a mass range better than 300 daltons, mass resolution better than 500, with sensitivity of at least $10 \text{ particles cm}^{-3}$.	Ion and Neutral Mass Spectrometer (INMS)	(1) Flyby Velocity of < 7 km/s, with slower speeds desirable. (2) Flight altitudes of < 200 km, with lower altitude passes desired (as low as 25 km).		✓	✓
		C.3 Characterize the chemical and compositional pathways in Europa's ocean.	C.3a Measure surface reflectance from 850-5000 nm with 10-nm resolution < 2500 nm and 20 nm from 2500-5000 nm. Targeted observations of ~100 representative landforms at 300-m/pixel sampling and global-scale coverage with a spatial sampling better than or equal to 10 km/pixel.	Shortwave Infrared Spectrometer (SWIRS)	(1) Ability to target specific geologic locations that are globally distributed: 6 equatorial panels (± 30 deg Lat) and 4 panels at each pole (± 60 deg in Lat); total of 14 panels. (2) Low-altitude flyby along a groundtrack within each panel at altitude < 1000 km, at ≤ 6 km/s, and with 25- to 100-km closest approach. Ability to collect data at different locations along the groundtrack to sample desired landforms. (3) Observations on the leading and trailing hemisphere are required in addition to at least one high-latitude pass. (4) Global-scale coverage with a spatial sampling better than or equal to 10 km/pixel that samples 70% of the surface at local true solar times (LTST) between 9:00 and 15:00 and at ~ 5 to 10° intervals in latitude and longitude. (5) Solar incidence angles at the equator of less than 45° (local true solar time between 9:00 to 15:00) [Note: Illumination requirements for the SWIRS have a higher priority than those for the Topographical Imager]. (6) Ability of spacecraft to smoothly scan over the surface to build up spectral image cube. (7) Spacecraft stability: Less than 1/2 IFOV over the integration time. (8) Regional scale (300 m/pixel) observations: <u>Floor</u> : Sampling in 8 of the 14 panels; <u>Baseline</u> : Sampling in 11 of 14 panels.	✓	✓	
			C.3b Characterize the composition of sputtered surface products over a mass range better than 300 daltons, mass resolution better than 500, with sensitivity of at least $10 \text{ particles cm}^{-3}$.	Ion and Neutral Mass Spectrometer (INMS)	(1) Flyby Velocity of < 7 km/s, with slower speeds desirable. (2) Flight altitudes of < 200 km, with lower altitude passes desired (as low as 25 km).	✓	✓	
			C.3c Correlate surface composition with geologic features through mapping at resolution of better than or equal to 100 m/pixel for locations measured spectroscopy.	Topographical Imager (TI) (stereo)	(1) Acceptable range for stereo imaging is incidence angles of $\sim 20^\circ$ to 80° . To the extent possible, imaging should be at solar incidence angles greater than 45° . Ideally, the incidence angle would be 70° . (2) The cross-track angular width (FOV) should be sufficient to cover the effective cross-track width of the radar sounder.	✓	✓	

Floor
 Baseline only

Water: Water in its liquid form as pertaining to habitability as an oxidizer and medium for the transport of chemical constituents.

Energy: Energy that supports and fosters a means for potential metabolism to be established and sustained.

Chemistry: The constituents that foster and sustain the processes and environment for metabolic activity.

Goal	Objective	Investigation	Measurement	Model Instrument	Mission Constraints/Requirements	Water	Chemistry	Energy
Explore Europa to investigate its habitability	G. Geology	G.1 Determine sites of most recent geological activity, and characterize localities of high science interest.	G.1a Characterize selected targets at ~20 m/pixel and characterize their topography at better than 50-m horizontal scale and better than or equal to 10-meter vertical resolution and accuracy.	Topographical Imager (TI) (stereo), Ion and Neutral Mass Spectrometer (INMS)	(1) Acceptable range for stereo imaging is incidence angles of ~20° to 80°. To the extent possible, imaging should be at solar incidence angles greater than 45°. Ideally, the incidence angle would be 70°. (2) The cross-track angular width (FOV) should be sufficient to cover the effective cross-track width of the radar sounder. (3) Flyby Velocity of <7 km/s, with slower speeds desirable. (4) Flight altitudes of <200 km, with lower altitude passes desired (as low as 25 km).	✓		✓

Floor
 Baseline only

Water: Water in its liquid form as pertaining to habitability as an oxidizer and medium for the transport of chemical constituents.
Energy: Energy that supports and fosters a means for potential metabolism to be established and sustained.
Chemistry: The constituents that foster and sustain the processes and environment for metabolic activity.

This profiling should be done in conjunction with colocated stereo imaging and a radar altimeter that could be used to register photogrammetric topography to vertical resolution of better than 20 m, permitting surface clutter effects to be removed from the radar data. Stereo imaging is susceptible to relative errors, and stereo vertical accuracy might vary across a scene. However, significantly higher vertical resolutions could be extracted using photogrammetry that is controlled by stereo imaging and radar altimetry data. By tying this high-horizontal-resolution relief to the high absolute vertical resolution of a radar altimeter, we could generate improved digital elevation models, which could be used to model and subtract radar clutter. Ultimately, shallow subsurface profiles should sample regions that are globally distributed across Europa's surface.

C.1.2.1.2 Investigation I.2: Search for an ice–ocean interface.

Subsurface signatures from lower-resolution but more deeply penetrating radar surveys might reveal the ice–ocean interface, which could be validated over a region by carefully correlating ice thickness and surface topography. An unequivocally thin ice shell, even within a limited region, would have significant implications for understanding direct exchange between the ocean and the overlying ice. Similarly, the detection of deep subsurface interfaces in these surveys and the presence or absence of shallower interfaces above them would test hypotheses regarding the convective upwelling of deep, ductile ice into the cold, brittle shell, implying indirect exchange with any ocean. Additional orbital profiling of the subsurface of Europa to depths of 30 km with a vertical resolution of about 100 m would establish the geometry of any deeper geophysical interfaces such as an ice–ocean interface.

Although warm ice is very attenuating to radar (Chyba et al. 1998), thick ice in a regime of steady-state thermal conduction could be sounded on Europa to depths of 25 to 40 km if

it is essentially free of impurities (Moore 2000). Although impurities are almost certainly present, the non-steady-state convective thermal regime could generate “windows” of very cold downwelling material within the ice shell, allowing local penetration to great depth (McKinnon 2005). Moreover, while the presence of meter-scale voids within the ice shell would confound sounding measurements at higher frequencies (>15 MHz) (Eluszkiewicz 2004), the presence of such large voids is probably unrealistic (Lee et al. 2005).

Deep ocean searches would produce data analogous to those of the Mars Advanced Radar for Subsurface and Ionosphere Sounding (MARSIS) instrument on the Mars Express spacecraft (Figure C.1.2-1). This profiling should establish the geometry of any deeper geophysical interfaces that might correspond to an ice–ocean boundary, to a vertical resolution of about 100 m (requiring a bandwidth of about 1 MHz).

Frequencies significantly less sensitive to any volume scattering that might be present in the shallow subsurface profiling detailed above (i.e., about 9 MHz) should be used on the anti-Jovian side of Europa, which is substantially shadowed from Jupiter's radio emissions. This low-frequency, low-resolution profiling should be complemented by high-frequency, low-resolution profiling over Europa's sub-Jovian surface (where Jupiter's radio noise is an issue for low-frequency sounding). Combined, the deep, low-resolution profiling should sample regions that are globally distributed across Europa's surface. Profiling should be performed along with colocated stereo imaging and radar altimetry of better than 100 m topographic resolution, permitting surface clutter effects to be removed from the radar data.

C.1.2.1.3 *Investigation I.3: Correlate surface features and subsurface structure to investigate processes governing material exchange among the surface, ice shell, and ocean.*

Targeted radar observations would lead to understanding the processes controlling the distribution of any shallow subsurface water and either the direct or indirect exchange of materials between the ice shell and its underlying ocean. Similarly, differences in the physical and compositional properties of the near-surface ice might arise due to age differences, tectonic deformation, mass wasting, or impact gardening. Knowledge of surface properties gained from spectroscopy and high-resolution image and topographic data would be essential for integrated interpretation of subsurface structure, and for understanding liquid water or ductile ice within Europa's ice shell.

Because of the complex geometries expected for subsurface structures, subsurface radar images should be obtained along profiles in globally distributed regions across Europa, either to a depth of 3 km for high-resolution imaging or to a depth of 30 km for lower-resolution imaging of deeper features, in conjunction with colocated topographic data.

C.1.2.1.4 *Investigation I.4: Characterize regional and global heat-flow variations.*

The thermal structure of the shell (apart from local heat sources) is set by the transport of heat from the interior. Regardless of the properties of the shell or the overall mechanism of

heat transport, the uppermost few kilometers at least are cold and stiff. The thickness of this "lid" is set by the total amount of heat that must be transported; thus, a measurement of the thickness of the cold and brittle part of the shell would provide a constraint on the heat production in the interior.

For a thin ice shell, the ice–ocean interface would form a significant dielectric horizon at the base of the thermally conductive layer. However, if warm pure-ice diapirs from the interior of a thicker convective shell approach the surface, they might be different from the pure-ice melting point and above the eutectic of many substances; this could create regions of melting within the rigid shell above them as the temperature increases above a diapir. Any dielectric horizon associated with such melt regions would also provide a good measurement of the thickness of the cold lid. Global radar profiles of the subsurface thermal horizons to depths of 30 km at a vertical resolution of 100 m would enable characterization of regional and global heat-flow variations in Europa's ice shell.

The key outstanding questions relating to Europa's ice shell (Table C.1.2-1) can be related to and addressed by the Objective I investigations described above, as summarized in FO C-1.

C.1.2.2 *Europa's Composition*

Surface composition forms the linkages that enable understanding of Europa's potential habitability in the context of geologic process-

Table C.1.2-1. Hypothesis tests to address selected key questions regarding Europa's ice shell.

Example Hypothesis Questions		Example Hypothesis Tests
I.1	Is Europa's ice shell very thin and conductive or thick and convecting?	Sound Europa's ice shell for a strong water reflector at shallow depth, or to observe a gradual absorption of the signal with depth, which might reveal diapiric structures.
I.2	Is there fluid transport from the ocean to the near-surface or surface, and vice versa?	Sound Europa's ice at shallow and greater depths for liquid water, and correlate to surface morphology, compositional, and thermal data.
I.3	What are the three-dimensional characteristics of Europa's geological structures?	Combine ice-penetrating radar and topographic measurements with high-resolution imaging to investigate the 3D structure of geological features.
I.4	Are there regional variations in the thickness of Europa's thermally conductive layer?	Sound Europa's ice shell to map dielectric horizons in globally distributed regions.

es. Composition is also a probe of the interior and records the evolution of the surface under the influence of internal and external processes. Investigations regarding Europa's chemistry and composition require synergistic, coordinated observations of targeted geological features, along with stereo imaging and radar sounding.

There are two basic approaches to determining the composition of Europa's surface: Materials could be measured on the surface using remote optical spectroscopy, or the surface composition could be inferred by measuring materials sputtered or ejected from the surface into an atmosphere. Optical measurements of the surface could determine the composition and distribution of materials at geologically relevant scales (tens to hundreds of meters). However, the spectroscopy of solids is complicated by the physical properties of the material (e.g., grain size and temperature), and by material mixing, and high-quality spectra of specific surface units are required to identify minor components. Materials with strong, narrow, isolated absorption features could be accurately identified with detection limits of ~1%, and much greater sensitivity (~0.1%) could be achieved for strongly absorbing components intimately mixed with a less-absorbing component such as water ice. Materials with broad, shallow features might have detection limits of $\geq 10\%$, and their identification might be limited to the mineral or functional group of material present (e.g., phyllosilicates). Some materials (e.g., NaCl) are optically inactive through much of the visible and infrared and are difficult to detect remotely. In addition, the surface composition can be inferred from measurements of daughter products that have been derived from the surface by sputtering and radiation-induced chemistry.

Before discussing the specific investigations for the objective related to Europa's composition, we first explore the techniques of infrared spectroscopy to understand surface composi-

tion, and ion and neutral spectroscopy to understand atmospheric composition.

Surface Composition through Infrared Spectroscopy

A well-established means to map surface composition at the spatial scales relevant to geologic processes is through infrared imaging spectroscopy. Data obtained by the Galileo NIMS for Europa and observations by the Cassini Visual and Infrared Mapping Spectrometer (VIMS) of the Saturnian system demonstrate the existence of a wealth of spectral features throughout the near-infrared spectral range (e.g., McCord et al. 1998b; Carlson et al. 1999a, b; Clark et al. 2005; Cruikshank et al. 2007).

Of the materials studied thus far in the laboratory, the hydrated sulfates appear to most closely reproduce the asymmetric and distorted H₂O spectral features observed at Europa. In these compounds, hydration shells around anions and/or cations contain water molecules in various configurations, held in place by hydrogen bonds. Each configuration corresponds to a particular vibrational state, resulting in complex spectral behavior that is diagnostic of composition. These bands become particularly pronounced at temperatures below 150 K as the reduced intermolecular coupling causes the individual absorptions that make up these spectral features to become more discrete (Crowley 1991; Dalton and Clark 1998; Carlson et al. 1999b, 2005; McCord et al. 2001a, 2002; Orlando et al. 2005; Dalton et al. 2003, 2005; Dalton 2000, 2007). As a result, the spectra of low-temperature materials provide highly diagnostic, narrow features ranging from 10 to 50 nm wide (Figure C.1.2-2).

Cryogenic spectra for all of the hydrated sulfates and brines in Figure C.1.2-2 display the diagnostic absorption features near 1.0, 1.25, 1.5, and 2.0 μm that are endemic to water-bearing compounds. These features generally align with those in water ice and with the features observed in the Europa spectrum. Other

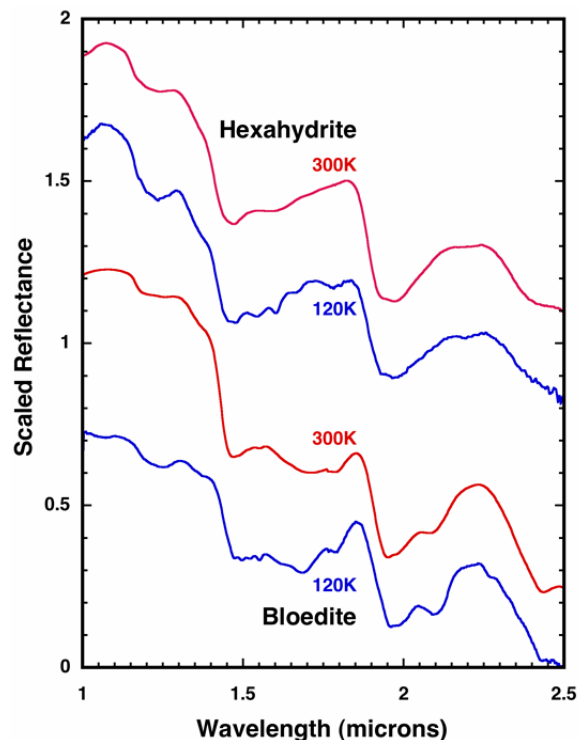


Figure C.1.2-2. Reflectance spectra of two hydrated salts at room temperature and at 120 K, as expected at the surface of Europa. The fine spectral structure apparent at high (~ 5 nm) spectral resolution could be exploited to discriminate between hydrates. From Dalton et al. (2003).

spectral features arising from the presence of water occur in many of the spectra, including features of moderate strength near 1.65, 1.8, and 2.2 μm (Figure C.1.2-3). An additional absorption common to the hydrates at 1.35 μm arises from the combination of low-frequency lattice modes with the asymmetric O-H stretching mode (Hunt et al. 1971a, b; Crowley 1991; Dalton and Clark 1999). Although weak, this feature is usually present in hydrates and has been used to place upper limits on abundances of hydrates in prior studies (Dalton and Clark 1999, Dalton 2000, Dalton et al. 2003).

Cassini VIMS observations of Phoebe provide additional examples of the wealth of information available in infrared spectra. Clark et al. (2005) reported 27 individual spectral features, indicating a complex surface containing a rich array of ices including H_2O and CO_2 ,

and organic species including CN-bearing ices. The 3- to 5- μm portion of the Phoebe spectrum includes absorptions tentatively interpreted as nitrile and hydrocarbon compounds. This spectral range is useful for detecting numerous organic and inorganic species anticipated at Europa (Figures C.1.2-3 and C.1.2-4).

Unexpectedly, the diagnostic spectral features of hydrated minerals are not seen in high-spectral-resolution 1.45- to 1.75- μm Keck telescopic spectra collected from regions of dark terrain on Europa that are several hundred kilometers in extent, suggesting that hydrated

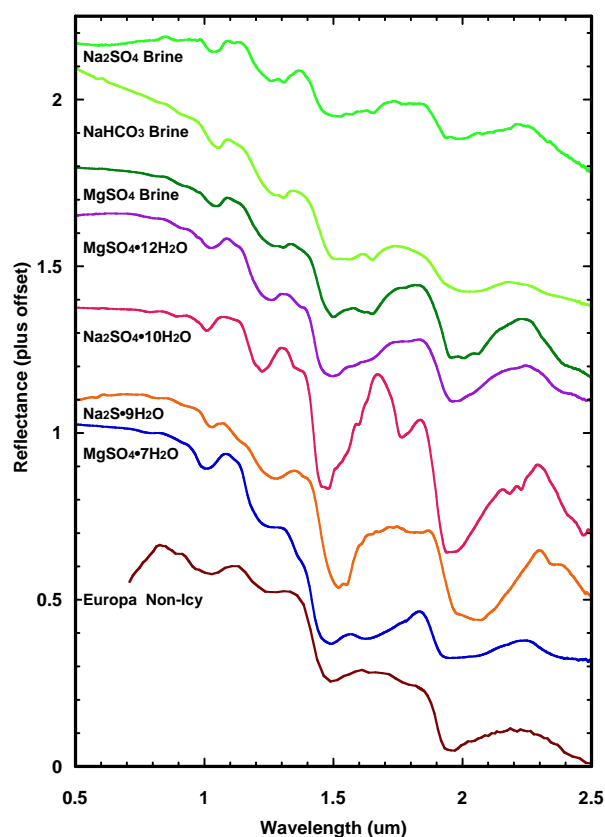


Figure C.1.2-3. Cryogenic reflectance spectra of hydrated sulfates and brines, compared to Europa. Spectra of epsomite ($\text{MgSO}_4 \cdot 7\text{H}_2\text{O}$), hexahydrate ($\text{MgSO}_4 \cdot 6\text{H}_2\text{O}$) and bloedite ($\text{Na}_2\text{Mg}(\text{SO}_4)_2 \cdot 4\text{H}_2\text{O}$) were measured at 100, 120, and 120 K, respectively (Dalton 2000, 2003). Spectra of sodium sulfide nonahydrate ($\text{Na}_2\text{S} \cdot 9\text{H}_2\text{O}$); mirabilite ($\text{Na}_2\text{SO}_4 \cdot 10\text{H}_2\text{O}$); magnesium sulfate dodecahydrate ($\text{MgSO}_4 \cdot 12\text{H}_2\text{O}$); and MgSO_4 , NaHCO_3 , and Na_2SO_4 brines were measured at 100 K (Dalton et al. 2005).

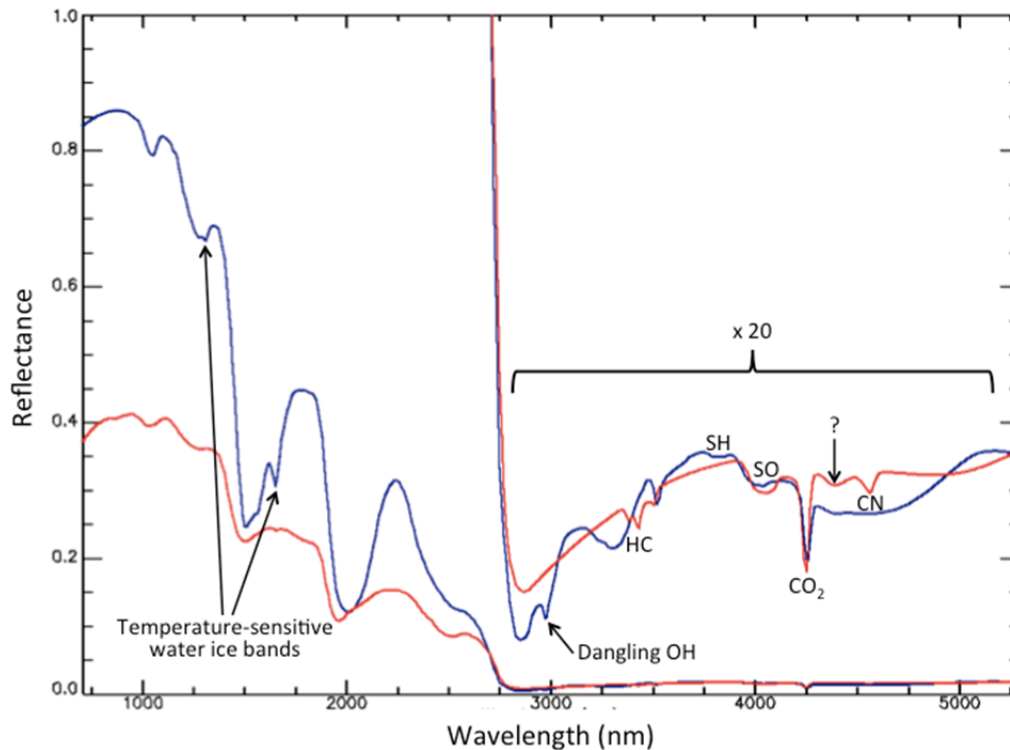


Figure C.1.2-4. Notional reflectance spectra for ice-rich regions (blue curves) and ice-poor regions (red curves) on Europa (based on observations of compounds observed on other Jovian and Saturnian satellites) at 10 nm spectral resolution in the 1–5 μm (1000–5000 nm) spectral range. A variety of materials and molecules have been identified or inferred from the Galileo results. The spectra shown here are composites to illustrate the types and variety of features found or expected. The detailed spectral structure observed in hydrates at high spectral resolution (e.g., Figure C.1.2-2, Figure C.1.2-3) is not fully represented here. The 2.8–5 μm range spectra are scaled by 20 compared to the shorter-wavelength range. Figure courtesy Diana Blaney.

materials might be noncrystalline (glassy) because of radiation damage or flash-freezing (Spencer et al. 2006)

Although these regions of Europa are dominated by dark materials, ice-rich materials probably occur within the observed area, and significant spatial mixing and dilution of the spectra of the optically active species might occur. It is also possible that the various hydrated species are mixed in such proportions that their diagnostic features overlap. It is expected that there would be smaller regions (perhaps the youngest ones) on Europa in which diagnostic spectral features could be found if observed at higher spatial resolution. An excellent example of the importance of spatial resolution is observed for Martian dark-region spectra, in which telescopic spectra in

both the thermal and short-wave infrared (e.g., Bell 1992, Moersch et al. 1997) did not reveal the mineralogical components until high-spatial-resolution spectra were acquired from orbit (e.g., Christensen et al. 2001, Bibring et al. 2005, Ehlmann et al. 2008, Mustard et al. 2008).

Laboratory studies have shown that at Europa's surface temperature, anticipated materials—in particular hydrates—exhibit fine structure, with the full width at half maximum (FWHM) of spectral features ranging from 7 to 50 μm (Carlson et al. 1999b, 2005; Dalton 2000; Dalton et al. 2003; Orlando et al. 2005). Analysis shows that to detect materials in relatively low abundance, or in mixtures with dark materials, signal-to-noise ratio (S/N) > 128 is desirable in the wavelength range 0.85 to 2.6

μm , and $S/N > 32$ is desirable in the wavelength range 2.6 to 5.0 μm (Figure C.1.2-5). An ideal spectral resolution of 2 nm per channel would be sufficient to identify all features observed in laboratory hydrates thus far (Dalton et al. 2003, Dalton et al. 2005). This would ensure multiple channels across each known feature of interest. However, at Jupiter's distance from the Sun, the reflected near-infrared radiance limits the achievable spectral resolution for high-spatial-resolution mapping. The S/N performance is further complicated by the severe radiation noise effects at Europa's orbit.

The spatial resolution required for compositional mapping is determined by the scale of critical landforms such as bands, lenticulae, chaos, and craters. Europa displays albedo and morphological heterogeneity at scales of ~ 100 m, suggesting that compositional variations also exist at this scale. However, the composition of these features remains unknown because Galileo NIMS observations are averages of light reflected from large areas containing both icy and "non-icy" terrain units (e.g., McCord et al. 1999, Fanale et al. 1999). Spectra of adjacent regions within an instru-

ment field of view combine to produce an average spectrum, with spectral features from all the materials. However, these composite spectra have potential overlap of spectral features and reduced spectral contrast relative to the spectra of the individual surface units. Because spectral mixing and reduced contrast will decrease detectability, it is desirable to resolve regions of uniform composition in order to map distinct surface units. While these in turn might be mixtures, spatially resolving dark terrains that have fewer components and are free of the strong and complex absorption features of water-ice would greatly facilitate identification of the non-ice materials. For reasonable statistical sampling, it is also desirable to have multiple pixels within a given surface unit. Adjacent measurements could then be compared with each other and averaged together to improve the signal and reduce noise.

Galileo images of Europa suggest geologically recent formation ages for ridges, chaos, and other features. The images also show abundant evidence for much younger materials exposed by mass wasting of faces and scarps (Sullivan

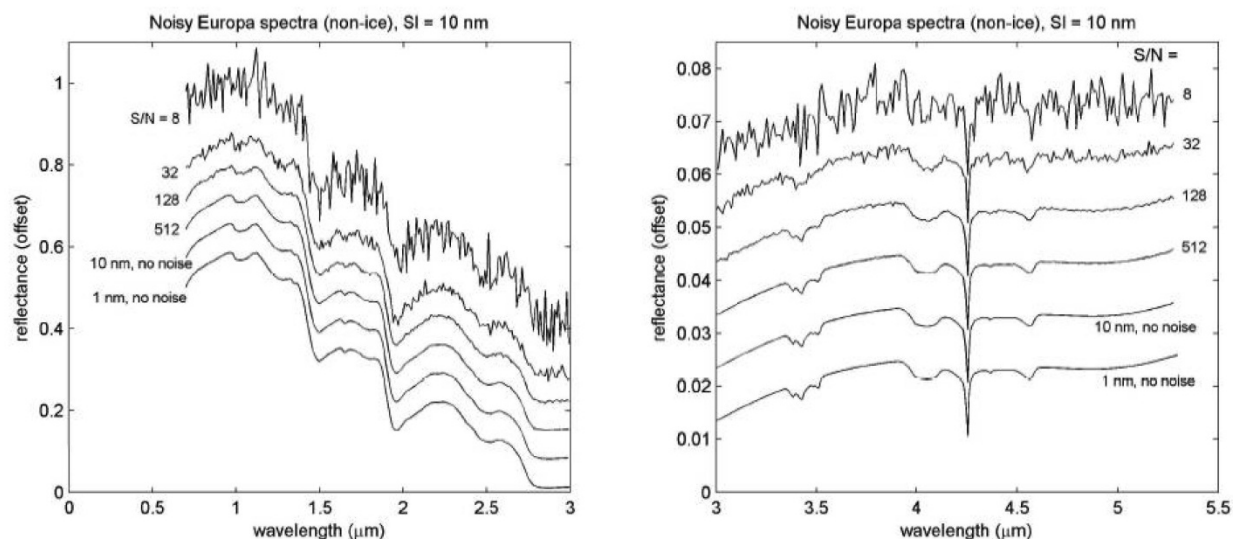


Figure C.1.2-5. Infrared reflectance spectra for a range of signal-to-noise ratios (S/N s) show that to detect absorption bands of materials in relatively low abundance, or in mixtures with dark materials, $S/N > 128$ is desirable in the shorter-wavelength range 0.85–2.6 μm , and $S/N > 32$ is desirable in the longer-wavelength range 2.6–5.0 μm (Tom McCord, personal communication). The model payload's Shortwave Infrared Spectrometer would achieve $S/N \sim 18$ with 1 row of target 100 at 5 μm (TMC 8), 18 at 5 μm (TMC 1).

et al. 1999). These postformational modification processes have likely affected many surfaces, potentially exposing fresh materials that are less altered than their surroundings. Spectroscopy at a resolution better than 300 m would isolate these surfaces and provide an opportunity to determine the composition of primary materials. Additional important compositional information could come from an Ion and Neutral Mass Spectrometer (INMS), which could measure sputtered materials. Integration of results from spectroscopic analysis and *in situ* INMS measurements would be key to identifying the non-ice materials on Europa's surface.

In summary, the multiple spectral features and fine (10 to 50 nm) structure of materials of interest in the 1 to ≥ 5 μm range in low-temperature spectra are sufficiently unique to allow these materials to be identified even in mixtures of only 5 to 10 weight percent (Dalton 2007, Hand 2007). The ability to fully resolve these features through high-spectral, high-spatial resolution observations would permit determination of the relative abundances of astrobiologically relevant materials on the surface of Europa.

Atmospheric Composition through Ion and Neutral Mass Spectrometry

Europa's composition is expressed in its sputtered atmosphere, with ties to the subsurface ocean and habitability. An INMS would provide a sensitive means to measure ions and neutrals present in Europa's atmosphere that are derived from the surface by sputtering, outgassing, and sublimation, considerably aiding

identification of surface materials. Europa's tenuous atmosphere, first postulated in the 1970s, has four observed components: O (Hall et al. 1995, 1998) near the surface, Na and K in the region from ~ 3.5 to 50 R_E (Brown and Hill 1996, Brown 2001, Leblanc et al. 2002, Leblanc et al. 2005), and H_2 in Europa's co-orbiting gas torus (Smyth and Marconi 2006). Robust plasma bombardment of Europa's surface is expected to produce many other components (e.g., Johnson et al. 1998). To date there have been few measurements of the European atmosphere, so models must be relied upon to infer its vertical structure, and especially the abundances of species other than those already detected (O, Na, and K).

Major volatiles would be easily detectable using current INMS technology. Figure C.1.2-6 shows one such model of Europa's atmosphere (Smyth and Marconi 2006), with sensitivity of

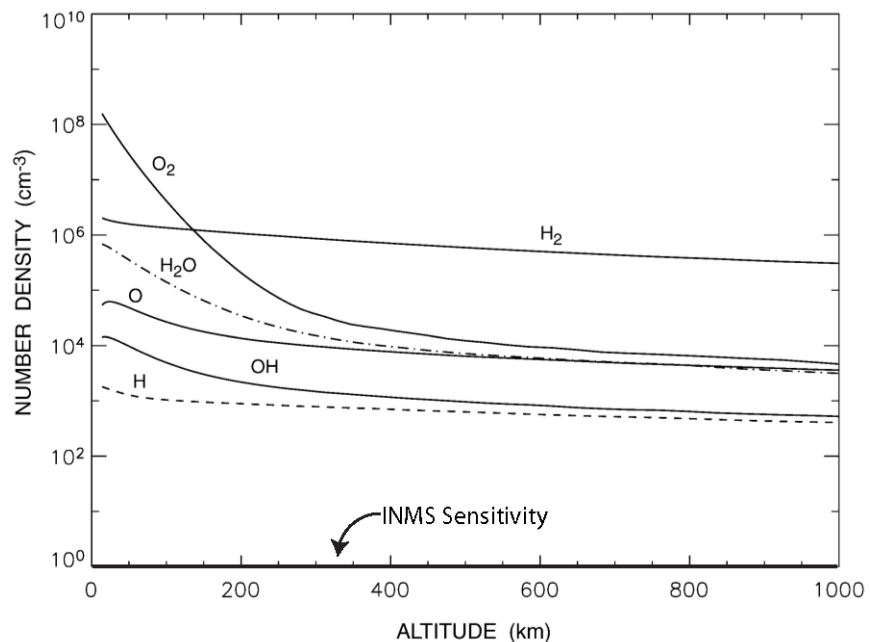


Figure C.1.2-6. Vertical distribution of the modeled abundance, globally averaged density of potential atmospheric components. The O_2 rate was set to reproduce the 135.6-nm O brightness of 37 ± 15 Rayleigh observation of Hall et al. (1995). Sublimation was taken into account but is unimportant except in the subsolar region. In both simulations, the ejecta energy distributions discussed in the text were used for H_2O and O_2 , and thermalization of returning H_2 and O_2 in the regolith is assumed. From Smyth and Marconi (2006).

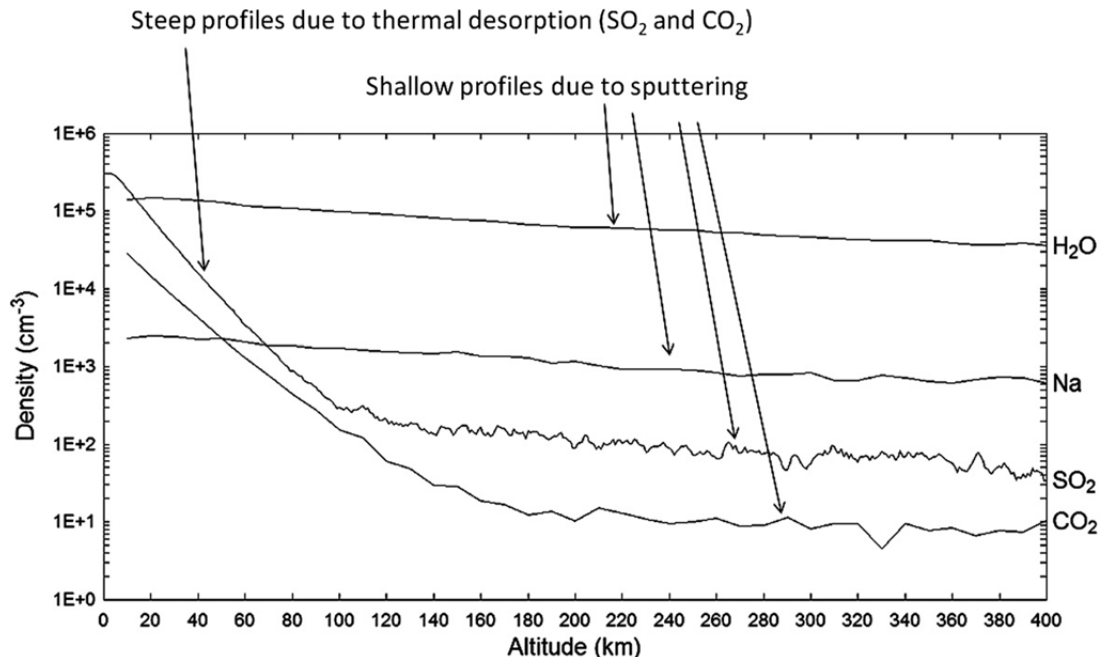


Figure C.1.2-7. Neutral density vs. altitude for selected species and cases. Shallow profiles decay much faster than $1/r^2$. At 100 km, a mass detection threshold of greater than 100 cm^{-3} is needed to characterize key volatiles. SO_2 and CO_2 abundances increase dramatically approaching the surface within about 150 km. From Cassidy et al (2009).

1 cm^{-3} for a model Flyby INMS superimposed.

Trace materials detected from surface spectroscopy (SO_2 , CO_2) should be readily detectable using INMS (Johnson et al. 2004). Further characterization of hydrate and associated dark materials could be accomplished for comparison to remote-sensing observations of the surface. For example, Mg should be present in the atmosphere if MgSO_4 , expected to dominate Europa's ocean composition, is present at the surface. Atmospheric emission measurements for Na and K have confirmed a surface source (Johnson et al. 2002, LeBlanc et al. 2002), with some evidence that the Na and K originate specifically from dark regions (LeBlanc et al. 2005, Cassidy et al. 2008). However, these have not yet been detected in surface spectral measurements.

Vented material or materials from flows that are emplaced on the surface are rapidly degraded by the incident radiation. This degradation process also produces sputtered products that could be detected and interpreted. Figure C.1.2-7 shows how sputtered atmospheric

density is predicted to rapidly increase approaching Europa's surface. The composition of Europa's atmospheric CO_2 , as shown in Table C.1.2-2, from Cassidy et al. (2009) sets the model INMS detection threshold of 1 cm^{-3} . From 100 km approach distance SO_2 , Na, and H_2O would be far above the model INMS performance of 1 cm^{-3} .

Ionospheric model results, shown in Figure C.1.2-8, are expected to be within INMS detection limits, indicated by the black line. From this analysis it is apparent that an INMS could detect vapor from an active vent, sublimation from a warm region, sputter products during the degradation process, and ions that are in all of these processes.

Another important contribution from an INMS, although not a scientific priority for the

Table C.1.2-2. Calculated global-average densities of sputtered Europa surface materials at 100 km.

Species	Predicted Densities @ 100 km
Na	60–1600 cm^{-3}
CO_2	36–193 cm^{-3}
SO_2	110–600 cm^{-3}

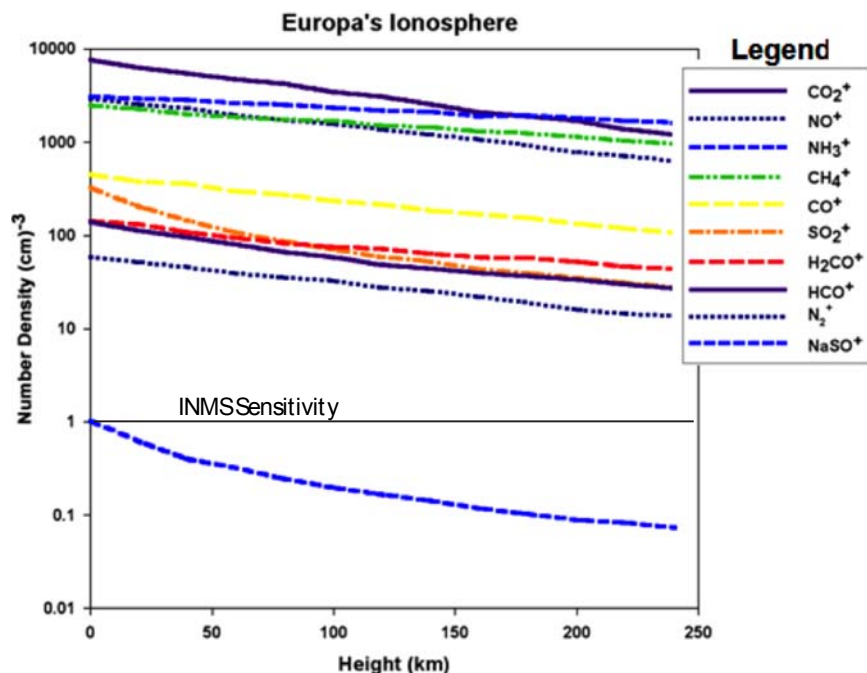


Figure C.1.2-8. Ionosphere densities vs. altitude, determined as discussed in Johnson et al. (1998) for molecules sputtered from the Europa's surface based on suggested surface materials. All densities, except those of NaSO^+ exceed the detection limit (1 cm^{-3} ; Y-axis) of the model Ion and Neutral Mass Spectrometer.

current mission, would be the ability to measure isotopic ratios. Variations in the $^{17}\text{O}/^{16}\text{O}$ and $^{18}\text{O}/^{16}\text{O}$ ratios in water vapor are the most useful system for distinguishing different planetary materials (Table C.1.2-3).

For example, it has been argued that two gaseous reservoirs, one terrestrial and one ^{16}O rich, are required to explain O-isotopic variations in meteorites. The terrestrial fractionation line is due to mass fractionation of the O isotopes in terrestrial materials, and the carbonaceous chondrite fractionation line represents mixing between different components. Obtaining similar isotope information for Europa would provide important constraints on the origin of water ice in the Galilean satellites. Based on other observations in the solar system, rare isotopes of oxygen are $\sim 10^4$ less abundant than their more common counterparts, which is still within the model instrument sensitivity of 1 cm^{-3} .

Trace organics would also be sputtered with the ice from the surface. Based on estimates by Cassidy et al. (2009) shown in Figure C.1.2-9, these would be detectable if sputtered from materials concentrated by geological processes at the surface, such as concentration and subsequent segregation of brine and organics (e.g., Schmidt et al. 2011).

C.1.2.2.1 Investigation C.1: Characterize the composition and chemistry of the Europa ocean as expressed on the surface and in the atmosphere.

The first-priority investigation for Europa's surface composition and chemistry is to identify the surface organic and inorganic constituents, with emphasis on materials relevant to Europa's habitability, and to map their distribution and association with geologic features. The search for organic materials, including compounds with CH, CO, CC, and CN, is especially relevant to understanding Europa's potential habitability. Moreover, identifying specific salts and/or acids might constrain the composition, physical environment, and origin of Europa's ocean (Kargel et al. 2000, McKinnon and Zolensky 2003, Zolotov and Kargel 2009). Additional compounds of interest include species that could be detected at UV wavelengths, such as

Table C.1.2-3. Water vapor components, including isotopes, in Europa's atmosphere expected to be measurable by an INMS (from Cassidy et al. 2009).

Species	Mass	Expected density (cm^{-3}) at 100 km
H ₂	2.01	10–6
O ₂	31.99	4×10^6 to 10^7
O	15.9	3×10^4 to 10^5
H ₂ O	18.0	10^4 to 2×10^5
OH	17.0	100 to 9×10^4

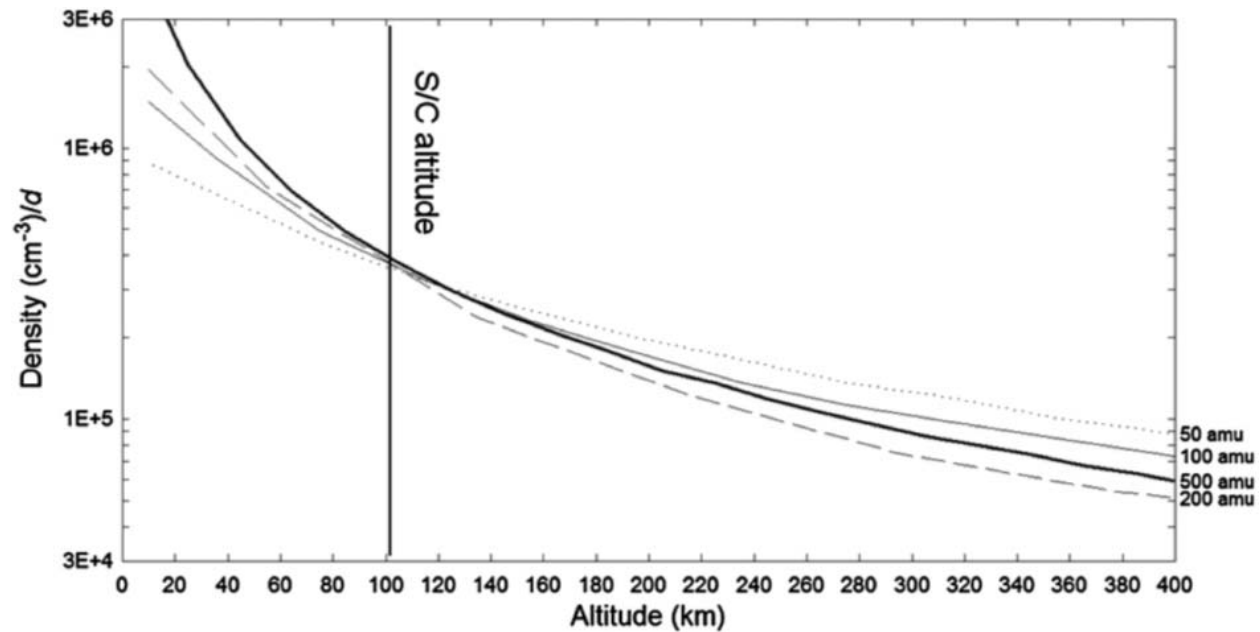


Figure C.1.2-9. Density vs. altitude for refractory molecules of different masses. The density of a given atmospheric species with a number fraction d in the surface is given by multiplying the plotted density by the number fraction, allowing estimates of minimum detectable surface concentration at the spacecraft (S/C) altitude. The different species happen to have similar densities at 100 km. From Cassidy et al. (2009).

water ice (crystalline and amorphous phases), products of irradiation (e.g., H_2O_2), compounds formed by implantation of sulfur and other ions, and other as yet unknown materials.

A spectral sampling of ~ 10 nm through the visible and near-IR wavelengths of 0.85 to ~ 2.5 μm and of ~ 20 nm from ~ 2.5 to ≥ 5 μm would provide the required S/N while maximizing spectral separability (Figures C.1.2-2, C.1.2-3, and C.1.2-4) (Dalton et al. 2003, Dalton 2007). Global observations (10 km/pixel) would be augmented with high-resolution observations having better than 300-m/pixel spatial resolution in order to resolve small geologic features, map compositional variations, and search for locations with distinctive compositions. High spectral resolution, coupled with high spatial resolution that could permit sampling of distinct compositional units at 100-m scales, would allow identification and quantification of the contributions of hydrated salts, sulfuric acid, sulfur polymers, CO_2 , organics,

and other compounds anticipated at the surface of Europa.

INMS observations would be performed to determine the composition of sputtered products. Such measurements should be made at a mass range better than 300 daltons, with a mass resolution ($m/\Delta m$) of greater than 500, and with sensitivity better than 10 particles/ cm^3 . Low-altitude measurements (< 100 km) are highly desirable in sampling denser portions of Europa's atmosphere.

C.1.2.2.2 Investigation C.2: Determine the role of Jupiter's radiation environment in processing materials on Europa.

In order to understand the surface composition, it is important to determine separately the effects of weathering by photons, neutral and charged particles, and micrometeoroids. In particular, radiolytic processes might alter the chemical signature over time, complicating efforts to understand the original composition of the surface. Assessing these relationships requires a detailed sampling of the surface with infrared spectroscopy, using global and

targeted observations. Efforts to separate the primary and alteration surface composition would be aided by the acquisition of high-spatial-resolution spectra on both leading and trailing hemispheres, in which younger, less altered materials might be exposed by magmatic, tectonic, or mass-wasting processes.

In addition, an INMS would provide a highly sensitive means to directly measure species sputtered off the surface, which might include organic fragments. A nonuniform atmosphere is anticipated, and its structure could be examined with INMS measurements.

C.1.2.2.3 *Investigation C.3: Characterize the chemical and compositional pathways in Europa's Ocean.*

In order to relate composition to geological processes, especially material exchange with the interior, composition interpretations need to be considered in the context of geophysical and morphological measurements. The suite of observation types discussed above provides a means to understand the three-dimensional structure of the near-surface crust and its relation to surface material units and processes of exchange between the interior and the surface. Specifically, compositional maps should be compared to detections of subsurface dielectric horizons obtained using Ice-Penetrating Radar, and to morphology and topography derived from stereo imaging. In addition, understanding tectonic and volcanic processes as manifested in structures and outcrops and their relation to surface materials will lead to a greater understanding of interactions between the ocean and the surface.

The key outstanding questions relating to Eu-

ropa composition can be addressed by the Objective C investigations described above, as summarized in Table C.1.2-4.

C.1.2.3 **Europa's Geology**

Europa's landforms are enigmatic, and a wide variety of hypotheses have been offered for their formation. Characterization of sites of most recent geological activity is especially significant for understanding the formation of surface features, including whether and how liquid water is involved in their formation. Moreover, the formation processes of surface landforms is important to how material is transported between the surface and the subsurface, and thus to whether and how surface oxidants could be transported to the ocean, providing chemical energy for life. In these ways, geology is directly pertinent to the potential habitability of Europa.

C.1.2.3.1 *Investigation G.1: Determine sites of most recent geological activity, and characterize localities of high science interest.*

Europa's incessant tidal activity leads to speculation that some landforms might be actively forming today and are the most likely locations for near-surface liquid (see Section C.1.2.1). The most promising regions for current activity are regions of chaos in which thermally or compositionally buoyant diapirs rise to the surface, or cracks that have recently formed in response to tidal stresses. Low-albedo smooth plains associated with some chaotic terrains might be composed of subsurface materials, such as brines, that have been emplaced onto the surface (Collins and Nimmo 2009, Schmidt et al. 2011). These

Table C.1.2-4. Hypothesis tests to address selected key questions regarding Europa's composition.

	Example Hypothesis Questions	Example Hypothesis Tests
C.1	Are there endogenic organic materials on Europa's surface?	Examine surface and sputtered materials for absorptions and masses consistent with organic materials, and correlate distributions to likely endogenic materials.
C.2	Is irradiation the principal cause of alteration of Europa's surface materials through time?	Determine the suite of compounds observable on Europa's surface, correlating to the local radiation environment and to the relative age of associated surface features.
C.3	Is chemical material from depth carried to the surface?	Determine whether hydrates and other minerals that might be indicative of a subsurface ocean are concentrated in specific geologic features, and correlate with evidence for subsurface liquid water at these locations.

plains might therefore represent sites of high scientific interest. Recently or currently active regions are expected to best illustrate the processes involved in the formation of some surface structures, showing pristine morphologies and distinct geologic relationships, and perhaps exhibiting associated plume activity such as that seen on Enceladus.

Determining the relative ages of Europa's surface features allows the evolution of the surface to be unraveled. Indication of relative age comes from the stratigraphy, derived from crosscutting and embayment relationships, and the relative density of small impact craters. These relationships enable a history to be assembled within local regions, for global extrapolation.

Of primary importance is the detailed characterization of surface features—especially their distribution, morphologies, and topography—at local to regional scales, to understand the processes by which they formed. Galileo images demonstrate that high-resolution data of a few tens of pixels is excellent for investigating the detailed formation and evolution of surface features such as bands, ridges, chaos, and impact features. Yet less than 0.05% of the surface was imaged at scales of 50 m/pixel or better, leading to only tantalizing and ambiguous glimpses of how these features formed (e.g., Figure C.1.2-2). Stereo imaging of the surface was extremely scarce, but the topographic models derived from it have contributed greatly to understanding how Europa's surface features formed. For example, digital terrain models (DTMs) of chaos regions suggest that these regions form from diapiric upwelling of material from below (e.g., Schenk and Pappalardo 2004, Prockter and Schenk 2005, Collins and Nimmo 2009), aided by brines in the subsurface (Schmidt et al. 2011). High-resolution Galileo images of Europa (Figure C.1.2-10) show abundant evidence for very young materials exposed by mass wasting of faces and scarps (Sullivan et al. 1999).

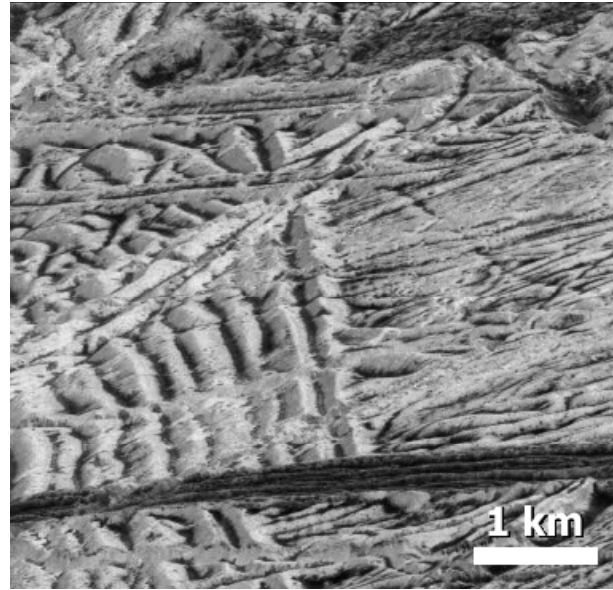


Figure C.1.2-10. Galileo Solid-State Imager image of ridged plains on Europa at 6 m/pixel horizontal resolution. The lineae in the central portion of the image have central troughs with deposits of dark material ~100 m wide, but with bright, presumably icy ridges and walls close by.

These postformational modification processes have likely affected many surfaces, potentially exposing fresh materials that are less altered than their surroundings. Topographical imaging of different feature types at several locations distributed across Europa's surface would allow detailed characterization of sites of high scientific interest, and would enable evaluation of sites of expected current or recent activity. Topographical mapping through stereo images acquired at regional scales can permit construction of digital elevation models with vertical resolution of ~10 m and horizontal resolution of 50 m, which would greatly aid morphologic characterization and geological interpretation of all known feature types on Europa. Images that are correlated with subsurface sounding measurements would allow the subsurface structure of geological landforms to be related to their surface expression, and the third dimension of these features to be fully characterized for the first time. Models of topography will also aid in the interpretation of compositional data.

Table C.1.2-5. Hypothesis test to address selected key questions regarding Europa's geology.

	Example Hypothesis Question	Example Hypothesis Test
G.1	Where are the youngest regions on Europa and how old are they?	Use stereo imaging and sputter measurements to determine the freshest, uncompensated surfaces, and potential locations of plumes.

The key outstanding questions relating to Europa geology (Table C.1.2-5) can be addressed by the Objective G investigation described above, as summarized in FO C-1.

C.1.3 Science Instrument Complement

The Europa Multiple-Flyby Mission focuses on measurements that can be taken over multiple flybys.

C.1.3.1 Mission Goal Relation to Core Measurements and Instrumentation

The overarching goal of the flyby mission would be to determine the habitability of Europa. As such, the recommended scientific measurements and scientific payload follow objectives (Section C.1.1) of characterizing the ice shell and any subsurface water (including the distribution of subsurface water and searching for an ice-ocean interface), understanding ocean habitability through composition and chemistry (as expressed on the surface and in the atmosphere), and addressing the surface geology (geological history and processes, including high science interest localities). In this way, the payload links tightly with the three science themes that relate to Water, Chemistry, and Energy. Particular to Europa, the presence of a subsurface ocean, the overall structure and thickness of the ice shell and the exchange of material between the subsurface (ice shell and ocean) and the surface layer over time, followed by the physical evolution of the surface, leads to a complex story of Europa habitability. Unraveling this story requires an integrated package of instruments that work ideally and effectively in coordination. The Flyby Mission offers unique abilities to observe the surface and address the goal of understanding Europa's habitability.

The recommended science measurements and payload utilize the strengths of each archetypal

instrument and technique to address key questions:

- Where is there subsurface water within Europa, and what are the mechanisms of surface-ice ocean exchange?
- What does surface composition and chemistry imply about the habitability of Europa's ocean?
- How do Europa's surface features form, and what are the characteristics of sites of recent or current activity?

C.1.3.2 Integration of Instrument Categories

Coordination and integration of observations and measurements acquired by different instruments is central to determining Europa's habitability. Spatially or temporally coordinated observations greatly enhance the scientific value of the mission. For example, obtaining clear insight into processes of material exchange at Europa requires various types of measurements working in concert. Understanding composition benefits from measuring chemical clues from both the surface and atmosphere. We can learn the most about the potentially active surface regions through complementary imaging and atmospheric analyses. In this way the suite of instruments integrates to address the broader questions of habitability in a way that cannot be accomplished by any instrument alone.

C.1.3.3 Instrument Payload

The choice of instruments for the scientific payload is driven by the need for specific types of measurements that trace from the overarching goal of Europa's habitability, as detailed in the Europa Multiple-Flyby Mission traceability matrix (FO C-1). These measurements are designed to focus on characterization of the Chemistry and Energy themes for Europa, but they also do an excellent job in addressing Water within Europa. These fundamental

Table C.1.3-1. Baseline and floor scientific instruments of the model payload. INMS (shaded) is additional to floor.

Model Instrument	Key Science Investigations and Measurements
Ice-Penetrating Radar (IPR)	Sounding of subsurface dielectric horizons to probe for water.
Shortwave Infrared Spectrometer (SWIRS)	Surface composition and chemistry through reflection spectroscopy.
Topographical Imager (TI)	Landform characterization and stereo topography.
Ion and Neutral Mass Spectrometer (INMS)	Atmospheric composition and chemistry through mass spectrometry.

measurements drive the recommendation of model instruments. These concentrate on remote sensing (Ice-Penetrating Radar, infrared spectroscopy, and high-resolution stereo imaging) along with in situ measurement of the atmospheric composition (by means of an ion and neutral mass spectrometer).

The baseline model payload of instruments is divided into three principal categories, as summarized in Table C.1.3-1. The first category, defining the science floor (unshaded in Table C.1.3-1), consists of those instruments fundamental to the mission objectives, without which the mission is not worth flying. The second category consists of a single additional scientific instrument which would greatly contribute to the scientific return of the mission, and thus is included in the baseline model payload, but which is not considered part of the floor payload: it could be descoped from the model payload if not accommodatable (shaded in Table C.1.3-1).

These model instruments work in concert to fully realize the value of data collected. For example, The Ice-Penetrating Radar (IPR) would be used to sound dielectric horizons within Europa's ice shell to search for liquid water. Simultaneously, the Topographical Imager (TI) would obtain stereo images that put the IPR observations into geological context and which provide topographic information necessary to process the IPR data. The Shortwave Infrared Spectrometer (SWIRS) and Ion and Neutral Mass Spectrometer (INMS) would work together in complemen-

tary ways to determine composition and chemistry through surface (SWIRS) and atmospheric (INMS) measurements. The Topographical Imager (TI) could be used to identify areas that are geologically young or active through stratigraphic relationships and by searching for surface changes, while the INMS could be used to search for unusual density and composition of the atmospheric components that might indicate currently active plumes. The combined investigations achievable from a Flyby Mission would fundamentally advance the state of knowledge and understanding of the habitability of Europa.

C.1.3.4 Potential Europa Ocean Science from a Flyby Mission

Three additional instruments were considered by the SDT as potentially attractive to enhance the scientific return of a Europa Multiple-Flyby Mission by addressing ocean science (Table C.1.3-2). However, these were not included in the baseline model payload because the Orbiter Mission would be the more appropriate platform for the associated measurements. If a Flyby Mission were chosen for Europa, then these valuable instruments might be considered in developing the optimal payload for a Flyby mission, to address a portion of the ocean science.

The science of the Europa Orbiter Mission concept (Section B) includes investigation of the deep interior structure of Europa by examining changes in the gravitational and magnetic fields of Europa, which are induced by rotational and orbital motions of Europa about Ju-

Table C.1.3-2. Potential enhanced instruments, not included in baseline model payload.

Model Instrument	Key Science Investigations and Measurements
Radio Subsystem (RS)	Gravitational tides and static gravity field to detect an interior ocean.
Magnetometer (MAG)	Magnetic measurements to derive ocean thickness and bulk salinity.
Langmuir Probe (LP)	Plasma correction for magnetic measurements.

piter. In both cases, the imposed fields (gravitational or magnetic) are well known, and the phase and amplitude of the response are diagnostic of Europa's internal structure. In the Orbiter Mission design, the spacecraft would be in a (nearly) circular and (nearly) polar orbit, and would make essentially continuous measurements of the magnetic and gravitational fields. In both cases, it is anticipated that these fields have static and time-dependent components. The primary interest here is in the time-dependent parts of the fields, as they are more diagnostic of deep interior structure. As an orbiting spacecraft moves through a gravitational or magnetic field of a body like Europa, the signal at the spacecraft will have time variations, even if the body-fixed field is constant. Separating the static and temporally varying components of the fields requires sufficient spatial and temporal coverage for the measurements, to recover a reasonably high fidelity spherical harmonic model.

Conducting similar investigations from the Flyby Mission can be done, but it places constraints on the encounter geometry. First we consider the gravitational investigation. The principal cause of time variations in the gravitational field is that Europa moving around Jupiter in a slightly eccentric orbit. As a result, the gravitational field of Jupiter, at the position of Europa, varies with orbital position. The deformation of Europa by the imposed tidal potential from Jupiter produces an additional gravitation potential with the same spatio-temporal pattern as the imposed field. The scaling factor, which relates the induced field to the imposed field, is known as the tidal Love number. It is large for a fluid body and small for an elastic solid. The desire is to determine the tidal Love number accurately enough to test the hypothesis of a global internal ocean, through precise measurements of the Doppler shift of the spacecraft's Radio Subsystem.

In order to measure the tidal changes in Europa's gravitational field, the flyby encounter

geometry needs to allow one or more locations on Europa to be visited repeatedly, at different phases of Europa's motion around Jupiter. That is largely because the tidal-induced changes in gravity are small compared to the static gravity field spatial variations. A recent analysis (Park et al. 2011) has shown that an orbit tour with three dozen Europa encounters can yield uncertainties in the degree-2 tidal Love number of 0.045 for X-band radio tracking data, and 0.009 for Ka-band. The latter value is sufficient to infer the presence of an ocean. The implication for a Europa Multiple-Flyby Mission, to meet this level of performance would be: use of Ka-band tracking, and having a steerable antenna, so that Doppler tracking can be performed during times of Europa close approach.

The magnetic induction experiment aims to characterize the salinity and thickness of Europa's ocean by measuring the induction signature of Europa at multiple frequencies. Similar to the tidal gravity experiment, determining magnetic induction requires repeat measurements at the same location on Europa, at different times in Europa's orbit around Jupiter. The magnitude and phase of the induced magnetic field are related to those of the imposed field, and the relationship between them is a measure of electrical conductivity variations within the interior. A salty water ocean would have a very different conductivity than ice or silicate rock (Khurana et al. 1998).

A major difference between the gravity and magnetic induction experiments is that the magnetometer measures the vector field, whereas the Doppler shift in gravity tracking data only delivers the projection of the spacecraft velocity onto the line-of-sight to Earth. Another difference is that the magnetic field at Europa has a more complex temporal variation. There is an effect due to Europa's orbital motion around Jupiter (85.2 hour period) and another due to Jupiter's rotation (11.2 hour period), among others. A partially compensating difference from tidal gravity is that any

permanent magnetic dipole field of Europa is expected to be small compared to the time-varying induced field, so there is not magnetic requirement on sampling the same location at different phases of the forcing periods.

We have not performed detailed simulations of magnetic induction experiments at Europa from a flyby geometry, but it seems that similarity in measurement requirements to the tidal gravity investigation suggests that it could potentially be done. The implications for the mission would be to carry a magnetometer deployed on a boom, to include a Langmuir probe or plasma instrument to permit corrections of plasma effects, and to reasonably control magnetic cleanliness of the spacecraft.

The ability to resolve tidal gravity and magnetic induction effects increase significantly with increasing number of flyby encounters. The actual increase in knowledge, per flyby, is a complicated function of the tempo and spatial pattern of encounters.

A currently unresolved challenge is how to accommodate the spatiotemporal sampling requirements of tidal gravity, magnetic induction, and the remote sensing investigations of the flyby spacecraft.

C.2 Multiple-Flyby Mission Concept

C.2.1 Mission Overview

The Multiple-Flyby Mission deploys a robust spacecraft with four science instruments into the Jovian system to perform repeated close flybys of Europa.

C.2.1.1 Flyby Study Scope and Driving Requirements

The purpose of the 2011 Europa Multiple-Flyby Mission study was to determine the existence of a feasible, cost effective, scientifically compelling mission concept. In order to be determined feasible, the mission had to have the following qualities:

- Accommodate the measurements and model payload elements delineated in the Science Traceability Matrix.

- Launch in the 2018-2024 timeframe w/ annual backup opportunities
- Use existing Atlas V 551 launch vehicle capability or smaller
- Utilize ASRGs (no limit on number, but strong desire to minimize ^{238}Pu usage)
- Mission Duration < 10 years, launch to EOM
- Use existing aerospace 300-krad radiation hardened parts
- Optimize design for cost (looking for the lowest cost possible while achieving baseline science)
- Maintain robust technical margins to support cost commitment

The study team's strategy in investigating this concept was to develop a well-defined, well-documented architecture description early in the mission life cycle. From that architecture space, lighter, more compact design solutions were favored to reduce shielding and overall system mass. Hardware procurement, implementation, and integration were simplified by using a modular design. Mission operation costs were reduced through best practice system robustness and fault tolerance capabilities to allow for extended periods of minimally monitored operations during the long interplanetary cruise and through repetitive operation for Europa science. Radiation dose at the part level was reduced to currently existing aerospace part tolerances. Specifically, the part total dose was reduced to levels demonstrated by geosynchronous and medium earth orbit satellites components.

These strategies, together, contribute to an overall reduction in mission cost while maintaining a compelling, high reliability mission.

C.2.1.2 Flyby Mission Concept Overview

The flyby mission concept centers around deploying a spacecraft into the Jovian system to perform repeated close flybys of the Jovian moon Europa to collect information on ice shell thickness, composition, and surface geo-

morphology. The science payload consists of four instruments: a Shortwave Infrared Spectrometer (SWIRS), an Ice-Penetrating Radar (IPR), a Topographical Imager (TI), and an Ion and Neutral Mass Spectrometer (INMS). Except for calibration and maintenance, these instruments are operated only during Europa flybys.

The nominal flyby mission performs 32 flybys of Europa at altitudes varying from 2700 km to 25 km. In the course of performing these flybys, the mission would also fly by the Jovian moons Ganymede and Callisto, although these flybys are solely to shape the orbit and are not driving science priorities.

The nominal Flyby mission launches from Cape Canaveral Air Force Station in November 2021 and spend 6.5 years traveling in solar orbit to Jupiter. During this time, the mission performs gravity assist flybys, first of Venus and then two of Earth, before swinging out to Jupiter. All terrestrial body flybys have a closest approach altitude greater than 500 km.

Jupiter orbit insertion would occur in April 2028 when the vehicle performs a nearly 2-hour main engine burn to impart a 900 m/s velocity change on the spacecraft. This maneuver places the spacecraft in an initial 200-day Jovian orbit. An additional burn at apoJove raises the periJove altitude. The spacecraft then performs four Ganymede flybys over the course of three months to reduce orbital energy and align the trajectory with Europa.

The Europa flyby campaign is comprised of four segments each designed to provide good coverage of a wide region on Europa with consistent lighting conditions. The first segment concentrates on the anti-Jovian hemisphere with seven flybys (Europa is tidally locked with Jupiter, so the side of the moon that faces toward or “sub-Jovian” and away or “anti-Jovian” never changes). Flyby closest approach altitudes range from 730 km to 25 km and cover latitudes from 80N to 80S.

During each flyby, a preset sequence of science observations would be executed. For any given flyby, the science team will have the opportunity to adjust some targeting and instrument performance parameters in advance, but the bulk of the sequence will execute unchanged for all Europa flybys. At approximately 60,000 km, the SWIRS instrument will begin a low-resolution global scan. This scanning is done via a “nodding” spacecraft pointing profile that is repeated for each encounter. At 2,000 km, the SWIRS instrument will switch to a targeted high-resolution scan mode. During these high-resolution scans the spacecraft is nadir-pointed. At 1,000 km the IPR, TI, and INMS power up, stabilize and perform calibration activities. The IP pass occurs from 400-km inbound altitude to 400-km outbound altitude during which TI and INMS data are acquired continuously. The spacecraft is nadir-pointed and the INMS is aligned near the ram direction. The SWIRS instrument, passive during the ± 400 km closest approach, then conducts additional high- and low-resolution scans as the spacecraft moves away from Europa.

The Europa flyby campaign continues through three more segments, the second also concentrating on the anti-Jovian side of Europa under different lighting conditions, and providing calibrating cross tracks for better interpretation of IPR data. The third and fourth segments concentrate on the sub-Jovian hemisphere providing comprehensive coverage of the other half of the moon.

Once the nominal mission has been completed, depending on consumable reserves and system reliability assessments, the flyby mission could continue to execute Europa flybys during an extended mission. However, the intent in this concept is to decommission the spacecraft via targeted Ganymede impact before consumable resources are fully depleted or system robustness has been compromised by radiation exposure.

C.2.1.3 Flyby Mission Elements

The flyby mission system would be composed of a flight system and a ground system. The ground system is responsible for planning, testing, transmitting, and monitoring all command sequences executed by the flight system, collecting and distributing the acquired science observation data, monitoring the flight systems health, and planning and executing any anomaly recovery activities required to maintain system health and mission robustness.

The flight system is composed of a modularly designed spacecraft with a vertical stack of three main modules: Avionics, Propulsion, and Power Source.

The Avionics Module hosts the bulk of the flight systems powered elements including the central computers, power conditioning and distribution electronics, radios, and mass memory. These units are housed in a vault structure that provides significant radiation shielding. The Upper Equipment Section (UES) of the Avionics Module hosts the batteries, reaction wheels, star-trackers as well as all of the science payload elements. Sensitive payload electronics are housed in a separate vault in the UES to increase flexibility during integration and test.

The Propulsion Module supports the fuel, oxidizer, and pressurant tanks, as well as the pressurant control assembly panel and the propellant isolation assembly panel. Four thruster clusters supported by tripod booms at the base of the Propulsion Module each contain four 1-lb reaction control system thrusters and one 20-lb thrust vector control thruster. The main engine is mounted to a baseplate suspended from the bottom of the Propulsion Module main structure.

The Power Source Module is composed of a ring and four vibration isolation systems, which each support an Advanced Stirling Radioisotope Generator (ASRG). The control units for the ASRGs are mounted directly to the Power Source Module's main ring struc-

ture. The launch vehicle adapter sits at the base of the Power Source Module's primary ring structure.

C.2.1.4 Flyby Mission Architecture Overview

Architecturally, the flight system's modular design offers several advantages and efficiencies. First, the Avionics Module is designed to place radiation sensitive components in a central vault structure. Centralization of sensitive components takes advantage of significant self-shielding benefits that are further enhanced by the vault structure. Late in the integration flow, the Avionics Module is stacked onto the Propulsion Module placing the avionics vault in the core of the spacecraft; surrounded on all sides by the Propulsion Module's structure and propellant tanks (the propellant itself does not provide significant additional shielding, since most of it expended during JOI and PJR). In this way, dedicated, single purpose radiation shielding mass is minimized while still providing an internal vault radiation environment comparable to the doses received by the electronics of geosynchronous satellites after a 20-year mission.

Additionally, the central vault avionics configuration allows waste avionics heat to be applied directly to warming the propellant. This configuration is so efficient that preliminary analysis indicates supplemental electrical heaters will not need to be used on the propellant tanks. There is sufficient heat collected from the avionics to keep the propellant above 15°C for the life of the mission.

Finally, the modular design allows for a flexible procurement, integration, and testing strategy, where each module is assembled and tested separately with schedule margin. Delays or problems on one module do not perturb the testing schedules of the other modules.

C.2.2 Model Payload

Proof of concept payload demonstrates feasibility of obtaining compelling science.

C.2.2.1 Payload

Instrument concepts and techniques that meet the mission objectives will be selected via NASA's Announcement of Opportunity (AO) process. Notional instruments and instrument capabilities presented within this report are not meant to prejudge AO solicitation outcome. Rather, this Europa Multiple-Flyby Mission model payload is used to deduce suitable engineering aspects of the mission and spacecraft design concept, including operational scenarios that could obtain the data necessary to meet the science objectives.

In addition, model payload instruments were defined well enough to demonstrate a plausible approach to meeting the measurement objectives, performing in the radiation environment, and meeting the planetary protection requirements. Therefore, instrument descriptions are provided here only to show proof of concept. Heritage or similarities discussed here refer only to instrument techniques and basic design approaches, and do not imply that specific implementations are fully viable in their detail. Physical and electrical modifications of any previous instrument designs would be necessary for them to function within the unique environmental context of this mission. Such

modifications are allowed for in the resource estimates. Instrument mass estimates assume performance only from currently available detectors.

The model payload selected for the Europa Multiple-Flyby Mission consists of a set of remote-sensing instruments and an *in situ* instrument. Instrument representatives on the Science Definition Team (SDT) (or identified by SDT members) were consulted extensively to understand the drivers for each notional instrument. Table C.2.2-1 presents the estimated resource demands of each instrument and for the total planning payload; Table C.2.2-2 summarizes the instruments and their capabilities. A more detailed mass estimate for each instrument is included in the Master Equipment List (MEL) (Section C.4.3) as input for the NASA Instrument Cost Model (NICM).

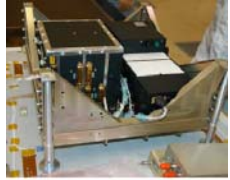
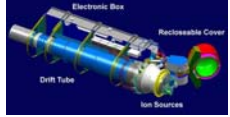
C.2.2.1.1 Payload Accommodation

All of the remote-sensing instruments in the model payload point in the nadir direction when flying by Europa, as shown in Figure C.2.2-1. Because the SDT analysis indicates that nominal nadir (or near-nadir) pointing of the remote-sensing instruments meets the science objectives, no spacecraft-provided scan platform is baselined. Individual instruments that need rapid scan systems for target tracking or target motion compensation are assumed to provide such a system as an inte-

Table C.2.2-1. Europa Multiple-Flyby Mission model payload resource characteristics.

Instrument	Acronym	Unshielded Mass (kg)	Shielding Mass (kg)	Total Mass (kg)	Operating Power (W)	Data Volume (Gb)/flyby	Telemetry Interface	Pointing
Ice-Penetrating Radar	IPR	28.0	5.0	33.0	55	25.2	SpaceWire	Nadir
Shortwave Infrared Spectrometer	SWIRS	11.6	9.1	20.7	19.1	1.3	SpaceWire	Nadir ± 45°
Ion and Neutral Mass Spectrometer	INMS	14.0	10.1	24.1	32.5	.002	SpaceWire	Ram
Topographical Imager	TI	2.5	4.5	7.0	5.9	3.1	SpaceWire	Nadir
TOTAL ALL INSTRUMENTS		56.1	28.7	84.8	112.5	29.6		
TOTAL ALL INSTRUMENTS + 30% contingency				110.2	146.3			

Table C.2.2-2. Europa Multiple-Flyby Mission model payload resource characteristics and accommodations.

Instrument	Characteristics	Similar Instruments		
Ice-Penetrating Radar (IPR)	Dual-Mode Radar Sounder Shallow Mode: 60 MHz with 10-MHz bandwidth Vertical Depth: ~3 km Vertical Resolution: 10 m Deep Mode: 9 MHz with 1-MHz bandwidth Vertical Depth: ~30 km Vertical Resolution: 100 m	Mars Express Mars Advanced Radar for Subsurface and Ionosphere Sounding (MARSIS) MRO Shallow Radar (SHARAD)	 	
Shortwave Infrared Spectrometer (SWIRS)	Pushbroom Spectrometer Detector: HgCdTe Spectral Range: 850 nm–5 μ m Spectral Resolution: 10 nm Spatial Resolution: 300 m @ 2000 km FOV: 4.2 deg cross-track IFOV: 150 μ rad	Chandrayaan Moon Mineralogy Mapper (M3)		
Ion and Neutral Mass Spectrometer (INMS)	Reflectron Time-of-Flight Mass Spectrometer Mass Range: 1 to 300 daltons Mass Resolution: >500 (m/ Δ m) Sensitivity: 10 particles/cm ³ FOV: 60 degrees	Rosetta Rosetta Orbiter Spec- trometer for Ion and Neutral Analysis (ROSINA) reflectron time-of-flight (RTOF) spectrometer Cassini Ion and Neutral Mass Spectrometer (INMS)	 	
Topographical Imager (TI)	Panchromatic Stereo Pushbroom Imager Detector: CMOS or CCD line arrays Detector size: 4096 pixels wide Spatial Resolution: 25 m from 100 km (@ C/A) FOV: 58 deg IFOV: 250 μ rad	MRO Mars Color Imager (MARI)	 MESSENGER Mercury Dual Imaging System (MDIS) New Horizons Multi- spectral Visible Imaging Camera (MVIC)	 

gral part of the instrument. Presently, for instance, one instrument in the model payload, the SWIRS, uses an along-track scan mirror in order to perform target motion compensation to increase the signal to noise. Slower scanning is accommodated by the spacecraft. For

instance, the spacecraft will perform slewing at long range from Europa in order for the SWIRS to perform global low-resolution mapping.

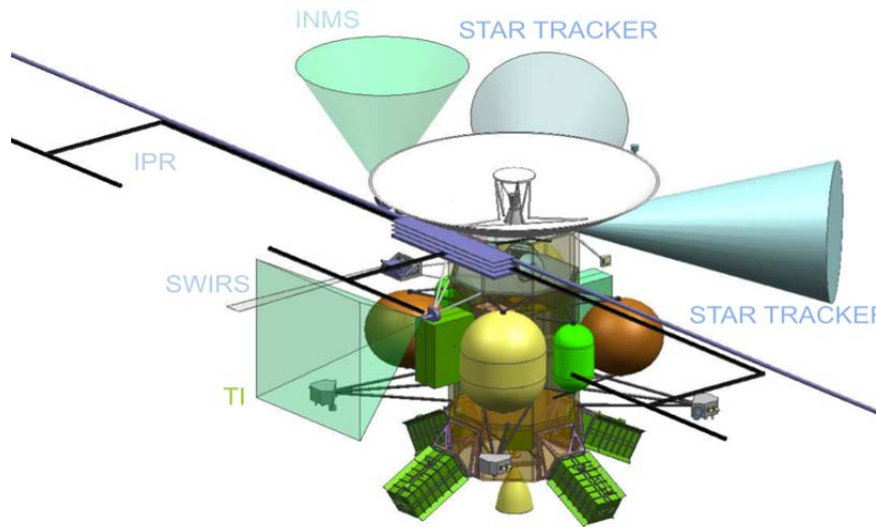


Figure C.2.2-1. Notional model payload accommodation and fields of view.

Adequate mounting area is available for the remote-sensing instruments on nadir-facing areas of the UES (see Figure C.2.2-1). Moreover, the Topographical Imager (TI) and SWIRS are mounted on brackets to ensure clear fields of regard for both instruments. The *in situ* instrument, the Ion and Neutral Mass Spectrometer (INMS), is pointing in the ram direction and is located next to the high-gain antenna (HGA). Note that the HGA is placed well clear of the INMS wide field of view. Instrument mounting and accommodation needs are summarized in Table C.2.2-1.

The science payload is expected to contain instruments with detectors requiring cooling to as low as 80 K for proper operation while dissipating perhaps 300 mW of heat. Cooling to this level would be accomplished via passive radiators, mounted so their view is directed away from the Sun and away from Europa to the extent necessary.

The remote-sensing instruments require spacecraft pointing control to better than or equal to 1 mrad, stability to 30 μ rad/s, and reconstruction to 0.15 mrad. Pointing performance is driven by SWIRS, which has a 150 μ rad pixel field of view and requires exposure times of up to 1 s, enabled by use of a scan mirror.

contingency. All of the instruments, other than IPR, perform data compression before sending the data to the SSR. IPR, with the highest instantaneous data rate, records raw data on the SSR, which is subsequently reduced before downlink. The notional model payload approach is to assume the data system architecture with SpaceWire interfaces baselined for all of the instruments.

The instrument electronics are currently baselined to be accommodated with each instrument, shielded separately. However, the spacecraft concept accommodates an additional science chassis that can house all of the payload electronics, as well as perform some of the data reduction for IPR. This approach results in a conservative mass estimate, adding further margin in radiation shielding. Further trades need to be conducted on the benefits of a separate science chassis and its functionality. Since the presented model payload is notional, the payload trade will be re-evaluated once the flight instruments are selected.

C.2.2.1.2 Radiation and Planetary Protection

The severe radiation environment at Europa presents significant challenges for the science instruments, as does the need to meet the planetary protection requirements outlined in Sec-

tion C.2.6.2. Payload radiation challenges have been addressed through a combination of generous shielding and radiation-hardened parts, while also identifying viable candidate technologies, such as detectors (as discussed below), for the notional instruments.

Detector Working Group

A thorough study of both radiation effects and the impact of planetary protection protocols on detectors were conducted for the 2008 Jupiter Europa Orbiter (JEO) study by a Detector Working Group (DWG) (Boldt et al. 2008). The DWG developed a methodology for determining the required radiation shielding for successful instrument operation in the transient radiation environment at Europa, assessed degradation of detectors due to total ionizing dose and displacement damage effects, and assessed the compatibility of candidate detectors with the planetary protection protocols. Because the radiation and planetary protection challenges for a Europa Multiple-Flyby Mission would be quite similar in nature and magnitude to those of JEO, the DWG conclusions apply here as well without alteration.

The DWG concluded that the radiation and planetary protection challenges facing the model payload for a Europa mission are well understood. The question of detector survivability and science data quality was not considered to be a significant risk, provided appropriate shielding is allocated to reduce cumulative total ionizing dose (TID), displacement damage dose (DDD), and instantaneous electron and proton flux at the detector. Specific activities have been identified to support early education of potential instrument providers in the complexity of meeting radiation and planetary protection requirements. A series of instrument workshops was also completed as part of the Europa Study. The Flyby Mission instrument detectors are a subset of those studied by the JEO DWG.

Payload Shielding Architecture

The mission radiation design point for the Flyby Mission is 2.01 Mrad behind an equivalent of 100 mil of aluminum shielding, as shown in Section C.2.3. Designs are required to tolerate twice this (a radiation design factor [RDF] of 2). Therefore, sensors and supporting electronics require significant radiation shielding. The most mass-efficient approach to providing radiation shielding is to centrally locate as much of the instrument electronics as possible deep in the interior of the spacecraft, minimizing the electronics that must be co-located with the sensor portion of the instrument. Besides utilizing a structurally nested configuration that exploits surrounding passive mass (such as propellant tanks) for self-shielding, this approach uses the large mass margins available from the flyby concept to maximize dedicated radiation shielding as well, thus providing a large reduction in radiation dose to the electronics.

Planetary Protection Protocols

The approach to planetary protection compliance for the Europa Multiple-Flyby Mission concept is presented in full in Section C.2.6.2 and can be summarized as follows:

- In-flight microbial reduction of exterior elements via radiation prior to completion of the orbit energy pump-down phase
- Prelaunch microbial reduction to control the bioburden for areas not irradiated in flight

The preferred prelaunch method is dry heat microbial reduction (DHMR). Our plan is to perform DHMR on the entire spacecraft upon completion of assembly. Current planetary protection protocols include a time vs. temperature profile ranging from 125°C for 5 hours to 110°C for 50 hours.

Planetary protection guidelines would be generated and disseminated to potential instrument providers early, allowing providers to adequately address planetary protection issues

during the instrument selection and design process. A mid-Phase B Payload Planetary Protection Review is baselined so that issues and mitigation strategies can be identified and addressed. Instrument-specific planetary protection concerns are addressed in subsequent sections. The Flyby Mission would dispose of the spacecraft at Ganymede. During Phase A and B the potential of following a Juno-like planetary protection approach would be explored, with the objective of showing that the probability of successfully disposing on Ganymede meets NASA requirements without DHMR.

C.2.2.2 Model Instrument Descriptions

C.2.2.2.1 *Ice-Penetrating Radar*

The notional Ice-Penetrating Radar (IPR) is a dual-frequency sounder (nominally 9 MHz with 1-MHz bandwidth, and 60 MHz with 10-MHz bandwidth). The higher-frequency band is designed to provide high spatial resolution (footprint and depth) for studying the subsurface above 3-km depth at high (10-m) vertical resolution. The low-frequency band, which can penetrate much deeper, is designed to search for the ice/ocean interface on Europa or the hypothesized transition between brittle and ductile ice in the deep subsurface at a depth of up to 30 km (and a vertical resolution of 100 m). This band mitigates the risks posed by the unknown subsurface structure, both in terms of unknown attenuation due to volumetric scattering in the shallow subsurface and thermal/compositional boundaries that may be characterized by brine pockets. Additionally, the low-frequency band is less affected by surface roughness, which can attenuate the reflected echo and add clutter noise.

Because the low-frequency band is vulnerable to Jupiter noise when operating on the sub-Jovian side of the moon, it is necessary to increase the radiated power as compared with spaceflight hardware currently deployed for subsurface studies of Mars. Jupiter noise should not impair radar performance on the anti-Jovian side of Europa. It should also be

noted that Jupiter noise is expected to be intermittent, even on the sub-Jovian side.

The IPR is similar to the Mars Advanced Radar for Subsurface and Ionosphere Sounding (MARSIS) instrument on Mars Express and the Shallow Radar (SHARAD) instrument on the Mars Reconnaissance Orbiter (MRO). The notional Ice-Penetrating Radar baselined for Europa Multiple-Flyby Mission is tailored to satisfy the science requirements identified in Section C.1. It requires simultaneous cross-track surface topography coverage of the radar swath via stereo imaging from the TI in order to support data interpretation through modeling of off-nadir signal clutter. The Europa Multiple-Flyby Mission design concept provides sufficient flybys to meet the requirements for globally distributed intersecting and adjacent swaths at <400 km altitude.

Instrument Description

The notional IPR uses a dual antenna system with a nadir-pointed 60-MHz dipole array, and a backing element that also serves as a dipole antenna for the 9-MHz system. Because this instrument is a depth sounder operating at relatively low frequencies and using a dipole antenna, the FOV is very wide and there are no strict pointing requirements. A 15-m dipole similar to those used by MARSIS and SHARAD is baselined (shown deployed in Figure C.2.2-1, and stowed in Table C.2.2-2). Deployment releases the folded antenna elements in the nadir direction and is planned for early in the mission.

A conceptual physical block diagram of the IPR is shown in Figure C.2.2-2. The transmitters and matching network are located close to the antenna array. The receivers, digital electronics, and power supply are located remotely, in the Avionics Module.

The IPR has essentially only one operating mode, where the radar performs both shallow and deep sounding of Europa's surface. This mode is a raw data mode, in which a burst of unprocessed data is collected below 400 km

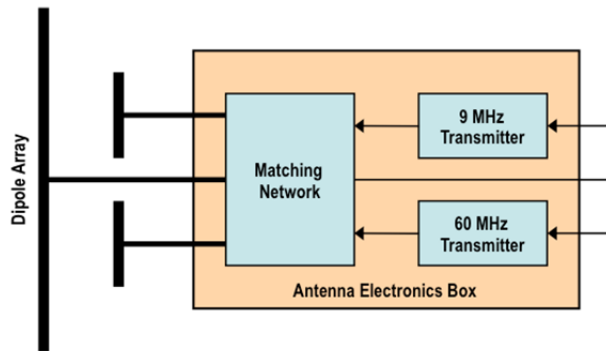


Figure C.2.2-2. Block diagram of the notional Ice-Penetrating Radar.

altitudes during the flyby. The radar is capable of bursts of raw data at a number of preselected rates up to a peak of ~130 Mbps. Due to the high data rate, the radar employs onboard processing elsewhere in the system to reduce the total data volume from the flyby to a manageable 25.2 Gbits. Processing will include range compression, presumming, Doppler filtering, data averaging, and resampling as needed to reduce output data volume.

Radiation Effects

Space-qualifiable parts that are radiation-hardened to 1 Mrad are currently available for use in the IPR transmitter and matching network. 5 kg of radiation shielding mass is allocated to protect this hardware, which is located adjacent to the dipole array. The rest of the IPR electronics are located in the UES of the Avionics Module, which provides shielding sufficient for parts tolerant to 300 krad or less (see Table C.2.6-7).

Planetary Protection

All of the IPR electronics can be prepared for planetary protection using dry heat microbial reduction. The deployed dipole array will be treated via radiation in flight.

Resource Estimates

The mass estimate for the IPR includes 6 kg for a stiffened 15-m dipole and 3 kg for a 5-m dipole array based on scaling from existing MARSIS and SHARAD designs. A mass es-

timate of 8 kg for the transmitter/matching network is derived from previous work performed under the High-Capability Instrument for Planetary Exploration (HCIPE) program with an additional 5 kg allocated for radiation shielding mass. Harness and antenna feeds are estimated at 3 kg, while remote digital electronics (including 4 receivers) are estimated at 8 kg, resulting in a total mass estimate for the IPR of 33 kg.

The power estimate for IPR is 55 W, driven by the use of both frequencies simultaneously.

C.2.2.2.2 Shortwave Infrared Spectrometer

The notional Shortwave Infrared Spectrometer (SWIRS) is a pushbroom spectrometer with a single-axis along-track scan mirror system for motion compensation. Functionality is similar to that of the Moon Mineralogy Mapper (M3) developed for the Chandrayaan-1 mission, shown in Table C.2.2-2.

Two primary modes of operation are defined for SWIRS. Inbound and outbound global-scale scans are obtained at ~10 km/pixel resolution, and inbound and outbound high-resolution scans are obtained at <300 m/pixel. The global scans are accomplished using a combination of spacecraft slews and internal scan mirror motion, while the high-resolution scans use the scan mirror as the spacecraft maintains a nadir orientation.

SWIRS is tailored to meet the science drivers identified in Section C.1.

- 150- μ rad IFOV spatial resolution from 0.85 to 5.0 μ m
- 10-nm spectral resolution from 0.85 to 5.0 μ m
- S/N >100 from 0.85 to 5.0 μ m (with target-motion compensation of up to 8 lines)

Instrument Description

The notional SWIRS consists of a single reflective telescope with a beam splitter feeding a grating spectrometer and detector. This op-

tics design concept yields an instrument IFOV of 150 μ rad.

The notional detectors are 640 \times 480 HgCdTe arrays, as used previously by M3 and by MRO's Compact Reconnaissance Imaging Spectrometer for Mars (CRISM). The wavelength cutoff is adjusted to 5 μ m, as dictated by the science drivers. Extensive radiation shielding will be required to minimize transient radiation noise in the HgCdTe detector elements. This effectively mitigates concerns over total dose effects on these detectors. The use of 480 cross-track pixels results in a 4.2 $^\circ$ instrument FOV. Spectral resolution of 10 nm from 0.85 to 5.0 μ m requires the use of 420 columns on the detector.

To achieve the required S/N at long wavelengths in the high-resolution targeted mode, target motion compensation is added via an along-track scan mirror that enables extended exposure times. S/N can also be improved by a selectable combination of spatial and spectral binning, similar to that implemented by MRO CRISM.

Preliminary SWIRS performance analysis has been completed assuming the pixel performance characteristics (quantum efficiency, well depth, 27- μ m pixel size) of the Teledyne TMC6604a HgCdTe image sensor. Low surface reflectance at Europa at 5 μ m limits system performance and drives the need for target motion compensation in the targeted mode. Assuming a 180-mm-focal-length telescope with 72-mm aperture ($f/2.5$), a 2:1 focal reducer, an optical efficiency of 75%, a grating efficiency of 66% at long wavelengths, 80% detector quantum efficiency, and 2% surface reflectance at long wavelengths, \sim 990 signal-electrons per pixel would be collected at 5 μ m per 120-ms exposure (2.5 km/s ground-track rate at 300 m/pixel, no target motion compensation). Assuming 100 electrons of read noise from the TMC6604a detector produces an S/N of 10. Applying target motion compensation via the scan mirror to allow 960-ms exposures,

\sim 7,900 signal-electrons are collected, resulting in an estimated S/N of 60 at 5 μ m. Due to increased solar flux, the S/N at 4 μ m improves to \sim 100 and at 2.6 μ m reaches \sim 210. The S/N values estimated for targeted mode and mapping mode do not include noise due to transient radiation noise in the HgCdTe detectors. Many data binning and/or editing options exist for data reduction in the mapping mode to achieve data volume allocation of 1.5 Gb per flyby.

A conceptual physical block diagram of the notional SWIRS is shown in Figure C.2.2-3. Consistent with the payload architecture described in Section C.2.2.1.2, minimal electronics are packaged at the focal plane with the detector, with most of the SWIRS electronics housed in the UES of the Avionics Module, which provides an environment shielded sufficiently for use of parts tolerant to a 300 krad or less total dose.

The scan mirror motor, with $\sim\pm 45^\circ$ range, is assumed to be a limited angle torque (LAT) motor with no internal electronic components. Scan mirror position sensing is assumed to be via a multispeed resolver or Inductosyn, also with no internal electronic components.

Motor drive and position sensing interface electronics and the SWIRS low-voltage power supply make up one of three electronics boards in the SWIRS electronics unit. The second board contains detector interface logic, pixel processing, and data compression. The third board contains the system controller and a SpaceWire interface to the spacecraft. These functions are implemented in radiation-hardened ASICs that use external radiation-hardened static RAM (currently available as 16-Mb devices) for temporary buffering of incoming spectrometer data, performing pipelined pixel processing, storing data compression intermediate products, and buffering incoming and outgoing SpaceWire command and telemetry data.

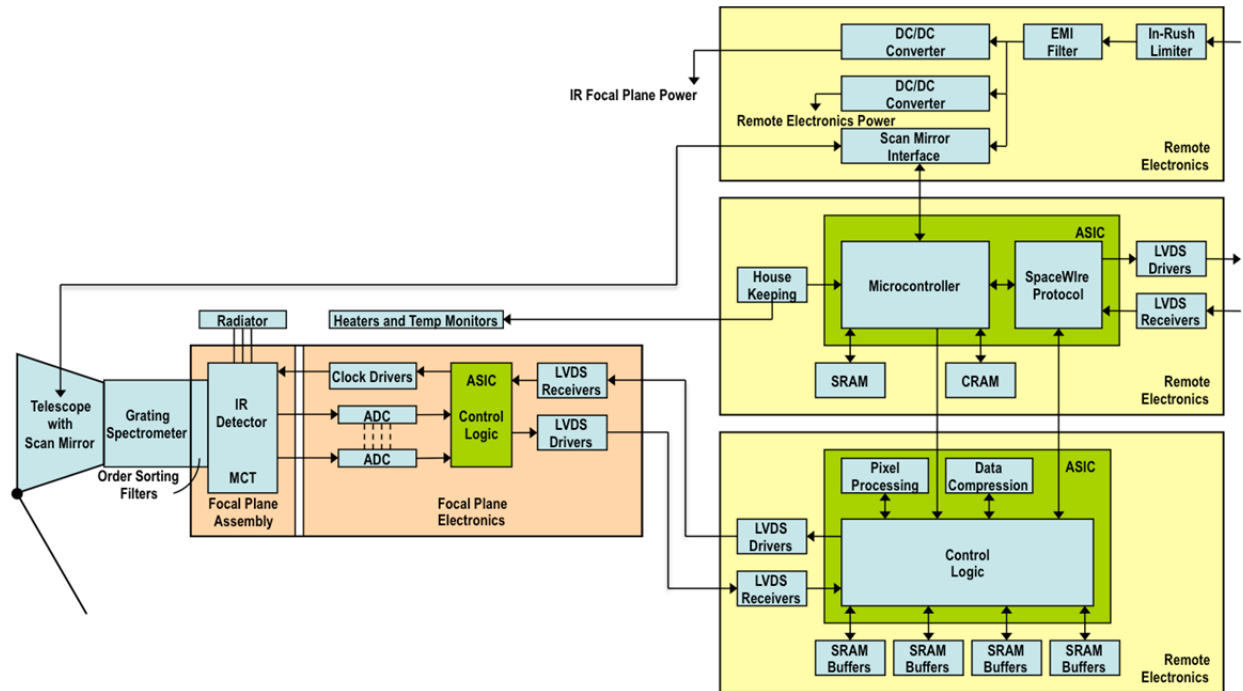


Figure C.2.2-3. Block diagram of the notional SWIRS.

Data compression is assumed to be wavelet based with commandable degrees of compression. Wavelet data compression algorithms developed for the Mercury Surface, Space Environment, Geochemistry, and Ranging (MESSENGER) mission have been tested using CRISM flight data and assuming onboard subtraction of a dark image (requiring ~8 Mb of SRAM) to remove fixed-pattern noise prior to compression. Results of this testing show acceptable noise levels with a 3:1 compression ratio.

A passive thermal design is baselined for SWIRS with a desired detector temperature of ~80 K. Accommodation of this radiator is discussed in Section C.2.2.1.1.

Radiation Effects and Shielding

While longer exposure times obtained through the use of target motion compensation can be used to increase the S/N, longer exposure times also increase the vulnerability to noise induced by background radiation. With 1 cm of Ta shielding, an estimated 4.3×10^5 electrons/cm²/s and 50 protons/cm²/s would reach the HgCdTe detectors through the shield while

in orbit at Europa (see Section C.2.2.1.2). Assuming 27- μ m pixels and 154-ms exposure times, an estimated 45% of all pixels would be struck by an incident electron during an integration period. Each incident electron is estimated to deposit an average of 12,000 signal-electrons in the HgCdTe detector (per Boldt et al. 2008), while ~990 signal-electrons due to optical input are estimated at 5 μ m for 120-ms exposures. Clearly, the SWIRS detectors will require additional radiation shielding. With 2 cm of Ta shielding, approximately 15% of SWIRS pixels would be struck during a 120-ms exposure. With 3 cm of Ta shielding, that rate is reduced to approximately 4%. For the notional SWIRS, a 3-cm Ta shield is assumed

The detector radiation shield is estimated at 4.6 kg with a notional configuration providing front-side detector shielding from the 2008 JEO study shown in Figure C.2.2-4. Shielding of the detector electronics, assumed to require an 8 \times 8 \times 2-cm interior volume, with 0.4 cm of Ta (100-krad components) is estimated at 1.30 kg each.

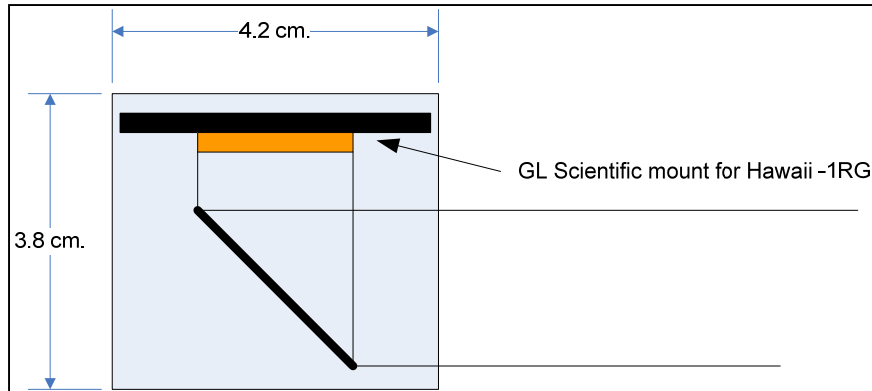


Figure C.2.2-4. Nominal SWIRS detector radiation shielding.

Transient radiation noise suppression in near-IR focal planes has seen considerable development effort due to its potential benefit to military systems. Various filtering approaches have been considered (Parish 1989) and some have been demonstrated within the readout integrated circuits (ROICs) underlining the HgCdTe detector elements. The Sensor Hardening Technology Program successfully implemented gamma noise suppression circuitry, including optical pulse suppression, within a ROIC using the BAE Systems 0.8- μm radiation-hardened complementary metal-oxide semiconductor (CMOS) process (Hairston et al. 2006). Transient suppression was achieved by dividing each image integration period into sub-frames using a Compact Signal Averager within each pixel to monitor each sub-frame and suppress outliers prior to charge integration within the ROIC. This technique is most effective in suppressing large transient events, and its overall effectiveness depends upon the pulse height distribution of the transient noise reaching the detector through the radiation shielding. While a factor-of-50 pulse suppression was achieved in the cited reference, the actual performance of such a system in the Europa environment is unknown at this time. Nonetheless, this approach looks promising. This technology suggests a possible radiation noise mitigation approach to be employed by SWIRS, but its implementation is not assumed for this report.

Planetary Protection

Planetary protection concerns would ideally be met for SWIRS through dry-heat microbial reduction, but survivability of the HgCdTe detector elements using the currently defined Europa Study planetary protection protocol is in question. A new “bake-stable” process has recently been developed that

produces HgCdTe focal plane arrays that can be baked at 90°C to 100°C for extended periods or 110°C for 24 hours. While this proprietary process has not yet been applied to the science-grade devices typically used for planetary space missions, it is thought that the bake-stable process can be applied to any HgCdTe focal plane array (James Beletic, Teledyne Imaging Sensors, private communication). A risk-reduction effort to fully quantify the performance impact of high-temperature bake-out on HgCdTe detector elements at the temperatures called for by the Europa Multiple-Flyby Mission planetary protection protocol is required. Alternatively, the SWIRS could be designed for removal of the focal plane during system DHMR, with a different microbial reduction technique performed on it.

Resource Estimates

The mass estimate for the notional SWIRS is based on an M3 system with scan mirror. The total mass estimate for SWIRS is 20.7 kg, of which 9.1 kg is radiation shielding.

Power dissipation for the notional SWIRS is estimated at 19.1 W, based on a bottoms-up estimate using M3 data.

The data volume estimate for the notional SWIRS in targeted mode is based on output of 480 cross-track pixels by 420 spectral pixels with 12 bits per pixel and a nominal 3:1 data compression ratio. Various combinations of spectral binning, spectral editing, spatial bin-

ning, and spatial editing can be used to reduce the compressed output data volume.

C.2.2.2.3 Ion and Neutral Mass Spectrometer

The notional INMS would determine the elemental, isotopic, and molecular composition of Europa's atmosphere and ionosphere during close flybys. Performing a role similar to that of the Cassini INMS, the Europa Multiple-Flyby Mission INMS concept has been adapted from the more recent design of the Reflectron Time-Of-Flight (RTOF) Rosetta Orbiter Spectrometer for Ion and Neutral Analysis (ROSINA). The Cassini and Rosetta spectrometers are both shown in Table C.2.2-2.

Due to the nature of Europa flybys, the SDT concluded that the INMS for the Flyby Mission requires greater sensitivity in a shorter integration time to achieve the science objectives than the heritage instruments offer. Research with potential INMS providers showed solutions for the Flyby Mission that could be tailored to the uniqueness of each INMS approach (quadrupole mass spectrometer vs. time-of-flight system, etc.). The notional model INMS represent a conservative merger of all of the solutions, considering resource needs. Therefore, while the INMS baselined for the Europa Multiple-Flyby Mission should satisfy the science drivers identified in Section C.1 (and listed below), the model instrument design concept has not been specified in as much detail as for other instruments.

The INMS is required to characterize the composition of sputtered products from energetic particle bombardment of Europa's surface, to include positive ions and neutral particles, with the following parameters:

- Mass range: up to 300 Da
- Mass resolution: $\Delta M/M \geq 500$
- Sensitivity: 10 particles/cm³

Instrument Description

The notional INMS collects exospheric ions and gases and forwards them to sensors that

determine their mass and mass-to-charge ratios. A clear 60°×60° FOV envelope in the spacecraft ram direction has been accommodated in the spacecraft configuration (see Figure C.2.2-1). Detectors of choice (either microchannel plate [MCP] or channel electron multipliers [CEMs]) detect the ion bunches, and their output is sampled by the instrument's data acquisition system. High-speed memory captures this output for postprocessing.

For the purposes of this study, it was assumed that the INMS data acquisition systems could be relocated from the sensor assembly to a separate electronics unit to make most efficient use of radiation shielding mass.

Radiation Effects and Shielding

There are two main areas of concern for radiation effects on the notional INMS: the high-speed data acquisition systems and detectors. The front end, consisting of mechanical parts at high voltage, would not be sensitive to radiation.

High-speed data acquisition systems on heritage instruments use analog-to-digital converters (ADCs) and high-speed memory. Existing ADCs from multiple sources are hardened to 300 krad and provide satisfactory 12-bit resolution at speeds of ≥ 20 MHz. Modern radiation-hardened memory offers access times as low as 20 ns with radiation hardness of up to 1 Mrad.

Transient radiation effects on the INMS detectors are mitigated by the extremely short duration of the burst of data acquisition produced when an ion bunch is released towards the detector. With 0.6 cm of Ta shielding, an estimated 8.7×10^5 electrons/cm²/s and 50 protons/cm²/s would reach the detectors through the shield during flyby of Europa (see Section C.2.2.1.2). As an example, for a notional 18-mm-diameter detector (similar to the ROSINA RTOF MCP), a 1-ns digitization window, and a worst-case assumption that each incident electron or proton generates an MCP output, ~0.2% of A/D samples will be

corrupted by background radiation. This represents a tolerable noise floor in a multisampled mass spectra. Given the small size of the detectors, only ~100 g of radiation shielding is required; however, a total of 1.1 kg of shielding has been allocated.

Electronics remaining in the notional INMS sensor unit (including front-end electronics, pulsers, and high-voltage power supplies) are assumed to be hardened to 1 Mrad, requiring a 0.2-cm Ta radiation shield and 2 kg of shielding mass.

Planetary Protection

Planetary protection concerns will be met for INMS through dry heat microbial reduction. The bare unpowered MCPs and CEMs can tolerate high-temperature soaks, but the drivers on the bake-out of the front end assembly and mass analyzer will need to be further investigated. The proposed INMS front-end assembly should tolerate up to 150°C bake-out temperatures.

Resource Estimates

The mass estimate for the notional INMS is derived by a conservative merging of inputs from the instrument community. The resulting mass estimate for the INMS sensor assembly is 24.1 kg. Of that mass, 10.5 kg is allocated to the sensor and an additional 3.1 kg to the sensor shielding. Two electronics boards in the science electronics unit (2.5 kg total) are assumed with additional shielding of 7.0 kg, and with 1 kg of harness mass allocated due to instrument partitioning. The notional INMS telemetry rate is estimated at 2 kbps, and power dissipation is estimated at 33 W.

C.2.2.2.4 Topographical Imager

The TI provides stereo imaging of Europa landforms to fulfill geology objectives, and it assists in removal of IPR clutter noise from off-nadir surface topography. The TI has basic functionality similar to that of the MRO Mars Color Imager (MARCI) instrument shown in Table C.2.2-2 and is tailored to satisfy the fol-

lowing science measurement requirements identified in Section C.1:

- High-resolution panchromatic imagery of Europa during flybys:
 - Along-track stereo
 - 58° cross-track coverage
 - 250- μ rad IFOV
 - Concurrent operation with the IPR

Instrument Description

The notional TI has a 0.25-mrad IFOV to produce a 25-m pixel footprint from a 100-km distance. Use of a 4096-pixel-wide image sensor results in an instrument FOV of ~58° full angle. A detector operating in pushbroom mode is baselined. A focal-plane detector, either dual charge-coupled devices (CCDs) or a CMOS active pixel sensor (APS) with multiple elements on a single substrate (similar to that developed by e2v Technologies for the New Horizons Multispectral Visible Imaging Camera [MVIC]) provides the along-track stereo image separation required. While future instrument proposers have a choice of available detectors, the higher radiation tolerance of CMOS APS devices and continued improvements in their performance for scientific applications (Janesick et al. 2008) make them the nominal detector choice for a notional TI.

Preliminary TI performance analysis has been completed using the pixel characteristics (quantum efficiency, 13- μ m pixel size, 100k e-well depth) of the e2v CCD47-20BT image sensor used by the New Horizons Long-Range Reconnaissance Imager (LORRI) instrument as an example of the performance expected from the TI sensor. Assuming a 52-mm-focal-length telescope with 13-mm aperture ($f/4$), an optical efficiency of 85%, an average detector quantum efficiency of 60%, and a surface reflectance of 20% at Europa, approximately 4.36×10^4 electrons per pixel are collected during the maximum exposure time of 5.5 ms. The required TI pixel readout rate (for 25-m resolution at 100 km with nominal ground speed of 4500 m/s) for a 4096-pixel line array

is 810 kHz, smaller than LORRI's readout rate of 1.2 MHz and its measured 20-electron system read noise. However, if the TI needs to take images at 25-km passes as well (though it is not a driving requirement), then the readout rate increases to 2.9 MHz, with corresponding increase of electron noise to ~ 30 electrons. Therefore, for the notional TI calculations, a 20-electron read noise is assumed. Coupled with photon noise and barring background radiation noise, the estimated panchromatic S/N is ~ 315 . The driving cases for TI are the flybys at 25 km. However, even then, the S/N exceeds 200.

A conceptual physical block diagram for the TI is provided in Figure C.2.2-5. Consistent with the instrument architecture described in Section C.2.2.1.2, minimal electronics are packaged at the focal plane with the detector. The signal chain shown in the focal plane electronics contains elements required for a CCD image sensor (clock drivers, correlated double sampler, A/D conversion) that either are not necessary or are typically implemented within a CMOS APS device. A highly integrated CMOS APS device is an ideal solution for the Europa Multiple-Flyby Mission TI, as it minimizes components at the focal plane that require radiation shielding.

The camera processor board contains camera interface logic, image data compression and a SpaceWire command and telemetry interface to the spacecraft. A single, radiation-hardened ASIC with 3:1 nominal wavelet-based data

compression is assumed. A second electronics board provides DC/DC power conversion.

The TI detector is cooled by a passive, Sun-protected radiator. A detector-annealing heater is baselined as a means to mitigate radiation damage.

Radiation Effects and Shielding

To protect the TI image sensor from total dose, displacement damage, and transient radiation noise, radiation shielding with 1 cm of Ta is baselined, comparable to shielding used by the Galileo Solid State Imager (SSI). The Europa Multiple-Flyby Mission radiation dose depth curve indicates a ~ 17.6 krad total dose behind 1 cm of Ta shielding. With a required RDF of 2, this allows use of detectors tolerant of 35.2 krad. While a CMOS APS device is favored for the notional Europa Multiple-Flyby Mission TI, this dose level allows a choice of silicon device technologies including CMOS APS, P-channel CCD, and arguably N-channel CCD.

Shielding mass of 4.5 kg is allocated for a 1-cm Ta, $5 \times 5 \times 4$ -cm enclosure. This is slightly larger than that shown in Figure C.2.2-6, which was designed to house a STAR1000-based CMOS APS and its interface electronics. The slight increase in dimensions allows for additional circuitry required for a CCD-based focal plane or additional electronics required by a multioutput CMOS APS device.

Background radiation noise is mitigated by the very short exposure times employed by TI.

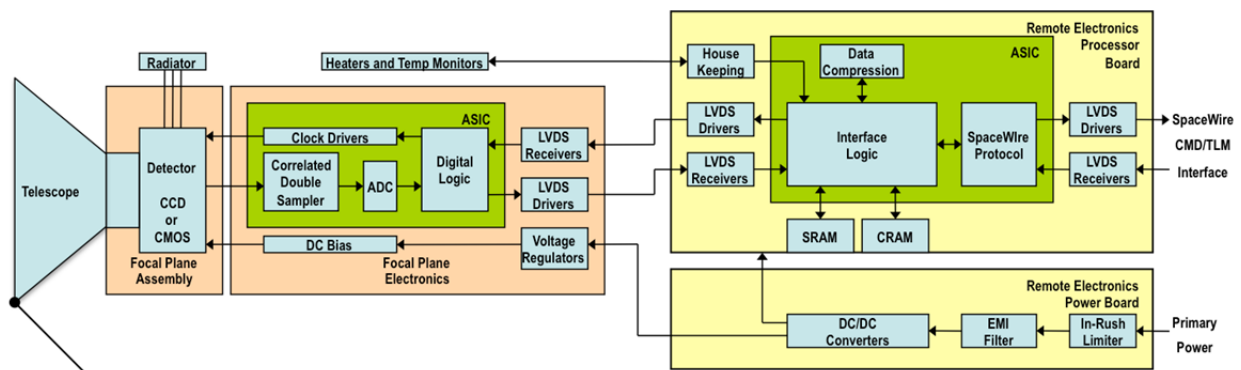


Figure C.2.2-5. Block diagram of the notional Topographical Imager

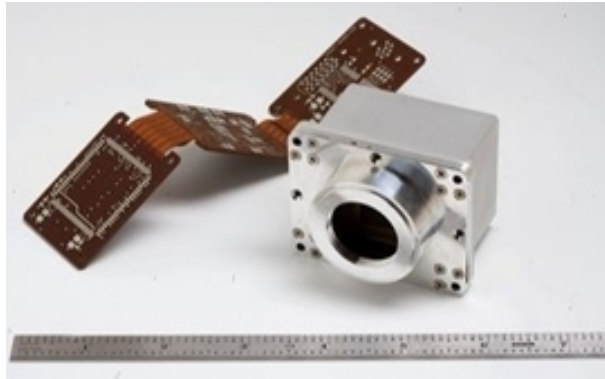


Figure C.2.2-6. Miniature focal plane assembly for a STAR1000 CMOS APS indicative of the TI focal plane electronics.

With 1 cm of Ta shielding, an estimated 4.3×10^5 particles/cm²/s would reach the detector through the shielding (see Section C.2.2.1.2). Assuming 13- μ m pixels and 5.5-ms exposure times, it is estimated that ~0.4% of all pixels would be struck by an incident electron during the integration period, which is a tolerable level. For a typical silicon image sensor, each incident electron can be expected to generate an average of 2,000 signal-electrons in the detector (per Boldt et al. 2008). With the assumption that the signal-electrons generated by the incident particles are concentrated on a single pixel, the method of calculating S/N adopted for the Galileo SSI camera can be employed (Klaasen et al. 1984). Based on empirical data, radiation-induced noise was approximated at $35 \times \text{SQRT}$ (mean radiation signal per pixel). For a 0.4% hit rate and 2,000 electrons per hit, the radiation-induced noise would contribute ~100 electrons to the TI S/N calculation. This reduces the TI S/N to 300 from 315.

The TI electronics present no significant radiation concerns beyond those particular to the detector; use of parts tolerant to 100 krad is assumed.

Planetary Protection

Planetary protection concerns for TI can be met through dry-heat microbial reduction. Temperature effects on optical materials, the

adhesives used in optical mounts, and the image sensor will require thorough testing early in instrument development.

Resource Estimates

The TI mass estimate of 7.0 kg (including 4.5 kg of shielding mass) is derived from similarity to the New Horizons LORRI instrument and assumed values for harness mass and separate electronics unit. Power dissipation is estimated at 5.9 W during image acquisition and is driven by pixel rate, data compression, and the high-speed SpaceWire interface.

For pushbroom operation at a range of 100-km orbit for a typical flyby, the TI line period is 5.5 ms. Assuming 14 bits/pixel, one 70-line stereo image is 8 Mb. Data volume from a typical flyby is estimated at 3.1 Gb, compressed 3:1, assuming ~1,100 images per flyby that can be allocated by the science team to meet the science objectives.

C.2.3 Mission Design

A fully integrated proof-of-concept trajectory has been developed for a compelling Europa Multiple-Flyby Mission that efficiently accomplishes high-quality scientific observations and measurements.

The trajectory design goal for this Europa Multiple-Flyby Mission study was to establish the existence and feasibility of a flyby-only Europa mission that meets the SDT observation and measurement requirements, as outlined in the traceability matrix (FO C-1). The focus for this study was to maximize IPR, TI, SWIRS and INMS coverage while minimizing total ionizing dose³ (TID), mission duration, and ΔV .

Current Europa Multiple-Flyby Mission concept needs are presently satisfied by the capabilities of an Atlas V 551 launched from Cape Canaveral Air Force Station on a Venus-Earth-Earth gravity assist (VEEGA) interplanetary trajectory. In this concept, after a cruise of

³ Total ionizing dose Si behind a 100-mil Al, spherical shell.

6.37 years, the spacecraft will fly by Ganymede just prior to performing Jupiter Orbit Insertion (JOI) via a large main engine maneuver. The spacecraft will then perform four additional Ganymede gravity assists over 11 months to lower its orbital energy with respect to Jupiter and set up the correct flyby conditions (lighting and relative velocity) at Europa. The spacecraft will then embark on an 18-month Europa science campaign. The first part of the science campaign will focus on Europa's then day lit anti-Jovian hemisphere (Figure C.2.3-1). After the first phase, six Eu-

ropa and three Ganymede flybys will be used to place the subsequent Europa flybys on the opposite side of Jupiter where the sub-Jovian hemisphere of Europa will then be day lit. These Europa flybys, constituting the second phase of the science campaign, will focus on Europa's sub-Jovian hemisphere. Finally, the mission will culminate with spacecraft disposal via Ganymede impact. FO C-2 depicts a summary of the mission design concept.

For a discussion of data acquisition scenarios, data return strategies, and communication strategies, see Section C.2.1.

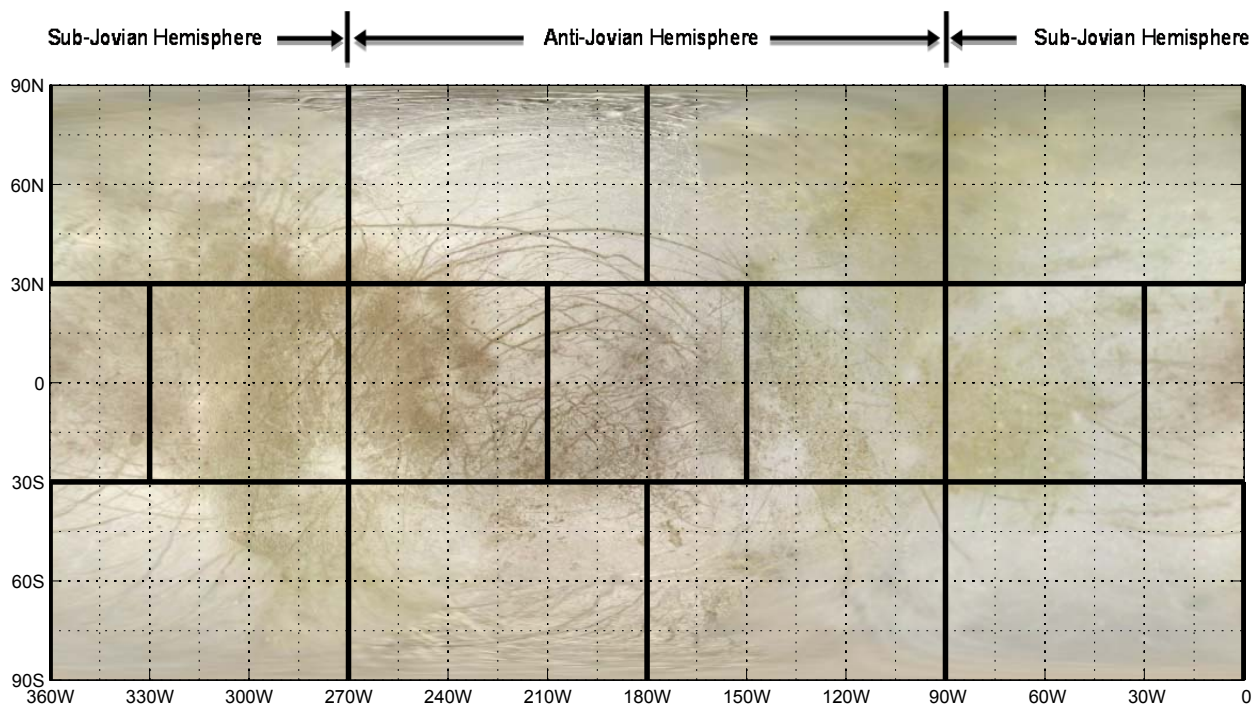
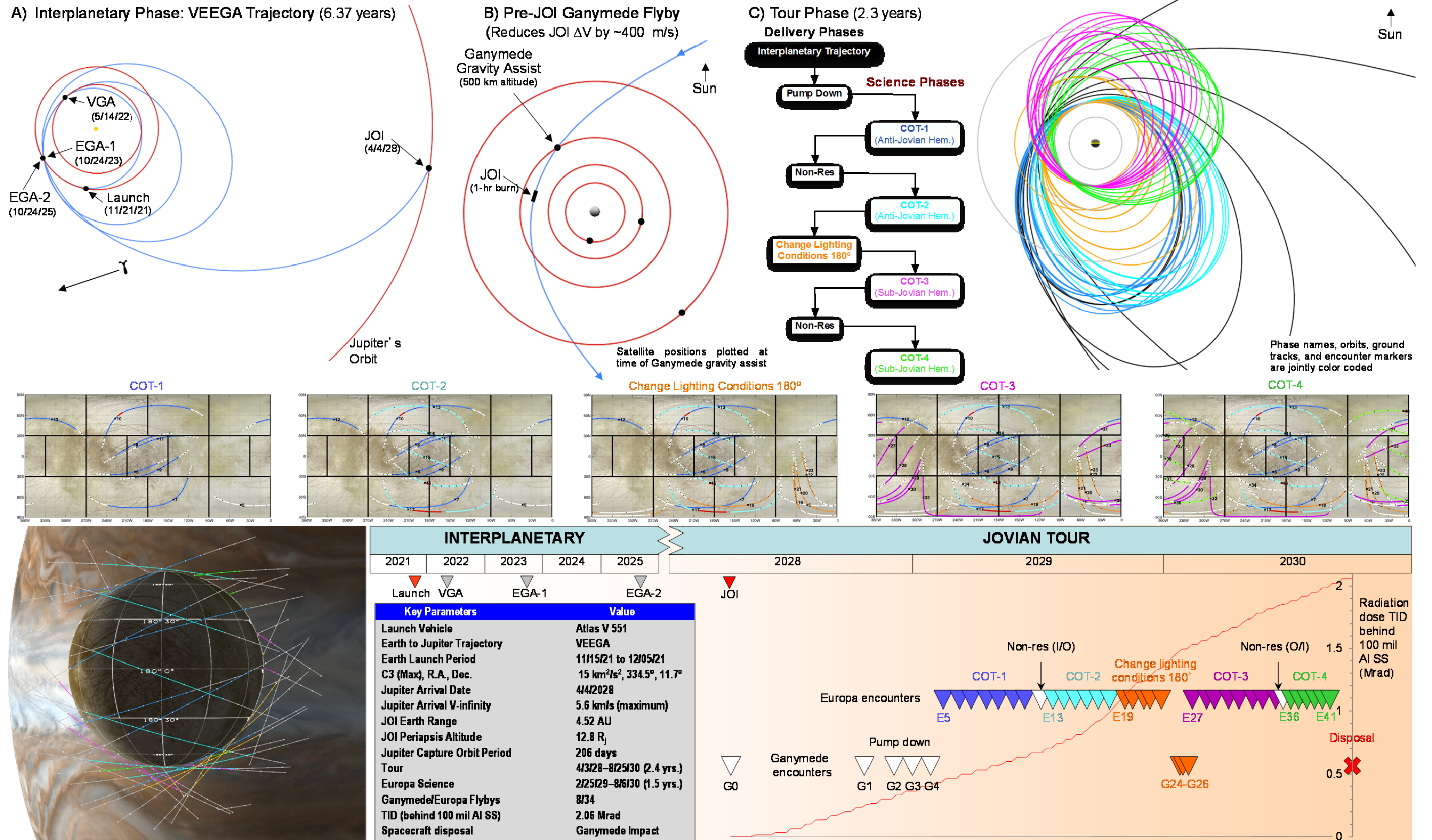


Figure C.2.3-1. Europa Mercator projection map including the 14 sectors defined by the SDT used to assess global coverage. In addition, since Europa is tidally locked, the same hemispheres (and associated sectors) always face towards (sub-Jovian) or away (anti-Jovian) from Jupiter.

Europa Multiple-Flyby Mission Design: Multiple-Flyby Approach to Explore Europa and Investigate Its Habitability



C.2.3.1 Mission Overview and Phase Definitions

General descriptions of each mission phase and related activities are summarized in Table C.2.3-1.

Table C.2.3-1. Mission phase definitions and descriptions.

Phase	Subphase	Activity	Start-End
Interplanetary	Launch and Early Operations	Begins with the launch countdown, launch, initial acquisition by the DSN, checkout and deployment of all major flight-system subsystems, and a moderate maneuver to clean up trajectory errors from launch vehicle injection.	Nov./Dec. 2021 + 30 days
	Cruise	Science instrument calibrations, Venus and Earth gravity-assist flyby operations, annual spacecraft health checks, trajectory correction maneuvers, and operations readiness tests (ORTs).	Jan. 2021–Oct. 2027
	Jupiter Approach	Training, and ORTs for all mission elements in preparation for JOI and Jovian tour. This phase includes the Ganymede (G0) flyby ~12 hours before JOI and ends with completion of JOI.	Oct. 2027–Apr. 2028
Pump-down		Reduces energy relative to Jupiter via four Ganymede gravity assists. The sequence of four outbound Ganymede flybys (G1–G4) following the inbound G0 flyby sets up the encounter geometry for the first Europa science phase such that an acceptable velocity relative to Europa is achieved and the anti-Jovian hemisphere is well illuminated.	Apr-2028–Feb. 2029 (11 months)
Europa Anti-Jovian Hemisphere Coverage	COT-1	A seven Europa-flyby crank-over-the-top (COT) sequence is used to systematically cover Europa's anti-Jovian hemisphere. Places groundtrack in all seven anti-Jovian hemisphere sectors. All Europa flybys occur at the ascending node. COT-1 sequence changes the flybys from outbound to inbound.	Feb. 2029–Jul. 2029 (4.7 months)
	Nonresonant Transfer	Inbound-to-outbound Europa nonresonant transfer to get back to outbound flybys such that another COT sequence can be implemented to cover the anti-Jovian hemisphere.	Jul. 2029–Aug. 2029 (0.5 months)
	COT-2	A five Europa-flyby COT sequence is used to systematically cross all COT-1 groundtracks to fulfill the IPR/TI requirements for <i>all</i> anti-Jovian hemisphere sectors. All flybys occur at the descending node. COT-2 changes the flybys from outbound to inbound.	Aug. 2029–Oct. 2029 (2.4 months)
Change Lighting Conditions	Pump-down, Crank-up	Reduces spacecraft orbit period and increases inclination to set up correct geometry for Europa-to-Ganymede pi-transfer.	Oct. 2029–Jan. 2030 (3.5 months)
	Pi-Transfers	Includes a Europa-to-Ganymede pi-transfer, a Ganymede pi-transfer (placing periapsis on the opposite side of Jupiter), and finally a Ganymede-to-Europa pi-transfer that places the subsequent Europa flybys approximately 180° from the location of the Europa flybys in COT-2.	Jan. 2030–Feb. 2030 (0.6 months)
Europa Sub-Jovian Hemisphere Coverage	COT-3	Eight Europa flybys are used to increase spacecraft orbit period while also cranking over the top to cover the sub-Jovian hemisphere. All Europa flybys occur at the descending node. COT-3 changes the flybys from inbound to outbound.	Feb. 2030–Jun. 2030 (3.7 months)
	Nonresonant Transfer	Outbound-to-inbound Europa flyby nonresonant transfer to get back to inbound flybys such that another COT sequence can be implemented to cover the sub-Jovian hemisphere.	Jun. 2030 (0.3 months)
	COT-4	A six Europa-flyby COT sequence is used to systematically cross the COT-3 groundtracks to fulfill the IPR/TI requirements for 6 of the 7 sub-Jovian hemisphere sectors. All flybys occur at the ascending node.	Jun. 2030–Aug. 2030 (2.4 months)
Spacecraft Disposal		Baseline strategy: Ganymede impactor (although many options exist—see Section C.2.3.9).	Aug. 2030

C.2.3.2 Launch Vehicle and Launch Period

An Atlas V 551 would launch the spacecraft with a maximum C_3 of $15.0 \text{ km}^2/\text{s}^2$ during a 21-day launch period opening on November 15, 2021. The optimal launch date within the launch period is November 21, 2021 (Figure C.2.3-2). The date of Jupiter arrival is held fixed throughout the launch period, incurring only a negligible penalty, while simplifying the design of the tour in the Jovian system. Launch vehicle and launch period parameters are shown on FO C-2. Launch vehicle performance is taken as that specified in the NASA Launch Services (NLS)-II Contract, which includes, in particular, a performance degradation of 15.2 kg/yr for launches occurring after 2015. The spacecraft propellant tanks are sized for maximum propellant, given the trajectory and launch vehicle capability, and are assumed to be fully loaded. The flight system is designed to launch on any given day in the launch period without reconfiguration or modification.

C.2.3.3 Interplanetary Trajectory

The baseline interplanetary trajectory used for the Europa Multiple-Flyby Mission is a VEEGA (FO C-2 and Table C.2.3-2). Cruise navigation will use Doppler and range observations from the Deep Space Network (DSN). The deep-space maneuver (DSM) ΔV required on the optimal day of the launch period is zero, but is about 80 m/s at the start of the launch period and reaches its highest level of 100 m/s

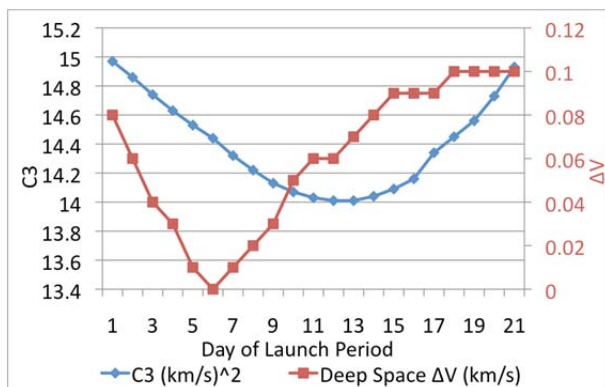


Figure C.2.3-2. Baseline interplanetary launch period

Table C.2.3-2. Baseline VEEGA interplanetary trajectory (for optimal launch date).

Event	Date	V_∞ or ΔV (km/s)	Flyby Alt. (km)
Launch	21 Nov 2021	3.77	-
Venus	14 May 2022	6.62	3184
Earth	24 Oct 2023	12.07	11764
Earth	24 Oct 2025	12.05	3336
G0	03 Apr 2028	7.37	500
JOI	04 Apr 2028	0.858	12.8 R_J

on the last day. The DSM occurs near aphelion on the Earth-Earth leg of the trajectory.

The interplanetary trajectory design will comply with all required National Environmental Policy Act (NEPA) assessments and safety analyses (see Section C.2.6). An aim-point-biasing strategy will be used for the Earth flybys.

The nominal flyby altitudes of Venus and Earth do not vary significantly over the launch period and are relatively high, as seen in Table C.2.3-2. For comparison, Cassini flew by Earth at an altitude of 1,166 km, and Galileo at altitudes of 960 and 304 km.

A 500-km Ganymede flyby will be performed approximately 12 hours before JOI, thereby saving about 400 m/s of ΔV (compared to the case of no Ganymede flyby). The JOI maneuver will last about 2 hours and occur at perijove at a range of $12.8 R_J$ (i.e., in the less intense outer regions of the radiation belts). Gravity losses are negligible due to the small angle subtended by the burn-arc. This also permits a far less complicated contingency strategy for this critical event.

C.2.3.4 Backup Interplanetary Trajectories

Many backup interplanetary trajectory options are available, offering launch opportunities every calendar year. The results of a comprehensive search of all 1-, 2-, 3-, and 4-gravity-assist trajectories are shown in Figure C.2.3-3. The best candidates from the search are shown in Table C.2.3-3, which includes launch period effects.

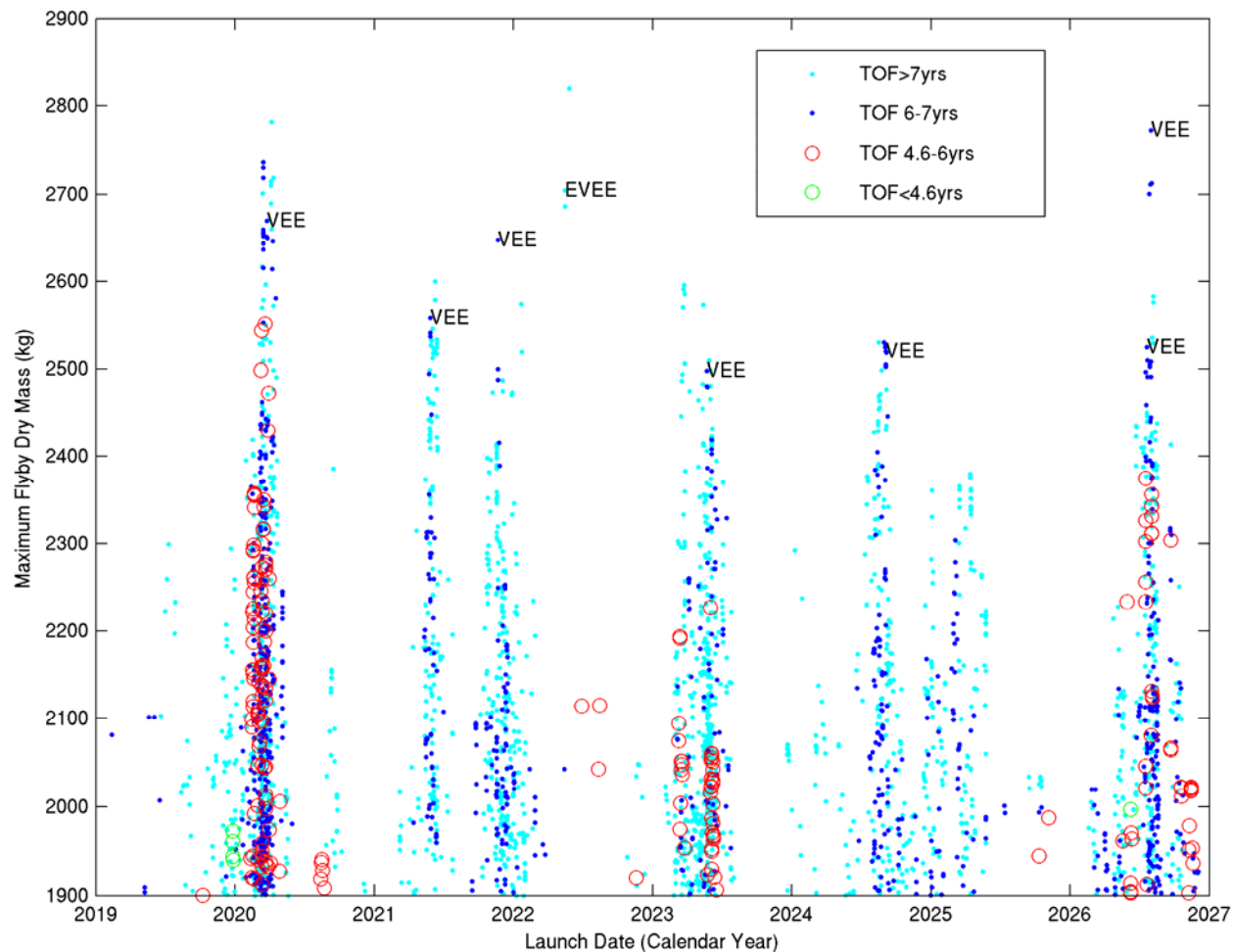


Figure C.2.3-3. Interplanetary trajectory options.

Table C.2.3-3. Short list of interplanetary trajectories, including launch period effects. Baseline trajectory is in bold; subsequent trajectories represent viable backup opportunities.

Launch Date	Flyby Path	TOF to JOI (yrs.)	C ₃ (km ² /s ²)	Atlas V 551 Capability (kg)	Max Prop Mass (MEV DV) (kg)	Max Dry Mass (kg)	Prop for CBE Dry Mass (kg)
25 Mar 2020	VEE	6.03	15.6	4456	1739	2717	864
27 May 2021	VEE	6.87	14.5	4541	1938	2603	1005
21 Nov 2021	VEE	6.37	15.0	4494	1846	2648	898
15 May 2022	EVEE	7.22	10.2	4935	2182	2753	1070
23 May 2023	VEE	6.18	16.4	4339	1797	2542	955
03 Sep 2024	VEE	6.71	13.8	4562	1998	2564	1052
01 Aug 2026	VEE	6.94	10.0	4893	2112	2781	1026
21 Jul 2026	VEE	6.15	15.2	4400	1831	2569	962

The table shows, for each trajectory, the optimal launch date of the launch period, the flight time to Jupiter, the expected maximum C_3 over the launch period, the launch vehicle capability at maximum C_3 for the indicated launch year (NLS-II contract), the propellant required for flying the mission (assuming the full launch vehicle capability is used), the maximum dry mass (i.e., the difference between the two preceding numbers), and the propellant required to fly the mission assuming the CBE value for the dry mass. In all cases, the MEV (maximum expected value) ΔV from Table C.2.3-5 is used.

It is worth noting that two types of commonly considered trajectories do not appear in the short list of Europa Multiple-Flyby Mission interplanetary trajectories because of their relatively poor mass performance. The first type is the ΔV -Earth gravity assist (ΔV -EGA), which is a V_∞ leveraging type of trajectory involving a large maneuver near aphelion before the Earth flyby. For the ΔV -EGA, the maximum dry mass that can be delivered in the years 2019–2027 is about 1,650 kg (about 1,000 kg less than the “Max Dry Mass” numbers in the short list, Table C.2.3-3). The required C_3 is in the range 25–30 km^2/s^2 , and the flight time is typically 4–5 years, corresponding to a 2:1 ΔV -EGA (4.5 years for the maximum-dry-mass case). The second type is the Venus-Earth Gravity Assist (VEGA), involving a large maneuver after the Venus flyby. For flight times of around 4.4 yrs., the maximum dry mass for the VEGA is about 1,740 kg. For flight times around 5.4 yrs., approaching the VEEGA flight times, the maximum dry mass becomes about 2,190 kg. Thus,

these two trajectory types significantly underperform in terms of delivered mass compared to the typical VEEGA trajectory. To save some flight time, these trajectory types may be considered in later phases of the mission design, once the vehicle mass is better characterized, assuming it does not grow significantly from current levels.

C.2.3.5 Jovian Tour (11-F5 Trajectory)

The current baseline Jupiter tour for the Europa Multiple-Flyby Mission is a fully integrated trajectory (i.e., flight-level fidelity, no approximations made), and one of many tours developed for this study. The baseline tour, referred to as 11-F5, begins after JOI and consists of 34 Europa and 9 Ganymede flybys over the course of 2.4 years, reaches a maximum Jovicentric inclination of 15° , has a deterministic ΔV of 157 m/s (post-PJR [perijove raise maneuver]), and has a TID of about 2 Mrad. This proof-of-concept trajectory employs a novel combination of mission design techniques to successfully fulfill a set of SDT-defined scientific objectives (see FO C-1) including global Ice-Penetrating Radar (IPR), Topographic Imager (TI), and Shortwave Infrared Spectrometer (SWIRS) observations, and Ion and Neutral Mass Spectrometer (INMS) *in situ* measurements. Navigational constraints concerning superior conjunctions of Jupiter, which occur every 13 months and require a several-day hiatus in spacecraft commanding, were not considered but are easily accommodated and will be included during Phase A. The 11-F5 trajectory can be broken into five distinct phases, each detailed in Table C.2.3-4 and depicted in FO C-2.

Table C.2.3-4. Detailed 11-F5 flyby and maneuver summary.

Phase	Flyby/ Maneuver	In/ Out	Date	Altitude (km)	B-Plane Ang (deg)	V-Infinity (km/s)	Inc. (deg)	Peri. (R _J)	Apo. (R _J)	Period (days)		TOF (days)	Total TOF (months)	
										m	n			
Jupiter Approach	Ganymede0	I	03-Apr-2028 14:56:45	500	0.1	7.382	5.17	12.96	-	N	R	-	202.1	0.00
	<i>JOI</i>		<i>04-Apr-2028 03:30:08</i>	$\Delta V =$	<i>857 m/s</i>		<i>4.97</i>	<i>12.78</i>	<i>268.5</i>	<i>-</i>	<i>-</i>	<i>205.7</i>	<i>0.5</i>	
	<i>PJR</i>		<i>13-Jul-2028 14:52:13</i>	$\Delta V =$	<i>114 m/s</i>		<i>4.95</i>	<i>13.6</i>	<i>264.5</i>	<i>-</i>	<i>-</i>	<i>202.6</i>	<i>100.5</i>	
Pump-down	Ganymede1	O	22-Oct-2028 16:52:57	100	-171.1	6.34	4.6	11.99	97.73	7	1	50.09	50.1	6.74
	<i>CU-Man-G1</i>		<i>25-Oct-2028 17:51:55</i>	$\Delta V =$	<i>0 m/s</i>							<i>3.0</i>		
	<i>Apo-Man-G1</i>		<i>16-Nov-2028 02:26:26</i>	$\Delta V =$	<i>0.427 m/s</i>							<i>21.4</i>		
	Ganymede2	O	11-Dec-2028 19:05:43	100	-136.4	6.42	1.54	11.16	64.37	4	1	28.61	28.6	8.41
	<i>Apo-Man-G2</i>		<i>25-Dec-2028 08:31:15</i>	$\Delta V =$	<i>4.821 m/s</i>							<i>13.6</i>		
	Ganymede3	O	09-Jan-2029 09:42:57	3496.3	-175.5	6.37	1.37	10.63	51.74	3	1	21.46	21.5	9.36
	<i>CU-Man-G3</i>		<i>12-Jan-2029 11:40:03</i>	$\Delta V =$	<i>0 m/s</i>							<i>3.1</i>		
	<i>Apo-Man-G3</i>		<i>19-Jan-2029 07:59:00</i>	$\Delta V =$	<i>0 m/s</i>							<i>6.8</i>		
	Ganymede4	O	30-Jan-2029 20:52:12	172.9	191.1	6.40	0.45	9.33	36.18	N	R	13.37	25.9	10.07
	<i>CU-Man-G4</i>		<i>02-Feb-2029 22:47:42</i>	$\Delta V =$	<i>0 m/s</i>							<i>3.1</i>		
	<i>Apo-Man-G4</i>		<i>05-Feb-2029 15:05:55</i>	$\Delta V =$	<i>0 m/s</i>							<i>2.7</i>		
Europa Anti-Jovian Hemisphere Coverage COT-1	Europa5	O	25-Feb-2029 17:45:14	724.3	104.6	3.84	2.32	9.27	34.04	7	2	12.43	24.9	10.94
	<i>CU-Man-E5</i>		<i>10-Mar-2029 02:14:25</i>	$\Delta V =$	<i>0 m/s</i>							<i>12.4</i>		
	<i>Apo-Man-E5</i>		<i>16-Mar-2029 06:24:12</i>	$\Delta V =$	<i>7.375 m/s</i>							<i>6.2</i>		
	Europa6	O	22-Mar-2029 14:52:04	100	25	3.92	3.33	9.42	37.93	4	1	14.20	14.2	11.77
	<i>CU-Man-E6</i>		<i>25-Mar-2029 14:59:58</i>	$\Delta V =$	<i>9.125 m/s</i>							<i>3.0</i>		
	<i>Apo-Man-E6</i>		<i>29-Mar-2029 15:26:54</i>	$\Delta V =$	<i>0 m/s</i>							<i>4.0</i>		
	Europa7	O	05-Apr-2029 19:35:07	100	73.6	3.92	5.98	9.45	33.89	7	2	12.43	24.9	12.24
	<i>CU-Man-E7</i>		<i>18-Apr-2029 04:34:59</i>	$\Delta V =$	<i>0 m/s</i>							<i>12.4</i>		
	<i>Apo-Man-E7</i>		<i>24-Apr-2029 09:45:13</i>	$\Delta V =$	<i>1.216 m/s</i>							<i>6.2</i>		
	Europa8	O	30-Apr-2029 16:28:04	100	-18.1	3.94	5.01	9.50	37.86	4	1	14.20	14.2	13.07
	<i>CU-Man-E8</i>		<i>03-May-2029 16:38:07</i>	$\Delta V =$	<i>0 m/s</i>							<i>3.0</i>		
	<i>Apo-Man-E8</i>		<i>07-May-2029 18:50:08</i>	$\Delta V =$	<i>2.201 m/s</i>							<i>4.1</i>		
	Europa9	I	14-May-2029 20:58:09	100	24.1	3.93	6.03	9.48	33.86	7	2	12.43	24.9	13.54
	<i>CU-Man-E9</i>		<i>27-May-2029 08:55:17</i>	$\Delta V =$	<i>0 m/s</i>							<i>12.5</i>		
	<i>Apo-Man-E9</i>		<i>02-Jun-2029 14:05:16</i>	$\Delta V =$	<i>1.951 m/s</i>							<i>6.2</i>		
	Europa10	I	08-Jun-2029 17:51:49	25	-72.3	3.92	3.27	9.42	37.92	4	1	14.20	14.2	14.37
	<i>CU-Man-E10</i>		<i>11-Jun-2029 18:15:35</i>	$\Delta V =$	<i>1.439 m/s</i>							<i>3.0</i>		
	<i>Apo-Man-E10</i>		<i>15-Jun-2029 22:22:27</i>	$\Delta V =$	<i>0 m/s</i>							<i>4.2</i>		
	Europa11	I	22-Jun-2029 22:24:10	100	-25	3.93	2.05	9.29	33.94	7	2	12.43	24.9	14.84
<i>CU-Man-E11</i>		<i>25-Jun-2029 23:12:45</i>	$\Delta V =$	<i>0 m/s</i>							<i>3.0</i>			
<i>Apo-Man-E11</i>		<i>11-Jul-2029 17:51:19</i>	$\Delta V =$	<i>11.635 m/s</i>							<i>15.8</i>			

Phase		Flyby/ Maneuver	In/ Out	Date	Altitude (km)	B-Plane Ang (deg)	V-Infinity (km/s)	Inc. (deg)	Peri. (R _J)	Apo. (R _J)	m	n	Period (days)	TOF (days)	Total TOF (months)	
Europa Anti-Jovian Hemisphere Coverage	Nonresonant	Europa12	I	17-Jul-2029 19:10:35	100	-124.6	3.90	0.34	9.34	38.12	N	R	14.25	14.4	15.67	
		CU-Man-E12		20-Jul-2029 19:24:29	$\Delta V =$	0 m/s									3.0	
		Apo-Man-E12		25-Jul-2029 01:26:55	$\Delta V =$	3.976 m/s									4.3	
	COT-2	Europa13	O	01-Aug-2029 05:25:51	100	-74.2	3.81	3.11	9.39	37.98	4	1	14.20	14.2	16.15	
			CU-Man-E13		04-Aug-2029 06:49:40	$\Delta V =$	0 m/s								3.1	
			Apo-Man-E13		08-Aug-2029 07:27:23	$\Delta V =$	2.142 m/s								4.0	
		Europa14	O	15-Aug-2029 10:30:01	100	-36.1	3.82	4.72	9.42	37.96	4	1	14.20	14.2	16.63	
			CU-Man-E14		18-Aug-2029 11:44:29	$\Delta V =$	0 m/s								3.1	
			Apo-Man-E14		22-Aug-2029 13:31:02	$\Delta V =$	2.498 m/s								4.1	
		Europa15	I	29-Aug-2029 15:32:40	100	1.4	3.82	4.55	9.37	38	4	1	14.20	14.2	17.10	
			CU-Man-E15		01-Sep-2029 16:39:17	$\Delta V =$	0 m/s								3.0	
			Apo-Man-E15		05-Sep-2029 19:49:51	$\Delta V =$	1.045 m/s								4.1	
		Europa16	I	12-Sep-2029 20:33:20	25	40.9	3.81	2.58	9.31	38.07	4	1	14.20	14.2	17.57	
			CU-Man-E16		15-Sep-2029 21:32:51	$\Delta V =$	0 m/s								3.0	
			Apo-Man-E16		20-Sep-2029 01:53:29	$\Delta V =$	4.581 m/s								4.2	
Europa17	I	27-Sep-2029 01:34:33	25	82.1	3.80	0.72	9.27	38.09	4	1	14.20	14.2	18.05			
	CU-Man-E17		30-Sep-2029 01:29:00	$\Delta V =$	0 m/s								3.0			
	Apo-Man-E17		04-Oct-2029 06:05:15	$\Delta V =$	2.908 m/s								4.2			
Change Lighting Conditions	Pump-down, Crank-up	Europa18	I	11-Oct-2029 06:13:06	100	74.2	3.82	3.36	9.22	34.12	7	2	12.43	24.8	18.52	
			CU-Man-E18		14-Oct-2029 06:21:55	$\Delta V =$	0 m/s							17.2		
			Apo-Man-E18		30-Oct-2029 00:14:13	$\Delta V =$	5.847 m/s							15.7		
		Europa19	I	05-Nov-2029 02:34:07	100	92.4	3.85	6.17	9.17	29.92	3	1	10.65	10.6	19.35	
			CU-Man-E19		08-Nov-2029 03:53:46	$\Delta V =$	2.465 m/s								3.1	
			Apo-Man-E19		10-Nov-2029 13:54:09	$\Delta V =$	0 m/s								2.4	
		Europa20	I	15-Nov-2029 18:02:04	100	97.7	3.85	8.73	9.22	25.39	5	2	8.88	17.7	19.70	
			CU-Man-E20		18-Nov-2029 19:32:54	$\Delta V =$	0 m/s								3.1	
			Apo-Man-E20		28-Nov-2029 13:38:02	$\Delta V =$	6.345 m/s								9.8	
		Europa21	I	03-Dec-2029 11:56:44	100	92.9	3.87	11.09	9.23	20.6	2	1	7.10	7.1	20.30	
			Apo-Man-E21		05-Dec-2029 16:04:02	$\Delta V =$	2.68 m/s								2.2	
			Europa22	I	10-Dec-2029 14:14:08	100	109.1	3.88	12.87	9.28	17.15	5	3	5.92	17.7	20.53
	CU-Man-E22		22-Dec-2029 11:06:26	$\Delta V =$	0 m/s									11.9		
		Apo-Man-E22		25-Dec-2029 10:07:17	$\Delta V =$	2.082 m/s								3.0		
		Europa23	I	28-Dec-2029 08:03:48	805.1	117.6	3.89	13.87	8.27	14.03	N	R	5.22	28.7	21.12	
Pi-transfers	CU-Man-E23		07-Jan-2030 20:29:36	$\Delta V =$	0 m/s								10.5			
	Apo-Man-E23		10-Jan-2030 11:09:44	$\Delta V =$	0 m/s								2.6			
	Ganymede24	O	26-Jan-2030 00:58:15	1346.7	-88.3	2.78	14.86	13.91	13.99	pi-tran		7.15	3.5	22.08		

Phase	Flyby/ Maneuver	In/ Out	Date	Altitude (km)	B-Plane Ang (deg)	V-Infinity (km/s)	Inc. (deg)	Peri. (R _J)	Apo. (R _J)	m	n	Period (days)	TOF (days)	Total TOF (months)
	CU-Man-G24		27-Jan-2030 13:36:44	$\Delta V =$	0 m/s								1.5	
	Ganymede25	O	29-Jan-2030 13:39:45	123.1	-2.7	2.79	11.93	12.64	17.3	1	1	7.11	7.1	22.20
	Apo-Man-G25		31-Jan-2030 14:18:35	$\Delta V =$	0 m/s								2.0	
	Ganymede26	O	05-Feb-2030 16:18:38	1584.7	-157.6	2.75	10.2	9.06	15.75	N	R	5.39	8.5	22.44
	Apo-Man-G26		06-Feb-2030 11:27:15	$\Delta V =$	0 m/s								0.8	
Europa Sub-Jovian Hemisphere Coverage	Europa27(e)	I	14-Feb-2030 04:41:04	100	-144.6	3.51	10.81	9.35	17.07	5	3	5.92	17.7	22.72
	CU-Man-E27		20-Feb-2030 08:02:04	$\Delta V =$	0 m/s								6.1	
	Apo-Man-E27		01-Mar-2030 05:07:30	$\Delta V =$	2.338 m/s								8.9	
	Europa28(e)	I	03-Mar-2030 22:40:57	100	166.1	3.50	9.63	9.43	20.41	2	1	7.10	7.1	23.31
	CU-Man-E28		07-Mar-2030 00:20:31	$\Delta V =$	1.92 m/s								3.1	
	Apo-Man-E28		08-Mar-2030 01:48:52	$\Delta V =$	0 m/s								1.1	
	Europa29(e)	I	11-Mar-2030 01:00:39	100	122.8	3.50	7.26	9.45	25.18	5	2	8.88	17.7	23.55
	CU-Man-E29		19-Mar-2030 22:37:34	$\Delta V =$	0 m/s								8.9	
	Apo-Man-E29		23-Mar-2030 19:59:29	$\Delta V =$	9.779 m/s								3.9	
	Europa30(e)	I	28-Mar-2030 18:58:34	100	112.4	3.50	4.52	9.42	29.67	3	1	10.65	10.6	24.14
Europa Sub-Jovian Hemisphere Coverage	CU-Man-E30		31-Mar-2030 19:59:29	$\Delta V =$	0 m/s								3.0	
	Apo-Man-E30		03-Apr-2030 03:11:29	$\Delta V =$	1.912 m/s								2.3	
	Europa31	O	08-Apr-2030 09:47:49	100	-135.6	3.48	6.56	9.39	25.25	5	2	8.88	17.8	24.49
	CU-Man-E31		17-Apr-2030 06:36:22	$\Delta V =$	0 m/s								8.9	
	Apo-Man-E31		21-Apr-2030 05:49:06	$\Delta V =$	5.931 m/s								4.0	
	Europa32	O	26-Apr-2030 04:12:11	100	89	3.50	3.51	9.38	29.71	3	1	10.65	10.6	25.09
	CU-Man-E32		29-Apr-2030 05:49:06	$\Delta V =$	7.373 m/s								3.1	
	Apo-Man-E32		01-May-2030 12:25:55	$\Delta V =$	0 m/s								2.3	
	Europa33	O	06-May-2030 19:02:35	25	-162.5	3.44	4.4	9.28	25.36	5	2	8.88	17.8	25.44
	CU-Man-E33		15-May-2030 15:19:14	$\Delta V =$	0 m/s								8.8	
Europa Sub-Jovian Hemisphere Coverage	Apo-Man-E33		19-May-2030 15:38:43	$\Delta V =$	11.098 m/s								4.0	
	Europa34	O	24-May-2030 13:26:26	601.8	45	3.47	2.52	9.34	29.78	3	1	10.65	10.6	26.03
	CU-Man-E34		27-May-2030 14:22:34	$\Delta V =$	0 m/s								3.0	
	Apo-Man-E34		29-May-2030 19:18:54	$\Delta V =$	10.07 m/s								2.2	
	Europa35	O	04-Jun-2030 04:55:10	100	113.6	3.49	0.47	9.32	29.66	N	R	10.58	10.3	26.39
	CU-Man-E35		07-Jun-2030 06:03:39	$\Delta V =$	0 m/s								3.0	
	Apo-Man-E35		09-Jun-2030 10:10:59	$\Delta V =$	13.642 m/s								2.2	
	Europa36	I	14-Jun-2030 13:13:38	100	111.6	3.48	3.47	9.31	29.79	3	1	10.65	10.7	26.73
	CU-Man-E36		17-Jun-2030 13:50:22	$\Delta V =$	0 m/s								3.0	
	Apo-Man-E36		20-Jun-2030 00:31:43	$\Delta V =$	3.714 m/s								2.4	

Phase	Flyby/ Maneuver	In/ Out	Date	Altitude (km)	B-Plane Ang (deg)	V-Infinity (km/s)	Inc. (deg)	Peri. (R _J)	Apo. (R _J)	m	n	Period (days)	TOF (days)	Total TOF (months)
	Europa37	I	25-Jun-2030 04:56:31	100	144	3.46	5.2	9.37	29.74	3	1	10.65	10.6	27.09
	<i>CU-Man-E37</i>		<i>28-Jun-2030 05:31:29</i>	$\Delta V =$	<i>0 m/s</i>								3.0	
	<i>Apo-Man-E37</i>		<i>30-Jun-2030 14:47:53</i>	$\Delta V =$	<i>9.232 m/s</i>								2.4	
	Europa38	I	05-Jul-2030 20:10:39	100	175.1	3.49	5.26	9.36	29.75	3	1	10.65	10.7	27.44
	<i>CU-Man-E38</i>		<i>08-Jul-2030 21:12:34</i>	$\Delta V =$	<i>0 m/s</i>								3.0	
	<i>Apo-Man-E38</i>		<i>11-Jul-2030 04:40:04</i>	$\Delta V =$	<i>2.909 m/s</i>								2.3	
	Europa39	O	16-Jul-2030 11:54:32	100	-147.6	3.49	3.52	9.33	29.76	3	1	10.65	10.6	27.80
	<i>CU-Man-E39</i>		<i>19-Jul-2030 12:53:40</i>	$\Delta V =$	<i>0 m/s</i>								3.0	
	<i>Apo-Man-E39</i>		<i>21-Jul-2030 18:49:52</i>	$\Delta V =$	<i>0.656 m/s</i>								2.2	
	Europa40	O	27-Jul-2030 02:56:52	25	-113.3	3.42	0.43	9.29	29.77	3	1	10.65	10.6	28.15
	<i>CU-Man-E40</i>		<i>30-Jul-2030 04:33:56</i>	$\Delta V =$	<i>0 m/s</i>								3.1	
	<i>Apo-Man-E40</i>		<i>01-Aug-2030 09:55:21</i>	$\Delta V =$	<i>0 m/s</i>								2.2	
	Europa41	O	06-Aug-2030 16:56:23	2661.5	-157.5	3.31	0.19	9.12	28.08	N	R	9.89	18.6	28.50
	<i>CU-Man-E41</i>		<i>09-Aug-2030 20:13:52</i>	$\Delta V =$	<i>0 m/s</i>								3.1	
	<i>Apo-Man-E41</i>		<i>11-Aug-2030 16:26:24</i>	$\Delta V =$	<i>0 m/s</i>								1.8	
Impact	Ganymede42	I	25-Aug-2030 06:48:55	100	17.8	5.77	-	-	-	-	-	-	-	29.12

B-plane = B-plane angle relative to the satellite's mean equator of epoch; V-infinity = Hyperbolic excess velocity; In/Out = inbound (I) or outbound (O) flyby; Inc., Peri., Apo., and Period = Spacecraft central body mean equator inclination, perijove, apojoive, and period after the encounter; m = Integer number of gravity-assist body orbits; n = Integer number of spacecraft orbits (NR=nonresonant transfer); TOF = time of flight; CU-Man = Postflyby cleanup maneuver; Apo-Man = Orbit shaping maneuver typically done near apojoive; e = Flyby in eclipse.

C.2.3.5.1 Jupiter Orbit Insertion and Energy Pump-Down

The purpose of the first mission phase is threefold: 1) insert into orbit around Jupiter, 2) reduce the spacecraft's energy relative to Jupiter, and 3) orient the spacecraft orbit such that the first set of Europa flybys has near-optimal relative velocity and lighting conditions for IPR, TI, and SWIRS observations (Figure C.2.3-4).

On the initial approach to Jupiter, the spacecraft will execute an inbound⁴ Ganymede gravity assist just prior to JOI. JOI, an 857-m/s maneuver, straddles the 12.8-Jovian-radii (R_J) perijove and puts the spacecraft into a 206-day period orbit. Near apojove of this first orbit, another large maneuver (PJR) is necessary to counter solar perturbations induced as a result of the spacecraft's large distance from Jupiter and to target an outbound⁵ Ganymede flyby. Four additional Ganymede flybys are then used to further pump-down the spacecraft's energy relative to Jupiter in order to reach the required hyperbolic excess velocity (V_∞) for the first Europa science campaign.

Lastly, since Europa is tidally locked (i.e., the prime meridian always faces towards Jupiter), the terrain illuminated by the Sun is simply a function of where Europa is in its orbit. By implementing a nonresonant G0–G1 transfer followed by three outbound resonant transfers, we can rotate the spacecraft's line of nodes clockwise such that the first set of Europa flybys will occur very near the Sun–Jupiter line (and hence Europa's anti-Jovian hemisphere will be well lit). This is necessary since visible wavelength stereo imaging must be done in unison with IPR measurements.

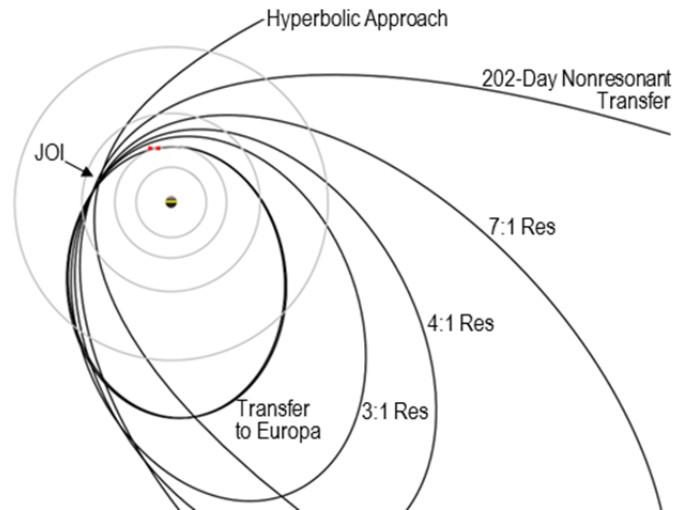


Figure C.2.3-4. View from Jupiter's north pole (Sun-fixed, towards top) of the pump-down phase of the 11-F5 trajectory. Black: spacecraft orbit; Gray: orbits of the four Galilean satellites.

C.2.3.5.2 Crank-over-the-Top

The mission design technique used to systematically cover a specific hemisphere of Europa is referred to as a crank-over-the-top (COT) sequence. This technique entails starting from an equatorial orbit, cranking the inclination up to the maximum⁶ (i_{max}) and then returning it to the equatorial plane via a set of resonant transfers. When starting from an inbound flyby, the COT sequence changes the flybys to outbound (transition occurs after i_{max} is reached, hence the term “over-the-top”), and vice versa when starting with outbound flybys. COT sequences starting from inbound flybys render coverage of the sub-Jovian hemisphere; COT sequences starting from outbound flybys cover the anti-Jovian hemisphere. The number of flybys—hence the density of groundtracks—for a given COT sequence is a function of spacecraft orbit period and its V_∞ relative to the gravity-assist body. Specifically,

- For a given period: The number of flybys increases/decreases as V_∞ increases/decreases.

⁴ Inbound flyby: Flyby that occurs prior to Jupiter perijove ($180^\circ < \text{spacecraft true anomaly} < 360^\circ$)

⁵ Outbound flyby: Flyby that occurs after Jupiter perijove ($0^\circ < \text{spacecraft true anomaly} < 180^\circ$)

⁶ Maximum inclination is a function of spacecraft period and the V_∞ relative to the gravity assist body.

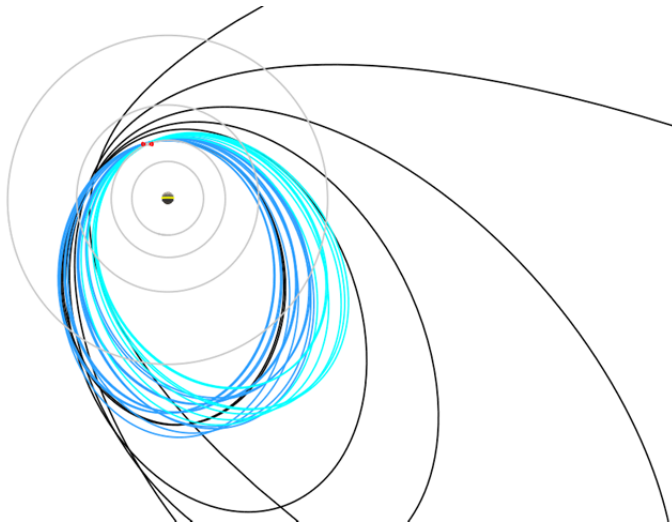


Figure C.2.3-5. View from Jupiter's north pole (Sun-fixed, towards top) of the anti-Jovian hemisphere coverage mission phase. Black: pump-down; blue: COT-1; cyan: COT-2; gray: orbits of the four Galilean satellites.

- For a given V_{∞} : The number of flybys increases/decreases as the spacecraft period decreases/increases.

Lastly, if the same period resonant transfers are used throughout a COT sequence (i.e., only cranking, no pumping), all closest approaches will lie very near the prime or 180° meridians (i.e., longitudinally 90° away from gravity-assist body's velocity vector). If different period resonant transfers are used during a COT sequence (i.e., cranking and pumping), the closest approach can be placed away from the prime or 180° meridians.

C.2.3.5.3 *Europa Science Campaign, Part I: Europa Anti-Jovian Hemisphere Coverage*

The first Europa science campaign focuses on Europa's anti-Jovian hemisphere (Figure C.2.3-5). This was done since it was more efficient (time, TID, and ΔV) to reach the proper lighting conditions—required by TI and SWIRS observations—on the anti-Jovian hemisphere given the Jupiter arrival conditions of the interplanetary trajectory. This strategy was also preferred by the SDT since IPR measure-

ments performed on Europa's anti-Jovian hemisphere yield a much higher S/N⁷.

To meet the science coverage requirements but also minimize the number of Europa flybys (and hence TID), the first COT sequence (COT-1) uses a combination of 4:1 ($T=14.3$ days) and 7:2 ($T=12.4$ days) resonant transfers with a V_{∞} of approximately 3.9 km/s. While alternating between the two resonances takes more time and leads to a higher TID (7:2 resonance has two perijove passages between Europa flybys), compared to using only 4:1 resonant transfers, it results in the closest approaches being pulled away from the 180° meridian enough to place a large portion of the groundtrack in the equatorial leading and trailing sectors (Figure C.2.3-6), as required for science coverage.

Once COT-1 is complete (which has changed the Europa flybys from outbound to inbound), a nonresonant Europa transfer is used to get back to an outbound flyby such that another COT sequence can be implemented to cover the anti-Jovian hemisphere of Europa. This nonresonant transfer also changes the local solar time (LST) of the Europa flybys by approximately half an hour (counter-clockwise away from the Sun–Jupiter line).

All flybys in COT-1 occur at the ascending node. COT-2 (using strictly 4:1 resonant transfers) instead cranks in the opposite direction, placing the flybys at the descending node. This results in the COT-2 groundtracks intersecting the COT-1 sequence groundtracks (instead of running nearly parallel), hence fulfilling the IPR requirements in all seven anti-Jovian hemisphere sectors to have groundtracks with intersections (Figure C.2.3-7).

⁷ Jupiter is a radio source in the operating spectrum of the IPR instrument. Hence, IPR measurements done on the hemisphere of Europa shielded from Jupiter render a higher S/N.

⁸ Variations in V_{∞} occur due to Europa's eccentricity and apsidal precession.

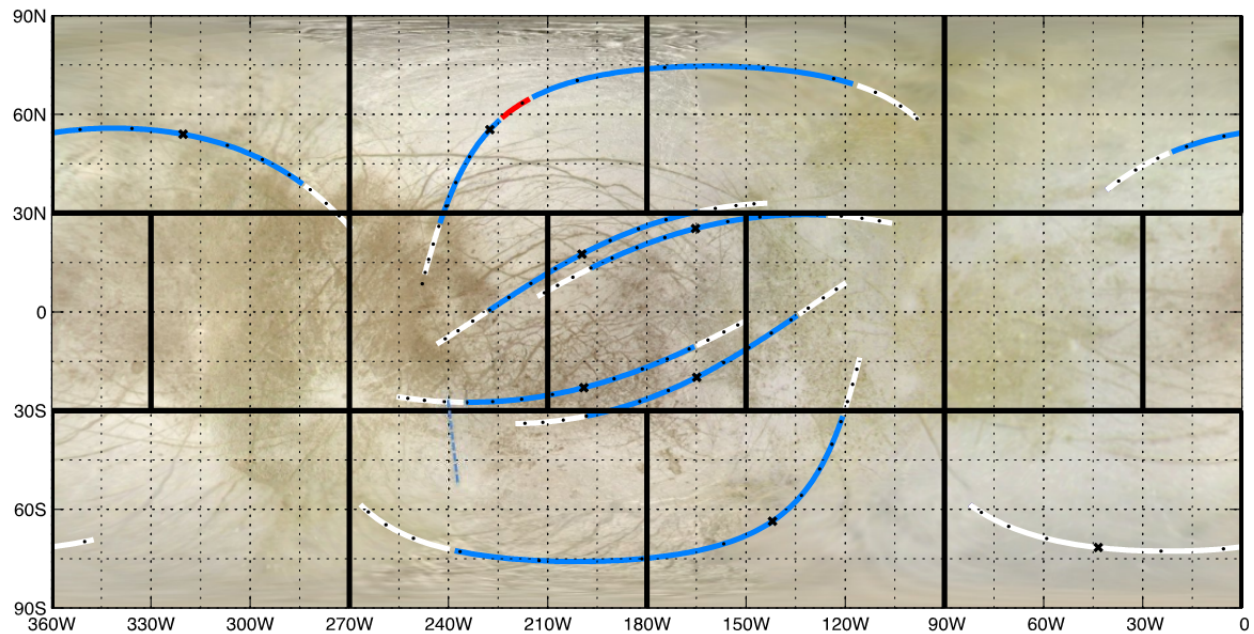


Figure C.2.3-6. Europa nadir groundtrack for COT-1. Closest approach is marked with an “x” and numbered in accordance with Table C.2.3-4. Red: $0 < alt \leq 25$ km; blue: $25 < alt < 400$ km; white: $400 < alt < 1,000$ km.

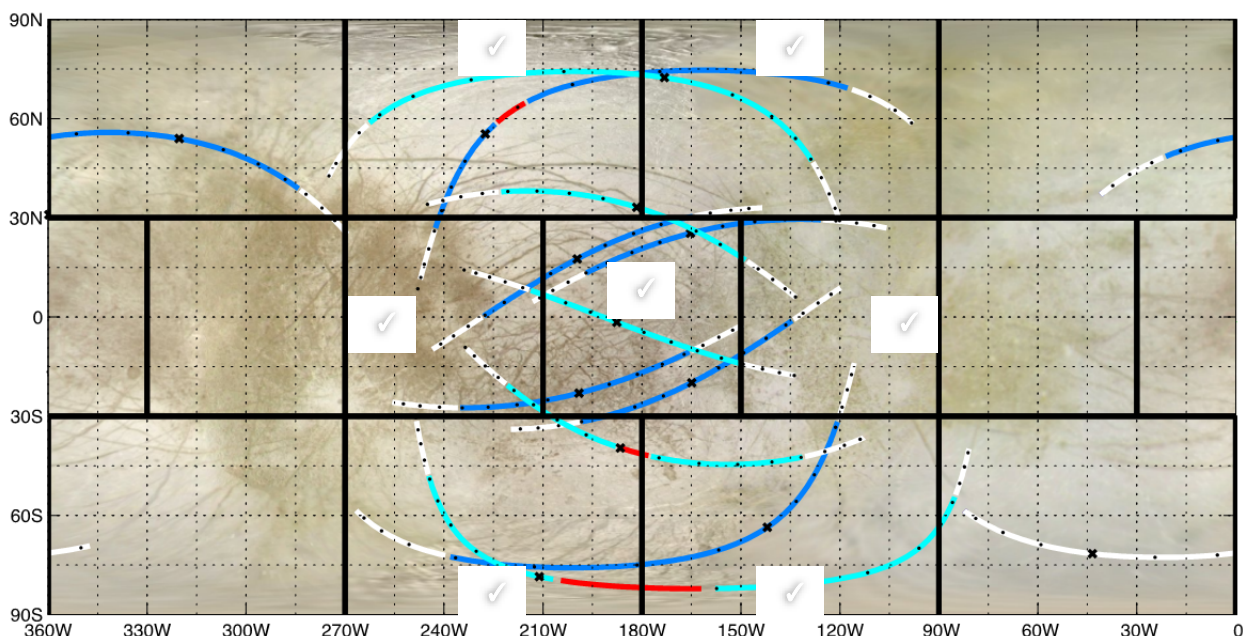


Figure C.2.3-7. Europa nadir groundtrack plot with COT-1 and COT-2. Green check marks indicate IPR requirements are met in specified sector. Closest approach is marked with an “x” and numbered in accordance with Table C.2.3-4. Red: $0 < alt \leq 25$ km; blue (COT-1) and cyan (COT-2): $25 < alt < 400$ km; white: $400 < alt < 1,000$ km.

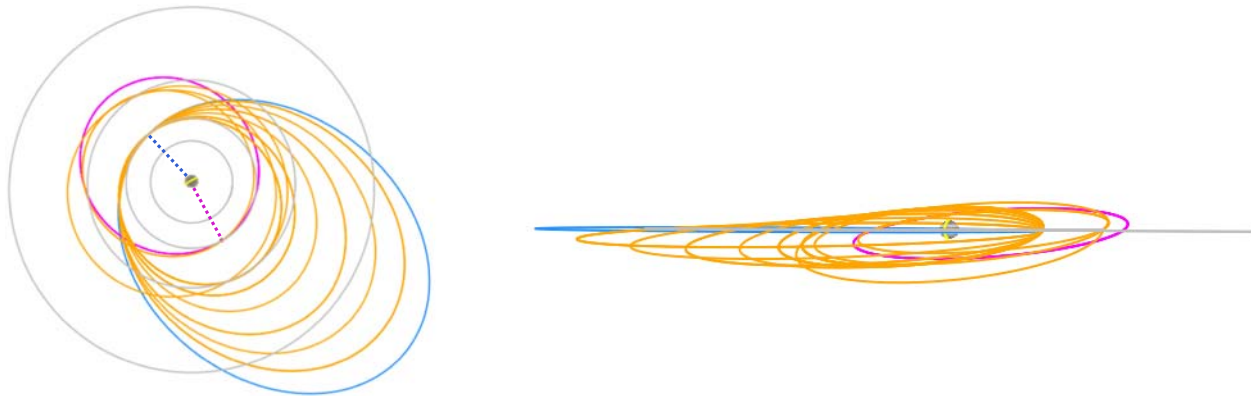


Figure C.2.3-8. “Switch-flip” method used to change the Europa lighting conditions by $\sim 180^\circ$. Dashed lines indicate locations of the Europa flybys before (blue) and after (magenta) the switch-flip. Blue: Last COT-2 orbit; orange: switch-flip sequence; magenta: first COT-3 orbit. Left: View from Jupiter’s north pole (Sun-fixed, towards top). Right: View from Jupiter’s equatorial plane, north pole towards top of the page.

C.2.3.5.4 Lighting Condition Change

Again, since visible wavelength stereo imaging must be done in unison with IPR measurements, it’s necessary to change the observation lighting conditions by 180° prior to taking IPR data on Europa’s sub-Jovian hemisphere. That is, the location of the Europa flybys needs to be moved to the opposite side of Jupiter so that Europa’s sub-Jovian hemisphere is well lit. Three different strategies can be implemented to accomplish this, using

1. Primarily nonresonant Callisto and/or Ganymede transfers
2. Only nonresonant Europa transfers
3. A “switch-flip” (Europa-to-Ganymede pi-transfer⁹ \rightarrow Ganymede pi-transfer \rightarrow Ganymede-to-Europa pi-transfer)

Each has its advantage. Option 1 will have the longest time of flight (TOF) but the lowest TID since perijove will be above Europa’s orbit radius the majority of the time. Option 2 will have the highest TID but will stay at Europa the entire time providing opportunities for continuous Europa observations over a wide range of geometries. Option 3 provides by far

⁹ A nonresonant transfer (typically inclined) in which two successive flybys are separated by 180° (or π -radians) in true anomaly (i.e., flybys occur on the opposite sides Jupiter).

the fastest way to get from one side of Jupiter to the other, but does have a fairly high TID (although not as high as Option 2).

For this study, the switch-flip option was employed due to its time efficiency (Figure C.2.3-8). The detailed sequence of events includes first cranking up the inclination and pumping down the orbit period to set up the correct geometry for a Europa-to-Ganymede transfer. A Ganymede pi-transfer is then executed (3.5-day TOF), followed by a 1:1 resonant Ganymede transfer that cranks down the inclination and sets up the Ganymede-to-Europa pi-transfer. The result: All subsequent Europa flybys are located $\sim 180^\circ$ away from the last Europa flyby in COT-2.

It should be noted that either Option 1 or 2 could instead be seamlessly added to the end of the 11-F5 COT-2 sequence.

C.2.3.5.5 Europa Science Campaign, Part II: Europa Sub-Jovian Hemisphere Coverage

The second Europa science campaign focuses on Europa’s sub-Jovian hemisphere. Immediately following the Ganymede-to-Europa transfer, Europa flybys are used to pump-up the orbit and crank-over-the-top. Like COT-1, the goal of COT-3 is to minimize the number of flybys while still providing adequate coverage for science. However, since the V_∞ is

~3.5 km/s (instead of 3.9 km/s in COT-1), the COT-3 sequence must alternate between 3:1 ($T=10.7$ days) and 5:2 ($T=8.8$ days) resonant transfers to accomplish this. Lastly the first four Europa flybys in COT-3 (Europa27 [E27] to Europa30 [E30]), are in Jupiter's shadow; hence no stereo imaging can be performed in unison with IPR measurement (see Figure C.2.3-9).

Once COT-3 is complete, a nonresonant Europa transfer is used to get back to an inbound flyby such that another COT sequence can be implemented to cover Europa's sub-Jovian hemisphere. This nonresonant transfer also changes the LST of the Europa flybys by approximately one hour (clockwise away from the Sun–Jupiter line).

Finally, COT-4 cranks in the opposite direction from COT-3 (i.e., switches the node at the Europa flybys from descending to ascending) with 3:1 resonant transfers to intersect the COT-3 sequence groundtracks, fulfilling the IPR requirements in six of the seven sub-Jovian hemisphere sectors (Figure C.2.3-10).

At the conclusion of COT-4, 13 of the 14 sectors have been covered sufficiently to meet the observational and measurement requirements of all four instruments on board as defined by the SDT (Figure C.2.3-10).

C.2.3.6 Navigational Feasibility

The 11-F5 trajectory (Figure C.2.3-11) is a proof-of-concept trajectory establishing the potential for a Europa Multiple-Flyby Mission that accomplishes high-quality scientific observations and measurements to significantly advance our knowledge of one of the most scientifically intriguing targets in our solar system. To prove we can—with a very high level of confidence—navigate the 11-F5 trajectory (or something similar) in the Jupiter system would require a high-fidelity covariance analysis, a task beyond the scope of the study. However, we can make a preliminary assessment of the 11-F5 trajectory by analyzing key mission events and comparing them to Cassini,

the most complicated gravity-assist trajectory ever flown.

Due to the distance from Earth of deep space missions, the spatial and temporal proximity of key/critical events (i.e., operational intensity) are among the most important factors in determining operational feasibility. In terms of navigation, analysis can be focused on two types of events, targeted flybys and propulsive maneuvers.

C.2.3.6.1 Targeted Flybys

A sufficient amount of time is required between successive targeted flybys to accurately determine the spacecraft's orbit after the first flyby, as well as design, uplink, and perform a series of maneuvers to target the subsequent flyby. This places a lower bound on the TOF between targeted encounters.

The delivery accuracy for a given targeted flyby is primarily a function of the spacecraft trajectory uncertainties, as well as the ephemeris uncertainties of the bodies in the system the spacecraft resides in (especially the targeted flyby body). The delivery accuracy for a given flyby directly affects the ΔV costs (i.e., how much propellant is required to cleanup flyby misses) and the minimum allowable flyby altitude of a body (probability of impact must be nil after the last maneuver to target the flyby has been executed). As the spacecraft and system uncertainties decrease—as knowledge of the system is gained via radiometric tracking data—so too does the minimum TOF between targeted flybys and the minimum flyby altitude. As such, the 11-F5 trajectory adheres to a two-prong strategy:

- 1) Temporally ratchet down minimum flyby altitudes (paying particular attention to the first encounter of each body).
- 2) Slowly decrease the average TOF between flybys.

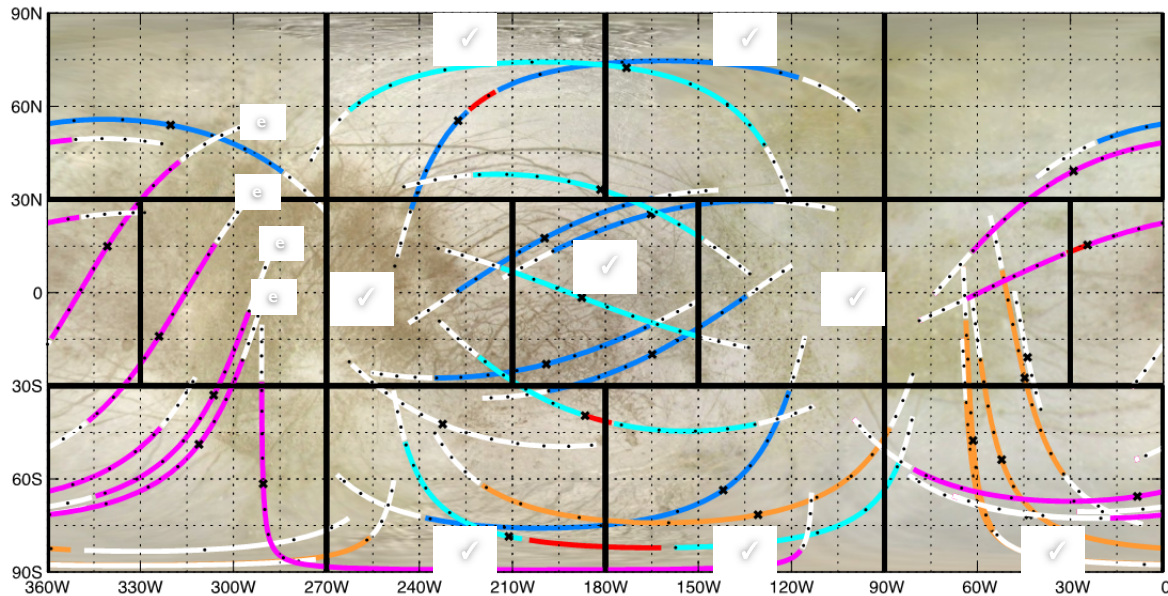


Figure C.2.3-9. Europa nadir groundtrack plot for COT-1 through COT-3. Green check marks indicate IPR requirements are met in specified sector. Red circles with “e” indicate flybys in eclipse. Closest approach is marked with an “x” and numbered in accordance with Table C.2.3-4. Red: $0 < \text{alt} \leq 25$ km; blue (COT-1), cyan (COT-2), orange (change lighting), and magenta (COT-3): $25 < \text{alt} < 400$ km; white: $400 < \text{alt} < 1,000$ km.

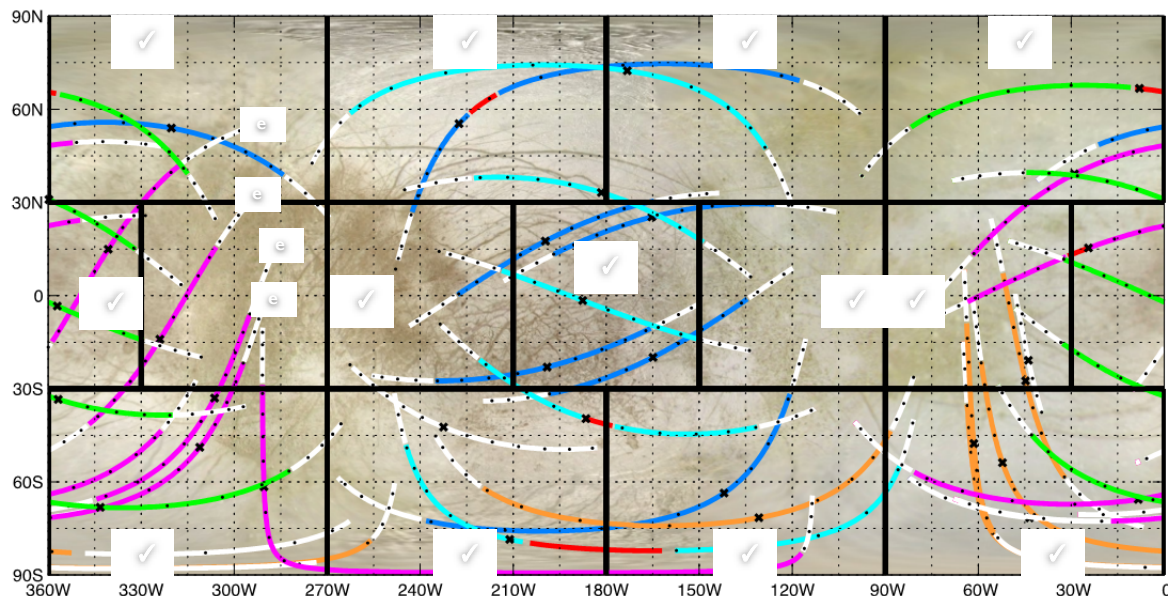


Figure C.2.3-10. Europa nadir groundtrack plot for entire 11-F5 baseline trajectory. Green check marks indicate IPR requirements are met in specified sector. Red circles with “e” indicate flybys in eclipse. Closest approach is marked with an “x” and numbered in accordance with Table C.2.3-4. Red: $0 < \text{alt} \leq 25$ km; blue (COT-1), cyan (COT-2), orange (switch-flip), magenta (COT-3), and green (COT-4): $25 < \text{alt} < 400$ km; white: $400 < \text{alt} < 1,000$ km.

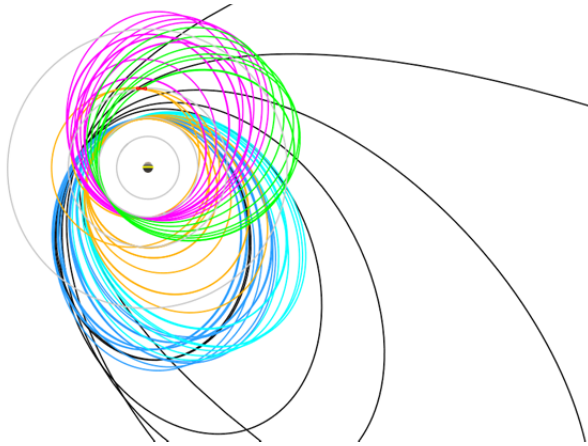


Figure C.2.3-11. View from Jupiter's north pole (Sun-fixed, towards top) of the 11-F5 baseline trajectory. Black: pump-down; blue: COT-1; cyan: COT-2; orange: switch-flip; magenta: COT-3; green COT-4; gray: orbits of the four Galilean satellites.

The first portion of the strategy is implemented by targeting the first Ganymede and Europa flybys to altitudes (500 and 724 km, respectively, as in Table C.2.3-4). These are relatively high when compared to minimum flyby altitudes executed by Galileo. Subsequent flybys of each body decrease uncertainties, and hence allow lower flybys to be carried out. Notice that all 25 km Europa flybys (done to maximize the quality of INMS measurements) will be performed at the end of COT sequences, where numerous 100 km flybys will have been completed and Europa's ephemeris will have become well known (at the particular LST the COT sequence occurs at). Lastly, it should be noted that since Ganymede and Europa are in a 2:4 orbital resonance, the first five Ganymede flybys (G0-G4) will provide knowledge of Europa's dynamics, thereby decreasing Europa's ephemeris uncertainties prior to the first Europa flyby.

The second portion of the strategy will be implemented by beginning with alternating 4:1 (TOF=14.2 days) and 7:2 (TOF=24.88 day) resonant transfers in the first COT sequence (COT-1). This oscillation in resonance transfers lessens the navigation intensity by interleaving longer-TOF multirevolution resonant

transfers between each shorter 4:1 resonant transfer, and results in a mean TOF/encounter equal to 19.5 days.

With decreased Europa ephemeris uncertainties, a 14.4-day non-resonant transfer will be followed by COT-2, consisting of five back-to-back 4:1 resonant transfers, translating to a mean TOF/encounter of 14.2 days.

The pump-down and pi-transfer phases of the tour continue the downward average TOF/encounter trend, namely a decrease to 14 days. Of notable interest is the 3.5-day Ganymede-to-Ganymede pi-transfer. This transfer was implemented to minimize total tour TOF and is believed to be navigationally feasible based on the ballistic nature of the transfer (i.e., no deterministic maneuvers) and the high altitude of the first Ganymede flyby (G24, 1,346 km), which will decrease the ΔV sensitivity of a flyby miss. The later characteristic will minimize the magnitude of the G24 cleanup maneuver, which is important since there will only be time for a single maneuver. For comparison, Cassini successfully executed an 8-day Titan pi-transfer in 2009. This transfer was also designed to be ballistic; in operations a single maneuver was executed with a magnitude of 0.75 m/s. If however the current baseline 3.5-day Ganymede pi-transfer is ultimately deemed too aggressive, a 3-, 5-, or 7-pi-transfer (i.e., TOFs of 10.5, 14, or 17.5 days, respectively) could be utilized instead.

COT-3 and COT-4 will proceed to further reduce the TOF/encounter, with values of 13.75 and 11.95, respectively. The former will use the same alternating resonance strategy as COT-1 (only this time with 3:1 [TOF=10.65 days] and 5:2 [TOF=25.44 days] resonances), and the latter will implement five back-to-back 3:1 resonant transfers.

As a reference, Cassini performed nine back-to-back 1:1 resonant transfers with Titan (15.9-day TOF) under much more dynamic

Table C.2.3-5. 11-F5 flyby ΔV summary.

Activity	CBE ΔV (m/s)	MEV ΔV (m/s)	Comments
Launch Injection Cleanup	20	20	Estimate to correct injection errors from launch vehicle.
Earth Bias ΔV	50	50	Needed for final correction of deliberate aim-point bias away from the Earth. ~25 m/s per Earth flyby. May be performed separately or integrated with other TCMs.
Deep Space Maneuver (DSM)	0–100	150	Maneuver on Earth–Earth leg near aphelion. Baseline launch period variation goes from 0 m/s up to 100 m/s.
Interplanetary Statistical & ΔV Cleanup	50	50	Multiple small maneuvers.
JOI at 12.8 R _J , 500-km G0 Flyby	857	900	200-day initial orbit.
Perijove Raise Maneuver	114	135	Counteracts solar perturbations, targets G1 flyby.
Tour Deterministic ΔV	157	200	Used primarily for targeting many resonant transfers.
Tour Statistical ΔV	63	170	~5 m/s per flyby for first 20 flybys, then 3 m/s for last 22 flybys (conservative). Rounded up. Expected average per-flyby values: 1.5 m/s per flyby
TOTALS	1311*	1675	

*Assumes maximum DSM value

conditions (12–63° inclination and much closer central body periapses) and higher ΔV loads¹⁰.

C.2.3.6.2 Maneuvers

Throughout a mission's lifetime, numerous deterministic maneuvers are required to shape the trajectory, and numerous statistical maneuvers are necessary to correct trajectory errors due to a number of sources. In the case of the 11-F5 trajectory, maneuver locations were generally placed 3 days after each flyby to cleanup any flyby errors, and near apoJove to target the subsequent flyby (where timing permitted). Due to time constraints associated with this study, the maneuvers have not yet been placed for optimal navigation robustness (i.e., provide time for apoJove backup maneuver locations prior to the targeted flyby). However, all transfers in the 11-F5 trajectory have, at most, only one maneuver with a deterministic component. In addition, the trajectory has very comfortable ΔV margins. These facts make future adjustments to maneuver locations of no foreseeable concern (based on extensive design experience on Cassini's prime and two extended missions).

C.2.3.6.3 Overall Flexibility

The proposed 11-F5-like trajectory will push the envelope of navigational complexity, but will do so in a very strategic manner. However, if future analysis reveals any portion of the trajectory is navigationally infeasible, or stresses the system in other ways, such as fault recovery time, many trajectory design options exist. As previously mentioned, phasing orbits can be inserted to lengthen the 3.5-day-TOF transfer, and other "lighting condition change" options can be implemented, whether it's the alternate options detailed in Section C.2.3.5.4 or a different switch-flip sequence to obtain a higher V_∞ at Europa, so the COT-3 and COT-4 sequences maintain a high average TOF between flybys.

C.2.3.7 Mission ΔV

Table C.2.3-5 summarizes both the estimated current best estimate (CBE) and maximum expected value (MEV) for the total ΔV needed to execute the Europa Multiple-Flyby mission. The two totals are comprised of both computed values (DSM, JOI, PJR and the tour's deterministic ΔV) and estimated values (launch injection cleanup, Earth bias ΔV , interplanetary statistical ΔV and tour's statistical ΔV).

¹⁰ Cassini's average ΔV budget was ~100 m/s per year during the Prime and Equinox missions.

The 11-F5 trajectory is a fully integrated trajectory from launch to end of mission in a high-fidelity force model including n -body perturbations. As such, high confidence can be placed on all computed ΔV components.

Statistical ΔV estimates are ultimately computed via a high-fidelity covariance analysis in unison with Monte Carlo simulations. Because this analysis is outside the scope of the Europa Study, the statistical ΔV s for this report were estimates based on previous operational experience with Cassini and Galileo.

See the Mass Margin Summary (Section C.2.4.7.1) for calculations of propellant loading based on ΔV and thruster usage.

C.2.3.8 Potential Extended Mission(s)

Given a healthy Europa Multiple-Flyby Mission spacecraft with demonstrable radiation margin at the end of the prime mission (and the necessary authorization, of course), a variety of different extended missions are possible from an orbital mechanics point of view. They include, but are not limited to

- Higher density core science observations (i.e., cover greater variety of terrain with higher frequency)
- New Europa campaigns:
 - Gravity/tides investigation
 - Regional mapping of the leading and trailing hemispheres
- Regional global-coverage missions at Ganymede, Callisto, or both
- Europa, Ganymede or Callisto orbit (if sufficient propellant is available)

C.2.3.9 Spacecraft Disposal

Planetary protection may require that, before control of the spacecraft is lost, action is taken to minimize the probability of biological contamination of Jupiter's moon Europa resulting from spacecraft impact. To preclude Europa impact, the study team chose Ganymede impact as the baseline spacecraft disposal scenario. This disposal scenario was chosen simply

because it was the transfer with the lowest TOF (post Europa-41) that resulted in impact. Many additional potential spacecraft disposal options exist that avoid collision with Europa, including (but not limited to) the following:

- Jovian system impacting trajectories:
 - Jupiter (via short- or long-period orbits, the latter using solar perturbations)
 - Io, Ganymede, or Callisto
- Long-term Jupiter-centered orbits:
 - Circular orbit between Ganymede and Callisto
 - Eccentric orbit outside of Callisto
- Jupiter system escape:
 - Heliocentric orbit
 - Saturn flyby, impactor, or potentially even capture
 - Icy-giant flyby or impactor
 - Trojan asteroid flyby or impactor

While theoretically all of these options are possible, numerical verification would need to be carried out to prove the existence (particularly the gas- and icy-giant flyby/impact trajectories) and quantify the TOF and associated ΔV costs of each.

C.2.4 Flight System Design and Development

The flyby flight system is a highly capable spacecraft tailored to the flyby science objectives of agile pointing, large data storage, and large data transmission.

C.2.4.1 Flight System Overview

The Europa Multiple-Flyby Mission flight system (FS) concept, pictured in Figure C.2.4-1, is a three-axis-stabilized spacecraft with three distinct modules arranged along the Z (vertical) axis from top to bottom.

The Avionics Module is dominated by the 3-meter high-gain antenna (HGA) on top of the UES along the +Z axis. This module also includes the science payload consisting of four instruments mounted beneath the HGA. Avionics and instrument electronics are carried in

an internal radiation vault descending into the core.

The Propulsion Module lies centrally, surrounding the electronics vault, with the main rocket engine at the bottom, directed along the $-Z$ axis. Tanks and the outrigger-mounted control thruster are at mid-span.

The ASRGs for power generation are mounted symmetrically about the main engine as part of the Power Source Module, which also includes the launch adapter.

These three modules are discussed in more detail below.

Instruments

The FS is configured to support the notional model payload described above, consisting of the following science instruments:

- Topographical Imager (TI)
- Shortwave Infrared Spectrometer (SWIRS)
- Ice-Penetrating Radar (IPR)
- Ion and Neutral Mass Spectrometer (INMS)

The TI, SWIRS, and IPR are coboresighted and configured for nadir-pointing during the close flyby of Europa. The INMS is configured to nominally point in the velocity vector direction during the flyby, roughly perpendicular to the nadir direction.

Attitude Control

The flyby spacecraft is three-axis-stabilized in all phases of flight. Stabilization is achieved through the use of inertial measurement and star measurement for attitude determination and thrusters or reaction wheels for attitude control.

Data Handling

During each flyby over 32 Gbits of data are generated by the instruments and engineering subsystems. This data can be stored multiple times in a large, redundant, solid-state data recorder (256 Gbits in total; 128 Gbits per card) that is part of the Command and Data

Handling Subsystem (C&DH). Concepts for data integrity using the excess storage capability will be studied during Phase A.

Power

The proposed power source for this spacecraft is four ASRGs. The power system is sized to accommodate one failure (mechanical or electrical) of an ASRG. Excess power is stored in the 59-A-hr lithium-ion battery or dumped as heat through a thermal shunt. For mission activities that are not power-positive, a positive energy margin is obtained by using the battery, which has been sized accordingly.

Thermal

To minimize the power demand of the spacecraft (because we desire to minimize the number of ASRGs), the spacecraft was designed to minimize the use of electrical heaters. To achieve this goal, the heat from spacecraft electronics is captured inside a thermal shroud surrounding the midsection. This allows the propellant to be kept near room temperature without the need for supplemental electrical heaters. The concept also includes 30 radioisotope heater units (RHUs) and/or variable RHUs (VRHUs), which will be used in select locations (e.g., thruster cluster assemblies) to minimize the need for electrical heaters.

Communications

The Communications Subsystem is designed to support the high volume of science data to be transmitted back to Earth after each flyby. This system consists of X-band downlink for low-data-rate telemetry, and Ka-band downlink using a 3-meter HGA for high-data-rate telemetry (including the science data collected during the flyby). X-band uplink is used for commands.

Propulsion

The Propulsion Subsystem must support attitude control, momentum management, trajectory correction, and Jupiter Orbit Insertion (JOI). To achieve these requirements the Pro-

pulsion Subsystem is a dual-mode, bipropellant architecture. The fuel, oxidizer, pressurant tanks, and supporting structure are distributed around the core of the spacecraft to provide radiation shielding to the internal electronics. During Phase A, a risk assessment will be performed on potential micrometeoroid damage to the tanks; if necessary, the thermal shroud can be upgraded with standoff Whipple bumper shields. The tanks are sized for maximum propellant for spacecraft on the Atlas 551 and can support up to 1.68 km/s of ΔV . The actuators consist of one 458-N main engine, four thrust vector control (TVC) thrusters, and sixteen attitude-control thrusters (eight primary, eight redundant) arranged in four clusters, each thruster cluster assembly (TCA) containing four attitude-control thrusters and one TVC thruster.

Redundancy

The spacecraft uses a redundancy philosophy similar to that of Cassini and comparable systems, where most active elements are redundant, with selected cross-strapping, and where the instruments are single-string. The main engine and TVC are also single-string; these single-string elements will undergo a risk assessment in Phase A to determine if the risk is acceptable. There is sufficient mass margin to accommodate dual redundancy here, if appropriate.

Radiation

This mission has a very demanding total ionizing dose (2.01 Mrad behind an equivalent of 100 mil Al Si), mostly from electrons). To support the use of standard aerospace EEE parts, we have employed a multilayered radiation shielding approach as part of the spacecraft design concept. Most of the spacecraft electronics are housed in a radiation vault (similar to that on the Juno spacecraft); this vault is also located inside the spacecraft to benefit from shielding provided by other spacecraft elements, such as the batteries, structure, and tanks. Inside the vault the end of

mission TID environment is 150 krad, with boards nearer the center encountering even less. Electronics will be tolerant to at least 300 krads, for a radiation design factor of 2 or better.

C.2.4.1.1 Flight System Configuration

The engineering configuration of the spacecraft concept is shown in Figure C.2.4-1. On the left side of the figure is the CAD model without the thermal shroud and with instruments stowed. On the right side of the figure is a cross-sectional view.

Avionics Module

The 3-meter HGA is at the top of the Avionics Module. Co-located on this structure is the medium-gain antenna (MGA) and one of three low-gain antennas (LGAs). Below the HGA is the UES. This holds the instruments, reaction wheels, and star-trackers. At the bottom of the Avionics Module is the avionics vault. Inside the vault is a majority of the spacecraft avionics, which is nested within the Propulsion Module to maximize the radiation shielding from the tanks, structure, and propellant. The Avionics Module attaches to the Propulsion Module. The equipment in the vault is accessible throughout integration and testing of the Avionics Module, while the equipment in the UES is accessible throughout integration and testing of the spacecraft as a whole. After spacecraft integration, a demate operation from the Propulsion Module will enable access to the vault.

Propulsion Module

The Propulsion Module is an integrated structure with all the tanks (fuel, oxidizer, pressurant), plumbing, pressurization control assembly (valves, filters, sensors, etc.), propellant isolation assembly (valves, filters, sensors, etc.), the thrusters mounted on four thruster clusters, and main engine mounted at the bottom of the module.

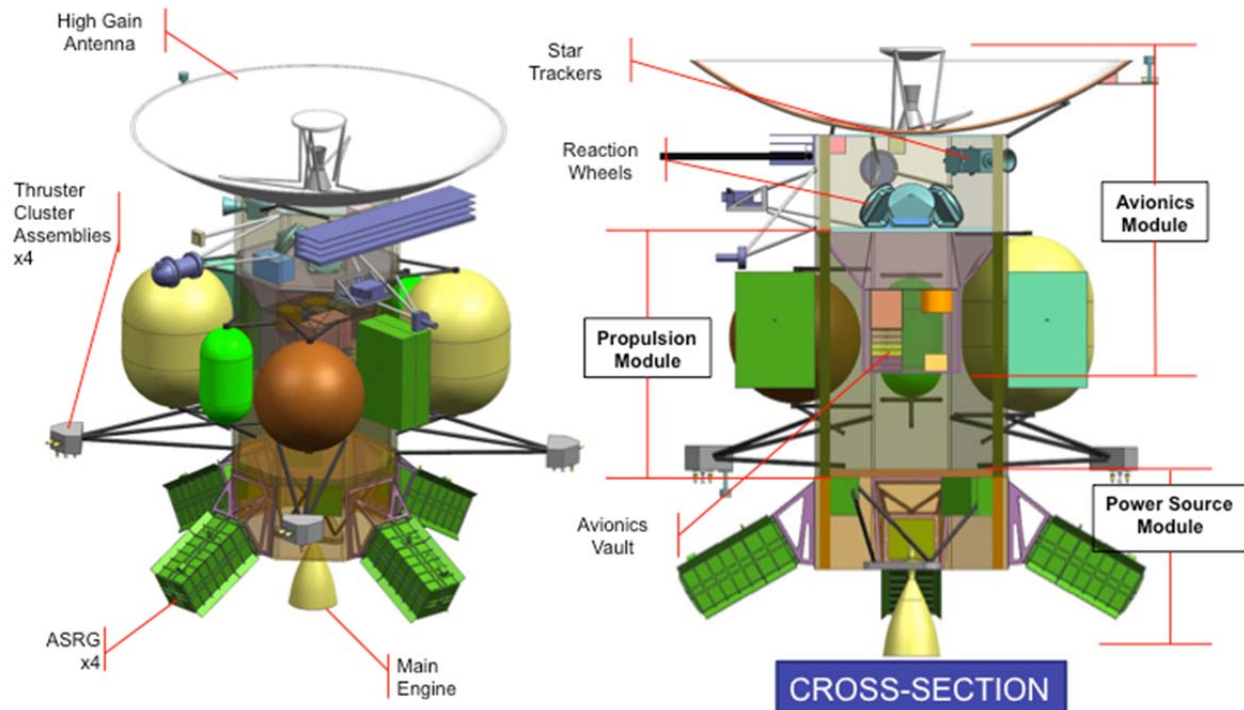


Figure C.2.4-1. The modular configuration shown provides maximum radiation shielding for the electronics (thermal shroud is not shown).

Power Source Module

The Power Source Module is an integrated structure with the launch vehicle adapter and ASRGs. The ASRG consists of the power sources, mounted externally, and their control electronics, located further inboard.

Thermal Shroud and Shading

The thermal shroud covers most of the spacecraft including parts of all three modules. Figure C.2.4-2 shows the spacecraft (with the 15-m IPR antenna deployed) enveloped by the thermal shroud, shown semi-transparently around the midsection. The bottom view shows how the HGA and thermal shroud protect the spacecraft from the high solar flux during the Venus flyby portion of the interplanetary cruise. Besides the HGA, the few elements exposed to the solar flux are the LGA, thruster clusters, and INMS (with cover). These elements can tolerate heating during the flyby without shading.

C.2.4.1.2 System Block Diagram

Figure C.2.4-3 shows the system block diagram for the flyby spacecraft. The top box is the Avionics Module. The middle box is the Propulsion Module. The bottom box is the Power Source Module. Note items like electrical heaters and temperature sensors are distributed across all the modules. The legend shows the key interface types between elements.

Note that some of the boxes in the block diagram (e.g., C&DH) do not show redundancy because they are internally redundant in configurations not yet determined.

C.2.4.1.3 Flight System Key Requirements

Table C.2.4-1 shows the key drivers on the FS from the science measurements. Two bands of measurement data from the IPR must be captured and processed. During the 15 minutes of data collection per flyby, nadir-pointing and low pointing jitter is required from GN&C.

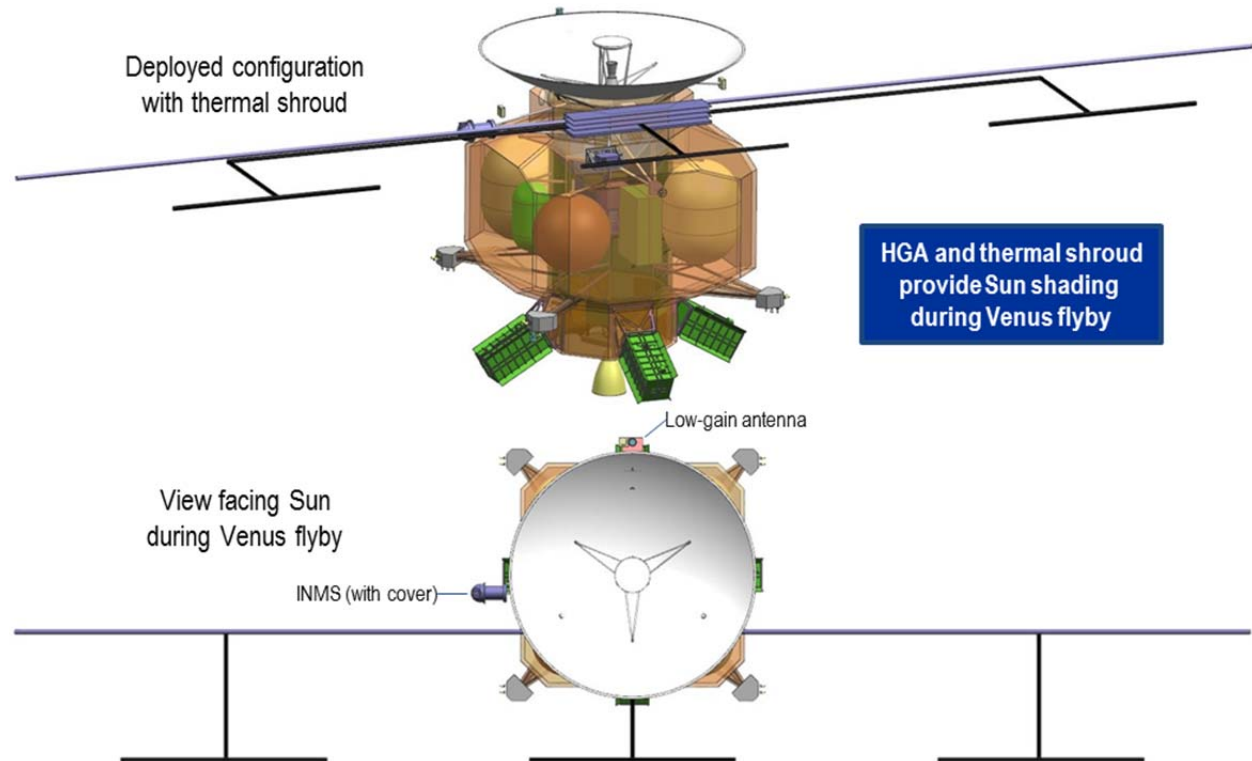


Figure C.2.4-2. The flight system provides thermal balance throughout all mission phases.

The 25 Gbit collected per Europa flyby is a driver on the solid-state recorder (SSR) size. It also drives sizing of the Telecom Subsystem for Ka-band downlink of the radar data. The need to process the radar data after collection but before downlinking drives the throughput capacity of the onboard computer. The 15-meter IPR antenna is required is stowed to fit within the launch vehicle faring at launch, and is deployed after separation from the launch vehicle.

Image resolution of the TI drives low pointing jitter capability from GN&C during nadir-pointing. Stereo imagery during the flyby adds several gigabits of science data and is a driver on the SSR size. The imager must be aligned with the IPR, and it needs a contamination cover that can be deployed after launch.

SWIRS is also aligned with the IPR and TI. Its integration time drives target motion compensation and pointing jitter drivers on GN&C. Its data volume over a 10-hour flyby is several Gbits, driving the SSR size. Finally, its ther-

mal radiator needs an unobstructed view of space during operation.

The INMS aperture must be aligned to the velocity vector during the Europa flyby. It also needs a contamination cover that can be deployed after the Venus flyby.

All brackets, struts, secondary structures, and mechanisms are mechanically grounded to the primary structure. Loads for these appendages are determined using the Atlas V mass acceleration curve.

The power demand of IPR, SWIRS and INMS together forms one of the sizing cases for the battery (JOI is the other)

Table C.2.4-2 shows the key drivers that flow down to the FS from the mission design.

The Venus flyby is a driver for the spacecraft thermal design. This has been addressed by configuring the spacecraft such that the HGA and a thermal shroud can shade the rest of the vehicle.

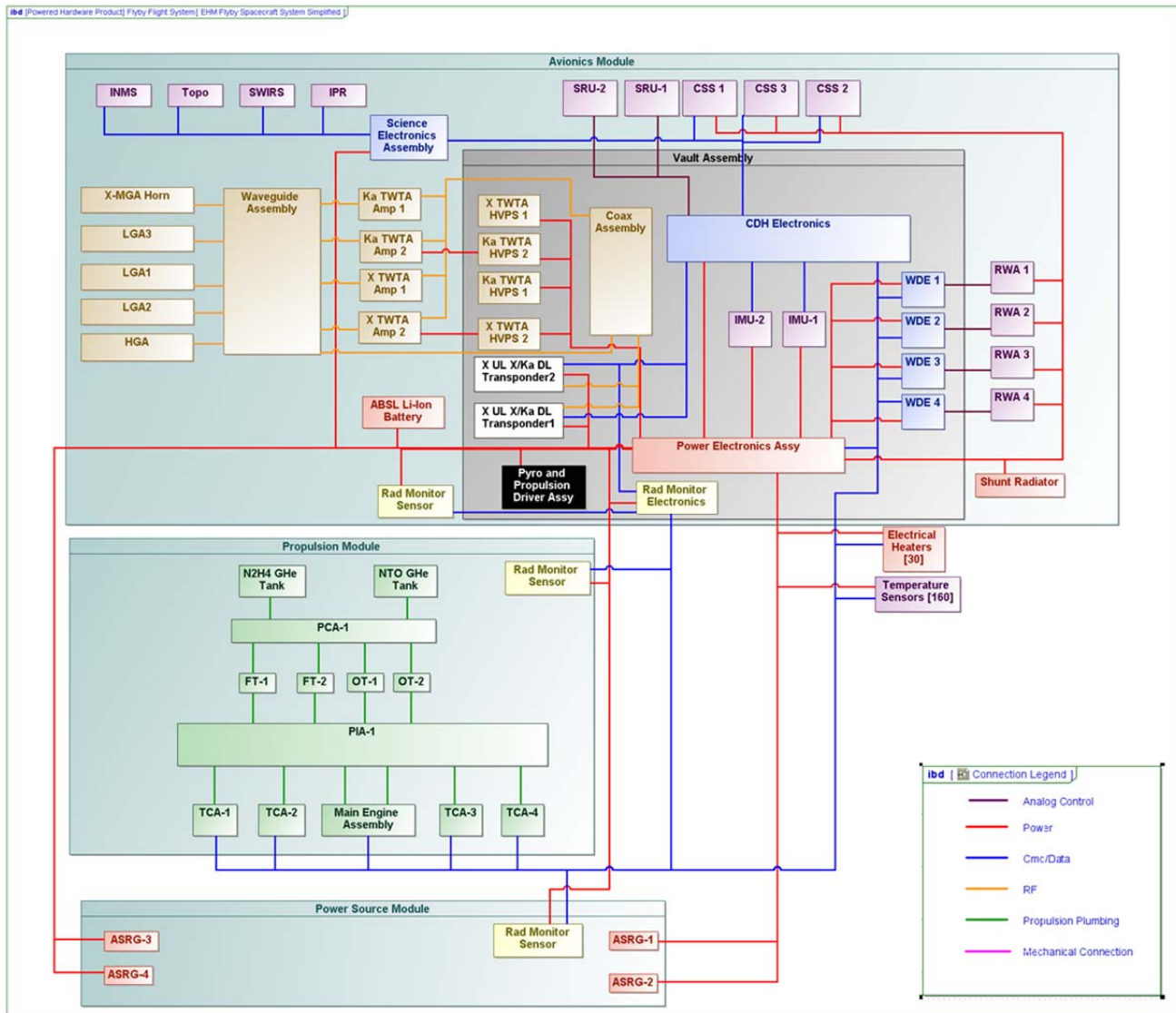


Figure C.2.4-3. The system block diagram shows the simple interfaces among modules on the spacecraft.

During inner solar system cruise, while the HGA must be pointed at the Sun for shading, geometric constraints on telecommunication has been addressed with an X-band system for uplink and downlink using 4- π steradian coverage from the LGAs.

During the outer-solar-system cruise, commanding and telemetry are accommodated with an X-band system for uplink and downlink using an MGA.

At all times in the outer solar system, cold conditions drive the thermal design of the

spacecraft. To minimize electrical heater power demand, internal heating from the electronics is captured within the thermal shroud to keep the spacecraft equipment within allowable flight temperatures. External elements will require electrical heaters or VRHUs. Even so, outer cruise safe mode is currently the sizing case for the number of ASRGs.

JOI is a fully autonomous critical event that requires robust system fault management. A cross-strapped dual-string architecture allows failures to be isolated so that recovery can occur on the backup hardware.

Table C.2.4-1. The spacecraft driving requirements from the science measurements appear to be feasible and consistent, and have been vetted through several Science Definition Team meetings.

Sci. Measure	Requirement	GN&C	Telecom	Power	C&DH	Prop Thermal	Mech
IPR	Capture & process 2 bands of radar data	Nadir pt	Telecom Ka down	Battery sizing	• Solid-state recorder • Through-put		Antenna deploy
TI	Image resolution	• Nadir pt • Jitter					
	Stereo imagery				Solid-state recorder		
	Accommodation						• Align with IPR • Cover
SWIRS	Image resolution, 1/2 IFOV over integration time	• Jitter					
	Data volume				Solid-state recorder		
	Accommodation			Battery sizing			Radiator view of space
INMS	Accommodation			Battery sizing			• Align to RAM • Cover

Table C.2.4-2. Flight system design elements flow down from the mission design driving requirements.

Msn Design	Req.	System	GN&C	Telecom	Power	C&DH	Prop	Thermal	Mech
Venus Flyby	Thermal control							Shade with HGA & shroud	
Inner-Solar-System Cruise	Command & telemetry			Xup/ Xdown with LGA					
	Earth flybys with ASRG	Fault management							
Outer-Solar-System Cruise	Command & telemetry		Sun-sensors	Xup/ Xdown with MGA					
Outer-Solar-System Cruise/ Europa Flybys	Thermal control				# of ASRGs			Thermal shroud/ RHU/ VRHU	
JOI	Critical event	Fault management	Dual-string/ hot-sparing	Dual-string/ hot-sparing	Dual-string/ hot-sparing	Dual-string/ hot-sparing	TVC size Engine size		
TCM	Navigation			Doppler					
Europa Flybys	Attitude control		Reaction wheel sizing						
	Radiation	Fault management	<300-krad parts	<300-krad parts	<300-krad parts	<300-krad parts			Vault & config

However, most fault tolerance complexity will be driven by the need to react cautiously to any type of disruption, suspending activity temporarily if needed, yet regaining control and resuming the orbit insertion with appropriate burn corrections for the interruption. This sort of capability is well established, as demonstrated several times throughout the solar system, including with GLL at Jupiter. JOI is presently the driving mode for battery sizing due to the long JOI burn of roughly 2 hours. The mission has several trajectory correction maneuvers (TCMs), both deterministic and statistical. The onboard communication system must support Doppler tracking to enable adequate navigation reconstruction of these maneuvers on the ground.

Attitude maneuvers during Europa flyby drive the sizing of reaction wheels. Radiation is also worst around flybys, driving fault-protection requirements on the ability to recover and continue science activities after a radiation-induced event (SEU, SEL, etc.). Radiation also drives the shielding design on the vehicle and the selection of EEE parts.

C.2.4.2 Structures and Mechanisms

The overall configuration of the spacecraft (Figure C.2.4-1) comprises the Avionics Module at the top, followed by the Propulsion Module and the Power Source Module at the bottom. The primary structure of these modules (Figure C.2.4-4) consists of these three commensurate octagonal segments, stacked vertically and joined mechanically to one another only via a simple octagonal ring interface. Each structure segment is based on an aluminum forging machined from the outside. Aluminum was chosen because it provides the

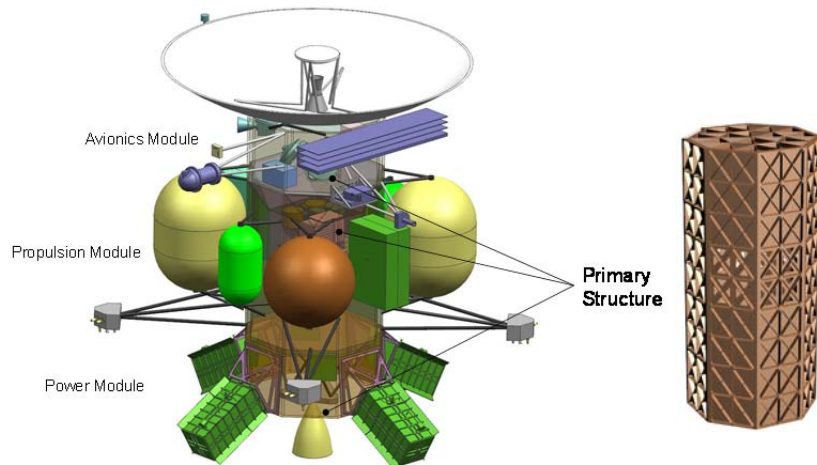


Figure C.2.4-4. Flyby primary structure.

best balance among weight, strength, stiffness, and radiation-shielding. After machining, deep stiffening ribs and a vertical wall remain. This provides for a lightweight, high-strength, and stiff structure. When all three modules are stacked, they form a superstructure that is able to meet the Atlas V launch vehicle's load and frequency requirements.

The predominant mechanism on the Europa Multiple-Flyby Mission spacecraft is the Ice-Penetrating Radar (IPR) antenna boom. Figure C.2.4-5 shows the stowed IPR antenna, and Figure C.2.4-6 shows the deployed IPR antenna.

The structures and mechanism in this concept require no new technology. Design approaches from past missions (like Cassini) can be adapted to address all of the structural and functional requirements for the Europa Multiple-Flyby Mission spacecraft. In addition, the overall numbers of mechanisms, consisting

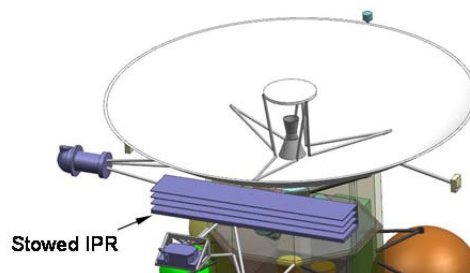


Figure C.2.4-5. IPR stowed.

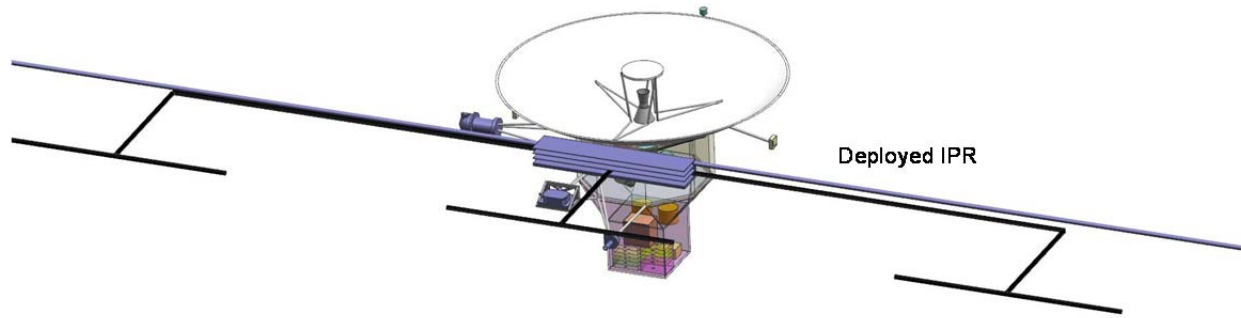


Figure C.2.4-6. IPR deployed.

mainly of small deployed items, such as covers, were minimized to reduce technical risk, cost, and schedule.

C.2.4.2.1 Key Mechanical Requirements

- First mode fundamental frequency: 8 Hz
- Primary structure lateral launch acceleration: 2 G
- Atlas V mass acceleration curve for appendages
- Isolation of the spacecraft to 20 Hz from a single Stirling converter failure at 102 Hz

C.2.4.3 Thermal Control

The thermal design concept uses, to the fullest extent practicable, waste heat, insulation, and louvers to control temperatures. This approach consumes little to no operational heater power, is low-mass, and has a flight-proven heritage.

C.2.4.3.1 Key Thermal Requirements

- Maintain the propulsion system and battery within allowable flight temperature (AFT) ranges (typically 15°C to 50°C and 10°C to 25°C, respectively).
- Maintain all instruments within the AFT limits.
- Accommodate the variation in environmental heat loads

from the Sun and Venus at 0.7 AU to Jupiter shadow at 5.5 AU (i.e., 2.0 to 0.03 Earth Suns).

- Tolerate limited transient off-Sun exposure (typically about an hour) at less than 1 AU during fault conditions or trajectory maneuvers.
- Minimize replacement heater power during outer solar system cruise and Jupiter operations.

C.2.4.3.2 Thermal Design

Figures C.2.4-7 and C.2.4-8 show the primary thermal components on the spacecraft. A lightweight thermal shroud surrounds the propulsion tanks and associated plumbing. Consisting of multilayered insulation (MLI) supported by a latticework, this shroud creates a

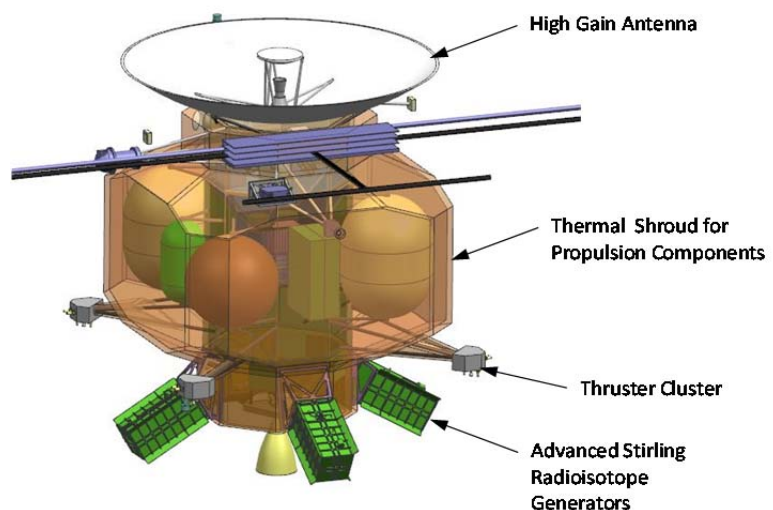


Figure C.2.4-7. Flyby spacecraft with thermal shroud surrounding propulsion tanks.

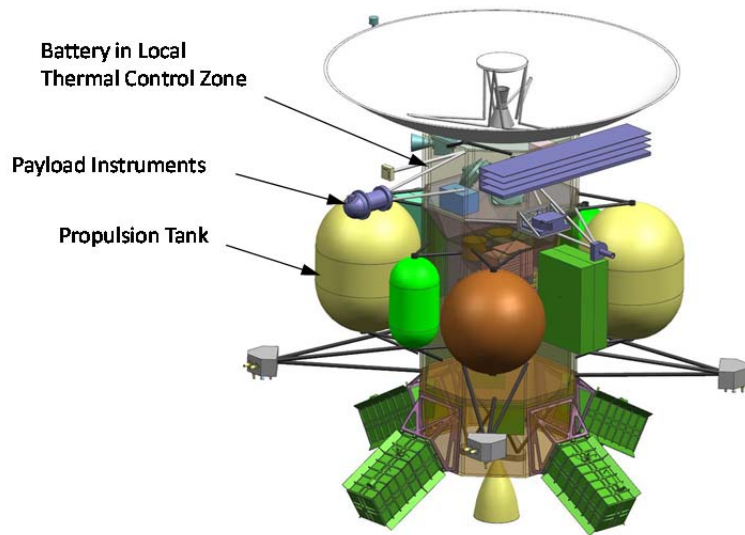


Figure C.2.4-8. Flyby spacecraft with thermal shroud removed.

radiative cavity around the tanks. A clearance of 100 mm between the propulsion components and shroud provides adequate view factors for radiation.

Waste heat from the avionics vault and advanced Stirling radioisotope generator (ASRG) electronics radiates into the cavity and warms the propulsion system. Openings in the primary structure allow heat to radiate from the vault onto the tanks and into the cavity.

A temperature-regulation system is necessary to accommodate the wide variation in environmental loads and internal dissipations. Accordingly, louvers over external radiators on both ends of the spacecraft regulate the cavity temperature to maintain acceptable vault and propulsion temperatures. Heat from the vault and ASRG electronics warms the shroud in the cold case, while louvers on the mounting structure reject excess heat to space in the hot case, thereby producing acceptable temperatures on the propulsion system and vault in all conditions.

This system of waste heat and louvers requires no additional electrical heaters for normal operation. With an MLI external area of 26 m^2 and a nominal effective thermal emissivity of 0.01, acceptable tank temperatures occur with a 200-W heat flow. During the mission, 216 W

to 416 W is available from the avionics vault and ASRG electronics. Hence, the heat balance is always positive. Fault conditions, where the avionics may be off and waste heat is low, are a factor in deciding the partitioning and placement of shunt radiators and replacement heaters. Survival operation will be studied in Phase A.

There are no driving temperature-stability requirements or temperature-gradient-control requirements; therefore louvers are adequate for overall temperature control.

The high-gain antenna (HGA) performs an important thermal-control function, shading the spacecraft from the Sun during the hot conditions of the inner solar system, especially near Venus. During this period, the spacecraft is oriented such that the HGA faces the Sun. This orientation preserves the heat balance on the thermal shroud and louvers. To tolerate a temporary disruption in attitude control under these thermal conditions, a hybrid MLI layup with five external layers of embossed Kapton protects against high exterior temperatures. Off-Sun illumination and the impact on temperatures will be studied during Phase A.

A separate thermal-control zone, with a dedicated radiator and louver, controls the temperature of the battery. This is accomplished by piggybacking the battery to structure in the Avionics Module's UES, but biased colder using a dedicated radiator.

Variable radioisotope heating units (VRHUs) control the temperature of the thruster clusters. Local heating from the VRHUs is required due to the remote location of the thrusters. Each VRHU consists of two to three individual RHUs mounted in a rotating cylinder. One half of the cylinder is painted white while the other half is insulated. A bimetallic spring positions the cylinder to radiate heat into the thruster

cluster when the cluster is cold, or out to space when the cluster is warm. There are four VHRUs per thruster cluster with a total of ten individual RHUs per cluster. Four thruster clusters yield a total of sixteen VHRUs and 40 individual RHUs. This design tolerates a failure mode where one VHRU is stuck fully open or fully closed.

Thermal control must be individually customized for each instrument via local radiators and heaters, orientation to thermal sources like the Sun, and control of the surrounding thermal context on the spacecraft. Addressing these issues in more detail for the model payload will be an important task during Phase A, and then again, once instruments are chosen.

Great care is also necessary, as in any thermal-control system, where thermal performance is affected by workmanship. The effective emissivity of MLI is a notable example. For the Europa Multiple-Flyby, this risk is mitigated by conservative design and by test. Margin in the active louver system provides tolerance for hardware variations. Also, thermal development tests of the louvers and critical areas of MLI reduce risk to acceptable levels.

C.2.4.3.3 Heritage

The thermal design concept for the Europa Multiple-Flyby Mission follows that of Cassini. In the Cassini design, the propulsion system was enclosed in a shroud that formed a radiative cavity. Heat for the Cassini shroud came from radioisotope thermoelectric generators (RTGs), whereas on the Europa Multiple-Flyby Mission spacecraft the heat comes from the avionics vault, the power shunt radiator, and the ASRG electronics. VRHUs control the temperature of the thruster clusters on Cassini, as planned for the Europa Multiple-Flyby Mission. HGA shading protected the Cassini spacecraft from solar loading at Venus and will do the same for the Europa Multiple-Flyby Mission. Other thermal hardware, such as louvers, heaters, MLI, and platinum resistance thermometers, also have good heritage

based on the flight experience of prior JPL missions.

C.2.4.3.4 Thermal Assessment of the Propulsion System

Thermal radiation from the Vault into the thermal enclosure provides passive temperature control for the propulsion tanks and lines, an approach similar to that used on Cassini. Three environmental conditions test the soundness of this approach.

Inner cruise takes the spacecraft near Venus. In this 0.7-AU hot condition, the high-gain antenna shades the spacecraft and prevents overheating. The internal heat dissipation is 290W, while the net heat loss from the thermal enclosure is 150W. Side-facing louvers reject the remainder of the heat, Figure C.2.4-9.

In the cold science mode, the internal heat dissipation drops to 216W while the heat loss off of the thermal enclosure increases to 200W. Sixteen watts remains to be rejected by the lower louver. The upper louver is closed, Figure C.2.4-10.

Power levels change again for orbit insertion and trajectory correction maneuvers. In this

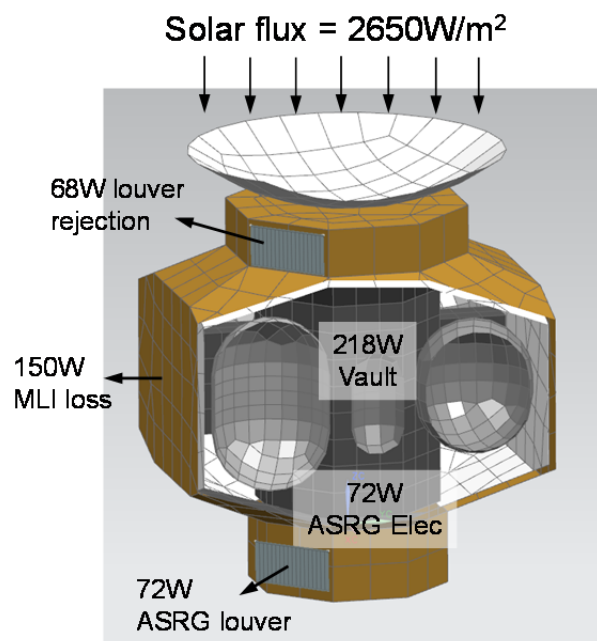


Figure C.2.4-9. Heat balance for inner cruise.

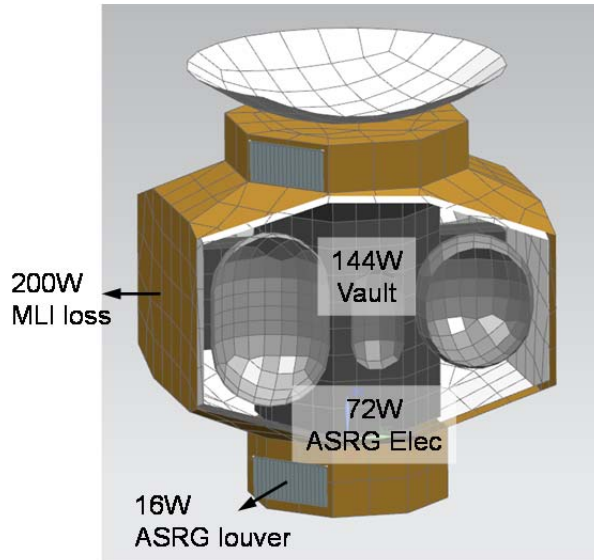


Figure C.2.4-10. Heat balance for Flyby science.

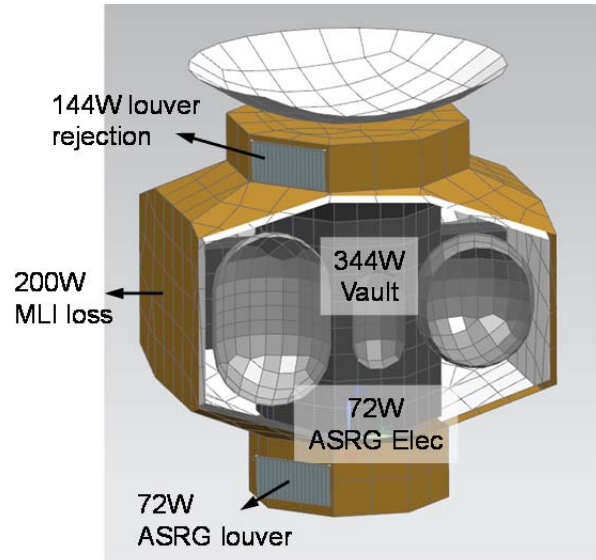


Figure C.2.4-11. Heat balance for orbit insertion and trajectory correction maneuvers.

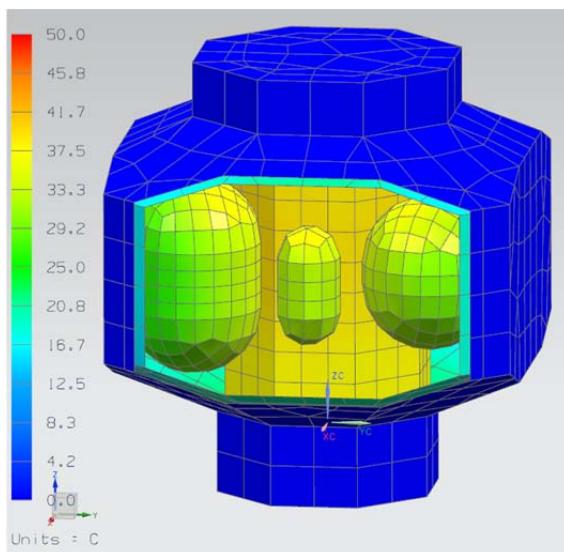


Figure C.2.4-12. Tank temperatures.

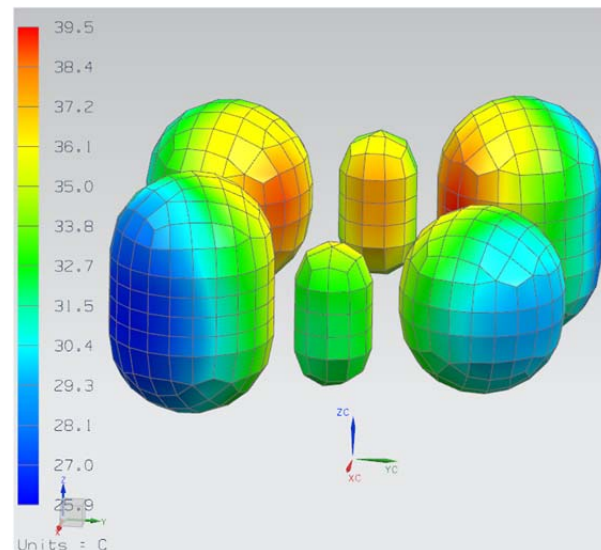


Figure C.2.4-13. Predicted tank temperatures, showing only the tanks.

high-power condition, 200W still leaks through the thermal enclosure, but the vault dissipates 344W. Both the upper and lower louvers participate in rejecting the balance of the heat and regulating the temperature, Figure C.2.4-11.

At Jupiter, in the worst-case cold condition, thermal equilibrium occurs with a heat flow of

200W from the inner structure to the insulation of the shroud. An initial thermal analysis for this case shows that the propulsion tanks remain within 25°C to 40°C, in compliance with their AFTs, without direct heating or active control. Figures C.2.4-12 and C.2.4-13 show predictions of the tank temperatures.

C.2.4.4 Propulsion Module

C.2.4.4.1 Propulsion

This Propulsion Subsystem, specifically designed for a long-life outer-planet mission, would provide the impulse and reliability necessary to meet the needs of the Europa Multiple-Flyby Mission.

The Europa Multiple-Flyby Mission spacecraft Propulsion Subsystem is a dual-mode bipropellant system. The propellants are hydrazine (N_2H_4) and nitrogen tetroxide (NTO). The hydrazine fuel and nitrogen tetroxide oxidizer are used by the bipropellant main engine, and the hydrazine fuel alone is used by the monopropellant Reaction-Control Subsystem (RCS) thrusters and thrust vector control (TVC) thrusters. Figure C.2.4-14 shows a schematic of the Propulsion Subsystem.

Driving Requirements

The requirements that drive the design of the Propulsion Subsystem are typical of those for outer-planet missions, with the possible exception of the requirement to configure the system to take advantage of the Propulsion Subsystem mass to provide radiation shielding for the

electronics. The key driving requirements for the Propulsion Module are to

1. Provide ΔV for maneuvers, including Jupiter Orbit Insertion (JOI).
2. Provide thrust vector control during main engine operation.
3. Provide for attitude control when the spacecraft is not using reaction wheels.
4. Provide for reaction wheel momentum unloading.
5. Configure the Propulsion Module to provide a substantial augmentation to radiation shielding of the spacecraft electronics.
6. Provide the central structure connecting the Power Source and Avionics Modules.
7. Support the thermal control concept with its shroud and internal radiative cavity.

Propulsion Module Configuration

Figure C.2.4-15 shows that the Propulsion Module configuration is based on a core octagonal structure with the propellant tanks, pressurant tanks, and component plates

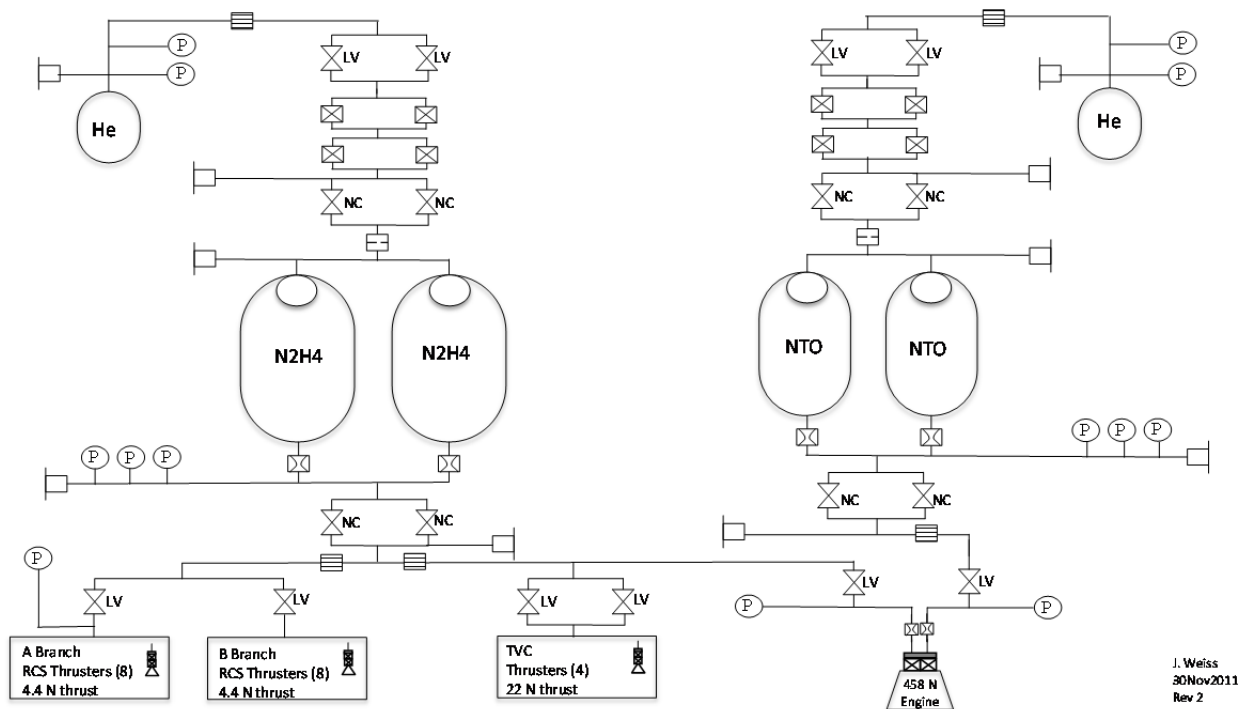


Figure C.2.4-14. Dual-mode, bipropellant Propulsion Subsystem schematic.

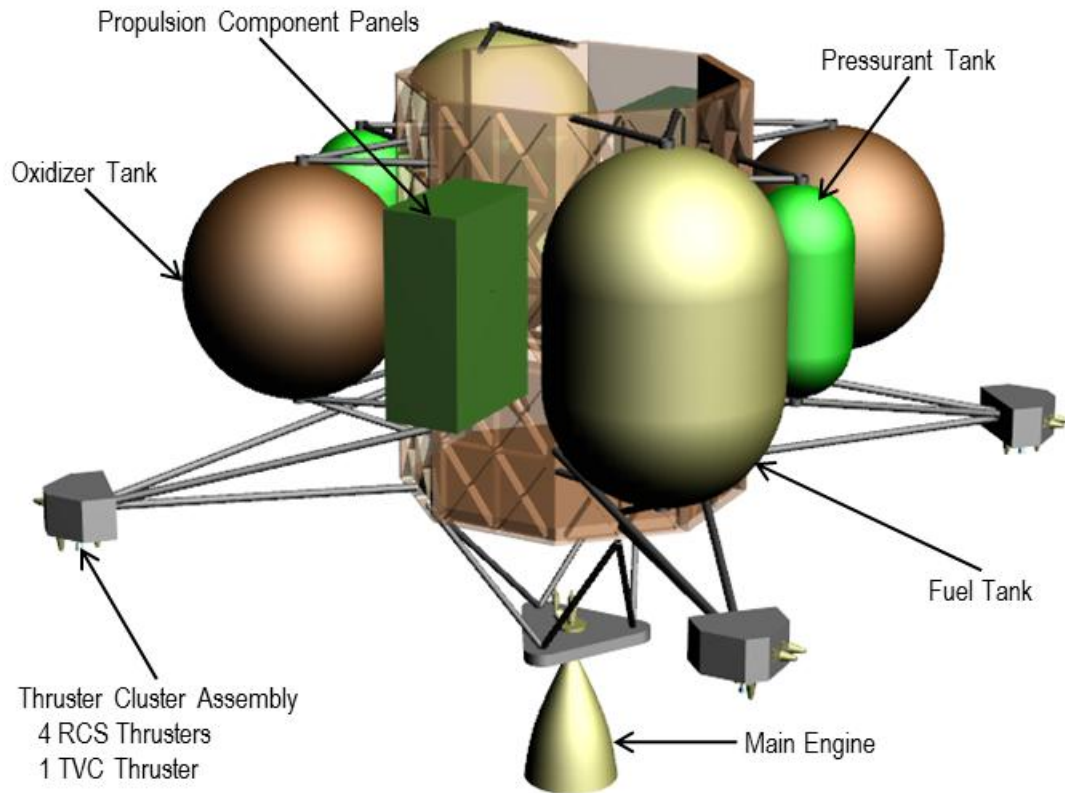


Figure C.2.4-15. Propulsion Module configuration.

mounted on the exterior sides of the octagonal structure. This configuration is driven by the necessity to maximize the radiation shielding for the spacecraft electronics, mounted on the Avionics Module and located internal to the Propulsion Module core structure. Mounting the tanks and the propulsion components on the external sides of the core structure provides additional shielding for the spacecraft electronics mounted internal to the vehicle.

Note that the propulsion components' plates are mounted perpendicular to the core structure (see Figure C.2.4-15). This is done because there is insufficient space to mount the component plates in a more traditional fashion (i.e., parallel) without increasing the length or diameter of the Propulsion Module. It was decided not to mount the component plates to an interior wall of the Propulsion Module because of limited accessibility during ATLO.

A single main engine, mounted using struts at the bottom of the Propulsion Module and protruding through the Power Source Module, provides for primary ΔV . The RCS and TVC thrusters are mounted on four thruster cluster assemblies (TCAs), which in turn are mounted on struts extending away from the spacecraft. This configuration is very similar to that of the Cassini RCS. Each TCA contains four RCS thrusters (two primary and two redundant) and a single TVC thruster. The RCS thrusters are block-redundant, in that there are two strings of eight thrusters. Each string of eight thrusters is isolated by a single latch valve and can perform all required functions. The second string is a backup. The RCS thruster configuration provides for coupled thrust about the Z-axis (roll) and uncoupled thrust in pitch and yaw, identical to the Cassini configuration. The spacecraft can be turned to align this axis with the reaction wheel momentum vector in order to minimize ΔV during momentum manage-

ment. Both the main engine and TVC thrusters are single-string in the present concept. This decision will be reassessed in Phase A.

Propulsion System Design

Engines and Thrusters. The baselined main engine for the Flyby spacecraft is the Ampac LEROS 1c (or equivalent). This is nominally a 458-N (103-lbf) engine. It operates at a nominal mixture ratio of 0.85 and has a minimum specific impulse of 324 seconds. This engine has been qualified for flight and has flown on numerous spacecraft. However, the engine will likely require a delta qualification test program for use on the Europa Multiple-Flyby Mission spacecraft. Although the total qualified throughput well exceeds the demands of the Europa Multiple-Flyby Mission, the tested single-burn duration of 60 minutes is insufficient. The Flyby Mission, as currently planned, requires a JOI maneuver on the order of 122 minutes. The vendor has indicated that they believe the risk of this delta qualification test to be very low.

It should be noted that the engine chamber interior wall is coated with R512E disilicide, which could be subject to micrometeoroid damage. The actual risk of failure and time to failure caused by damage is unknown, and likely indeterminate. The presented concept does not include an engine cover but the design does not preclude its addition. This would be reevaluated during Phase A.

The TVC thruster currently assumed for the flyby spacecraft is the Aerojet MR-106 thruster (or equivalent), providing approximately 22 N (5 lbf) of thrust. A preliminary analysis has been performed showing that this thruster provides adequate control authority for the vehicle during main engine operation, given different deployment configurations, but with assumptions on balanced propellant flow. Explicit measures to ensure propellant balance will be studied in Phase A. For now, ballast mass is included in the mass budget to keep the dry system center of mass near the sym-

metry axis of the tanks. The RCS thruster currently assumed is the Aerojet MR-111 thruster (or equivalent), providing approximately 4.4 N (1 lbf) of thrust. Both thrusters are qualified for flight and have high heritage.

Pressurization System. The baselined pressurization system allows for independent pressurization and regulation of the oxidizer and fuel tanks. Rather than using a traditional mechanical regulator, this system uses a set of four solenoid valves configured to be parallel and series-redundant (i.e., for a minimum of single fault tolerance), allowing for electronic regulation using pressure transducer feedback. Flight software would provide closed-loop control using pressure transducers measuring tank pressure. In the present concept, three pressure transducers would be polled to protect from a transducer failure scenario (though further study is required during Phase A to consider common mode issues). There are several advantages of this system over a more traditional pressurization system using mechanical regulators, especially for long-duration outer-planet missions:

1. Separate pressurization and regulation of the oxidizer and fuel tanks eliminates the risk of propellant vapor mixing in the pressurization system. It also eliminates the need for numerous check valves and pyro-valve isolation, reducing dry mass.
2. Elimination of the mechanical pressure regulator reduces the risk of regulator leakage. The series-redundant solenoid valves are less susceptible to leakage than are mechanical regulators.
3. The design allows for active control of oxidizer and fuel tank pressures. This is advantageous because the oxidizer-to-fuel mixture ratio can be adjusted during the mission. It allows for more accurate control of mixture ratio, which in turn reduces residual propellant.

The schematic in Figure C.2.4-14 shows that the quad-redundant solenoid valves are isolat-

ed above by parallel redundant, high-pressure latch valves and below by parallel redundant, normally closed pyro valves. The pyro valves would remain closed until first use of the regulating solenoid valves is required.

Systems similar in concept to this have been used in the past on other spacecraft (e.g., MiTE_x Upper Stage, Clementine, GeoLite, and Orbital Express).

Propellant and Pressurant Tanks. The propellant tanks are sized for a total propellant load of 1,872 kg. This assumes the maximum launch capability of the 21 November 2021 launch window, providing a ΔV of 1.52 km/s. Table C.2.4-3 shows the rack-up of propellant, including residual and ACS propellant. The hydrazine tanks are about 130 cm high by 90 cm in diameter (6% ullage), and the oxidizer tanks are 90-cm diameter spheres. The oxidizer tanks are significantly oversized for the current propellant load. These dimensions are based on available tanks. The tanks are oversized for these mission drivers; sizing will be revisited in Phase A.

The pressurant tanks are essentially off-the-shelf tanks and significantly oversized for the current propellant load. The pressurant tank sizing will be optimized as the design matures.

Propellant Isolation. The propellant tanks are isolated from the thrusters using parallel redundant, normally closed pyro valves and low-pressure latch valves. This design concept provides sufficient mechanical inhibits to meet

Table C.2.4-3. Maximum propellant load case for Flyby spacecraft propellant tank sizing.

Required Propellant	Mass (kg)
Propellant load for 1.52 km/s ΔV	1711
Hydrazine (MR=0.85)	925
NTO	786
Hydrazine for TVC	75
Allocation of ACS propellant (N ₂ H ₄)	40
Hydrazine residual/hold up (2.5%)	26
NTO residual/hold up (2.5%)	20
Total hydrazine	1066
Total NTO	806
Total Propellant Load	1872

KSC launch safety requirements.

Careful design of the propellant tank surface-tension propellant-management devices (PMDs) and the venturis downstream of the tanks will be necessary in order to prevent propellant transfer between the two tanks, or preferential draw of propellant from one tank. It may also be necessary to take more positive measures to prevent propellant transfer, such as the addition of latch valves to isolate the propellant tanks from each other when not in use and to regulate differential flow. Further detailed analyses will be required before this design concept can be finalized.

Heritage

The majority of the components used in the flyby propulsion system are flight qualified and considered off-the-shelf. This includes the RCS thrusters, TVC thrusters, service valves, pressure transducers (except for required shielding), filters, and solenoid and latch valves. As discussed above, the baselined main engine is also flight-qualified and has flown before. However, it will likely require a delta qualification test to qualify the single-burn duration for JOI. Regarding the propellant tanks, it is the intent to size them based on a heritage design that makes use of qualified hemisphere forgings. The current design concept makes use of an 89.15-cm (35.1-in.) tank, but will likely require a change in length of the cylindrical section. In addition, a new PMD for the oxidizer and fuel tanks will need to be designed and integrated. Hence, the propellant tanks will likely require a new qualification test program. A similar approach has been taken with the pressurant tanks, using a qualified design that best meets the requirements for the Europa Multiple-Flyby Mission.

The pressurization system, which makes use of electronic regulation, will need to go through a program that develops and qualifies it as an integrated system, including the propulsion hardware, controller, and flight software.

C.2.4.4.2 Propulsion Module Structure

The Propulsion Module (Figure C.2.4-15) supports the fuel tanks, TVC and RCS thrusters, propellant-isolation assembly (PIA), pressurant-control assembly (PCA), and main engine. The propulsion fuel tanks are supported by bipod and tripod combinations and are attached to the primary structure. The main engine is attached at the bottom and extends through and below the Power Source Module. Four thruster clusters are supported at the ends of four tripods sized for adequate control authority and minimal plume impingement. The PIA and PCA are attached together, back to back and parallel to each other. The PIA/PCA assembly is in turn attached to the Propulsion Module’s primary structure.

The Propulsion Module’s primary structure has triangular holes in the wall at the location where the warm avionics has a radial view to the propulsion tanks. These holes allow for a direct radiation path to the tanks. In this region, the primary structure’s wall thickness is increased to compensate for the holes. The necessary radiation shielding is still maintained due to the position of the tanks and the thickness of the vault.

C.2.4.5 Power Source Module

The Power Source Module (Figure C.2.4-16) would include four ASRGs, the launch vehicle adapter, the main engine thermal shroud, and

structure to support these items and carry the Propulsion and Avionics Modules above. Each ASRG provides a power and command interface to the Avionics Module. Electrically heated units will be used during system integration and test, after which the Power Source Module will be demated and return for fueled ASRG integration. The Power Source Module will then be delivered directly to the launch site for reintegration (Section C.2.4.8). The thermal dissipation of the ASRGs inside the primary structure contributes to the overall thermal input inside the thermal shroud of the spacecraft. The main engine assembly of the Propulsion Module goes through the center of the Power Source Module with a thermal shroud protecting against the heat of the engine.

C.2.4.5.1 Power Source

The power source would be the combined contribution of four ASRGs. Its power interface to the rest of the system is through a single industry-standard power bus with a 22 to 34-V range defined at the load interface with the Power Source Module. The power bus is a direct energy transfer architecture, with the power source output connected to the Power Subsystem in the Avionics Module. The Power Subsystem provides power bus voltage regulation, not the Power Source Module.

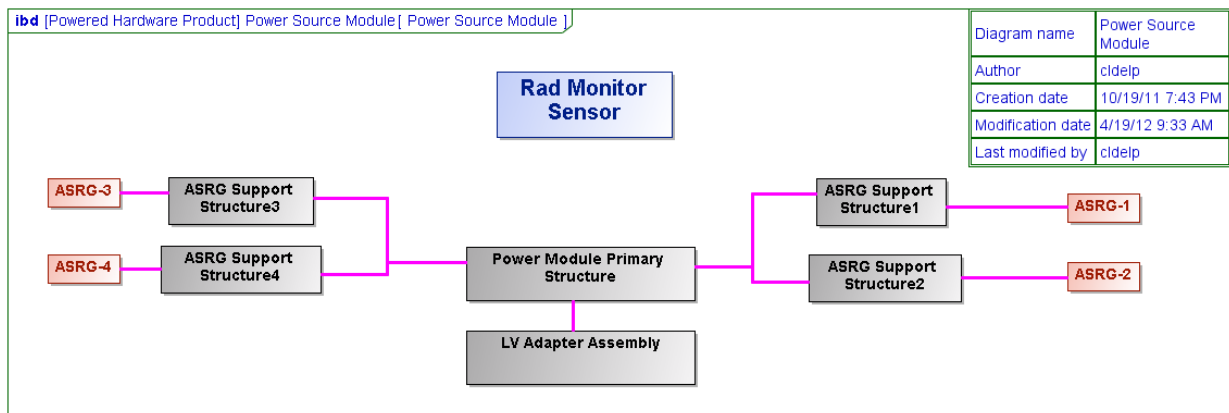


Figure C.2.4-16. Power Source Module block diagram.

Power Source Driving Requirements

The key drivers for the power source are to

1. Provide 392 W at EOM, assuming a single Stirling engine failure in one ASRG.
2. Provide constant power over the nominal power bus voltage operating range of 22 to 34 V as defined at the power source output.
3. Tolerate a power bus overvoltage up to 40 V for an indefinite period of time.
4. Provide diminished but positive power to the power bus if the voltage drops to less than 22 V in order to support recovery from a bus overload.

C.2.4.5.2 ASRG

ASRG Functional Description

Each ASRG (Figure C.2.4-17) consists of two General-Purpose Heat Source (GPHS) mod-

ules, two ASRG Stirling converters (ASCs), a generator housing assembly (GHA), a shunt dissipater unit (SDU), an ASC controller unit (ACU), and associated internal cables.

The GPHS contains plutonium dioxide fuel pellets and is designed to meet all safety and handling requirements. The GPHS produces from 244 W to 258 W at encapsulation when the fuel mixture is set in the pellet and placed in the module. From the point of encapsulation, the GPHS thermal output will degrade with the radioactive decay rate of plutonium-238, which is approximately 0.8% per year. It has been assumed that the average GPHS encapsulation will be 3 years before launch.

The ASC converts the thermal energy from the GPHS to AC electrical current using a piston and linear alternator. The ACU rectifies the AC power to DC power and provides it to the power bus with a constant power I-V curve

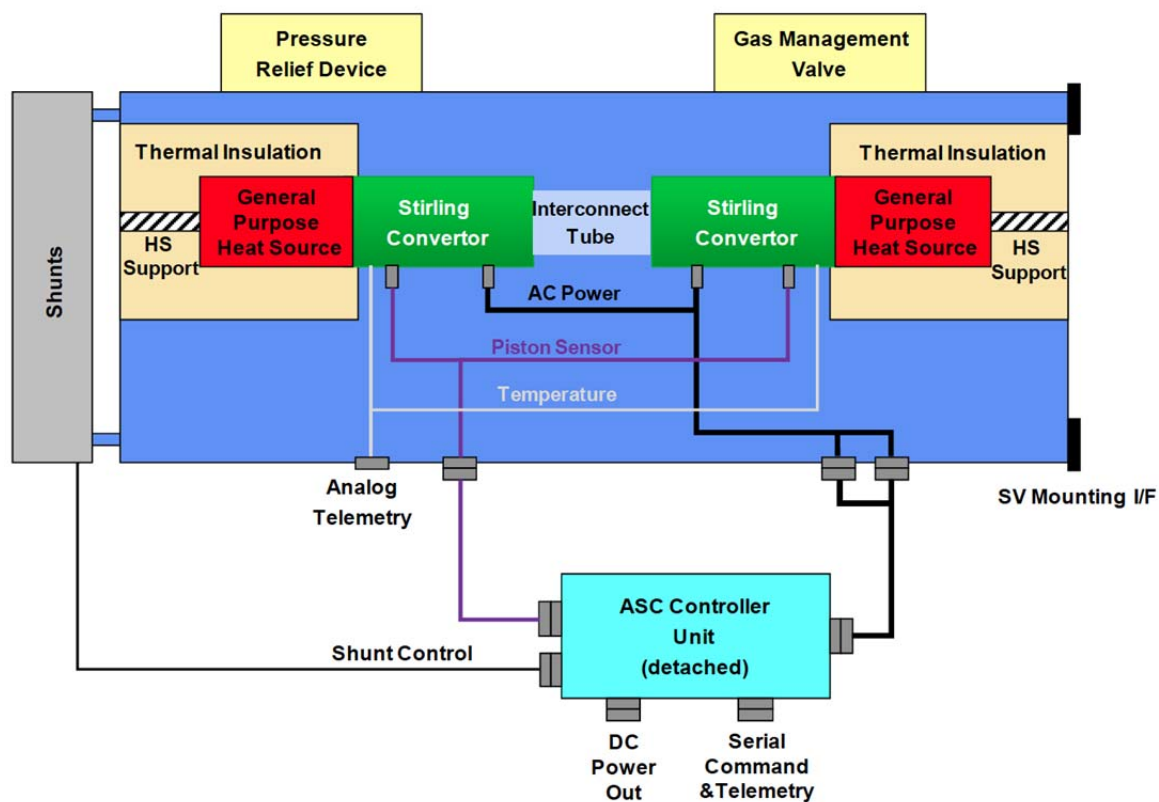


Figure C.2.4-17. This ASRG block diagram includes all functional elements that make up the ASRG, including the detached controller that provides the electrical interface with the spacecraft.

over the power bus voltage range controlled by the spacecraft. The constant power I-V curve allows for more than one ASRG to be connected to the same power bus and share the power.

The ASRG protects itself if the bus voltage goes outside of the specified range of 22–34 V at the ASRG output. The ACU disengages the output from the power bus and shunts the power to the attached radiator if the bus voltage exceeds $35\text{ V} \pm 1\text{ V}$. The internal ASRG shunt regulator is independent of the Power Subsystem shunt regulator used to regulate the power bus voltage. The ASRG shunt radiator is on the outboard end of the GHA and is used during flight only for the off-nominal bus voltage. The power system maintains the bus voltage range at less than 34 V at the ASRG interface to prevent disengagement. The ASRG reengages once the bus voltage drops back into the safe range. The ASRG provides a current limited to 3.5 A if the bus voltage drops below 22 V, enabling the system to recover by charging the battery.

The ACU is detached from the GHA (Figure C.2.4-18) and mounted on the inside of the Power Source Module primary structure.

The ACU is single-fault-tolerant with an N+1 internal voting architecture and two 1553 data

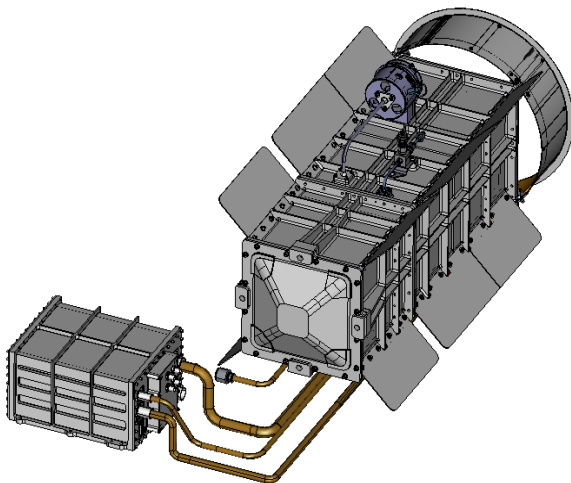


Figure C.2.4-18. ASRG CAD model shows the detached controller with cabling and outboard shunt radiator.

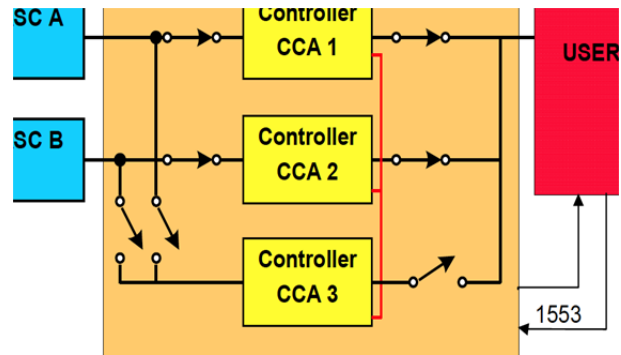


Figure C.2.4-19. ASC controller unit block diagram shows the spare controller # 3 to which the internal fault management switches with the detection of a failure.

bus interfaces (Figure C.2.4-19). The ACU needs to be within 1.8 meters (by cable length) due to impedance constraints from the controller. The ACU also needs to be greater than 1 meter away (by geometric distance) to tolerate self-generated radiation levels.

The ACU has internal fault management to switch automatically to the spare controller board with the detection of a fault. Additional shielding mass was allocated to the ASRGs so that the ACU would be shielded to 50 krad with a radiation design factor of 2 at the component level, including radiation from the ASRG as well as from the environment.

ASRG Performance

ASRG output power is a function of time and environment. The power graphs below show the predicted power output of the four ASRGs, with degradation due to natural decay of the plutonium dioxide fuel as a function of the time from encapsulation, and assuming each GHA has a direct view to space after launch (Figure C.2.4-20). Three graphs are shown. The graph for total power CBE (current best estimate) assumes the nominal specified GPHS thermal output of 250 W at encapsulation. The graph for total power specification is from the ASRG user guide with a BOM power at 130 W, assuming a failure of one single Stirling converter shortly after launch, and 1% degradation per year. The graph for lowest expected value (LEV) assumes the minimum

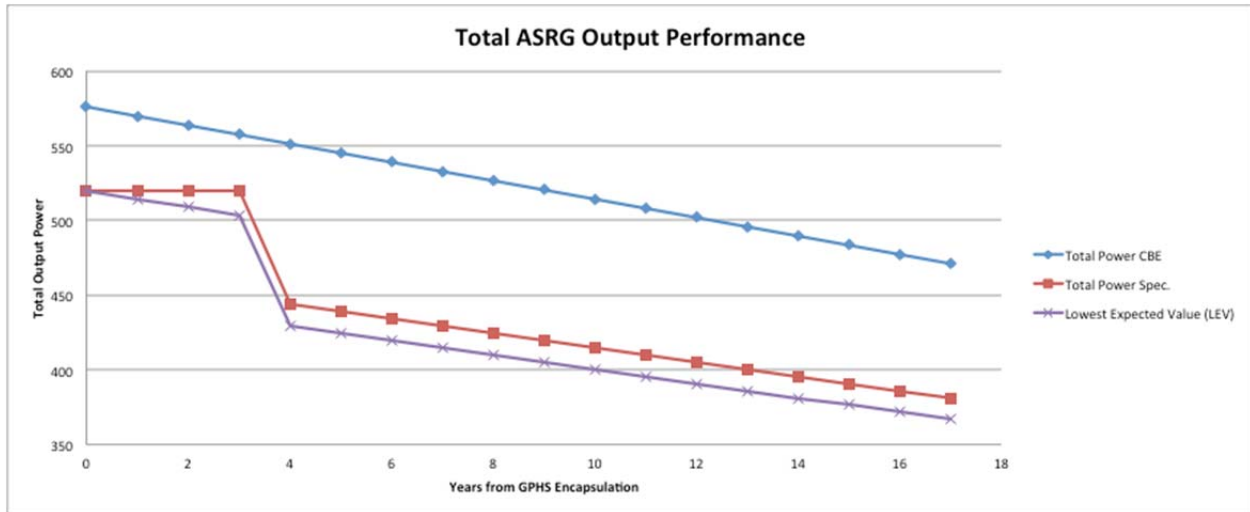


Figure C.2.4-20. The Europa Study Team uses conservative ASRG performance that includes end-of-life output and takes into account the failure of one Stirling engine.

specified GPHS thermal output of 244 W at encapsulation, 1% degradation per year, and failure of a single Stirling converter shortly after launch. The LEV graph has been assumed for the Europa Multiple-Flyby Mission concept. The main difference between this and the Department of Energy (DOE) specification is that the 1% degradation per year is presumed in the LEV case to begin 3 years prior to launch at the average GPHS encapsulation date. With a Europa Multiple-Flyby Mission duration at 12 years, at least 392 W is expected at EOM.

The curve above assumes a direct view to space with a sink temperature equivalent to 4 K. The power output graph below shows the degradation as the sink temperature increases due to the environment (Figure C.2.4-21).

The spacecraft configuration uses the high-gain antenna and thermal blanket envelope to shade the ASRGs from the Sun within 1 AU. For the changing environment of launch, inner cruise, and Venus gravity assist, a commands are sent to the ASRGs to adjust an internal operational set point to make sure the ASRGs are safe from over-temperature which would impact the output power. This operation is independent of the power bus voltage set points

controlled by the spacecraft. The spacecraft has adequate power margin for such environmentally impacted mission phases.

C.2.4.5.3 Power Source Module Structure/LVA

The four ASRGs would reside on the Power Source Module (Figure C.2.4-22). The Propulsion Module’s main engine assembly passes through the center of but does not directly attach to the Power Source Module’s primary structure.

Each ASRG has two opposing advanced Stirling converters (ASCs). To counter vibration,

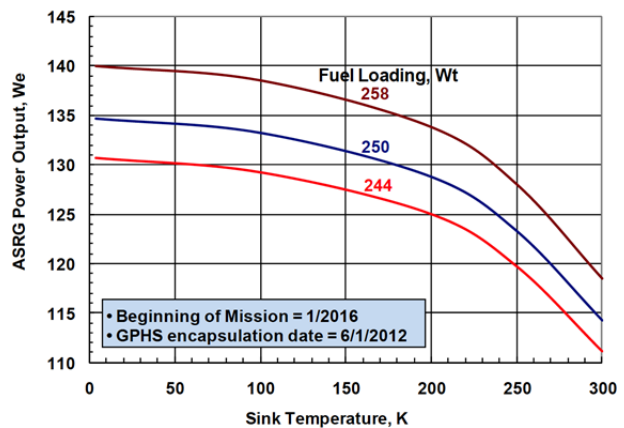


Figure C.2.4-21. ASRG output power vs. sink temperature shows that depending on the environment the output power will degrade. The ASRG power output power will depend on the view to space.

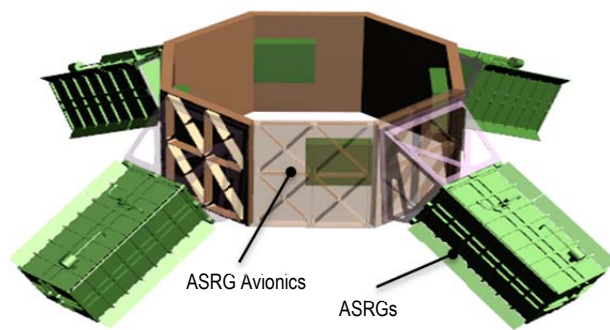


Figure C.2.4-22. ASRGs and their avionics on the Power Source Module.

they are paired in an opposing configuration and tuned through active control by the ACU. As long as both ASCs are working, the ACU controls the phase to reduce the vibration. If an ASC fails, the mechanical interface must dampen or counter the resulting vibration from operating a single ASC.

In the present concept, compression spring assemblies are assumed, oriented parallel to the long axis of the ASRG. These can be tuned to couple poorly with the ASC's frequency of 102 Hz, while still ensuring margin against launch accelerations. However, other ways to accomplish isolation have been identified. These would need to be studied in detail during Phase A.

Because the Power Source Module is the bottom-most module, it experiences the largest moment loads during launch. This will require its primary structure to have a slightly greater wall thickness than the Propulsion and Avionics Modules.

At the bottom of the Power Source Module is the launch vehicle adapter (LVA, Figure C.2.4-23). The LVA provides for a



Figure C.2.4-23. Launch vehicle adapter.

transition between the octagonal geometry of the upper Power Source Module structure and the circular Marmon clamp separation interface.

C.2.4.6 Avionics Module

The Avionics Module concept results in radiation shielding that enables the use of standard aerospace industry radiation tolerant parts.

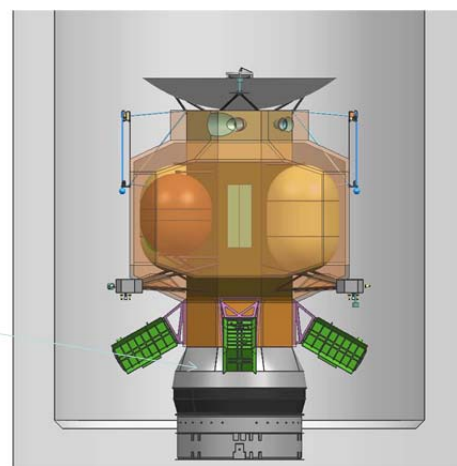
Avionics Module Overview

The Avionics Module described below includes the following subsystems:

- Telecom
- Power
- Guidance, Navigation, and Control
- Command and Data Handling
- Software
- Structure, along with instrument accommodation

Besides supporting instruments and the mission design, some of the unique design objectives for the Avionics Module have been as follows:

- Modular design for parallel I&T with Propulsion and Power Source Modules
- Avionics vault to shield a majority of the spacecraft electronics
- Enabling of late integration of instruments
- Simple interfaces with Propulsion and



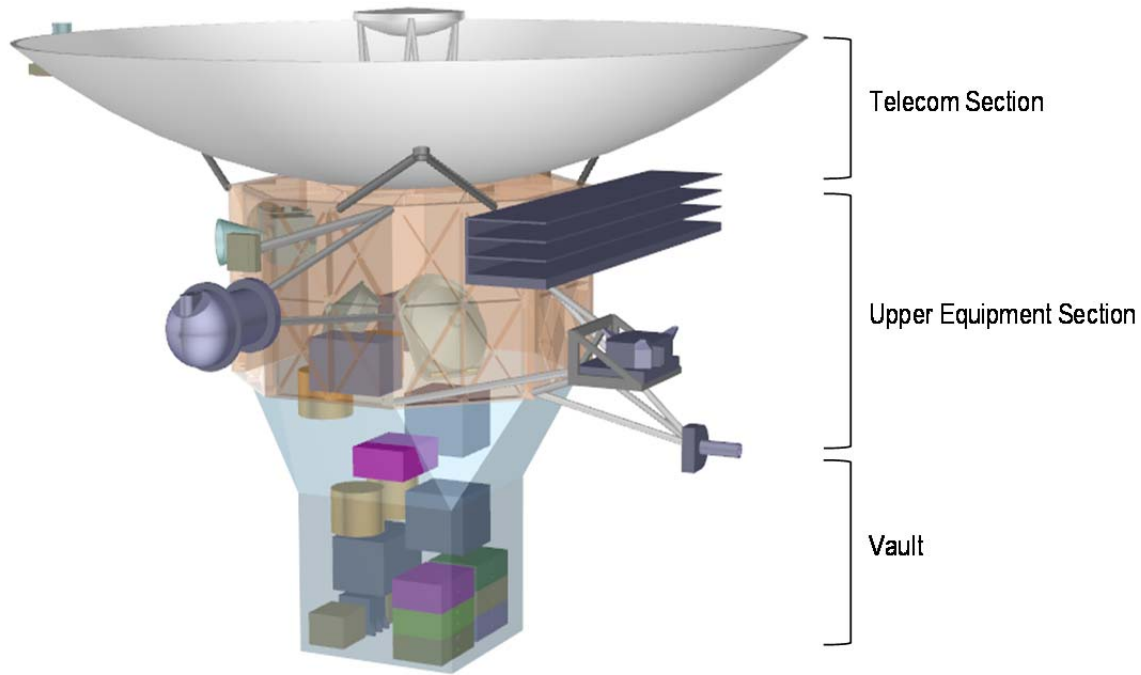


Figure C.2.4-24. The three assemblies of the Avionics Module (telecom, Upper Equipment Section, and Avionics Vault Section) are configured for simple interfaces to enable parallel integration and test.

Power Source Modules

Figure C.2.4-24 shows the configuration of the Avionics Module. It consists primarily of three separate entities: the Telecom Section, the UES, and the Avionics Vault Section.

Figure C.2.4-25 shows the system block diagram of the Avionics Module. The red inter-

faces are DC power; the blue interfaces are data; and the gold interfaces are RF.

Inside the avionics vault are the C&DH electronics (this box is internally redundant), four-for-three reaction wheel electronics(RWE), internally redundant power electronics, internally redundant pyro/propulsion drive elec-

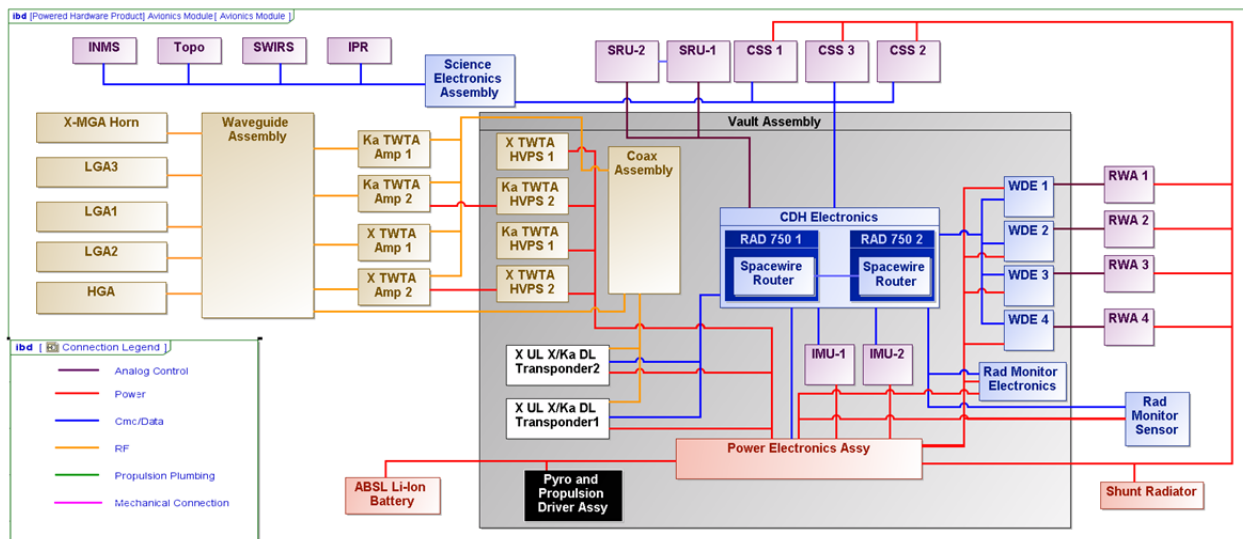


Figure C.2.4-25. A majority of the spacecraft electronics protected in the avionics vault.

tronics, block-redundant IMUs, and block-redundant small deep-space transponders (SDSTs). In the UES are the instruments (TI, SWIRS, IPR, and INMS) and instrument electronics. Also in the UES are the following GN&C components: four-for-three reaction wheel mechanical assemblies (RWA), block-redundant Sun-sensors, and block-redundant SRUs. All the elements outside the vault are individually shielded for total-dose radiation. In the case of instrument and star-tracker detectors, the shielding also mitigates the effect of the electron flux, which is likely to drive shielding mass. The Power Subsystem components outside the vault are the shunt radiator, and battery (both internally redundant). The Telecom Section houses the following components: the TWTAs, coax, waveguide, switches, and antennas configured in a single-fault-tolerant configuration for Ka-band and X-band communication.

C.2.4.6.1 Telecom Subsystem

The Telecom Subsystem performs a dual role for the spacecraft: two-way communications with Earth and Earth-to-spacecraft ranging and Doppler to support navigation.

Driving Requirements

There are a number of drivers for the subsystem. It must accept uplinked commands through all postlaunch mission phases, as well as transmit engineering telemetry and science data to Earth. Key data rates required are

- Engineering telemetry: ~2 kbps
- Uplink commanding: ~1 kbps
- Safe mode commanding: ~7.8 bps
- Safe mode telemetry: ~10 bps
- Science data return: ~112 kbps

Implicit in the above is communications with the Deep Space Network (DSN) 34-m subnet for routine communications and the 70-m subnet (or equivalent) for emergency/safe mode communications.

Subsystem Features

The implementation of the Telecom Subsystem includes X-band uplink and downlink capabilities as well as a Ka-band downlink. Ka-band downlink enables the mission to meet science data volume drivers concurrently with stringent drivers for DC power. While the downlink data volume drivers could be met with X-band alone (assuming a much more powerful X-band TWTAs), a trade study between available DC power and science data volume return informed the selection of a more DC-power-efficient architecture for high-rate science data. A similar trade study was undertaken for the Dawn mission. For Dawn, however, more DC power was available, thus enabling a higher DC/RF power X-band downlink for science data; no Ka-band downlink was required. For the Europa Multiple-Flyby Mission, by contrast, the use of Ka-band for high-rate science downlink directly lowers the number of ASRGs required to meet mission objectives.

The Telecom Subsystem features a 3-m-diameter X/Ka-band high-gain antenna (HGA), three LGAs, an MGA with dual polarizations, redundant 35-W (RF power) Ka-band TWTAs, redundant 20-W (RF power) X-band TWTAs, redundant SDSTs, and a complement of microwave waveguide and coax elements. The SDSTs are X-band uplink and downlink capable as well as being Ka-band downlink capable. There is no capability for Ka-band uplink.

The Telecom Subsystem is also expected to be single-fault-tolerant. This drives The Telecom Subsystem architecture to include redundant transponders (small deep-space transponders [SDSTs]), redundant X-band and Ka-band traveling-wave tube amplifiers (TWTAs), a waveguide transfer switch (WTS) network to support cross-strapping, as well as a set of low- and medium-gain antennas. One X-band low-gain antenna (LGA) and the medium-gain antenna (MGA) are tolerant of a single WTS failure. Even though there is a single High

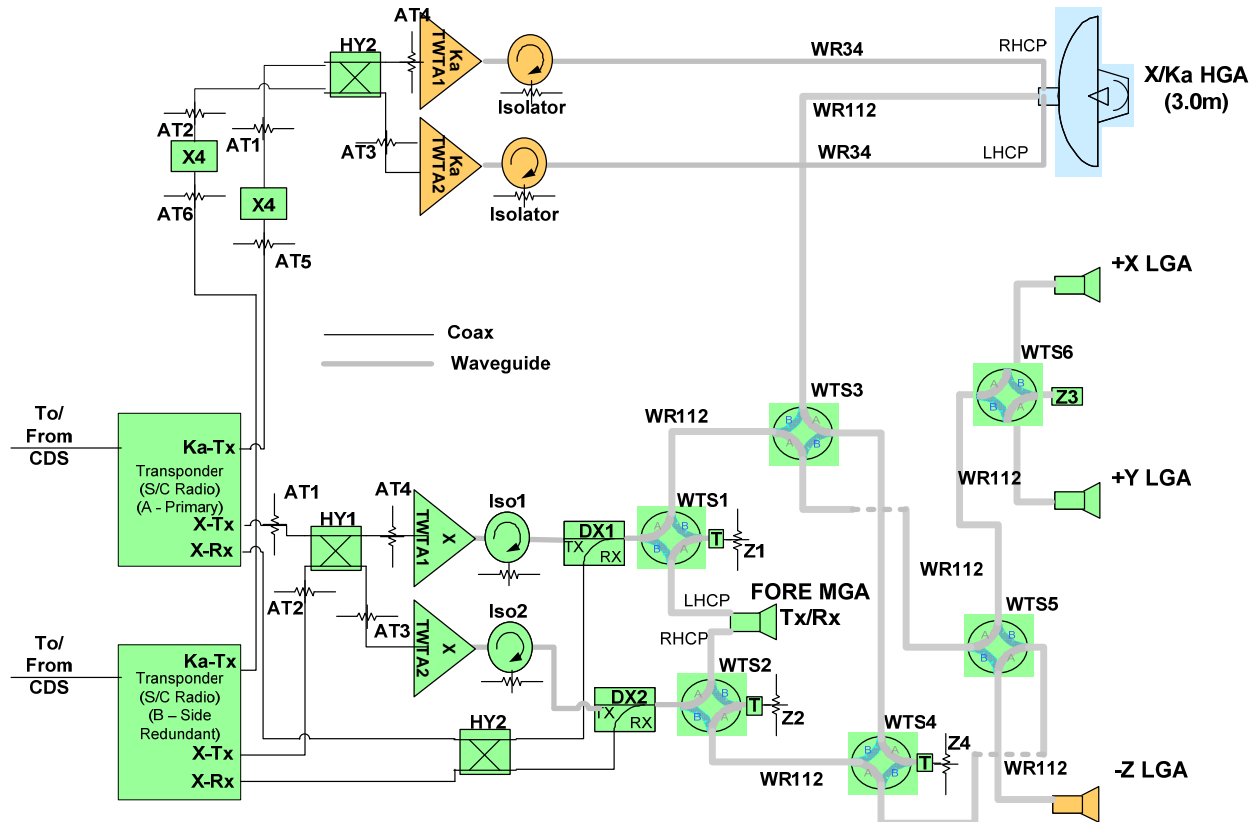


Figure C.2.4-26. The Telecom Subsystem provides robust fault-tolerance through a simplified architecture that minimizes potential for single-point failures.

Gain Antenna (HGA), the HGA features the capability of two downlink polarizations for fault tolerance to a single failure in the Telecom Subsystem's transmitter/receiver hardware chain.

Block Diagram

The equipment configuration shown in the Telecom Subsystem block diagram (Figure C.2.4-26) is based upon many years of deep-space communications heritage. For example, the -Z LGA is fault-tolerant to a single WTS failure in order to provide fault-tolerance for communications during the inner-cruise portion of the mission when the spacecraft uses its HGA as a sunshield. The LGA configuration enables communications through all cruise periods out to approximately 2 to 3 AU from Earth after which the MGA takes over the safe-mode and general cruise communications. Ka-band downlink redundancy is pro-

vided through the use of redundant hardware chains and downlink antenna polarizations. This simplified architecture promotes a more robust system fault-tolerance than could be achieved with the inclusion of an additional WTS to switch between the redundant downlink TWTAs. Similarly, for the X-band uplink, an RF hybrid is used (HY2) in place of a WTS. This alone eliminates a potential single-point failure in the critical X-band uplink path. Similarly the MGA has dual polarizations that enable single-fault-tolerant safe-mode communications at Europa. Overall the Telecom Subsystem presents a robust, fault tolerant, and low risk posture for the mission.

Equipment Heritage

Telecom hardware heritage comes from a number of previous missions. The HGA will be similar to the Juno HGA. It will be redesigned for higher gain by scaling up Juno's



Figure C.2-27. Juno's 2.5-m HGA (X/Ka-band) provides the basis for the Europa HGA.

2.5 m in diameter to 3 m. The Europa Multiple-Flyby Mission's HGA will leverage technology developed for the Juno HGA reflector (Figure C.2.4-27) to meet the surface-tolerance requirements for precision Ka-band pointing and efficiency. The Juno HGA optics will be redesigned to improve Ka-band performance for the Europa Multiple-Flyby Mission's high-rate downlink communications needs.

The TWTA's have heritage from multiple JPL missions: Juno, Dawn, and MRO (X-band) and Kepler (Ka-band). A good example here is the X-band TWTA for the Dawn mission, shown in Figure C.2.4-28. We propose to leverage a long history of downlink TWTA's designed specifically for the requirements of deep-space missions.

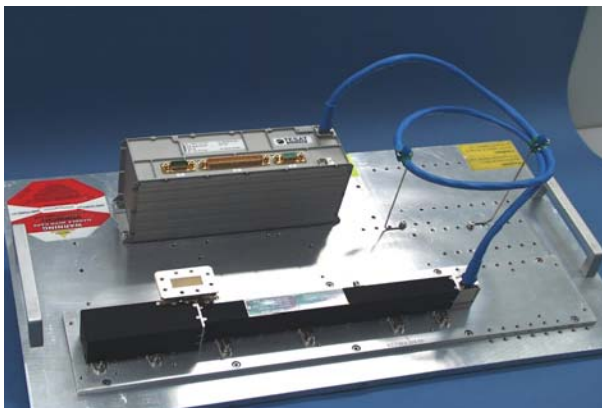


Figure C.2.4-28. Candidate X-band TWTA (flown on MRO, MSL, and Dawn).



Figure C.2.4-29. The SDST product line provides the mission-critical communications link to Earth.

We propose to use the SDST, a very mature product, to provide the mission-critical uplink and downlink functions. The SDSTs have heritage from Juno (X/X/Ka-bands), Dawn (X-band), MRO (X/X/Ka-bands), MSL (X-band), Kepler (X/X/Ka-bands), and others. A candidate SDST, flown recently on the Dawn mission, is shown in Figure C.2.4-29. Due to the extensive heritage inherent in the SDST product line, the use of the SDST lowers the overall residual mission risk.

Characteristics and Sizing

The average Telecom Subsystem downlink data rate must be at least 112 kbps during Europa science operations. The telecom link budget is designed to meet this with the parameters shown in Table C.2.4-4. We've sized the Telecom Subsystem to have a worst case bit rate of 112 kbps. This yields a nominal average bit rate of 134 kbps.

The HGA is body-fixed to the spacecraft and requires a ≤ 1 -mrad pointing accuracy to meet communications throughput requirements. We've taken a conservative approach with the telecom link by requiring 3 dB margin minimum and by making conservative estimates of individual contributors to the link. Parameters such as RF losses in the downlink path, DSN station performance due to low station elevations, link degradation at low Sun-Earth pointing (SEP) angles and Jupiter's hot-body noise

Table C.2.4-4. Telecom link budget inputs.

Parameter	Required Capability	Notes
Throughput Rate (worst case)	112 kbps	Average = $1.2 \times$ worst case = 134 kbps
TWTA RF Power	35 W (Ka), 20 W (X)	2 \times for Power Dissipation
HGA Diameter	3.0 m	Body fixed HGA, 60% efficiency
HGA Pointing Error	≤ 1.0 mrad	Reaction-wheel control
DSN Weather	90% cumulative dist.	
Canberra Elevation	20°	Worst-case, fixed
Earth S/C Range	6.5 AU	Average mission design
Hot Body Noise	16 K	About 0.6 dB loss
Turbo Coding	Rate=1/6, 8920-bit frame	
TWTA to HGA Losses	2 dB	Conservative estimate
Link Margin	3 dB	Per Institutional guidelines
SEP Angle	20°	Worst-case assumption
Operational Configuration	X-band up, Ka-band down	X-band downlink for safe mode & cruise
Gravity Science Doppler	None	
Hardware Configuration	X-band up, X/Ka-band down 3 LGAs, MGA, HGA, TWTAs	Possible X-band SSPA in lieu of TWTA

at Ka-Band are all taken into account. Overall, we propose very conservative and robust X-band and Ka-band communications links.

The LGA complement provides full 4π -steradian coverage; this enables command uplink at any spacecraft attitude unless the line-of-sight to Earth is blocked, which occurs only for brief episodes. Spacecraft communications during the inner cruise portion of the mission (<1 AU solar distance) use a single-fault-tolerant LGA (-Z LGA). The distances to Jupiter, however, prevent LGA communications at the required safe mode rates. To meet safe mode communications rate requirements in this situation, a body-fixed MGA with an approximate full-cone beamwidth of 20 deg, pointed at the sun using the spacecraft sun sensors, is used. All high-rate communications are performed through the HGA. Turbo coding at rate = 1/6 is also part of the baseline communications architecture.

C.2.4.6.2 Power

The Flyby Power Subsystem electronics and energy storage provide the power bus regulation and distribute power from the ASRGs and battery to the loads.

Power Driving Requirements

1. Be single-fault-tolerant

2. Provide energy storage to level the mission load profile
3. Provide power bus regulation
4. Provide battery charge control
5. Accept power from the ASRGs
6. Distribute power to the loads
7. Actuate valves
8. Fire pyro events

Power Subsystem Description

The Power Subsystem electronics regulates the power bus, directly connected to the ASRGs, and distributes power to the loads on the spacecraft. The Power Subsystem provides rechargeable energy storage to cover the transient load profiles of the different Flyby Mission scenarios. It is single-fault-tolerant, using a combination of block-redundancy with cross-strapping and some majority-voted functions. It provides valve-drive and pyro-firing functions with range and mission safety inhibits for hazardous functions.

The Power Subsystem consists of a Li-ion battery, a shunt radiator, a shunt driver slice (SDS), two multimission power switch slices (MPSSs), two power bus controllers (PBCs), two power converter units (PCUs), two pyro-firing cards (PFCs), and four propulsion drive electronics slices (PDEs) (Figure C.2.4-30).

ibid [Powered Hardware Product] Flyby Flight System [Power Electronics Connectivity]

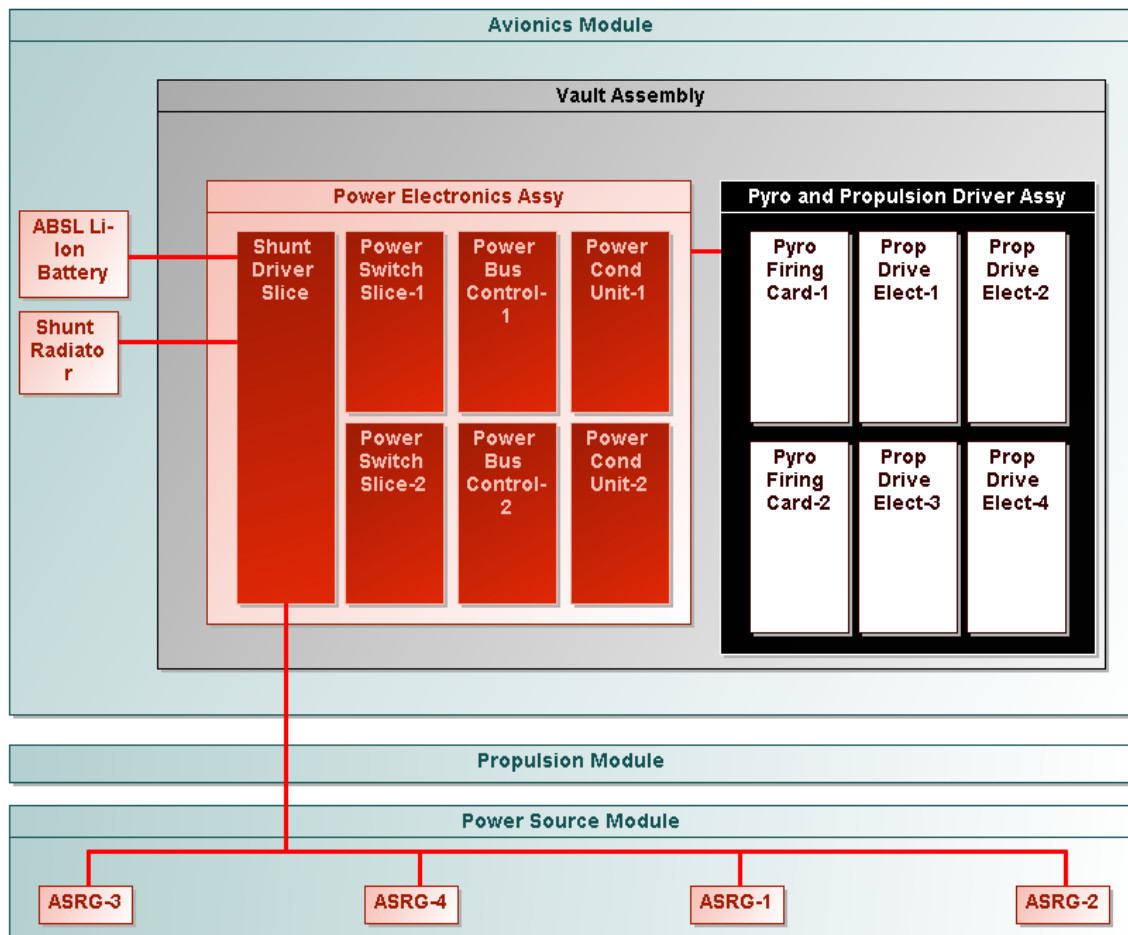


Figure C.2.4-30. The power electronics are shielded inside the vault.

Power Control

The PBC slices provide the SpaceWire command interface to C&DH. The PBC provides a low-power serial data bus to all of the other power electronics slices. It converts commands from the C&DH via the SpaceWire interface and distributes them to other slices through a low-power serial data bus. The PBC collects Power Subsystem telemetry and makes it available to C&DH via the SpaceWire interface.

The PBC contains control algorithms for regulating the power bus by commanding shunt switches in a shunt regulator. The ASRG power source has a constant power I-V curve over

a power bus voltage range of 22 to 34 V at the ASRG output. The control function senses the current in the battery and adds or subtracts shunt current to limit the battery charge current to C/5 (full Charge in 5 hours). The PBC commands discrete shunt driver switches in the SDS that drive power to the shunt radiator to control the power bus. The current regulation will taper to 0 current at the voltage set point correlating to the desired state of charge. We are using 32.8 V as the 100% state of charge for the selected Li-Ion battery technology. The PBC has several commanded set points to set the battery at the desired state of charge.

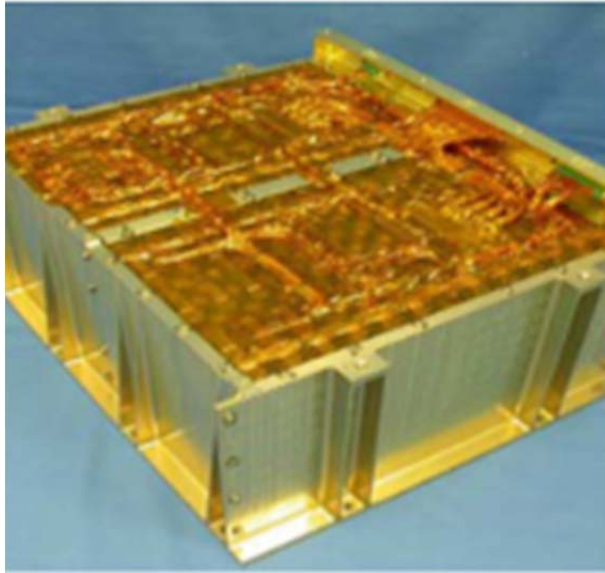


Figure C.2.4-31. Small-cell ABSL reference battery is the same size as the SMAP battery configured with 8 cells in series and 52 strings in parallel.

The energy storage technology assumed for this study is based upon the characteristics of the small-cell ABSL Li-ion battery used on the Soil Moisture Active Passive (SMAP) mission (Figure C.2.4-31). The battery is configured with eight cells in series to get the desired bus voltage operating range, and 52 cells in parallel to get the desired 59 Ah of energy storage at the beginning of life. The battery has a capacity of 40 Ah at EOM after a single-string failure, including degradation for life, discharge rate, and operating temperature. The reference scenario that defines the energy storage needed for the Europa Multiple-Flyby Mission is the 2-hour JOI maneuver, which requires 13 Ah at 10°C with a 6.5-A discharge rate. JPL Design Principles allow for a 70% depth of discharge (DOD), making a 19-Ah battery adequate for the Flyby Mission (JPL 2010a).

The small-cell battery approach does not implement individual cell monitoring and balancing due to the matched cell behavior; however, a trade between the large cell with cell balancing and the small cell needs to be studied.

Power Distribution

The power distribution function is a combination of centralized power switches in the MPSS and distributed power switches on the primary side of each PCU. This combination enables the system to optimize the mass of the cabling by using centralized switches for heater buses and other loads that do not require a PCU and distributed switches for each PCU, reducing point-to-point cabling for the major subsystems. A slice packaging approach enables the addition of centralized power switches without affecting the mechanical footprint and cabling and without modifications to a chassis or backplane. Growth in the command and telemetry interface is handled by the addition of addresses on the serial bus implemented in cabling. The thermal interface scales with the mechanical footprint.

Independent high- and low-side switches prevent any single failure from resulting in a stuck-on load and permit the resolution of load shorts to chassis. Commanding is cross-strapped to the power switches through each PBC, such that no single failure will prevent the commanding of any power switch. Each set of load switches is part of the load fault-containment region, regardless of the centralized or distributed location of the switch.

Power Conversion

The power conversion function for each electronic assembly uses a distributed point of load (POL) architecture (Figure C.2.4-32), where appropriate. This approach has a single isolated power converter on the PCU board, providing an intermediate power bus voltage that is distributed to each subassembly in the assembly. Where this is used (e.g., C&DH), the front end of each subassembly can cross-strap the intermediate power bus and provide on and off capability with fault management to enable low-power operating modes and improve fault-containment regions. The primary side power switch is controlled by the Power Subsystem, and the POL regulators are command-

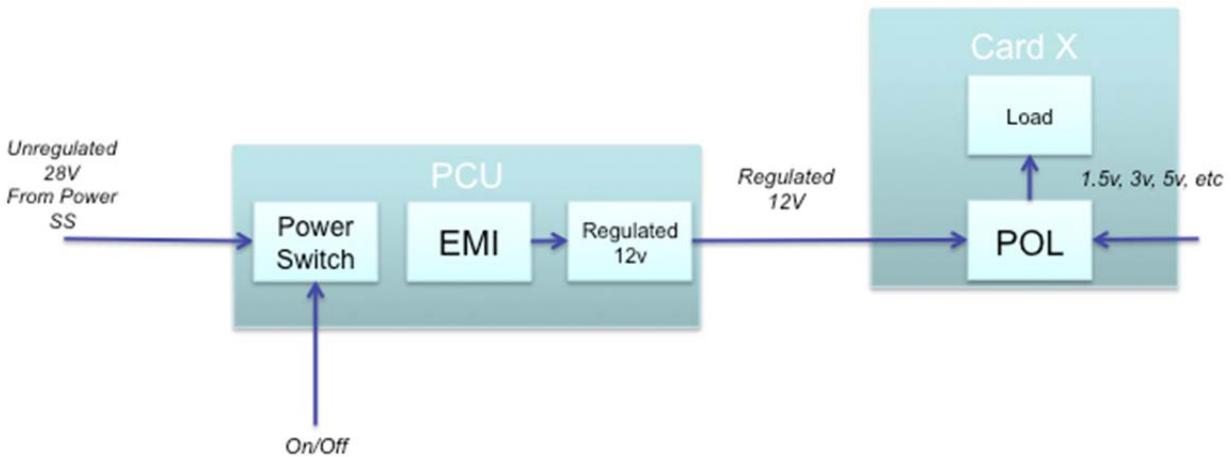


Figure C.2.4-32. POL power conversion architecture shows the primary power bus interface with distributed switch controlled by the Power Subsystem. The distributed POL converters are controlled by the local assembly.

ed by the assembly. In electronic assemblies where POL switching is not needed, primary side power switching would still be used.

PCUs in other subsystems would not be part of the Power Subsystem, but the PCU design would be a common delivery from the Power Subsystem to other subsystems/payloads, both to minimize cost through commonality and to ensure the greatest integrity of the overall system power architecture.

Pyro Firing and Valve Drive

Pyro-firing and valve-drive functions are provided by a set of centralized power switches in the Power Subsystem electronics commanded by C&DH via the PBC. The PFCs are fail-safe off, with two cards providing block-redundancy. Each PFC fires up to 32 NASA Standard Initiators (NSIs) from a protected load power bus that provides all of the safety inhibits required for launch. The PFC controls the current into each NSI, with the ability to fire six events simultaneously.

The PDE actuates valves for the main engine and the ACS thrusters. The PDE also actuates propulsion latch and solenoid valves and switches power from the protected load bus with necessary safety inhibits in place. The PDE is fail-safe off with single-fault-tolerance provided by a block-redundant set.

Power Subsystem Heritage

This Power Subsystem concept uses the same architecture as SMAP, and many of the slice designs are the same. The power bus control algorithm is the same as used on SMAP, as is the slice packaging design and designs for the PFC and PDE. The MPSS is the high-side and low-side variant of the design used on SMAP. The PBC has a new command interface, but the control of the shunt regulator is the same as for SMAP. The ABSL battery is the same design as used on SMAP, and the cell technology has flight heritage with Kepler.

C.2.4.6.3 Guidance, Navigation, and Control

The GN&C Subsystem provides an agile pointing platform for science data collection and a stable platform for science telemetry transmission.

The Europa Multiple-Flyby Mission GN&C Subsystem provides three-axis attitude control through all mission phases after separation from the launch vehicle in order to meet science and engineering pointing needs for instruments, antennas, radiators, shades, and so on. All pointed elements (except the SWIRS mirror for image integration) are body-fixed, so pointing is via spacecraft orientation. GN&C also detumbles the spacecraft after separation, controls ΔV maneuvers and performs momentum management. During JOI or

larger TCMs, when the fixed main engine is used, GN&C provides thrust vector control using dedicated TVC thrusters mounted on the thruster clusters.

At flyby ranges greater than 1,000 km, the spacecraft points at areas of interest for SWIRS images. During flyby maneuvers with ranges less than 1,000 km, the spacecraft is pointed to nadir to enable science instrument data collection; after each flyby, the spacecraft points the HGA towards Earth to downlink the science data.

The C&DH Subsystem hosts GN&C software, which is developed in a GN&C design and simulation environment.

GN&C hardware consists of reaction wheels, inertial measurement units (IMUs), sun sensors and stellar reference units (SRUs). Four reaction wheels and block redundant IMUs and SRUs provide single fault tolerance. The reaction wheel, IMU, and SRU electronics are heavily shielded from radiation, allowing the use of standard space products. The SRU head with detector is shielded to reduce the electron/proton flux so that $<4^{\text{th}}$ -magnitude stars can be tracked. Analysis of attitude determination capabilities in the Europa environment demonstrated pointing knowledge capability exceeding the requirements driven by HGA pointing with Ka-band.

As on Cassini, the location over time of the spacecraft and of pointing targets will be stored on board, enabling ephemeris-based tracking, including target relative pointing profiles and motion compensation, as necessary. Cassini demonstrated that this improves performance and reduces operations complexity. The use of thrusters for thrust vector control eliminates the development cost and complexity for a gimballed engine and reduces the number of unique interfaces on the vehicle. When the redundancy of the main engine is revisited in Phase A, this configuration would be subject to change, including possibly the need for gimbals.

Table C.2.4-5. The GN&C Subsystem design provides an agile platform with precise pointing control.

Item	Value	Sizing
Reaction Wheel Momentum	12 Nm	Handle flyby maneuvers
Attitude-Control Thruster Size	4.45 N	Minimum torque impulse bit for deadband control during cruise/safe mode
TVC Thruster Size	22 N	TVC control for CM offset
Ka-Pointing	1 mrad	Support HGA link budget at required data rate with 3 dB of margin
X-Pointing	112 mrad	MGA communication while Sun-pointing
Ti Jitter	25 μ rad/ 3.5 ms	
IPR Jitter	5 cm/32 s	Assumes 15-m IPR antenna

Table C.2.4-5 shows the key characteristics of the GN&C Subsystem. The reaction wheel sizing is driven not by environmental momentum accumulation but by the flyby maneuver. The momentum sizing of 12 Nms was based on vehicle inertias and the maximum flyby rate, with 100% margin for unknowns. The torque sizing of 95 mNm was based on vehicle inertias and maximum acceleration during the flyby, with 100% margin for unknowns (on top of the torque required to overcome losses inside the wheel). Figure C.2.4-33 shows the thruster configuration.

Given a thruster moment arm of approximately 2 meters, the attitude-control thruster sizing of 4.45 N is to provide a sufficiently small minimum torque impulse for deadband attitude

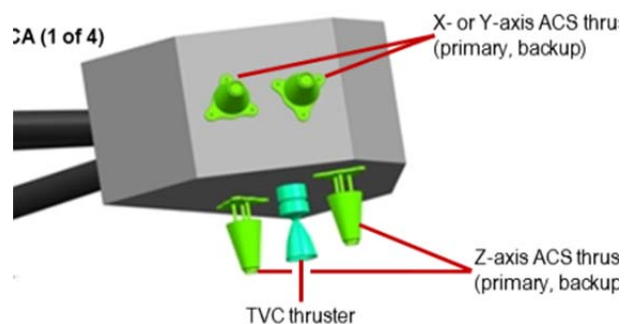


Figure C.2.4-33. The thruster configuration leverages the proven Cassini approach.

control during interplanetary cruise (or safe mode). The TVC thruster sizing of 22 N is provides sufficient control authority for up to a 9-centimeter shift of the vehicle center of mass (CM) during the mission. Ballast mass is included in the MEL (Section C.4.3) to provide initial center of mass alignment. Methods of controlling CM offset from propellant migration will be studied in Phase A.

The 1 mrad Ka-pointing control requirement is a radial, three-sigma number derived from the telecom link analysis. The X band pointing for safe mode is 112 mrad, based on a beam width that allows Sun-pointing with Sun-sensors while still communicating with Earth from Europa. The TI jitter is 25 microradians over the exposure time of the camera of 3.5 milliseconds. The IPR jitter is based on keeping the antenna beam aligned with the orbit normal such that there is no more than a 5 centimeter deflection off that line at the ends of the 15 meter boom over 32 seconds. The capability of the concept will be assessed when more details about spacecraft flexible-body effects and propellant slosh are modeled.

Figure C.2.4-34 shows the block diagram of

the GN&C Subsystem. At the center of the subsystem is the FSW that resides in the RAD750 processor in the C&DH electronics. For Sun-pointing modes of operation, the knowledge of the Sun vector with respect to the vehicle reference frame is provided by three Sun-sensors distributed on the Avionics Module to provide near 4π -steradian coverage. If there are any gaps in the coverage a spiral scan attitude maneuver can quickly bring the Sun into a sensor's FOV. For precise attitude determination a combination of inertial measurements corrected by stellar updates is provided by the IMUs in the avionics vault and shielded SRUs outside the vault.

For precision attitude control, three of four reaction wheels are used; accumulated angular momentum from external torque is eliminated, as needed, by the attitude-control thrusters. The reaction wheel drive electronics (RWE) are in the avionics vault while the mechanical assembly (RWA) is outside the vault. For less precise attitude control during cruise or during safe mode, the attitude-control thrusters can be used. Note that using the Cassini configuration for thrusters uncouples forces and torque in

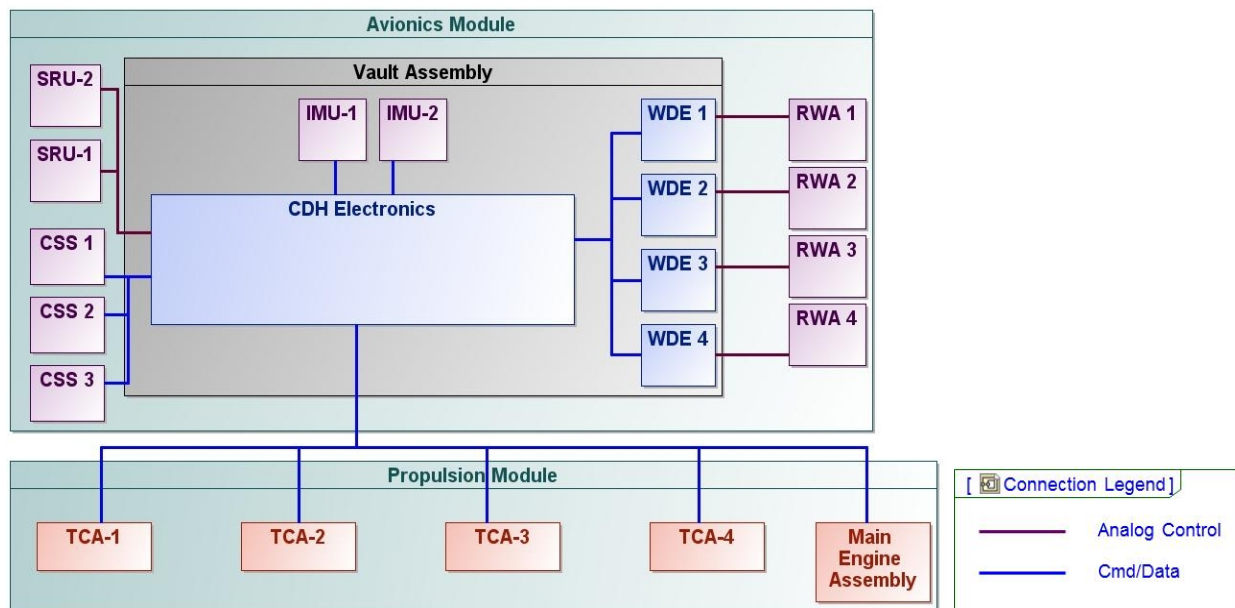


Figure C.2.4-34. The GN&C Subsystem is redundant and cross-strapped to provide robust fault-tolerance to radiation events.

Table C.2.4-6. GN&C hardware items, and approach to deal with radiation.

Item	Radiation Approach
Reaction Wheel	Sensitive wheel-drive electronics in avionics vault Mechanical assembly radiation-hard by design
Sun-Sensor	Radiation-hard by design
Stellar Reference Unit	Shielding for flux and total dose
Inertial Measurement Unit	In avionics vault

roll, but not in pitch or yaw. For attitude control during TCM or JOI (when the main engine is fired), the TVC thrusters are used for pitch and yaw control while the attitude-control thrusters are used for roll control.

The GN&C architecture is cross-strapped such that any SRU can be used with any IMU to provide the attitude information to any computer. Attitude control can be accomplished with any three of four reaction wheels or with any set of eight block-redundant thrusters.

Given the radiation shielding provided by the rest of the spacecraft, the GN&C Subsystem can use standard space GN&C products with high TRL. Table C.2.4-6 shows the GN&C hardware items, and the approach to deal with radiation.

C.2.4.6.4 Command and Data Handling Subsystem

The C&DH provides a cross-strapped and redundant radiation-hard platform to support the data storage and processing needs of flyby science.

The Europa Multiple-Flyby Mission C&DH is the control center for most activities on the spacecraft, including nominal command sequencing; general system operation; GN&C, propulsion, and thermal control algorithms; and fault management. Both science and engineering data are also gathered, stored, and processed in C&DH for telemetry.

Several additional key requirements drive the C&DH, as follows. The design must be single-fault-tolerant and cross-strapped. It must be able to fail operational during single-event ef-



Figure C.2.4-35. The RAD750 provides high heritage for both the C&DH electronics and FSW designs.

fects in the high-radiation environment of the Jovian system, and should allow easy swapping of redundant subassemblies to enable rapid transition of control after a fault. A RAD750 single-board computer (see Figure C.2.4-35) was selected to leverage the processor's flight heritage and radiation-hardness, and JPL's software architecture heritage. Onboard data storage is sized to accommodate multiple copies of the flyby science data. Concepts for data integrity using this redundant storage capacity will be investigated in Phase A.

The C&DH electronics occupies a single box that is internally redundant. Given the use of SpaceWire (see Figure C.2.4-36) as the primary interface, there is no need for a backplane or motherboard within the box; this increases the C&DH box reliability and simplifies packaging. A standard-size chassis of a 6U × 220 mm cards was selected to enable the use of heritage single-board computers and provide sufficient board area for the I/O and memory cards.

Time broadcast and synchronization are part of the SpaceWire standard so no external timing

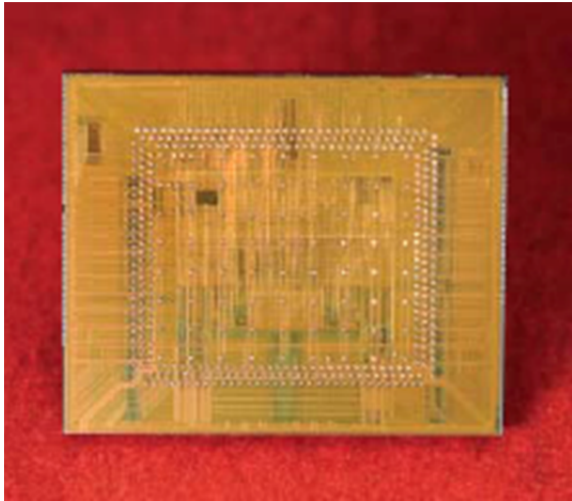


Figure C.2.4-36. The SpaceWire interface chip is radiation-hard and provides a high-speed standard interface to the cards in the C&DH.

network is required. Remote I/O units handle all the low-level interfaces such as analog and discrete measurements, and serial I/O; they also provide the Telecom Subsystem interface, critical relay commanding, and processor swap functions. I/O is multiplexed through an enhanced SpaceWire interface that can support programmable I/O functions. I/O circuits are standard designs from other JPL spacecraft.

The solid-state recorder provides 128 Gbit of storage using Flash memories. Although Flash memories are commercial parts, recent testing shows several radiation-tolerant options. A

radiation characterization risk-mitigation activity in Phase A will identify the best part, followed by a lifetime buy for the project. The memories are interfaced to the spacecraft through a SpaceWire interface with embedded processor that will allow it to behave as “network-attached” storage: Reading from and writing to this recorder doesn’t require involvement of the RAD750, freeing this processor for other functions, such as IPR data processing. The power-conditioning unit (PCU) takes in unregulated 28 V off the power bus, provides EMI filtering, and converts it to a regulated 12 V that is distributed to each card in the box. The PCU on/off switch is controlled by the Power Subsystem. The local card on/off is software controlled via the processor and commands issued via the remote I/O.

A physical block diagram of C&DH is shown in Figure C.2.4-37. This shows the cards in the C&DH box. The box is internally redundant and cross-strapped (both data and power). SpaceWire supports multiple topologies (e.g., star or daisy chain). The box consists of two RAD750 single-board computers with SpaceWire router, two mass memory cards, two remote I/O cards, and two PCUs. The mass memory card interfaces to the single board computer via SpaceWire. The remote I/O cards interfaces to the single-board computer via SpaceWire.

The C&DH electronics does not require any new technologies. The RAD750 single-board computer with SpaceWire is an off-the-shelf product. The SpaceWire interface chip is an off-the-shelf product. The I/O circuits, power supply, and mass memory have analogs on previous projects. The $6U \times 220$ mm packaging standard has been qualified and used on previous projects.

C.2.4.6.5 Software

Highly reliable software for mission-critical applications is essential for this long-life mission. The flight software (FSW) baseline extends JPL's long heritage in FSW architecture development, and will be implemented in accordance with JPL requirements for NASA Class B (non-human-space-rated) software development. JPL has established a set of institutional software development and acquisition policies and practices as well as design principles that apply to mission-critical and mission-support software. These practices conform to NASA Software Engineering Requirements, NPR 7150.2 (NASA 2009b) and are an integral part of the JPL Design Principles (DPs) and Flight Project Practices (FPPs) (JPL 2010a, b). All Europa Multiple-Flyby

Mission FSW will be developed in accordance with JPL institutional policies and practices for deep space missions, including JPL's Software Development Requirements (JPL 2010c), which address all Capability Maturity Model Integration (CMMI) process areas up to maturity level 3. Software identified as safety-critical will comply with safety-critical requirements, regardless of software classification. Software safety-criticality assessment, planning, and management will be performed for all software, including new, acquired, inherited, and legacy software and for supporting software tools. Software is identified and documented as safety-critical or not safety-critical based upon a hazard analysis conducted prior to start of development activities.

Key functions allocated to software include system command and control, health and safety management, attitude and ΔV control (such as maintaining concurrent HGA Earth pointing during telecom sessions, or instrument surface tracking during science operations), science data collection and processing, onboard data management, and reliable delivery using Consultative Committee for Space Data Systems (CCSDS) File Delivery Protocol (CFDP).

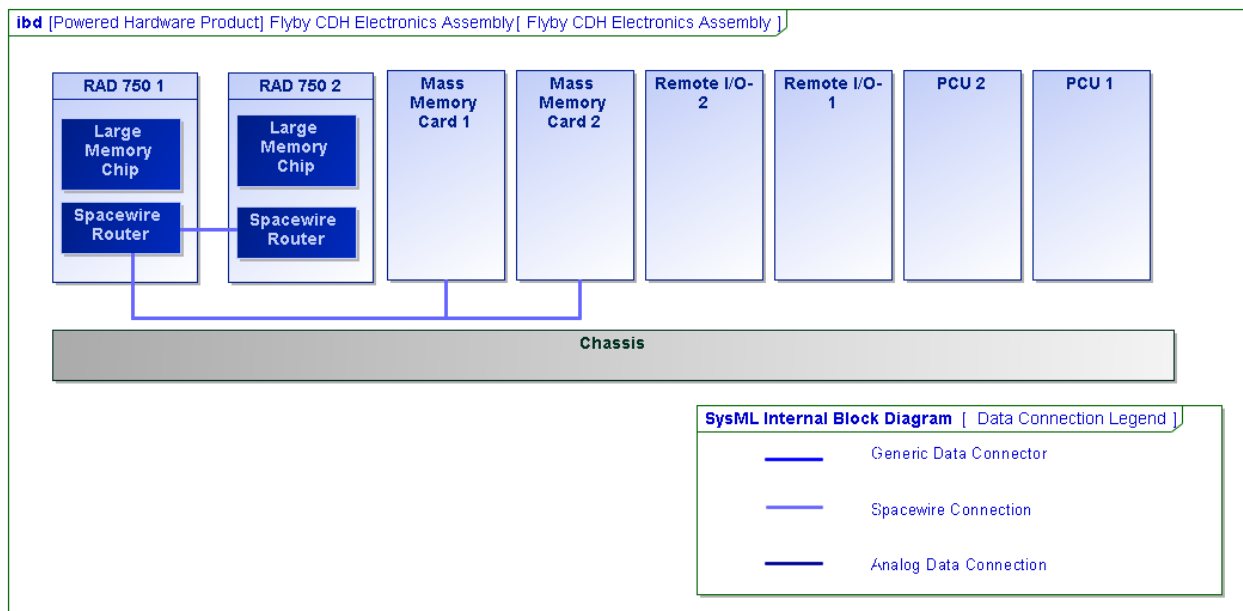


Figure C.2.4-37. The C&DH is redundant and cross-strapped to provide robust fault-tolerance.

Onboard ephemeris-based pointing and the use of CFDP help to simplify operations and thus reduce long-term operations costs. None of these capabilities are new technology, and significant algorithm and architecture heritage is available from Cassini, MSL, SMAP, MESSENGER, and other missions.

Flight software has a key role in system fault management. Critical activities are expected to include postlaunch separation, detumble, and acquisition, Jupiter orbit insertion, and possibly a moderate number of propulsive maneuvers needed to achieve the planned sequence of flybys. Although the flyby sequences are expected to be less complex than comparable Cassini or Galileo flybys, due to having fewer instruments and no articulation, they repeat at a more demanding rate than experienced in previous missions, and occur in the hostile radiation environment around Jupiter and Europa. Moreover, coverage objectives require most of the flybys to complete with minimal disruption. For this reason the FSW coordinates a system fault-management approach, consistent with current best practices, aimed at protecting essential resources, but trying to

maintain scheduled operations using automatic fault responses such as resetting devices, switching to redundant devices, or selectively trimming subsets of planned activities.

The FSW is organized in a layered architecture, as shown in Figure C.2.4-38.

The Platform Abstraction layer interfaces directly with the hardware. This layer contains drivers that provide control, and data abstractions to the device-manager and services layers. The drivers communicate with the hardware using the device-specific syntax and protocol, allowing higher layers of software to interact with these devices using system-standard communication protocols and message formats. Notably, the use of industry-standard SpaceWire as a common hardware communications medium reduces the number of different device types that must be supported, with commensurate reductions in software system complexity. Furthermore, the ability of SpaceWire interface devices to buffer data and perform other control functions in hardware (as demonstrated by MESSENGER) is expected to further reduce the complexity and time-criticality of the FSW implementation.

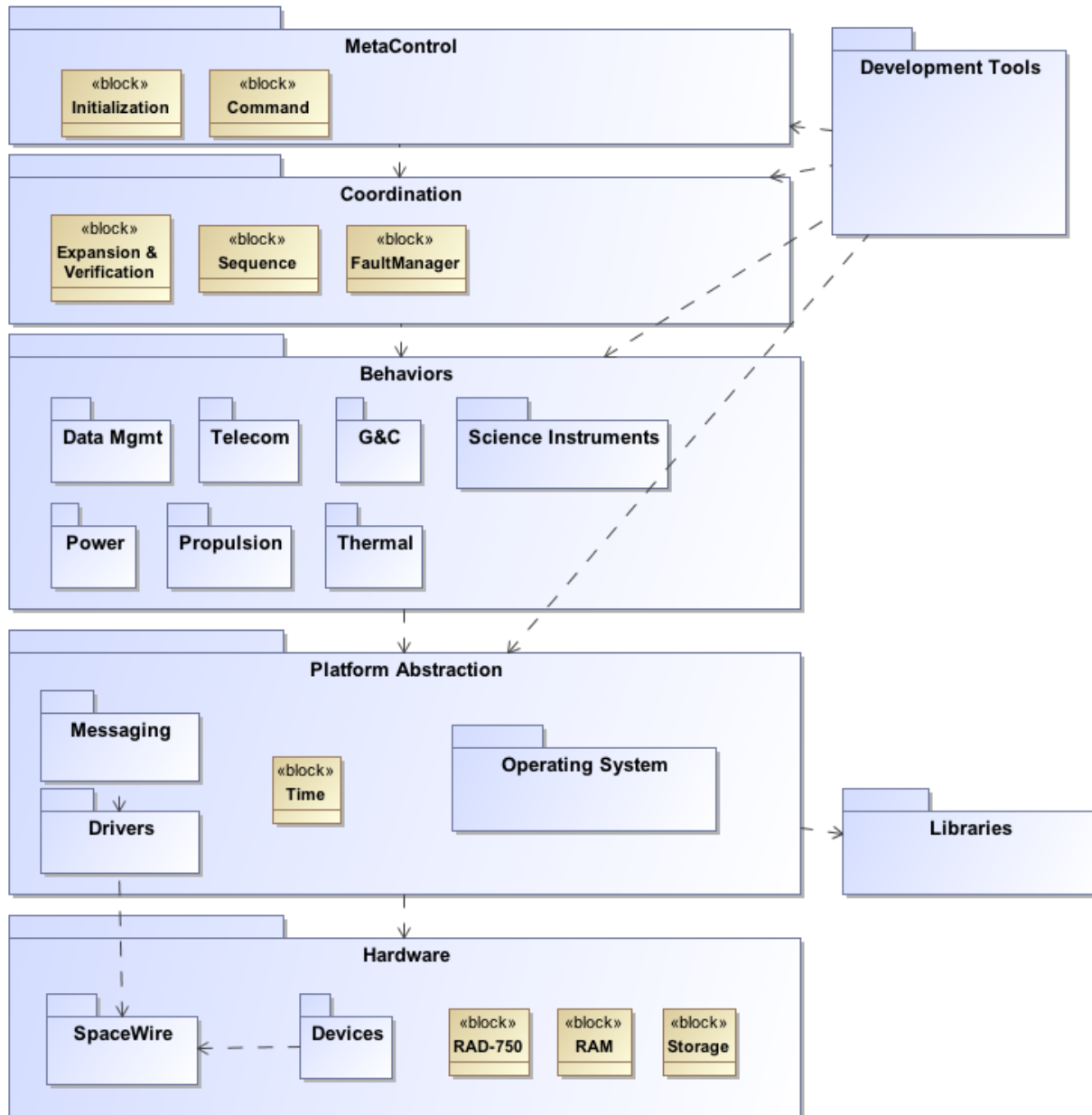


Figure C.2.4-38. Flight software benefits from appropriate reuse and evolution within a layered architecture.

The Platform Abstraction layer also encapsulates the real-time operating system, device drivers, and all interprocess communications, leveraging flight heritage with the RAD750 platform and all JPL missions since Pathfinder. The commercial operating system provides real-time task scheduling, memory management, and interfaces to I/O devices immediately associated with the processor board.

The Behaviors layer includes software elements that perform closed-loop control around specific system behaviors. These behaviors are typically responsible for the management of one or more hardware devices or subsystems, as well as integrated behaviors associated with them, such as attitude control. Closed-loop behaviors also incorporate fault detection and localized fault management capabilities.

Behavior coordination is provided in a separate Coordination layer that can sequence and coordinate the control of underlying behaviors. This layer is also responsible for coordinating any fault responses at a system level.

The MetaControl layer provides services for initializing and supervising reliable operation of the rest of the software and computing system and for supporting external commanding and configuration (such as changing system behavior from the ground).

Instrument-embedded software is developed by instrument providers and tested locally using a spacecraft simulator (see Testbed Approach). It is delivered with the instruments. Some engineering devices may also include embedded software. All other software is developed in-house.

C.2.4.6.6 Structure

The Avionics Module (Figure C.2.4-24) supports the majority of the avionics, batteries, science instruments, star-trackers, Sun-sensors, and reaction wheels. Its vault houses and shields most of the avionics components and extends below the Avionics Module's mechanical interface with the Propulsion Module. This configuration optimizes radiation-shielding by making use of the existing structure in all directions: From the top the octagonal primary structure, reaction wheel mechanical assemblies, and batteries provide shielding; from the sides the primary structure, tanks, and thermal enclosure provide shielding; and from the bottom the Power Source Module's primary structure and the Propulsion Module's main engine assembly provide shielding, complementing the vault's thick walls. Waste heat from the avionics is allowed to radiate out from the vault into an enveloping thermal shroud to help maintain the propulsion tanks at their required temperatures.

The topmost part of the Avionics Module, called the Upper Equipment Section (UES), is also octagonal. The vault is box-shaped. The structure that connects the UES of the Avion-

ics Module to the vault is composed of machined stringers riveted to sheet-metal panels. An octagonal ring is riveted to the top of the module, and a square interface ring is riveted to the bottom.

The vault consists of six machined panels that are riveted together, with access panels integrated to allow for installation and removal of the avionics.

The batteries and reaction wheels reside inside the UES of the Avionics Module.

Instrument Accommodation Structures

The INMS, TI, SWIRS, and IPR are all mounted to the Avionics Module's primary structure, as shown in Figure C.2.4-39. Each instrument has been positioned to accommodate the required aperture and radiator fields of view to support its science function.

Thermal Section Structures

The thermal enclosure consists of blankets made from aluminized Kapton, aluminized Mylar, and Dacron net separators, supported by a lightweight, carbon-fiber tubular frame.

C.2.4.7 Technical Budgets

Three primary technical margins are addressed here: mass, power/energy, and data balance.

Other key technical margins are covered elsewhere in this report: Radiation tolerance margin is treated in Section C.2.6.1.

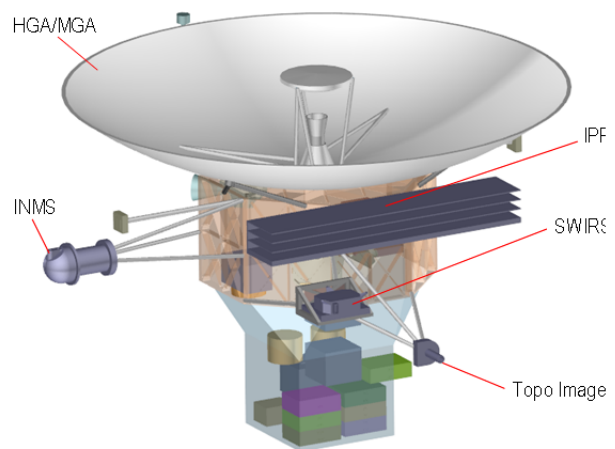


Figure C.2.4-39. Avionics Module primary structure.

The approach to technical resources in this study has been to model what is well understood, and then include conservative margin based on past experience to account for items not known well enough to model.

To minimize cost and schedule risk, we have striven to achieve high levels of technical margin wherever possible.

C.2.4.7.1 MEL and Mass Margins

Mass margin follows the definitions and conventions specified in the JPL Design Principles, Section 6.3.2 (JPL 2010a). The earliest milestone at which the Design Principles specify a mass margin, however, is the Project Mission System Review (PMSR), when at least 30% is required. In consideration of the fact that the Europa Multiple-Flyby Mission concept is in a study phase, we have set a more conservative policy of $\geq 40\%$ mass margin for this report. This is consistent with the expected evolution of JPL's institutional guidance. The method of calculating the Design Principles margin is shown in Table C.2.4-7.

The dry mass current best estimate (CBE) includes tanks sized to carry the maximum propellant load, plus radiation shielding, and the launch vehicle adapter (LVA). Each of these is discussed in more detail below.

Use of "Max Propellant"

The Design Principles explicitly require that the propellant load assumed for the margin calculation be that amount of propellant needed to provide the required ΔV for the maximum possible launch mass on that launch vehicle (LV), given ΔV requirements for the

chosen trajectory. In addition, the dry mass of the propellant tanks reflects tanks sized for this maximum propellant load. This approach gives an accurate reading of the overall dry mass margin, *assuming* that the flight system grows

Table C.2.4-7. Europa Multiple-Flyby Mission mass margin.

Flyby Mass Margin				
T. Bayer 24 Apr 2012 Flyby Model - Final Report Update	LAUNCH			
	Flight System Mass, kg			
	CBE	Cont.*	MEV	
Ion & Neutral Mass Spectrometer	24	50%	36	
Ice Penetrating Radar	33	50%	50	
ShortWave IR Spectrometer	21	50%	31	
Topographical Imager	7	50%	11	
Payload	85	50%	127	
Power	59	21%	72	
C&DH	39	30%	51	
Telecom	98	29%	126	
Structures	529	27%	673	
Thermal Control	44	30%	57	
Propulsion	175	28%	224	
GN&C	68	23%	84	
Harness	70	50%	105	
Radiation Monitor	8	30%	10	
ASRGs (4)	174	45%	252	
Spacecraft	1264	31%	1655	
Flight System Total Dry	1349	32%	1782	Max Prop
Bipropellant	860		1277	1711
TVC Monopropellant	75		75	75
ACS Monopropellant	40		40	40
Pressurant	6		6	6
Residual and Holdup	24		35	46
Propellant	1005		1432	1877
Flight System Total Wet	2354		3214	
Capability (21-Nov-21 VEEGA)	Atlas V 551:		4494	
System Margins				
JPL DWP (Capability - Max Prop - CBE Dry) / (Capability - Max Prop)			48%	
Total payload shielding	48	42%	68	
Total spacecraft shielding	170	29%	220	
LV adapter	89	25%	111	
*Using ANSI/AIAA Guide G-020-1992, "Estimating and Budgeting Weight and Power Contingencies for Spacecraft Systems", applied at the component level.				

to the maximum launchable mass.

Specifically, in Table C.2.4-7, propellant mass is computed from the ΔV required for the 21 November 2021 Venus-Earth-Earth gravity assist (VEEGA) trajectory. The CBE propellant is computed using the CBE dry mass and CBE ΔV . The maximum expected value (MEV) propellant is computed using the MEV dry mass and the MEV ΔV . The max propellant is computed using the maximum possible dry mass and the CBE ΔV .

Radiation Shielding

The mass model tracks the amount of shielding necessary to protect each piece of sensitive electronics. This mass is accounted for at the appropriate level of assembly (card, box, or module), and shown as a payload and engineering total in Table C.2.4-7.

Launch Vehicle Adapter

A standard Atlas LVA is assumed. The mass shown in Table C.2.4-7 includes both the part that remains with the spacecraft and the part that remains with the Centaur upper stage but is considered by launch services as “payload mass” for the purpose of LV performance. Delta-V calculations carry only the part that remains with the spacecraft.

This margin calculation adds “growth contingency” mass to the CBE masses to arrive at an MEV mass and the propellant required for that mass. It then compares this value to the LV capability. For determination of contingency factors, the Europa Study Team has used the ANSI/AIAA Guide G-020-1992 (American National Standards Institute 1992), applied at the component level. This specifies the *minimum* contingency factor based on project phase and component sizing and maturity, and

allows a higher factor where the project deems it appropriate. The guideline is generally consistent with traditional JPL practice, but provides a more rigorous grounding through its use of historical data.

As can be seen in Table C.2.4-7, the Europa Multiple-Flyby Mission has excellent mass margins. A more detailed mass breakdown can be found in the MEL (Section C.4.3).

C.2.4.7.2 PEL and Power/Energy Margins

The Power Equipment List (PEL) contains the CBE power needs for power loads in various modes, with a contingency for maturity. Europa Multiple-Flyby Mission power modes are based on the mission scenarios described previously (see Section C.2.1.2). The policy established for Europa Multiple-Flyby Mission policy has been to maintain 40% of the power source capability after an ASRG single failure as power margin on the load for all mission power modes. Each mission mode is assessed against this policy. Transient modes are assessed with power margin on the load included, and using the JPL Design Principles depth of discharge (DOD) guidelines for actual battery capacity, assuming a single failure. Others are steady state (S/S). Summary results of the mission mode power analysis are shown in Table C.2.4-8.

The PEL provides the CBE capability of the power source and its LEV for each mission mode. The power source estimate takes into account degraded performance of the ASRG during launch due to the environmental conditions inside the shroud. The LEV of the ASRG assumes a failed Stirling converter after launch, effectively producing the power of 3.45 ASRGs.

Table C.2.4-8. Europa Multiple-Flyby Mission power analysis compares the power source capability to the estimated load for all phases of the mission. There are two mission modes that rely on the battery, and the DOD is displayed.

Mission Phase	Flyby Power Analysis					Margin %	Stdy State or Transient?	Max Bat DOD, %
	ASRG Power, W		Flight System Power, W					
	CBE	LEV	CBE	Cont.	MEV			
Launch	426	334	113	19%	135	66%		
Inner Cruise	535	420	224	24%	279	47%	S/S	
Inner Cruise (Safe)	535	420	245	23%	302	42%	S/S	
Outer Cruise	514	403	177	23%	217	56%	S/S	
Outer Cruise (Safe)	514	403	245	23%	302	39%	S/S	
Orbit Insertion/TCM	505	403	355	24%	438	40%	Transient	32%
Flyby Science (all instruments)	498	391	264	27%	391	40%	Transient	2
Flybys Science (without IPR)	498	391	207	25%	258	47%	S/S	
Telecom Downlink	498	391	224	27%	284	43%	S/S	

The PEL reports for each load a CBE, a contingency to cover estimated growth based on maturity, and a maximum expected value (MEV), which includes transient loads. Each identified power mode is covered in the PEL, along with a summation of all of the loads that are on in that mode. The mission mode total is compared to the power source capability for the same mission mode, with the power margin calculated per the JPL Design Principles approach of $(\text{Capability} - \text{CBE}) / \text{Capability}$ (JPL 2010a). The transient modes are modeled to estimate the battery DOD with the actual battery capacity.

One mission mode that needs some investigation is the outer Cruise Safe Mode, in which the power margin is slightly below the Europa Multiple-Flyby Mission policy at 39%. This is a steady-state mode that cannot rely on the battery, so sizing adjustments will be analyzed in Phase A to comply with the mission policy margin.

The two transient modes in the PEL are Orbit Insertion /TCM and Flyby Science (all instruments). Orbit insertion is presently the driving mode for battery sizing due to the long JOI burn of roughly 2 hours. However, this is based on very conservative assumptions regarding backup strategies that will be revisited in Phase A. Under such assumptions, the load profile and battery DOD are shown in Figure C.2.4-40, given a battery capacity estimat-

ed to be 40 Ah with a 6.5-A discharge at 10°C near EOM.

The JPL Design Principles allow for a 70% DOD for events such as orbit insertion that involve less than 100 cycles (JPL 2010a).

The other transient mode is the Flyby Science (all instruments) mode, in which the different instruments are turned on, depending on the distance range from Europa. The system is power-positive until the Ice-Penetrating Radar (IPR) is turned on for 16 minutes near closest approach to Europa (see Figure C.2.4-41).

We presently have only 2% DOD for this Flyby Science mode. The JPL Design Principles allow 60% DOD for less than 5,000 cycles (JPL 2010a).

Because both transient modes presently possess generous margins, there may be an opportunity to adjust the size of the battery to reduce mass, if necessary.

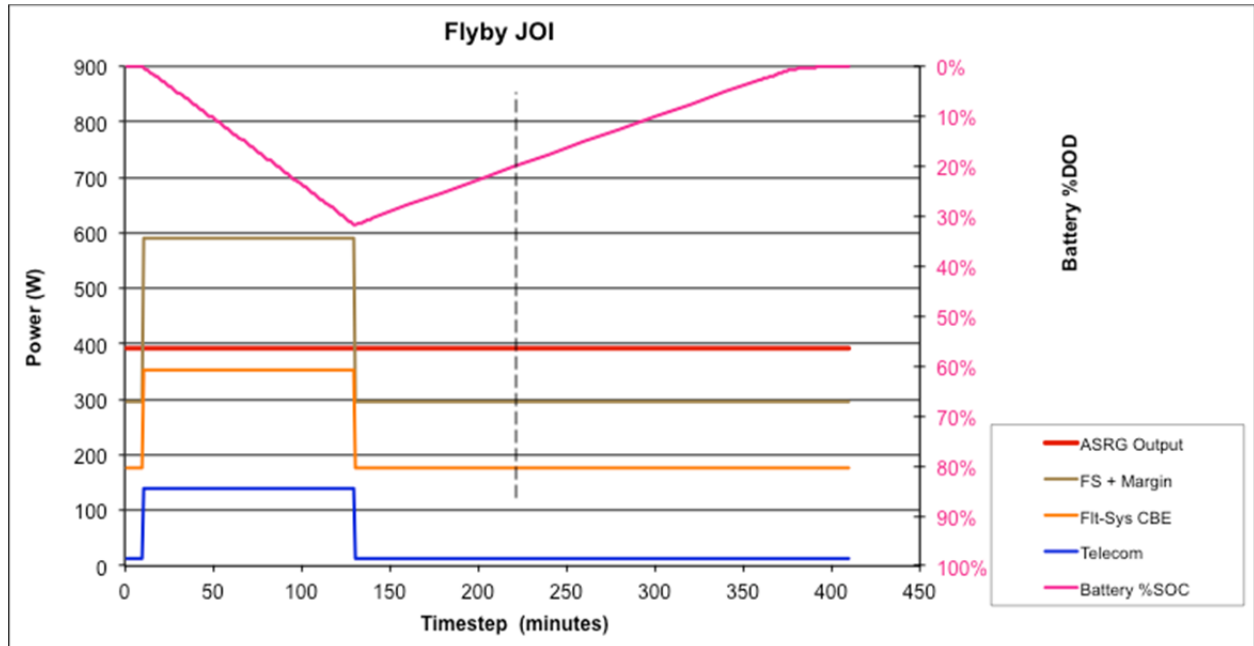


Figure C.2.4-40. Flyby JOI power analysis shows a 2-hour discharge of the battery using the Europa Study policy of 40% margin on the load profile.

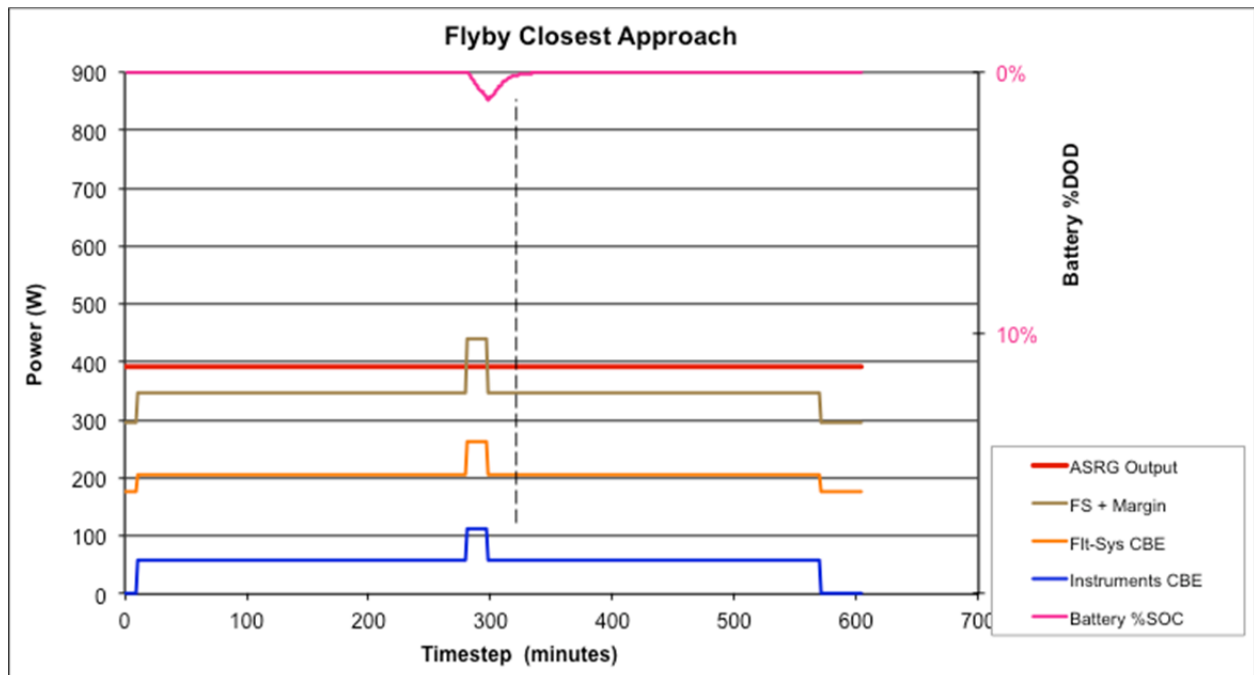


Figure C.2.4-41. Flyby science mode power profile shows that the system is power-negative only when the IPR is on for 16 minutes of each flyby.

C.2.4.7.3 Data Balance

Mission data balance is driven by the science objectives described in Section C.2.1, and the corresponding operations strategy described in Section C.2.5. This science scenario is viewed as the driving case for data collection rates because this is the only time the science instruments are operated, and because all must be operated concurrently when under 1,000 km in altitude. Each flyby is nearly identical, so the concept is to use essentially the same sequence of science observations each time, resulting in about the same data volume each time, as well. The notional instruments have a small number of operating modes where data output rate changes significantly. Operating modes for the nominal scenario are assumed to be producing data at the maximum expected rates.

The majority of orbits in the present mission concept have a 4:1 resonance with the period of Europa's orbit, so a 4-Eurosol period is used as the nominal repeat cycle for science operations to determine the time available for downlink. Each cycle begins with about 10 hours of science observations during the closest approach to Europa, producing about 32 Gbit of stored. The observation phase is followed immediately by a short battery-recharge period and then data playback during the ascending petal of the orbit. During this period, data is transmitted on Ka-band to maximize downlink throughput. Ground tracking is provided using 34-m DSN stations operating alternate 8-hour passes until the data from the flyby is recovered (this provides the option of inserting additional station passes to recover

from a missed pass). Additional downlink time is available during the descending petal of the orbit to recover any data missed during the first playback.

256 Gbit of solid-state data storage is provided by the C&DH Subsystem to provide redundant storage for the data from a single flyby, and/or data from an additional flyby to accommodate missed passes or other downlink interruptions (e.g., from weather). This strategy also accommodates the small number of flybys in transitional orbits that may have less downlink time between them, requiring downlink over subsequent orbits.

Downlink margins are shown in Table C.2.4-9. The 32 Gbit of accumulated data include the quantities of science data shown plus engineering data collected at 2 kbps. Downlink capacity is computed using the Ka link budget described in Section C.2.4.6.1, computed for a worst-case range of 6.5 AU, and DSN elevation angle of 20 degrees, and then multiplied by a factor of 1.2, based on the 2008 JEO analysis, to account for the ability to step downlink bit rates over each pass to maximize the throughput. Note that the telecom link budget already includes some margin for weather, and the downlink strategy described here includes additional margin in the form of time available to use different or alternate DSN stations if one station is disabled due to failure or weather.

Stored data is managed as products (files) in the onboard store; CFDP is used to ensure reliable transport of this data to the ground. At the

Table C.2.4-9. Data balance and margin.

	IPR	TI	SWIRS	INMS	Total/Flyby
Raw Data Rate (kbps)	28000	10258	116	2	
On-time per flybys (min)	15	15	554	15	
Compression Factor	1	3	3	1	
Effective Output Rate (kbps)	28000	3419	47	2	
Average Data Per Flyby (Gbit)	25.2	3.1	1.3	0.002	32 Gbit
Average Downlink Rate (kbps)					134 kbps
Downlink Time Required (hr)					66.3 hr
Downlink Time Available (hr)					326.8 hr
Downlink Margin					80%

average rate of 134 kbps data accumulates on the ground at a rate of about 3.8 Gbit/pass, or about 5.8B Gbit/day. Over the course of 27 science flybys, the mission accumulates a total of about 1 Tb of data. Because the rates given in Table C.2.4-9 are computed assuming worst-case conditions, the actual downlink rates could be higher for some flybys, requiring slightly more time to recover the data. Maximum downlink rates have yet to be determined.

C.2.4.8 Module Development, Integration, and Test

The modular approach for the spacecraft allows parallel testing before delivery to system integration and test at a higher level of integration than was possible for previous spacecraft.

The spacecraft would be comprised of the Avionics Module, the Propulsion Module, and the Power Source Module.

Development of the spacecraft modules begins with the design and fabrication of a developmental test model (DTM) of the spacecraft structure. The DTM is populated with appropriate mass mockups as required to properly represent the mass properties of the spacecraft. After assembly, a full set of structure qualification tests is performed, including static loads, modal survey and pyro-shock testing. The DTM is also used later as a “trailblazer” to ensure that all facilities (such as the launch site and LV) and mechanical ground support equipment (MGSE) characteristics are compatible. Because the DTM components are built to the same drawings as flight, elements of the DTM could also be used as surrogates for the flight structure, if required.

As the DTM program progresses, the flight model (FM) structural components are fabricated and delivered to the module teams (Avionics Module, Propulsion Module and Power Source Module) for integration with active components and secondary structure, and for module-level testing, including environments, prior to the start of system integration and test. 2 months of schedule margin is allocated for

the structure deliveries to the Module Development Teams, and a minimum of 1.5 months schedule margin is allocated for the delivery of the tested flight modules for system integration. Since the Avionics Module is the most complex functionally, 3.5 months of margin are allocated in recognition of its schedule criticality to System Integration and Test.

The module concept adopted for the spacecraft permits testing, both functional and environmental, to be performed with flight cabling and flight structure at a higher level of integration prior to delivery than has been performed on similar previous missions, such as Cassini. Development of more highly integrated modules allows more parallel path testing, reducing the number of interfaces that need to be verified at the system level, compared to a project like Cassini, where individual components and subsystems were delivered and integrated during System Integration and Test.

The major deliveries to system integration are the Avionics Module (consisting of the UES with science instruments (see below), the avionics vault and its contents, and the telecom assembly), the Propulsion Module (with tanks, other propulsion components, and harnessing), and the Power Source Module. The Power Source Module is populated with advanced Stirling radioisotope generators (ASRG) that are electrically heated to permit realistic testing and evaluation of the end-to-end power delivery system for the spacecraft. Emulations of other modules at electrical interfaces will be used to support module-level integration in each case.

All module deliveries are planned to occur at the start of System Integration and Test to maximize flexibility. The UES is initially delivered with Engineering-Model (EM) Science Instruments. The Flight Model (FM) science instruments are delivered later as shown in the System Integration and Test flow, permitting any interface or performance issues to be resolved before the flight deliveries.

C.2.4.8.1 Testbed Approach

Consistent with longstanding practice, the Europa Multiple-Flyby Mission has adopted a system integration approach that is supported by an additional set of software and hardware testbeds, enabling early and thorough integration of key hardware and software interfaces prior to ATLO. This development and validation approach begins with scenario development during formulation and design, and progresses incrementally to system validation using an ever-growing battery of regression tests that verify and validate system architecture as it is designed and developed. Figure C.2.4-42 depicts the proposed testbeds described in the following paragraphs.

Since science instruments are likely to be developed externally, instrument developers must be provided with a testbed environment that includes an emulator for engineering subsystems (hardware and software) that simulates the power, data, and control interfaces with which the instrument must integrate. This ensures that all interface issues have been resolved prior to delivery, thereby helping to keep the ATLO work focused on system integration and on the concerns that can be verified only in an assembled system context. Similar subsystem assembly testbeds are provided for early integration testing of major subsystems (telecom, propulsion, power, etc.).

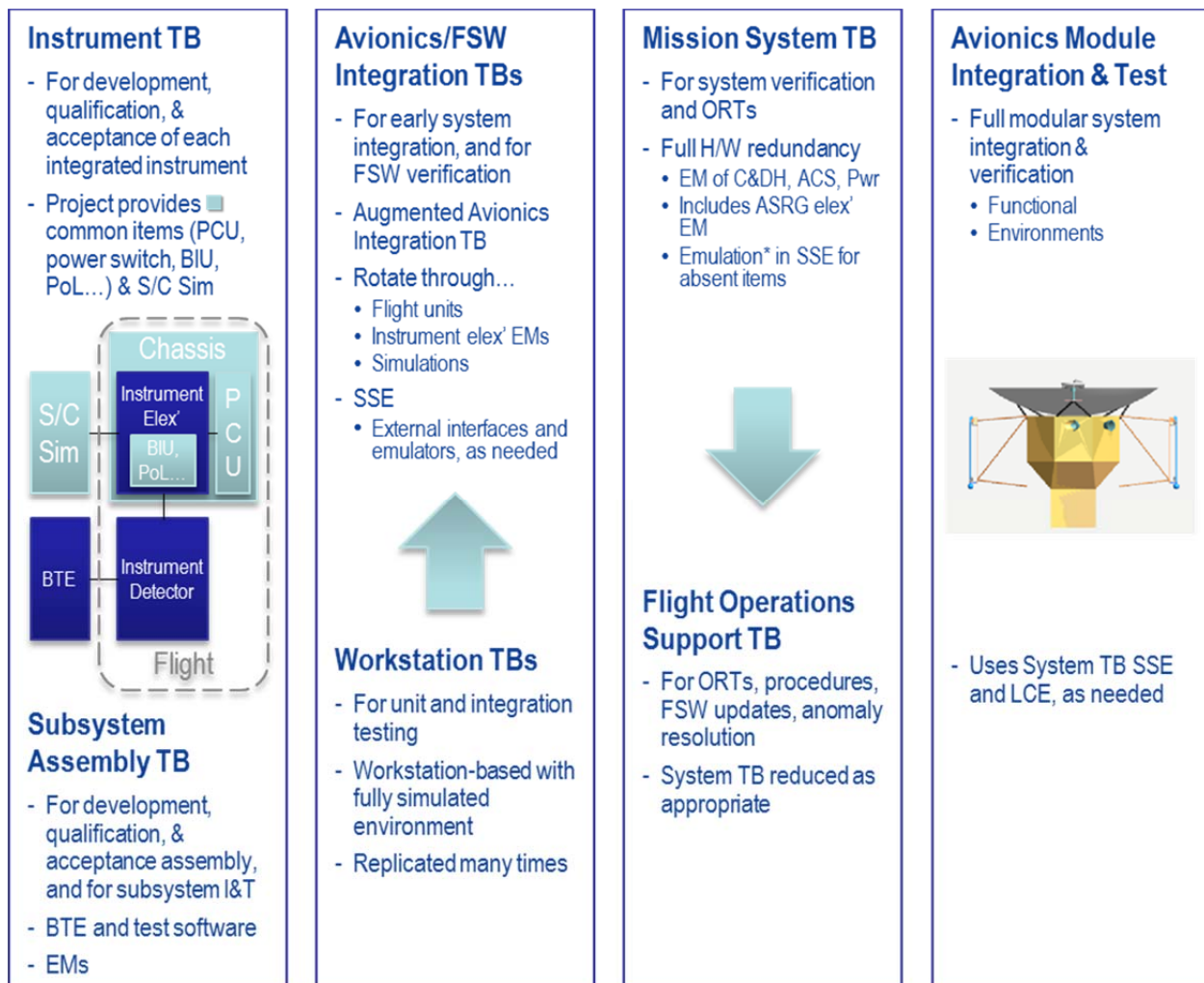


Figure C.2.4-42. System integration testbeds.

A high-fidelity model-based simulation capability (known as the workstation test set [WSTS] on MSL and SMAP) is baselined for FSW development test and verification. This includes but is not limited to fault management development and test, attitude control system-level verification and validation (V&V), and mission activity development and test; so several groups will exploit this capability, which can be replicated cheaply as often as necessary. The software simulation of hardware must be of sufficient fidelity to allow seamless migration of FSW and test cases from simulation to hardware-in-the-loop testbeds. This capability is important and necessary because certain software services are needed to support the instrument testbeds and the testing and integration of devices. Therefore, emphasis will be placed during hardware testing on validating simulation model fidelity.

The first workstation-based spacecraft simulator version will be available in time to support development of the first FSW release, and will progress with expanded capability, as needed to support testing of subsequent FSW builds. It will be available on all software developers', systems engineers', and testers' workstations. Capabilities will include closed-loop spacecraft behaviors operating in both nominal and off-nominal modes. These simulators are built to allow for interchangeability between software models and hardware engineering models (EMs) later in the "hardware-in-the-loop" testbeds in a manner that is transparent to the FSW and to test scripts, at least at the interface level. This enables use of the same test scripts whenever the testbed models are interchanged with EMs or hardware emulators.

In addition to the simulation capability described above, the Europa Multiple-Flyby Mission would have three system testbeds. The first two are the Avionics/FSW integration testbeds, which are similarly configured with single-string avionics. These support the development and test of ground support equipment (GSE) hardware and software, the devel-

opment and validation of test scripts, and the maturation of databases, such as command and telemetry dictionaries. First on line is the Real-Time Development Environment (RDE), which is dedicated to GSE hardware and software development and test. The next instance of this testbed, the Flight Software Testbeds (FSWTBs), becomes available later in the development process to allow V&V to proceed in parallel with FSW development. The third system testbed is the Mission System Testbed (MSTB), a full redundant, high-fidelity testbed dedicated to system V&V, FSW fault management tests, mission system tests, and AT-LO support.

These system testbeds include the C&DH, GN&C, Power, Telecom, and Harness subsystems, as well as Ground Data System (GDS) hardware and software. The EM versions of all flight system engineering subsystems and instruments will pass through these testbeds for integration and interface verification. No flight units are required to pass through the testbeds unless there are major modifications from the EM. However, the testbeds can support flight hardware integrations, if needed. The V&V simulation environment can offload the hardware-in-the-loop testbeds and use the EM integration effort to help evaluate model fidelity. The simulation environment interfaces and procedures are compatible with those of the hardware testbeds. These testbeds are also used to train test analysts to support system testing, as well as to support ATLO procedure development and anomaly investigation. All FSW versions are verified on the system testbeds prior to being loaded onto the flight system during ATLO or flight operations. The flight system testbed transitions to operational use for this purpose after launch.

C.2.4.8.2 System Integration and Test

The conservatively derived system integration and test program is based on actual durations from the Cassini project. Launch operations durations are based on actuals from the MSL project along with operations unique to the Europa Multiple-Flyby Mission.

The System Integration and Test (SI&T) Phase, described graphically in Figure C.2.4-43, begins with the delivery of the flight Avionics Module components, Propulsion Module, and Power Source Module for system integration. The Avionics Module components, consisting of the telecom assembly, UES (with EM science instruments) and the Avionics Vault, is integrated initially using extender cables. These permit access to circuits for integration and troubleshooting, as well as for connection of direct access equipment needed for closed-loop operation of the Attitude Control Subsystem during mission scenario and comprehensive performance testing. During integration, interface signal characteristics are measured and recorded for comparison with requirements.

Even though traditional EMC/EMI system engineering methods will be employed during development, the early integration of the Telecom Subsystem permits monitoring of spectral characteristics as other hardware is added to the system for detection and identification of any interfering spurious signals. A thorough telecom functional test is included in the flow to establish baseline performance while operating with the rest of the Avionics Module.

The Propulsion Module is electrically integrated through extender cables next in the flow to demonstrate signal characteristics to propulsion valves and thrusters, and to perform an initial verification of proper phasing. The design of the extender cables and the layout of the modules in the test facility address cable length issues, as appropriate. Phasing of propulsion components (as well as G&C components) is repeated after spacecraft stacking to remove any influence of the extender cables.

Finally, the Power Source Module is electrically integrated through extender cables. Plans call for fully functional ASRGs that are electrically heated and can be used to verify end-to-end performance, as well as to verify integration procedures that will be used for the flight ASRG integration at KSC.

A Deep Space Network (DSN) compatibility test is performed at this point (with the DSN compatibility test trailer) followed by an Engineering Baseline Comprehensive Performance Test (CPT). This and other configuration-dependent baseline tests are performed throughout the ATLO program in order to detect performance changes resulting from either trending or environments.

A series of fault management tests is performed to establish correct operation of the fault management system software in conjunction with associated hardware detections and responses.

The first mission scenario test is the launch sequence test, executed both nominally and with selected fault and off-nominal conditions. Subsequently, a trajectory correction maneuver test (including orbit insertion) is performed in both nominal and off nominal conditions. Other capabilities of the spacecraft to support required operational modes, science observations, and other noncritical mission scenarios will be incorporated in CPT(s) rather than in specific scenario tests so that spacecraft capabilities are fully established, rather than merely performing point-design mission scenario verifications. Since all operations described above are first-time events, one-month schedule margin is included at this point to prevent any delay to the science instrument integration.

At this point, any outstanding science instruments are delivered and integrated into the Avionics Module, replacing their EMs that have been serving as surrogates throughout system testing.

Europa Study System Integration & Test

12-19-11

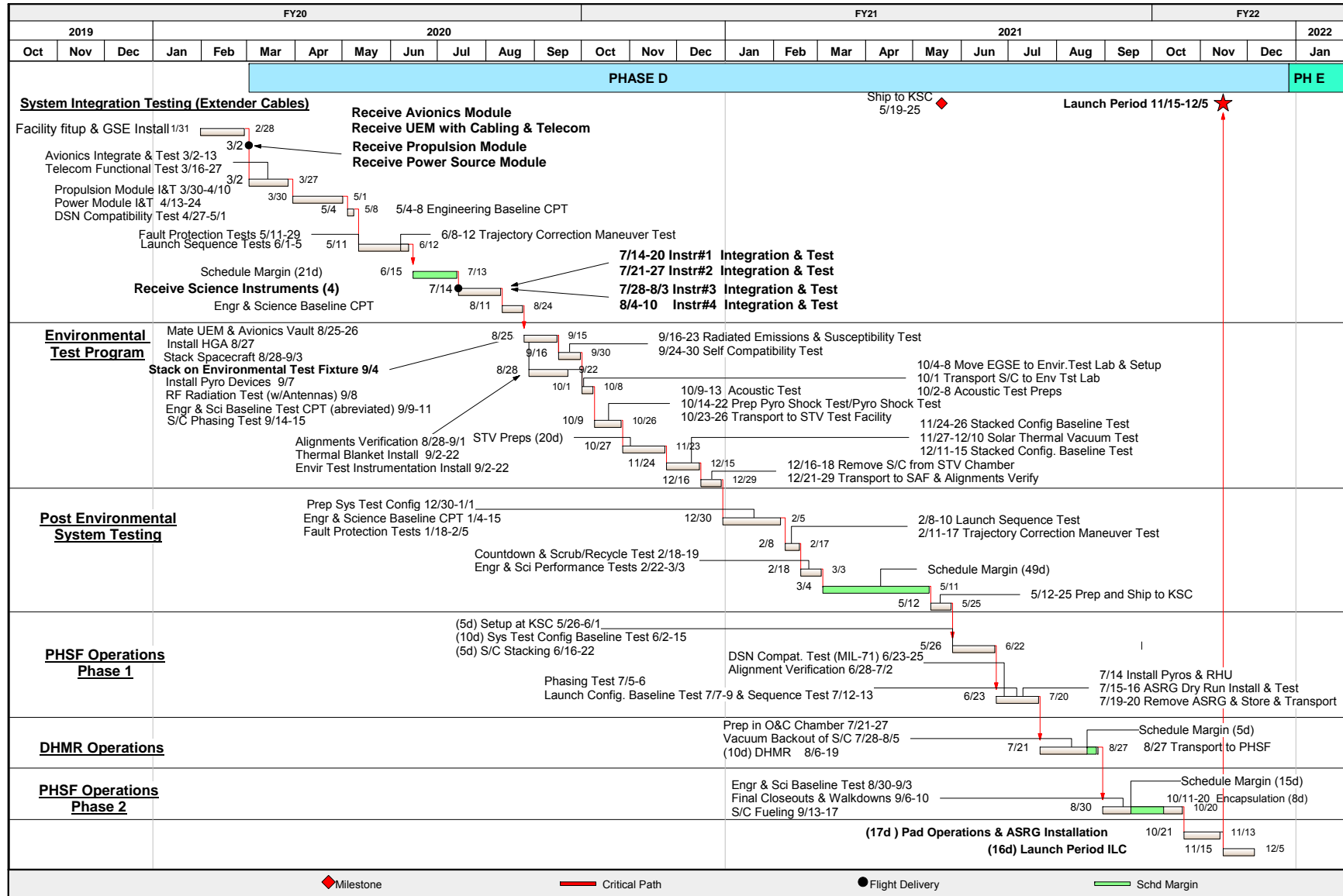


Figure C.2.4-43. The comprehensive ATLO program is based on as-run durations from Cassini and MSL plus JPL-required schedule margins.

An Engineering and Science CPT follows integration, with all spacecraft components present to establish the performance of the spacecraft before reconfiguration for environmental test. The environmental test program starts with the mechanical and electrical integration of the UES, avionics vault and the telecommunications assembly to complete the Avionics Module. Stacking of the Propulsion Module, Power Source Module, and Avionics Module to each other, stacking the spacecraft on the Launch Vehicle Adapter (provided by the Launch Service) and the installation of pyro devices needed for pyro-shock testing. An Abbreviated Baseline CPT is performed, as well as an RF radiation test using the flight antennas, and a phasing test to demonstrate proper phasing without extender cables. This is the first time the spacecraft is in a flight-like electrical and mechanical configuration.

Radiated emissions and radiated susceptibility tests are then performed, as well as a self-compatibility test. This is followed by an alignment verification to establish pre-environmental alignment data. Thermal blankets (including the thermal shroud) and environmental test instrumentation are installed after the spacecraft is stacked.

The spacecraft is then transported to the Environmental Test Lab (ETL), where acoustics tests and pyro-shock tests are performed. The pyro-shock test also verifies the LV separation mechanical interfaces.

The spacecraft is then moved to the 25-foot Space Simulator, where a baseline test is performed to verify configuration and performance prior to starting solar thermal-vacuum (STV) tests. The STV test is primarily a verification of worst-case hot and cold performance, as well as selected thermal balance conditions. Additional tests (such as science instrument modes that require vacuum conditions) are performed during thermal transitions, if they are not otherwise required for the worst-case thermal tests that verify margins required by

JPL Design Principles and Flight Project Practices (JPL 2010a, b).

After STV test, the spacecraft is transported back to the Spacecraft Assembly Facility (SAF), where post-environmental alignment verifications are performed, followed by de-stacking to a system test configuration. The Engineering and Science CPT is repeated for post-environmental performance verification. Launch sequence tests, trajectory correction maneuver tests, countdown and scrub/recycle tests, and engineering and science performance tests are performed prior to shipment to KSC. Two months of schedule margin are included at this point to protect the ship date and KSC operations. Shipment to KSC is performed at the module level because of the large size of the stacked spacecraft and to permit access to direct access signals for the final comprehensive performance testing at KSC.

After arrival at the KSC Payload Hazardous Servicing Facility (PHSF), the spacecraft modules, interconnected with extender cables, are put through a System Test Configuration Baseline CPT to reestablish the health of all spacecraft systems. Spacecraft stacking is then performed, followed by a DSN Compatibility Test with MIL-71, alignment re-verification, and a final Phasing Test using the launch version of flight software. A Launch Configuration Baseline Test is performed, followed by a Launch Sequence Test from prelaunch through early cruise. Flight pyrotechnic devices (excluding those for spacecraft separation) are installed. A dry-run installation of the flight ASRG(s) is performed as well. After the flight ASRG(s) are removed and secured, the spacecraft is transported to the KSC Operations and Checkout (O&C) facility for dry heat microbial reduction (DHMR). ASRG fueling is performed during this time in a separate facility. The descriptions of operations with the ASRG assume that they can be handled in similar fashion to the MMRTG used on Mars Science Laboratory (MSL). These operations will be

refined as the ASRG requirements and development proceed.

At the O&C the spacecraft is installed in an existing thermal chamber in the O&C high bay. Vacuum bakeout of the spacecraft is performed, followed by backfill to an appropriate convective atmospheric environment for heating (either nitrogen or filtered air at the preference of the Planetary Protection Engineer). Spacecraft temperatures are elevated and verified, at which point the DHMR operation is conducted. Because of uncertainty in the durations of each of these operations, five days of schedule margin are allocated at this point. Over one month of schedule is allocated to the end-to-end DHMR operation. The spacecraft is then transported back to the PHSF. Conservative planetary protection handling is planned beyond this point, consistent with a spacecraft that could impact Europa.

At the PHSF, a baseline test is performed to confirm the status of all spacecraft systems after DHMR. Since the ASRG(s) would not be present, the spacecraft will be powered by ground support equipment power supplies. Final spacecraft closeouts and walk-down inspections are performed, followed by propellant and pressurant loading of the Propulsion Module. Three weeks of schedule margin are included at this point to protect the date of delivery to the LV for integrated operations.

At this point, the spacecraft is ready for integrated operations with the LV, including mating to the flight LVA, encapsulation with the fairing, transport to the launch pad, and fueled ASRG installation for flight, countdown, and launch.

Durations for most of the spacecraft test operations (including setup, reconfiguration, preps, and transportation) are based on actual “as-executed” durations from Cassini. Cassini was used as a reference because its ATLO plan was executed without any holiday work, or any work on a holiday weekend, minimal Saturday work, and a nominal five-day-per-week, sin-

gle-shift operation. Integrated operations with the LV are based on actuals from MSL, which had similar operations with the same/similar LV and integration of an MMRTG. These estimates have been informed by MSL complications of MMRTG installation inside the MSL aeroshell and implementation of required cooling systems. Cooling may not be required for the Europa Multiple-Flyby Mission, given the characteristics of ASRGs.

The ATLO flow described above has not been optimized to incorporate opportunities for parallel operations, except in the case of preparations for environmental testing, where such operations are customary. The flow described also includes the 20% schedule margin at JPL, and one day per week schedule margin at KSC, as required by the JPL Design Principles (JPL 2010a).

C.2.5 Mission Operations Concepts

Repetitive activities, centralized operations and focus on Europa science enables realization of efficient, low-cost operations.

Europa and its vicinity pose a challenging and hazardous environment for operating any science mission. Based on the cost-reduction mandate from the decadal survey for 2013–2022 (Space Studies Board 2011), and hand-in-hand with the design of the Europa Multiple-Flyby Mission and spacecraft, the operations strategies described herein have been developed principally to achieve the intended Europa science described in Section C.1 at the lowest feasible cost, yet while minimizing mission risk in this environment. Therefore, the central guiding theme of Europa Multiple-Flyby Mission operations has been to deliver the spacecraft to Europa safe and fully capable of conducting science observations, consisting of remote and in situ measurements that can be accomplished best via multiple flybys.

Europa science is the driver of mission architecture. No tangential activities have been allowed to drive the design of the operations systems and concepts. All design decisions—

be they for the spacecraft or operations—are studied, often with the applications of models and/or scenarios, to measure the cost, performance, and risk across all phases of the project, including operations.

Operations development has drawn much wisdom from the many NASA-wide studies of Europa exploration from as early as 1997. In addition, two key studies in 2008 were conducted to capture relevant operations lessons learned from past and present missions, incorporating members from JPL, APL, and NASA Ames (Paczkowski et al. 2008, Lock 2008). These studies focused in particular on flight and ground system capabilities needed to simplify science operations, on early integrated development of flight and ground concepts to ensure appropriate implementation, and on postlaunch activities and development to ensure practiced functional capabilities and simplified operations. All of these operations assessments, from the many studies and from scenario work of highly experienced engineers, emphasize early consideration of operability issues in the system architecture and design. All system trades (spacecraft, operations, science, etc.) are treated as collective mission trades to work toward the best cost/risk for the overall mission, rather than optimizing a single element and unknowingly adding significant cost/risk to another.

C.2.5.1 Operations Concept—Science Phase

The Europa Multiple-Flyby Mission science phase described in Section C.2.3 begins after the pumpdown phase of the in-orbit trajectory and is achieved via 34 flybys of Europa, spaced over 18 months of Jupiter orbit. These occur over a total of 55 orbits at flyby spacings that vary typically from 11 to 25 days (there is also one 7-day encounter-to-encounter leg). Each flyby has a unique geometry, and the altitudes do vary across the mission; however, simple, repeated observations flowing from one conceptual design are capable of delivering all of the science goals. The Europa en-

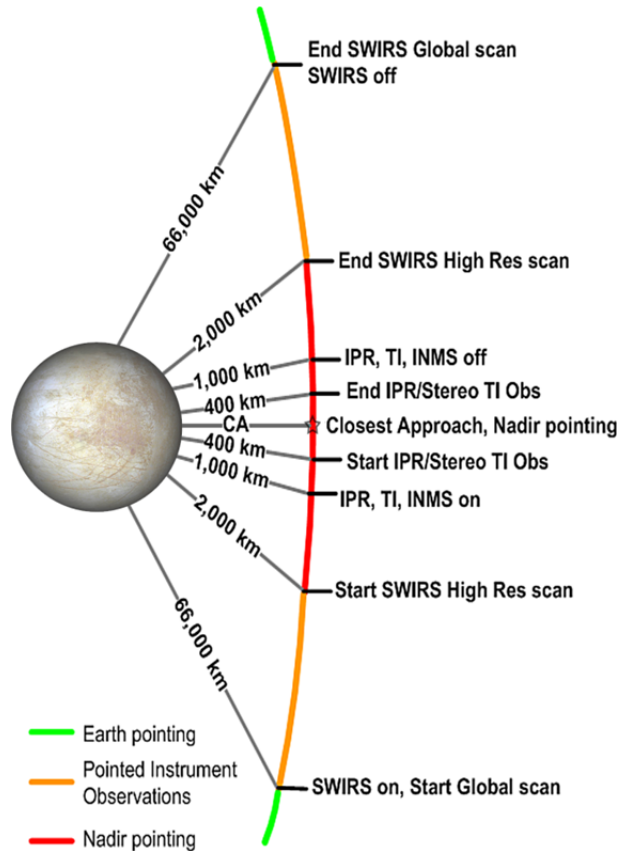


Figure C.2.5-1. Europa encounter concept—Multiple-Flyby Mission.

counter template (i.e., one conceptual design for all encounters) is shown in Figure C.2.5-1. This sequence of activities is described in Section C.2.1.

Operating durations for the various instruments are shown in Table C.2.5-1.

Away from the science flybys, orbit operations are shown in a rudimentary fashion in Fig-

Table C.2.5-1. Instrument on times per flyby.

Altitude Range (km)	Time at Altitude (minutes)	Instrument On Time (minutes)			
		IPR	TI	SWIRS	INMS
66,000 to 2,000	265			265	
2,000 to 1,000	5			5	
1,000 to 400	4	4	4	4	4
400 to CA	4	4	4	4	4
CA to 400	4	4	4	4	4
400 to 1,000	4	4	4	4	4
1,000 to 2,000	5			5	
2,000 to 6,000	265			265	
Total Minutes	554	15	15	554	15

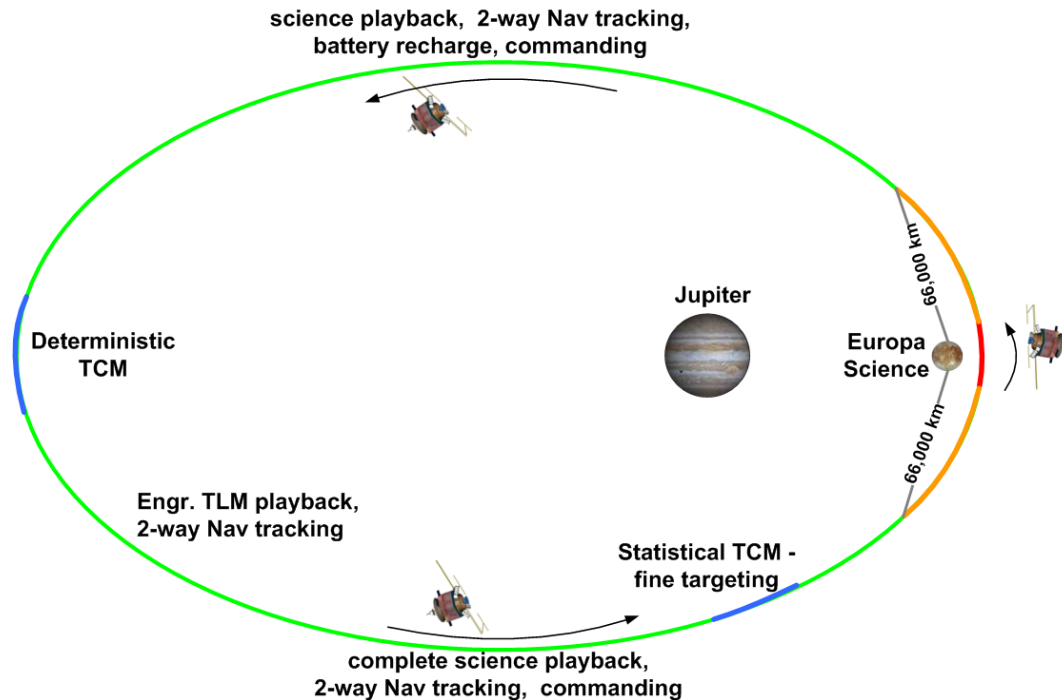


Figure C.2.5-2. Orbit concept—Multiple-Flyby Mission (not to scale).

ure C.2.5-2. The flyby concept permits a store-and-forward data-return strategy via at least daily DSN passes between science operations, and it also exploits battery use for short intervals with ample time for recharging between science operations. In addition, because science observations and data collection occur at different time, instruments can be fixed on the spacecraft body. During the downlink and recharging interval, the spacecraft is Earth-pointed (except for trajectory correction maneuvers), with science playback, engineering telemetry, and two-way navigation during DSN passes scheduled at least daily. The data balance described in Section C.2.4.7 allows for reasonable DSN tracking and healthy data volume margin in returning each encounter's science observations.

This data collection and pointing profile is quite similar in nature for each flyby. Mainly, the geometry and timing change. Therefore, given nominal operation, these observations can be laid down algorithmically with the same approach for each encounter. No negotiation for resources or case-by-case optimiza-

tion is necessary. Simple, repeated operations are sufficient to accomplish this. The instruments are on during each science flyby, and off otherwise. All flybys follow a single science profile of activities. There is no optimization per flyby, and the sharing of pointing is clearly defined and needs no negotiations. Maneuvers occur every few days; and other than maneuvers and encounters, activity intensity is low, with continuous, simply sequenced background activities.

The Europa Multiple-Flyby Mission design concept, along with the groundtrack geometry, has been described in Section C.2.3. Combined with the operations approach described above, the instrument coverage of Europa's surface that can be achieved as shown in Figures C.2.5-3 through C.2.5-6. These coverage profiles meet the science goals described in Section C.1. Each figure is shown as an equirectangular projection of Europa's surface. The center of the figure (longitude 180°) is anti-Jovian, whereas the edges (longitude $0/360^\circ$) are sub-Jovian. Europa's north pole is at the top.

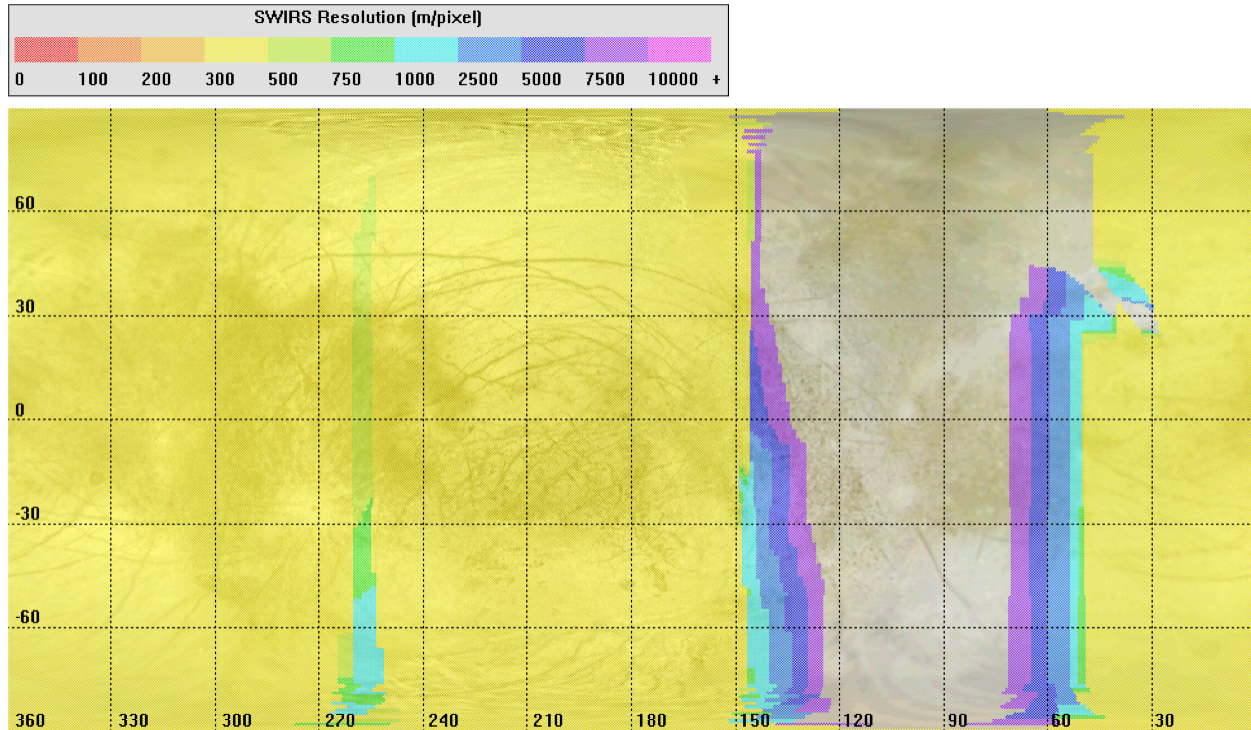


Figure C.2.5-3. SWIRS low-resolution coverage (66,000 km to 2,000 km altitude).

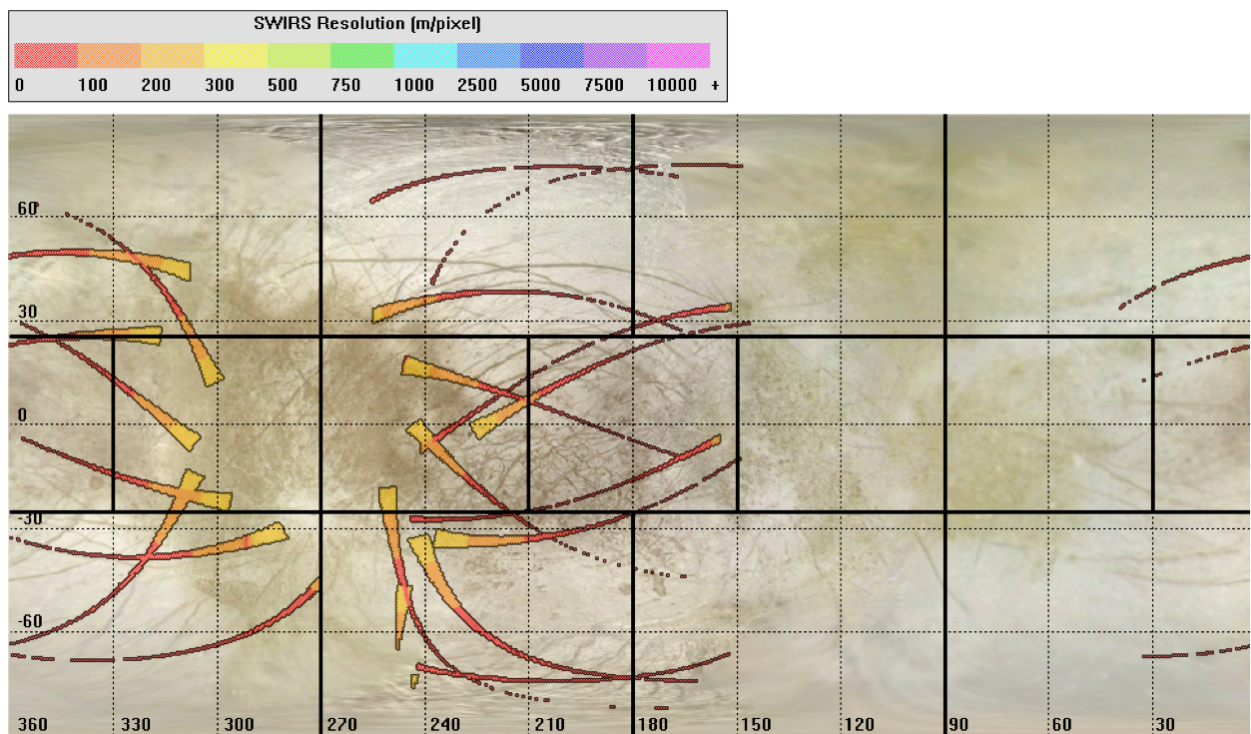


Figure C.2.5-4. SWIRS high-resolution coverage (under 2,000 km altitude).

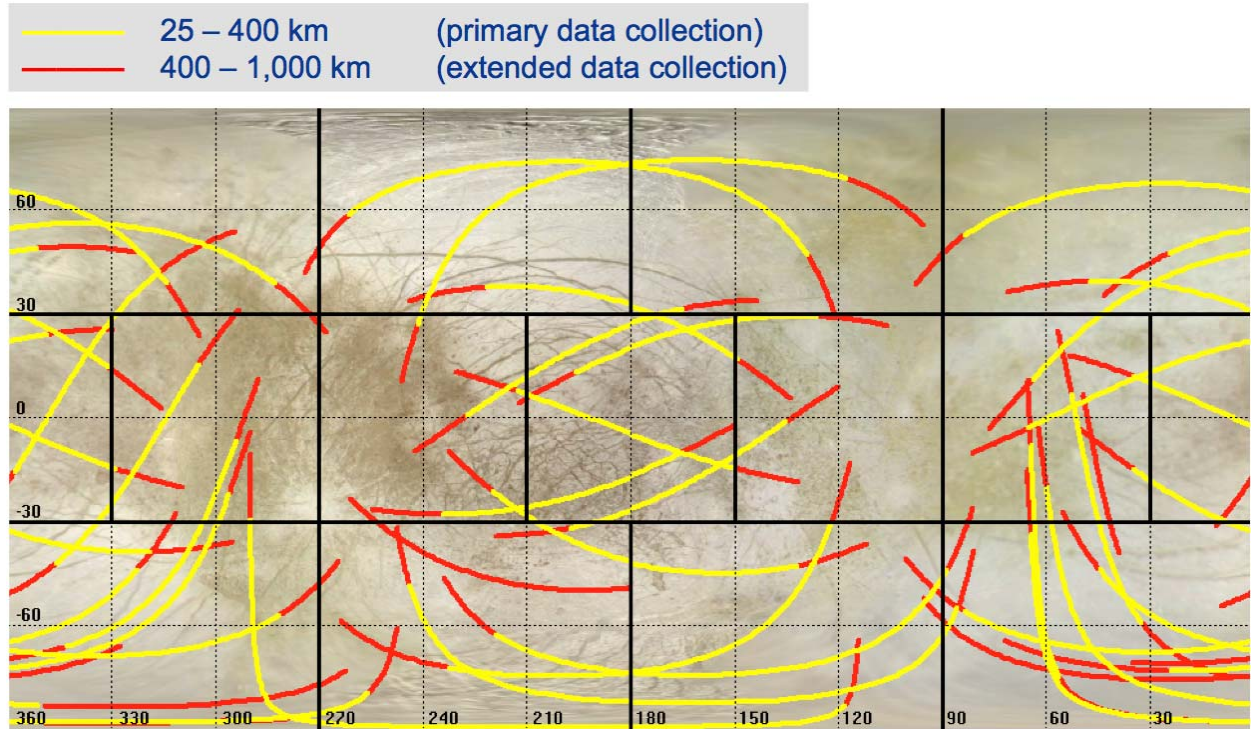


Figure C.2.5-5. IPR ground coverage.

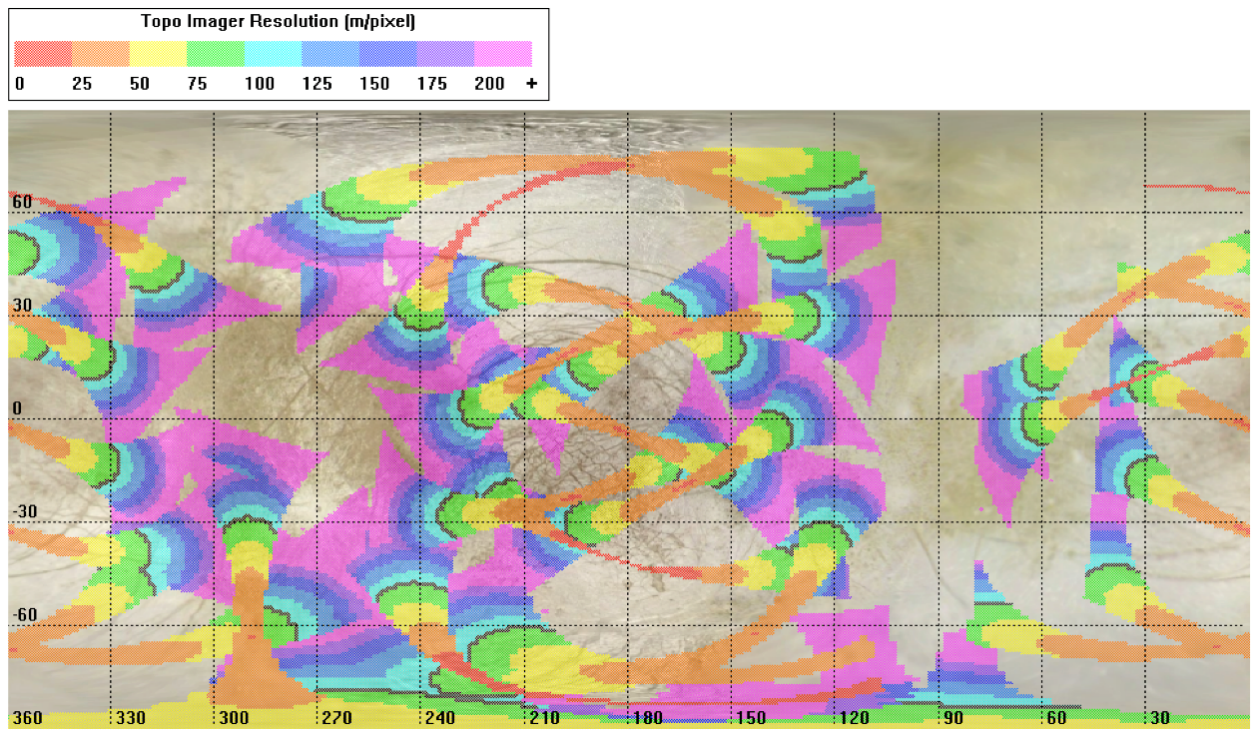


Figure C.2.5-6. TI instrument coverage.

C.2.5.2 Interplanetary and Jupiter Cruise

After launch, mission focus is on the checkout, characterization, and deployment of all flight systems. In the first few weeks of cruise, DSN coverage is nearly continuous, driven to some extent by real-time commanding for schedule flexibility. Once postlaunch configuration and checkouts are complete, the mission transitions to interplanetary cruise.

Interplanetary cruise is quiescent, save for elevated activity required for gravity assists and maneuvers. The spacecraft is minimally operated, with basic telemetry expected only once per week; however, 24-hour coverage is expected around maneuvers, and daily to continuous tracking is expected prior to gravity assists, particularly for nuclear safety prior to gravity assists involving Earth. In between gravity assists, the project focuses efforts on development and improvement of operations processes and tools for Europa encounters, as well as science team meetings to refine the Europa template of operations. After JOI, instrument characterization and checkout resume, and operations readiness tests (ORTs) and instrument calibrations are conducted prior to the first Europa encounter.

C.2.5.3 Development Supporting Europa Operations

As mentioned at the beginning of Section C.2.5, early consideration of operability issues in the system architecture and design is of great importance. The Europa Multiple-Flyby Mission plans significant operations scenario development during Phases A-D. Science operations will be a strong element of the prelaunch flight systems engineering. Science operations scenarios will be developed early and at a level of detail that permits flight system design choices to be assessed thoroughly. Operations and ground system architecture, requirements, models, and software will be developed to a level sufficient to support prelaunch development and flight system trade studies. Science planning tools will be devel-

oped such that they can be used to evaluate the ground and flight system requirements and capabilities. Based on these preparations, refinements can then be made much more confidently in cruise and throughout the mission to this unified ground and flight system architecture and its software requirements.

Modeling will be conducted to simulate representative operations in deep space, including Europa flyby operations. The ATLO phase includes testing of at least one representative operational sequence to be used during Europa encounters. These efforts, though they add early cost, should bring net savings to the project over all life cycle phases because they make possible more efficient operations, and uncover problems at a time when something can be done to mitigate them.

Opportunities for process improvement are built into the schedule after launch. A long cruise period presents some challenges, among them the risks of personnel attrition and ground system obsolescence. However, the varying level of intensity—lower between gravity assists, for example—also offers opportunities to improve processes, software, IT infrastructure, and operations concepts and the science template for Europa observations. A Europa Flyby Mission project would aim to fill the “bathtubs” between major events in cruise with periods of further development and training. The project would strategically defer some operations development until after launch. Doing so has several advantages. First, it obviates the need to staff the project up for major cruise events and down afterwards. Second, it allows the project to take advantage of improvements in technology as they become available and to work with a flight team more likely to be present during later operations than is the flight team in place at launch. Third, it affords the flight team opportunities to contribute to the design of the operations system, improving staff skill and possibly retention as team members choose to remain with the project in part to see their efforts bear fruit in Jupiter orbit. Finally, it ensures that the

operations team on the line during orbital operations is deeply familiar with the system, such that disruptions from faults or radiation issues can be handled in an expeditious, reliable, and expert manner.

Staffing levels should remain at approximately the late Phase D workforce level through launch and initial checkouts, after which it can drop to a more sustainable cruise staffing level. Cruise staffing should be relatively flat thereafter, with a moderate increase in development staff in the later portion of interplanetary cruise. Because the navigation team must be fully capable for JOI, they would staff up to Jupiter cruise/Europa flyby levels no later than six months before JOI. Spacecraft system and subsystem support needed to support navigation and maneuvering would also be added at this time. Other operations teams would staff up at around JOI to test final processes, the science template, and software, with the first ORTs for Europa beginning 1 to 2 months thereafter.

C.2.6 Systems Engineering

Through key investments in infrastructure, engineering products, and team-building, the Europa Study Team is well positioned to move into pre-project formulation.

This section outlines the overall systems engineering approach and plan. The subsections that follow address three specific systems engineering challenges: radiation, planetary protection, and nuclear safety.

In general the Europa Multiple-Flyby Mission can be said to have the following technical and programmatic characteristics:

- Technical:
 - Functioning in the presence of radiation flux, SEEs, radiation damage to parts and materials
 - Satisfying planetary protection of the European ocean, as well as of Ganymede and Callisto, from delivered bioburden
 - Lifetime and reliability over a long mission

- Maintaining conservative resource margins
- Integrating a suite of competitively selected science instruments from a diverse field of providers
- Integrating radioisotope power sources
- Contrasting thermal environments at Venus flyby and Jupiter
- Critical orbit insertion at Jupiter
- Intense science operations schedule at Europa after years of unhurried cruise
- Keeping a 10-year-plus “corporate memory” of the requirements, detailed design, and the rationales for design choices
- Programmatic:
 - Succeeding in a cost- and cost-profile-constrained environment
 - Coordinating the efforts of a large, diverse engineering team
 - Integrated the project and design with competitively selected instruments
 - Accommodating development and maturation issues of the radioisotope power sources
 - Multi-institution and potential multinational partnerships (JPL, APL, PIs)

To help address these concerns, the following overarching systems engineering objectives have been set for formulation:

- By System Requirements Review (SRR), produce a Baseline System Specification (L1-L3 Baseline; L4 Preliminary; L5 Key and Driving), a committed systems engineering schedule and cost profile, and a committed mission architecture.
- By Preliminary Design Review (PDR), produce a released set of procurement specifications, a fully developed preliminary design, and a committed project schedule and cost.

Institutional project and line management is uniformly committed to making major strides in systems engineering, supporting and enforcing the following approach:

- Exercise rigorous engineering discipline. Expect engineering rationale to be documented as complete and logical chains of thought, and in appropriate tools (Mathematica/Maple not PowerPoint; IOMs not emails)
- Make use of emerging new systems engineering capabilities as appropriate, including system modeling language standards and tooling, model integration and exchange standards and tooling, and Web-based report generation.
- Starting from the beginning, build persistent and evolvable artifacts.
- Starting from the beginning, build a core team of systems engineers who can faithfully promulgate the architecture later as the project grows.
- Proactively align with forthcoming NPR 7120.5E (NASA 2012).
- Emphasize architecture and design space exploration through MCR. An architectural approach keeps the team properly focused on the “why,” and design space keeps us properly focused on the concept rather than a point design. In this endeavor, trusted models and analytical tools are essential investments.
- Make decisions by a process that is explicitly guided by Architecture, is timely and responsive, is transparent to all stakeholders, and includes balanced consideration of multiple experienced viewpoints.

The Europa Multiple-Flyby Mission is well positioned to move into preproject formulation. The Europa Study Team has made key investments in infrastructure, engineering artifacts, and team-building, as described below:

- Infrastructure has been under development for the long term. Already set up and in initial use are a collaborative Systems Modeling Language (SysML) environment (MagicDraw/Teamwork Server), a collaborative architecture development environment (Architecture Framework Tool), the project document repository (DocuShare), and the project workflow management system (JIRA).
- Key plans and processes are in place. Key parts of the architecture description are in preliminary form, as outlined in this report. The core of a system model is established.
- Our team processes and practices are maturing. Cost estimates, some technical margin estimates, and mechanical configuration changes have been improved over past practice.

From this strong starting point, a plan that achieves robust maturity at SRR and PDR has been constructed. The sketch of this plan, expressed as key artifacts per life-cycle phase through PDR, is shown in tables C.2.6-1 through C.2.6-4. In these tables the changes from one table to the next are shown in **bold blue font**, and the parentheticals following the artifact names denote required maturity levels:

- (A): Approach is defined, and possibly a sketch of the artifact.
- (K&D): Key and Driving cases are identified and covered.
- (P): Preliminary. A full version for review and discussion leading to a baseline version.
- (B): Baseline. The artifact is under configuration control.
- (U): Update.

After PDR, systems engineering focus changes from development to implementation: managing the change-control process while maintaining architectural integrity, implementing I&T and V&V programs, and preparing for flight operations.

Table C.2.6-1. Present maturity of systems engineering artifacts.

Systems Engineering Plan: Key Artifacts per Life-Cycle Phase							
At Tech Review	Artifact Type						
	Plan	Scenario	Model	Analysis & Sim	Report	Spec	
SCOPE	Program (L1)					L1 Rqmts (K&D)	
	Project (L2)	Arch Dev Plan (P) SEMP (A) Model Mgt Plan (A)	Driving Mission (K&D)	Trajectory (P) Science Margin (A) Data Margin (P) FS Radiation (P)	Delta-V/Prop (P) Science Margin (A) Data Margin (P) FS Radiation Life (P)	Concept Report (P) Msn Arch Descr (P) Ops Concept (A) Tech Assessment (A) Eng Dev Assess (A) Top Risks (A)	L2 Rqmts (A) Env Definition (A)
	System (L3)		Flight Sys Ops (K&D)	FS Functional (P) FS Physical (P) FS Shielding (P) FS Power (P) FS Static Mech (P) FS Thermal (P) FS Telecom Link (P) FS Attitude Ctrl (P)	FS Mass Margin (P) FS Shield Mass (P) FS Pwr Margin (P) FS Mass Props (P) FS Therm Balance (P) FS Link Margin (P) FS Pntg Margin (P)	L3 Rqmts (A)	
	Subsystem (L4)			Power (K&D) Thermal (K&D) Propulsion (K&D) Telecom (K&D) Avionics (K&D) Structure (K&D)	Power Bus Sim (P) Therm Balance (P) JOI Perf (A) EIRP, G/T (P) C&DH Throughput (A) LV Static Envel (P)		
	Component (L5)			Radiation Effects (P) DHMR Effects (P)	Component Life (P) Parts/Matl Issues (P)	Approved Parts (A) Approved Matls (A)	

(A) Approach (K&D) Key & Driving (P) Preliminary (B) Baseline (U) Update **Blue = Change**

Table C.2.6-2. Maturity of systems engineering artifacts at MCR.

Systems Engineering Plan: Key Artifacts per Life-Cycle Phase							
At MCR	Artifact Type						
	Plan	Scenario	Model	Analysis & Sim	Report	Spec	
SCOPE	Program (L1)					L1 Rqmts (P)	
	Project (L2)	Arch Dev Plan (B) SEMP (P) Model Mgt Plan (P) Integr Plan (A) V&V Plan (A)	Driving Mission (P)	Trajectory (B) Science Margin (B) Data Margin (B) FS Radiation (B)	Delta-V/Prop (P) Science Margin (P) Data Margin (P) FS Radiation Life (P) Rqmt Traceability (P)	Concept Report (B) Msn Arch Descr (P) Ops Concept (P) Tech Assessment (P) Eng Dev Assess (P) Top Risks (P)	L2 Rqmts (P) Env Definition (P) External ICDs (K&D) Intersystem ICDs (K&D) S/C-P/L ICD (K&D)
	System (L3)		Flight Sys Ops (P)	FS Functional (P) FS Physical (P) FS Shielding (P) FS Power (P) FS Static Mech (P) FS Thermal (P) FS Telecom Link (P) FS Attitude Ctrl (P) FS Behavior (P) FS Fault Contnmt (P)	FS Mass Margin (P) FS Shield Mass (P) FS Pwr Margin (P) FS Mass Props (P) FS Therm Balance (P) FS Link Margin (P) FS Pntg Margin (P)	L3 Rqmts (K&D) Intra-FS ICDs (K&D)	
	Subsystem (L4)			Power (P) Thermal (P) Propulsion (P) Telecom (P) Avionics (P) Structure (P)	Power Bus Sim (P) Therm Balance (P) JOI Perf (P) EIRP, G/T (P) C&DH Throughput (P) LV Static Envel (P)		
	Component (L5)			Radiation Effects (P) DHMR Effects (P)	Component Life (P) Parts/Matl Issues (P)	Approved Parts (P) Approved Matls (P)	

(A) Approach (K&D) Key & Driving (P) Preliminary (B) Baseline (U) Update Blue = Change

Table C.2.6-3. Maturity of systems engineering artifacts at SRR.

Systems Engineering Plan: Key Artifacts per Life-Cycle Phase								
At SRR	Artifact Type							
	Plan	Scenario	Model	Analysis & Sim	Report	Spec		
SCOPE	Program (L1)					L1 Rqmts (B)		
	Project (L2)	Arch Dev Plan (U) SEMP (B) Model Mgt Plan (B) Integr Plan (P) V&V Plan (P) S/W Mgt Plan (P)	Mission Plan (K&D)	Trajectory (U) Science Margin (U) Data Margin (U) FS Radiation (U)	Delta-V/Prop (B) Science Margin (B) Data Margin (B) FS Radiation Life (B) Rqmt Traceability (B)	Concept Report (U) Msn Arch Descr (B) Ops Concept (B) Tech Assessment (B) Eng Dev Assess (B) Top Risks (B) Instrument AO PIP (B)	L2 Rqmts (B) Env Definition (B) External ICDs (B) Intersystem ICDs (P) S/C-P/L ICD (P)	(A) Approach (K&D) Key & Driving (P) Preliminary (B) Baseline (U) Update Blue = Change
	System (L3)		Flight Sys Ops (B)	FS Functional (B) FS Physical (B) FS Shielding (B) FS Power (B) FS Static Mech (B) FS Thermal (B) FS Telecom Link (B) FS Attitude Ctrl (B) FS Behavior (B) FS Fault Contnmt (B)	FS Mass Margin (P) FS Shield Mass (P) FS Pwr Margin (P) FS Mass Props (P) FS Therm Balance (P) FS Link Margin (P) FS Pntg Margin (P) FS PRA (A) FS Func FMECA (A) FS TAYF Exceptions (A)	Ground Sys Arch (P) Payload Arch (P)	L3 Rqmts (B) Intra-FS ICDs (P) Procurement Specs (P)	
	Subsystem (L4)			Power (B) Thermal (B) Propulsion (B) Telecom (B) Avionics (B) Structures (B)	Power Bus Sim (P) Therm Balance (P) JOI Perf (P) EIRP, G/T (P) C&DH Throughput (P) LV Static Envel (P)		L4 Rqmts (P) Intrasubsystem ICDs (P)	
	Component (L5)			Radiation Effects (B) DHMR Effects (B)	Component Life (P) Parts/Matl Issues (P)	Approved Parts (P) Approved Matls (P)		

Table C.2.6-4. Maturity of systems engineering artifacts at PDR.

Systems Engineering Plan: Key Artifacts per Life-Cycle Phase								
At PDR	Artifact Type							
	Plan	Scenario	Model	Analysis & Sim	Report	Spec		
SCOPE	Program (L1)					L1 Rqmts (B)	(A) Approach (K&D) Key & Driving (P) Preliminary (B) Baseline (U) Update Blue = Change	
	Project (L2)	Arch Dev Plan (B) SEMP (U) Model Mgt Plan (U) Integr Plan (B) V&V Plan (B) S/W Mgt Plan (B)	Mission Plan (P)	Trajectory (U) Science Margin (U) Data Margin (U) FS Radiation (U)	Delta-V/Prop (U) Science Margin (U) Data Margin (U) FS Radiation Life (U) Rqmt Traceability (U) Mission Fault Tree (P)	Concept Report (U) Msn Arch Descr (U) Ops Concept (U) Tech Assessment (U) Eng Dev Assess (U) Top Risks (U) Instrument AO PIP (B)		L2 Rqmts (B) Env Definition (B) External ICDs (B) Intersystem ICDs (B) S/C-P/L ICD (B)
	System (L3)		Flight Sys Ops (U)	FS Functional (B) FS Physical (B) FS Shielding (B) FS Power (B) FS Static Mech (B) FS Thermal (B) FS Telecom Link (B) FS Attitude Ctrl (B) FS Behavior (B) FS Fault Contnmt (B)	FS Mass Margin (B) FS Shield Mass (B) FS Pwr Margin (B) FS Mass Props (B) FS Therm Balance (B) FS Link Margin (B) FS Pntg Margin (B) FS PRA (P) FS Func FMECA (P) FS TAYF Exceptions (P)	Ground Sys Arch (B) Payload Arch (B)		L3 Rqmts (B) Intra-FS ICDs (B) Procurement Specs (B)
	Subsystem (L4)			Power (B) Thermal (B) Propulsion (B) Telecom (B) Avionics (B) Structures (B)	Power Bus Sim (B) Therm Balance (B) JOI Perf (B) EIRP, G/T (B) C&DH Throughput (B) LV Static Envel (B)	Subsys Des Desc (P) P/L Design Desc (P)		L4 Rqmts (B) Intrasubsystem ICDs (B)
	Component (L5)			Radiation Effects (B) DHMR Effects (B)	Component Life (B) Parts/Mat Issues (B)	Approved Parts (B) Approved Matls (B)		L5 Rqmts (P)

C.2.6.1 Radiation

The effects of radiation on the spacecraft are mitigated by the efficient use of inherent shielding provided by the spacecraft itself and additional dedicated shield mass, combined with radiation-tolerant materials and electronics.

The Europa Multiple-Flyby Mission spacecraft would be exposed to both naturally occurring and self-generated radiation from launch to the end of the mission. The self-generated radiation, composed of neutrons and gamma rays, is produced from the Advanced Stirling Radioisotope Generators (ASRGs). The naturally occurring radiation encountered during the cruise phase between launch and Jupiter Orbit Insertion (JOI) consists of solar flare protons. Between JOI and the end of the mission, the spacecraft is exposed to protons, electrons, and heavy ions trapped in the Jovian magnetosphere. In addition, there is a background of galactic cosmic rays throughout the entire mission.

The radiation encountered during the mission can affect onboard electronics, thermal control materials, surface coatings, and other nonmetallic items by depositing energy that can disrupt the properties of these materials. Cumulative damage in electronics can through ionization, called total ionizing dose (TID), or displacement of atoms in the crystalline lattice, called displacement damage dose (DDD). The expected accumulated TID from launch to end of mission as a function of effective aluminum shielding thickness is shown in Table C.2.6-5.

Radiation can also cause noise in science instrument and star-tracker detectors due to the intense proton and electron flux encountered in the Jovian system. Peak electron and proton fluxes for the mission are shown in Table C.2.6-6.

The selection of electronic parts with respect to their radiation tolerance and reliability in the Europa radiation environment will be achieved through a combination testing and analysis. The minimum acceptable total ioniz-

Table C.2.6-5. Expected Flyby Mission accumulated total ionizing dose as a function of shield thickness.

Aluminum Thickness (mil)	Total Ionizing Dose (krad Si)				
	Electron	Photon	Proton	ASRG	Total
100	1960	7.0	46.6	1.3	2010
200	893	7.9	10.9	1.3	913
400	341	8.9	1.9	1.3	353
600	178	9.5	0.8	1.3	189
800	107	9.9	0.5	1.3	118
1000	70.5	10.0	0.4	1.3	81.1
1200	48.9	10.0	0.3	1.3	60.4
1400	35.2	9.8	0.2	1.3	46.5
1600	25.9	9.6	0.2	1.3	37.0

ing dose hardness of electronic devices will be 100 kilorad. The minimum single-event-effects (SEE) hardness will be documented in a Parts Program Requirements (PPR) document. A combination of radiation testing (TID, DDD, and SEE) of electronic devices and buying vendor guaranteed radiation hardened parts that meet the minimum TID and SEE requirements will ensure that robust electronics will be used in spacecraft and instrument electronics. Radiation testing will be done at industry-standard high-dose-rates and at low-dose-rate for electronic devices types that are susceptible to Enhanced Low Dose Rate Sensitivity (ELDRS) effects (primarily bipolar devices). Electronic part parameter degradation observed during radiation testing will be documented and used as input into the spacecraft and instrument electronics end of mission worst-case analysis (WCA). Electronic devices that do not meet the minimum TID and SEU hardness requirements will not be used within the spacecraft electronics or instruments unless approved by a requirements waiver.

The guidelines for selecting nonmetallic mate-

Table C.2.6-6. Expected Flyby Mission peak electron and proton flux.

Particle Energy (MeV)	Flux (#>Energy cm ⁻² sec ⁻¹)	
	Electron	Proton
10	1.7 E6	1.5 E5
20	4.8 E5	3.2 E4
30	2.2 E5	8.7 E3
50	7.9 E4	8.6 E2
100	1.8 E4	2.0 E1

rials for radiation susceptibility and reliability have been documented by Willis (2011). Detailed evaluations will be performed for these materials after exposure to end-of-mission radiation environment to ensure end of life performance requirements are met. Radiation testing will be performed for materials which do not have available radiation data.

The Europa Multiple-Flyby mission will develop an Approved Parts and Materials List (APML) for the purpose of identifying standard parts approved for flight equipment developed under the project's cognizance. The APML will be populated with EEE parts and materials, as well as many critical parts such as sensors, detectors, power converters, FPGAs, and non-volatile memories. Each entry will be accompanied with a Worst Case Datasheet (WCD) and application notes describing proper use of the part at selected radiation levels. Dissemination of this information early in the design process is critical to enable the spacecraft electronics and instrument providers to adequately design for the radiation environment.

Every approved part listed on the APML will meet the reliability, quality, and radiation requirements specified in the PPR. The APML will be updated as new radiation data become available. Parts not listed as approved on the APML are defined as non-standard parts and will require a Nonstandard Parts Approval Request (NSPAR) for use in the Europa Multiple-Flyby mission. All non-standard parts will be reviewed, screened, and qualified to the requirements of PPR.

Every part on the APML will be approved by the Parts Control Board (PCB). The PCB recommends and approves parts for inclusion in the APML. Criteria will be based on absolute need, the number of subsystems requiring the part, qualification status, TID, Single Event Effects (SEE), and procurement specification review. Mission designers should use standard parts to the maximum extent possible so that

they can reduce the radiation testing and qualification expenditure to the minimum.

Radiation-induced effects on instrument detectors and other key instrument components ultimately impact the quality and quantity of the mission science return and the reliability of engineering sensor data critical to flight operations. High-energy particles found within the Europa environment will produce increased transient detector noise as well as long-term degradation of detector performance and even potential failure of the device. Transient radiation effects are produced when an ionizing particle traverses the active detector volume and creates charges that are clocked out during readout. Radiation-induced noise can potentially swamp the science signal, especially in the infrared wavebands where low solar flux and low surface reflectivity result in a relative low signal. Both TID and DDD effects produce long-term permanent degradation in detector performance characteristics. This includes a decrease in the ability of the detector to generate signal charge or to transfer that charge from the photo active region to the readout circuitry; shifts in gate threshold voltages; increases in dark current and dark current non-uniformities, and the production of high-dark-current pixels (hot pixels or spikes). It is important to identify and understand both the transient and permanent performance degradation effects in order to plan early for appropriate hardware and operations risk mitigation to insure mission success and high-quality science returns.

A JEO Detector Working Group (DWG) was formed in FY08 to evaluate the detector and laser components required by the planning payload and stellar reference unit. The DWG participants included experienced instrument, detector, and radiation environment experts from APL and JPL. For each technology required for the payload, the DWG (i) reviewed the available radiation literature and test results, (ii) estimated the radiation environment incident on the component behind its shield,

and (iii) assessed the total dose survivability (both TID and DDD) and radiation-induced transient noise effects during peak flux periods. The assessment included the following technologies: visible detectors, mid-infrared and thermal detectors, micro-channel plates and photomultipliers, avalanche photodiodes, and laser-related components (pump diode laser, solid-state laser, fiber optics).

The DWG assessment, reported in Boldt (2008), concluded that the radiation challenges facing the JEO notional payload and SRU detectors and laser components are well understood. With the recommended shielding allocations, the total dose survivability of these components is not considered to be a significant risk. In many cases, the shielding allocation was driven by the need to reduce radiation-induced transient noise effects in order to meet science and engineering performance requirements. For these technologies—notably mid-infrared detectors, avalanche photodiode detectors, and visible detectors for star-tracking—the extensive shielding (up to 3-cm-thick Ta) for transient noise reduction effectively mitigates all concern over total dose degradation. For the remaining technologies, more modest shielding thicknesses (0.3–1.0 cm Ta, depending upon the specific technology) were judged to be sufficient to reduce the total dose exposure and transient noise impact to levels that could be further reduced with known mitigation techniques (detector design, detector operational parameters, algorithmic approaches and system-level mitigations). The DWG conclusions reached for the JEO are applicable for the science detectors and the SRU onboard the Europa Multiple-Flyby mission.

A rigorous “test-as-you-fly” policy with respect to detector radiation testing, including irradiation with flight-representative species and energies for TID, DDD, and transient testing, will be adopted for the Europa Multiple-Flyby mission.

The Jovian electron environment also causes dielectric materials and ungrounded metals to collect charge, both on spacecraft external surfaces and within the spacecraft. This can cause damaging or disruptive transient voltages and currents in the spacecraft when an electrostatic discharge (ESD) event occurs.

Surface charging effects are mitigated by limiting the differential charging of external materials. This is accomplished by using materials that have surface coatings and treatments that allow the accumulated charges to bleed to spacecraft ground. A significant number of such surface materials have been used extensively in severe charging environments for spacecraft with long lifetimes (typically geosynchronous communications spacecraft, but also Juno, GLL, and others) and are usable for the Europa Multiple-Flyby Mission. These materials include

- Carbon-loaded Kapton thermal blankets
- Indium-tin-oxide-coated gold Kapton thermal blankets
- Germanium-coated, carbon-loaded Kapton thermal blankets
- Electrostatic-conductive white paint
- Electrostatic-conductive black paint
- Composite materials
- Metallic materials

When surface discharge does occur, the voltage and current transients are mitigated by shielding around harness lines and using interface electronic devices that can tolerate the energy from ESD-induced transients that couple into the harness center conductors.

Internal ESD is controlled by shielding to reduce the electron flux present at dielectric materials within the spacecraft (typically circuit boards) and by limiting the amount of ungrounded metal (ungrounded harness conductors, connector pins, device radiation shields, part packages, etc.). The shielding required to reduce the TID to acceptable levels for the Europa Multiple-Flyby Mission is more than suf-

efficient to reduce the electron flux to levels that preclude discharge events to circuit boards. Grounding of radiation shields, part packages, harness conductors, and connector pins through ESD bleed wires or conductive coatings limits the ungrounded metals to small areas that cannot store enough energy to cause damaging discharges to electronic devices.

This surface and internal charging methodology has been used extensively in a severe charging environment for spacecraft with long lifetimes and was used specifically on the Juno project.

The spacecraft's exposure to radiation is attenuated to acceptable levels by providing shielding between the external environment and the sensitive materials and electronic parts in the spacecraft. Most of the spacecraft electronics are placed in a shielded vault. Payload electronics and sensor heads external to the vault have shielding tailored for their design and location on the spacecraft. Science instrument detector shielding to suppress radiation-induced background noise and permanent damage effects is achieved through a combination of instrument-level shielding for detector support electronics and internal high-Z (high-atomic-number) material shielding for the detector devices.

Efficient use of dedicated shield mass is achieved through a nested shield design concept, shown in Figure C.2.6-1. Spacecraft structure and placement of the Propulsion Subsystem hardware (fuel tanks, oxidizer tanks, helium pressurant tanks, and propellant that remains in the tanks after JOI) provide significant collateral shielding to the electronics packaged within the vault. The vault's wall thickness and material composition, 7.3-mm-thick aluminum, further limit the Flyby Mission TID to 150 krad for the enclosed electronics. Localized shielding at the assembly level then reduces the Flyby Mission TID even more, from 150 krad to 50 krad at the device level for all electronics.

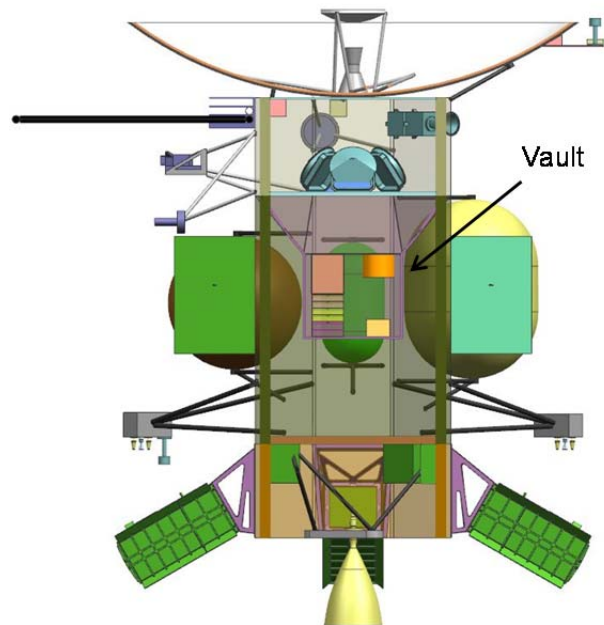


Figure C.2.6-1. Flyby Mission electronics are shielded by the spacecraft structure, propulsion tanks, and a dedicated electronics vault.

The dedicated shield mass for the Europa Multiple-Flyby Mission is a total of 218 kg, as shown in Table C.2.6-7. The shield mass was calculated based on a detailed radiation transport analysis that takes into account the spacecraft configuration shown in Figure C.2.6-1, material composition and thickness of the spacecraft structural elements and propulsion tanks, and the locations of electronic units and science instruments. Analysts used the following process:

1. Generate spacecraft element configuration and locations from a CAD model.
2. Explicitly calculate the shielding effectiveness of materials used in spacecraft structure, propulsion tanks, electronics unit chassis, dedicated vault, and added electronics assembly shielding based on material composition, density, and location using the NOVICE radiation transport code. The NOVICE code results have been correlated against a ray tracing code shielding code FASTRAD that is used by Aerospace contractors in both European and the United

States. For this analysis, the propulsion tanks are modeled as empty tanks.

3. To minimize the cost and risk of assuming electronic parts with higher radiation tolerance, assume all spacecraft electronics use 100-krad-tolerant electronic parts.
4. Understand science instrument front-end electronics co-located with detectors to have radiation tolerances that are instrument-specific (see Section C.2.2).
5. Through adjustments to assembly-level shielding mass, shield all spacecraft electronics assemblies to a TID of 50 krad or less at end of mission (i.e., to account for environmental uncertainty, they are given a radiation design factor [RDF] greater than or equal to 2 at the end of the mission).
6. Shield science instrument front-end electronics to have a minimum RDF of 2 for TID at the end of the mission.
7. To minimize cost, use aluminum shielding for all spacecraft electronics except science instrument and star-tracker detectors.
8. To minimize the radiation-induced noise at each detector location, shield science instrument and star-tracker detectors using high-Z materials (such as tantalum) (see Section C.2.2).
9. At the individual assembly level, to allow the use of off-the-shelf electronics without modification, wrap shielding around each assembly rather than integrating it into the assembly chassis.
10. Model circuit boards within the electronic assemblies as unpopulated boards. (Modeling component layouts on boards will be performed as the project progresses into Phase B. Including component layout in the radiation transport model will further reduce TID at the device level.)

Significant opportunities to reduce the dedicated shield mass have been identified although they have remained unexercised at this time. These opportunities include the following:

1. Change electronics unit placement within the vault to better protect units with lower-TID-capable electronic parts.
2. Place electronics cards within units to provide the lowest local TID at the part level.
3. Use a more efficient shield material than aluminum.
4. Add detail to the radiation transport model by including populated boards and individual device shielding.
5. Integrate the shielding into the electronics chassis.
6. Use multiple-material layered shielding, which is known to improve shielding efficiency.

The shield masses in Table C.2.6-7 have been incorporated into the spacecraft MEL (Section C.4.3).

Table C.2.6-7. Calculated shield masses to reduce the mission TID to 50 krad within each assembly.

Item	Shield Mass (kg)
Vault Structure	51.9
C&DH Subsystem	5.9
Power Subsystem	12.6
MIMU (2)	10.1
SDST (2)	6.1
WDE (4 slices)	4.4
Ka HVPS (2)	6.8
X HVPS (2)	6.0
ASRG (4)	45.9
Star-Tracker (2)	16.8
Pressure Transducer (10)	3.9
Science Electronics	21.8
INMS	10.1
Ice-Penetrating Radar	5.0
Topographic Imager	1.5
SWIRS	9.1
Flyby Spacecraft Total	218

C.2.6.2 Planetary Protection

NASA Planetary Protection policy (NPR 8020.12C [NASA 2005]) specifies requirements for limiting forward contamination in accordance with Article IX of the 1967 Outer Space Treaty. As Europa is a body of extreme interest to the astrobiological community as a possible location for the emergence of extra-terrestrial life, contamination of Europa with Earth-derived biology must be carefully avoided.

The mission's plan for responding to planetary protection requirements is to perform Dry Heat Microbial Reduction (DHMR) on as much of the spacecraft as possible, as late in the integration flow as possible. DHMR involves raising the bulk temperature of the spacecraft above the survival threshold for microbes and their spores. For materials contamination reasons, this bake out is typically done in vacuum or inert gas (nitrogen). To the extent possible, all spacecraft components will be designed to accommodate late integration DHMR without disassembly or recalibration. However, components or instrumentation unable to comply with DHMR requirements may be removed and sterilized through other means.

The extent to which DHMR sterilization and subsequent recontamination must reduce the spacecraft bioburden before liftoff is greatly influenced by the expected impact of post-launch sterilization processes and contamination probabilities. These include:

- a) Probability of organism survival during interplanetary cruise
- b) Probability of organism survival in the Jovian radiation environment
- c) Probability of impacting Europa
- d) Probability of organism survival on the surface of Europa before subsurface transfer
- e) The duration required for transport to the European subsurface
- f) Organism survival and proliferation after subsurface transfer

Each of these factors will be carefully examined to determine the ultimate allowable bioburden at launch and the required effectiveness of DHMR to maintain compliance with NASA regulation and international treaty.

C.2.6.3 Nuclear Safety

Missions to the outer solar system generally require the use of nuclear energy sources for electrical power and heating. The radioactive material used for this purpose is potentially hazardous to humans and the environment unless precautions are taken for its safe deployment. The following circumstances are of concern:

- Handling: People will be in the vicinity while nuclear sources (ASRGs or RHUs) are being constructed, transported, and installed on the spacecraft.
- Launch: In the event of a catastrophic LV failure, the spacecraft with its nuclear components is potentially subject to explosion, fire, impact, or the heat and forces of immediate reentry.
- Injection: If injection into interplanetary flight is not achieved, the spacecraft may be left in an Earth orbit that could decay to reentry after some time, thus exposing nuclear components to reentry conditions.
- Earth Flyby: If unplanned trajectory errors cause the spacecraft to reenter Earth's atmosphere, nuclear components would be exposed to reentry conditions.

Safety from nuclear hazards in each of these circumstances is essential.

The National Environmental Policy Act of 1969 (NEPA) specifies measures intended to address these concerns. Project compliance with NEPA is mandatory and is described in more detail below.

C.2.6.3.1 NEPA Compliance

Environmental review requirements will be satisfied by the completion of a mission-

specific Environmental Impact Statement (EIS) for the Europa Multiple-Flyby Mission. In accordance with the requirements of NPR 7120.5D, NPR 7120.5E and NPR 8580.1 (pending) (NASA 2007, 2012), the Record of Decision (ROD) for this EIS is finalized prior to or concurrent with project PDR.

The Europa Multiple-Flyby Mission Launch Approval Engineering Plan (LAEP) is completed no later than the Mission Definition Review (MDR). This plan describes the approach for satisfying NASA's NEPA requirements for the mission, and the approach for complying with the nuclear safety launch approval process described in Presidential Directive/National Security Council Memorandum #25 (PD/NSC-25) (1977) and satisfying the nuclear safety requirements of NPR 8715.3 (NASA 2010b). The LAEP provides a description of responsibilities, data sources, schedule, and an overall summary plan for preparing the following:

- A mission-specific environmental review document and supporting nuclear safety risk-assessment efforts
- LV and flight system/mission design data requirements to support nuclear risk assessment and safety analyses in compliance with the requirements of NPR 8715.3 (NASA 2010b) and the PD/NSC-25 nuclear safety launch approval process
- Support of launch site radiological contingency planning efforts
- Earth swing-by analysis
- Risk communication activities and products pertaining to the NEPA process, nuclear safety, and planetary protection aspects of the project.

It is anticipated that NASA HQ would initiate the Europa Multiple-Flyby Mission NEPA compliance document development as soon as a clear definition of the baseline plan and option space has been formulated. The Department of Energy (DOE) provides a nuclear risk

assessment to support the environmental review document, based upon a representative set of environments and accident scenarios compiled by the KSC Launch Services Program working with JPL. This deliverable might be modeled after the approach used for the MSL EIS.

DOE provides a Nuclear Safety Analysis Report (SAR) based upon NASA-provided mission-specific launch system and flight system data to support the PD/NSC-25 compliance effort. The SAR is delivered to an ad hoc Interagency Nuclear Safety Review Panel (INSRP) organized for the Europa Multiple-Flyby Mission. This INSRP reviews the SAR's methodology and conclusions and prepares a Safety Evaluation Report (SER). Both the SER and the SAR are then provided by NASA to the Environmental Protection Agency, Department of Defense, and DOE for agency review. Following agency review of the documents and resolution of any outstanding issues, NASA, as the sponsoring agency, would submit a request for launch approval to the Director of the Office of Science and Technology Policy (OSTP). The OSTP Director reviews the request for nuclear safety launch approval and can either approve the launch or defer the decision to the President.

As part of broader nuclear safety considerations, the Europa Multiple-Flyby Mission would adopt requirements for ATLO, spacecraft design, trajectory design (e.g., for sufficiently high orbit at launch, and for Earth flybys), and operations that satisfy the nuclear safety requirements of NPR 8715.3 (NASA 2010b).

Development of coordinated launch site radiological contingency response plans for NASA launches is the responsibility of the launch site Radiation Protection Officer. Comprehensive radiological contingency response plans, compliant with the National Response Framework and appropriate annexes, is developed and put in place prior to launch as required by NPR 8715.2 and NPR 8715.3 (NASA 2009a,

2010b). The Europa Multiple-Flyby Mission would support the development of plans for on-orbit contingency actions to complement these ground-based response plans.

A project-specific Risk Communication Plan would be completed no later than the MDR. The Risk Communication Plan details the rationale, proactive strategy, process, and products of communicating risk aspects of the project, including nuclear safety and planetary protection. The communication strategy and process would comply with the approach and requirements outlined in the Office of Space Science Risk Communication Plan for Deep Space Missions (JPL D-16993).

C.3 Multiple-Flyby Programmatic

C.3.1 Management Approach

The management approach for the Europa Multiple-Flyby Mission draws upon extensive experience from Galileo and Cassini. It follows NPR 7120.5E and incorporates NASA lessons learned.

The project approach includes a conventional Work Breakdown Structure (WBS), technical management processes conducted by veteran systems engineers, and integrated schedule/cost/risk planning and management. The project will take advantage of existing infrastructure for planning, acquisition, compliance with the National Environmental Policy Act (NEPA), compliance with export control regulations (including International Traffic in Arms Regulations and Export Administration Regulations), independent technical authority (as called for in NPR 7120.5E [NASA 2012]), mission assurance, ISO 9001 compliance, and earned value management (EVM).

The Europa Multiple-Flyby Mission employs JPL's integrated project controls solutions to manage and control costs. Skilled business and project control professionals are deployed to projects, utilizing state of the art tools and executing processes that support the project cost, schedule, and risk management requirements.

Key attributes of the project controls solution are as follows:

- The Business Manager, project focal point on all business management issues, and the project control staff lead project planners and managers in application of effective and efficient implementation of project control processes.
- Mature and successfully demonstrated cost and schedule tools are employed.
- Cost and schedule data are tied directly to work scope.
- “Early warning” metrics are provided monthly to key decision makers. Metrics include 1) cost and schedule variances based on the cost value of work performed and 2) critical-path and slack analysis derived from fully integrated end-to-end network schedules. Each end-item deliverable is scheduled with slack to a fixed receivable. Erosion of this slack value is tracked weekly and reported monthly.
- An integrated business management approach is applied to all system and instrument providers. This approach includes relative performance measurement data integrated into the total project database for a comprehensive understanding of project cost and schedule dynamics.
- Risk management processes are integrated with the liens management process for full knowledge of project reserve status. Early risk identification is emphasized, with each risk tracked as a potential threat to project reserves. Reserve utilization decisions are made with the knowledge of risks and risk mitigation, project performance issues, and increases in scope.

JPL flight projects that have used this integrated project controls approach include Juno, GRAIL, MSL, and Phoenix.

Requirements for project controls evolve throughout the project life cycle. Pre-Phase A and Phase A will require less support than phases B, C, and D. During Phase B, the project controls capability is established at full strength to establish all the appropriate databases and gate products required for a successful Confirmation Review. During phases C and D, full application of project controls will continue, with recurring performance measurement analysis and cost and schedule tracking reports. During phases E and F, the project controls function is reduced to lower levels commensurate with the scale of postlaunch activities.

C.3.2 WBS

The Europa Multiple-Flyby Mission Work Breakdown Structure (WBS) is structured to enable effective cost, schedule and management integration.

The WBS is derived from JPL's Standard Flight Project WBS Version 5 (JPL 2009) and is fully compliant with NPR 7120.5E. This WBS is a product-oriented hierarchical division of the hardware, software, services, and data required to produce end products. It is structured according to modular design of the spacecraft, and reflects the way the work would be implemented, and the way in which project costs, schedule, technical and risk data are to be accumulated, summarized, and reported.

The top-level WBS is shown Figures C.3.2-1 and C.3.2-2.

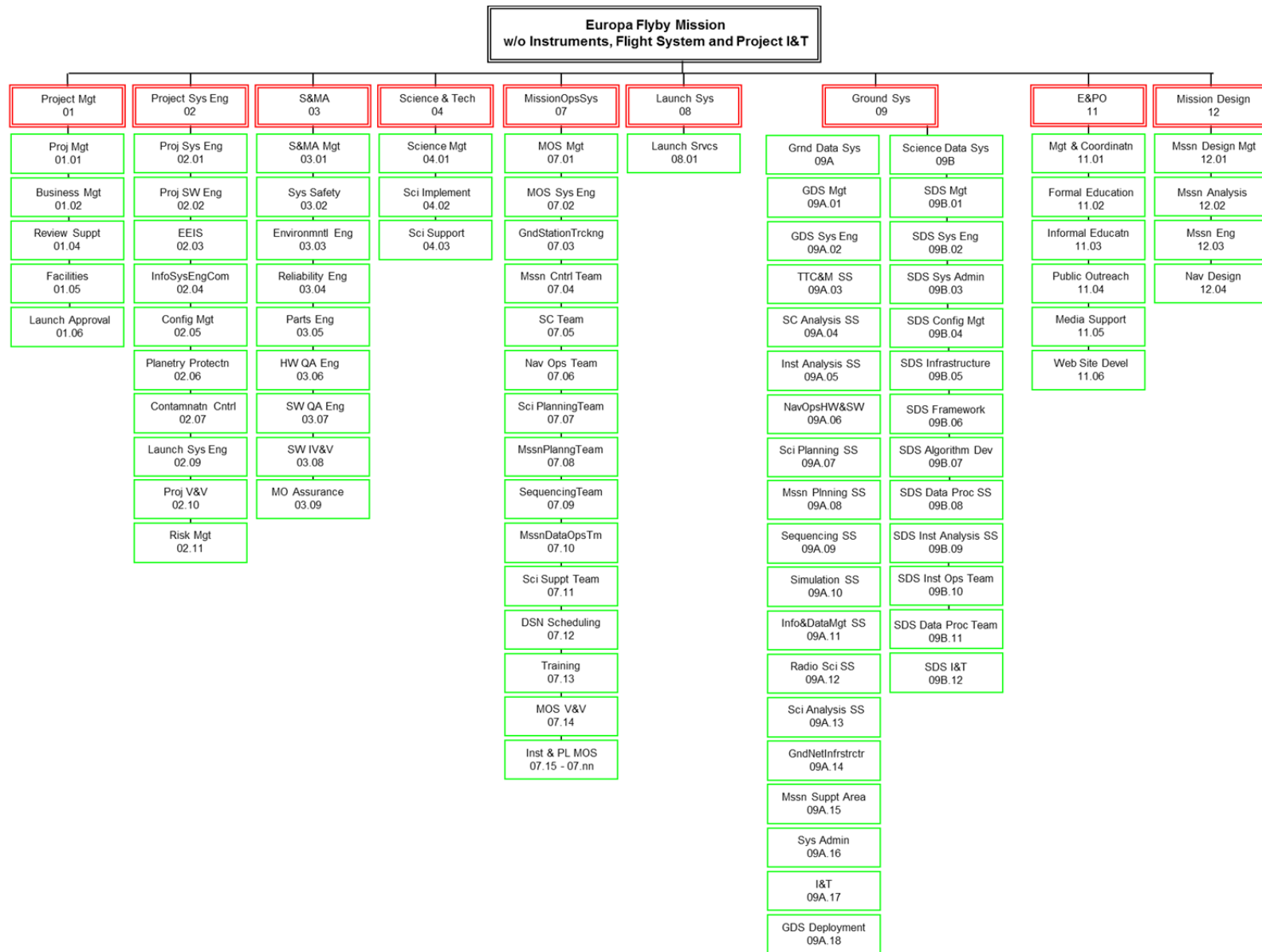


Figure C.3.2-1. Europa Multiple-Flyby Mission concept work breakdown structure.

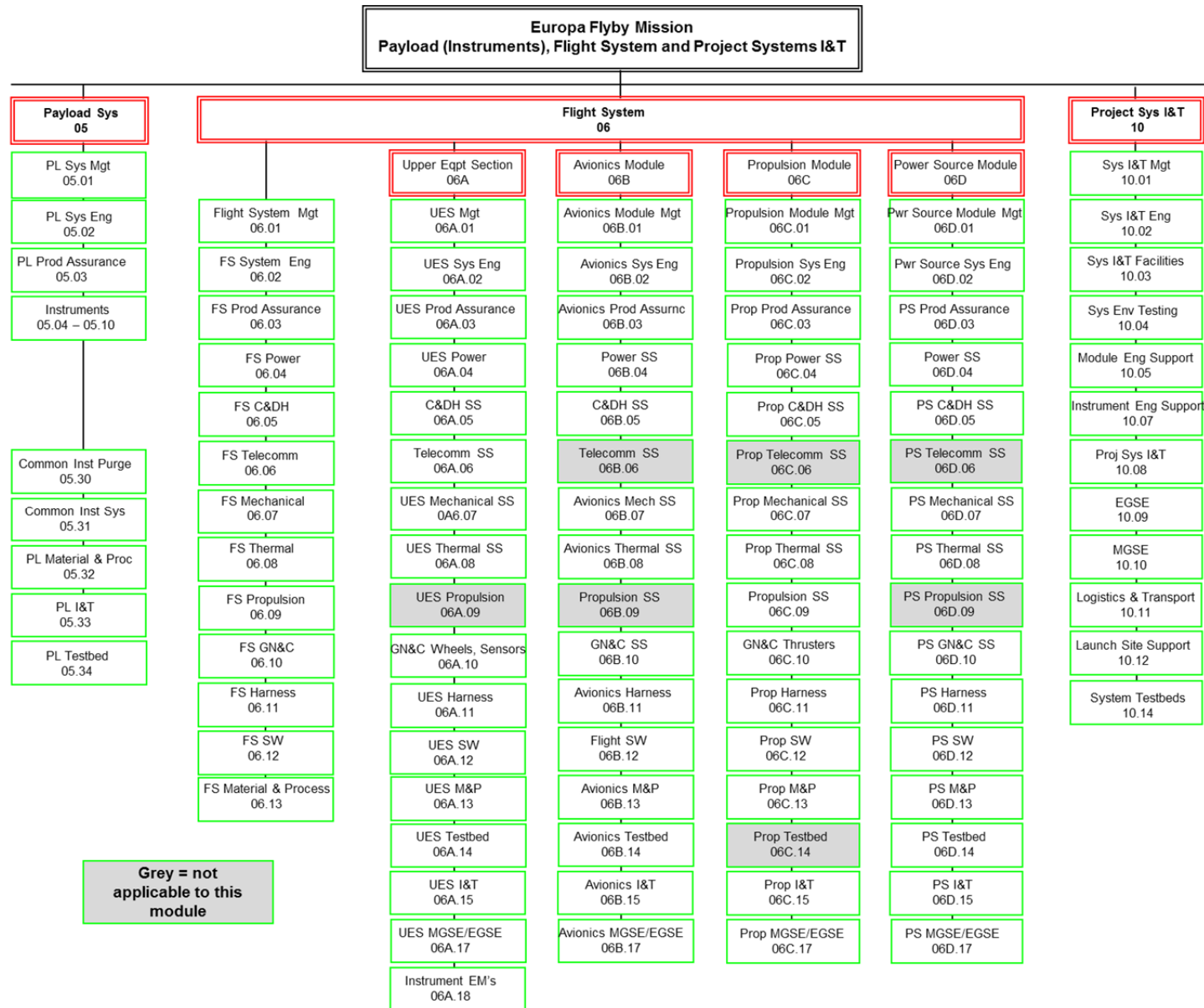


Figure C.3.2-2. Europa Multiple-Flyby Mission work breakdown structure: Payload, Flight Systems, I&T.

C.3.3 Schedule

The low-risk schedule is informed by previous outer planet missions.

A top-level schedule with implementation flow is shown in Figure C.3.3-1. The phase durations draw on experience from previous outer planet missions and are conservative. A bottom-up, WBS-based integrated schedule will be generated during Pre-Phase A.

C.3.3.1 Pre-Phase A

In preparation for this report, many alternative concept studies have been conducted. Should the Flyby concept be carried forward to Pre-Phase A, a preproject team will be formed to refine the baseline mission concept and implementation plan to align with programmatic goals and objectives. This refinement, along with interactions with NASA and other stakeholders, will result in further definition of the mission concept and draft project-level requirements.

Pre-Phase A activities include completion of NPR 7120.5D-specified Pre-Phase A Gate Products (NASA 2007), preparation of a Project Information Package (PIP) in support of NASA's development of an Announcement of Opportunity (AO) for instrument acquisition, and a Mission Concept Review leading to Key Decision Point (KDP) A. In addition to those activities required for transition to Phase A, the team will identify additional planning, advanced development, and risk-reduction tasks that could provide a prudent and cost-effective approach to early reduction of cost and schedule risk and have the potential to reduce the estimated cost of the mission. Primary activities include reducing the radiation and planetary-protection risks associated with instrument and spacecraft development.

C.3.3.2 Phases A–F

The Phase A–F schedule reflects the total project scope of work as discrete and measurable tasks and milestones that are time-phased through the use of task durations, interdepend-

encies, and date constraints. To ensure low risk, the schedule includes margin for all tasks.

The Project Manager controls the project schedule, with support from a Project Schedule Analyst. An Integrated Master Schedule identifies key milestones, major reviews, and receivables/deliverables (Rec/Dels). Schedule reserves for the November 2021 launch opportunity meet or exceed JPL Design Principles (DPs) requirements (schedule reserves of 1 month per year for phases A through D, with schedule reserves of 1 week per month for activities at the launch site) (JPL 2010a). The project utilizes an integrated cost/schedule system in Phase B, in order to fully implement an EVM baseline in phases C, D, and E. Inputs are supplied to NASA's Cost Analysis Data Requirement (CADRe) support contractor for reporting at major reviews. Schedule and cost estimates at completion (EACs) are prepared at regular intervals as part of the EVM process. Major project review milestones (not all shown) are consistent with NPR 7120.5D (NASA 2007).

C.3.3.3 Phases A–B

The length of phases A and B (24 months for A, 26 months for B) is primarily driven by the schedule to select the instruments in response to the AO and advance the selected instruments to the PDR level of maturity. In Phase A the primary tasks are completing the Gate Products required and facilitating the selection of the science instruments. The 8-month period between instrument selection and the system Mission Definition Review (MDR) allows instrument designers to work directly with the project personnel on issues related to accommodation, requirements, radiation, and planetary protection. The schedule is front-loaded with a long Phase A to give adequate time to define requirements early in the mission development life cycle. A basic approach to meeting the planetary protection requirements has been outlined and agreed to by the Planetary Protection Officer at NASA Headquarters.

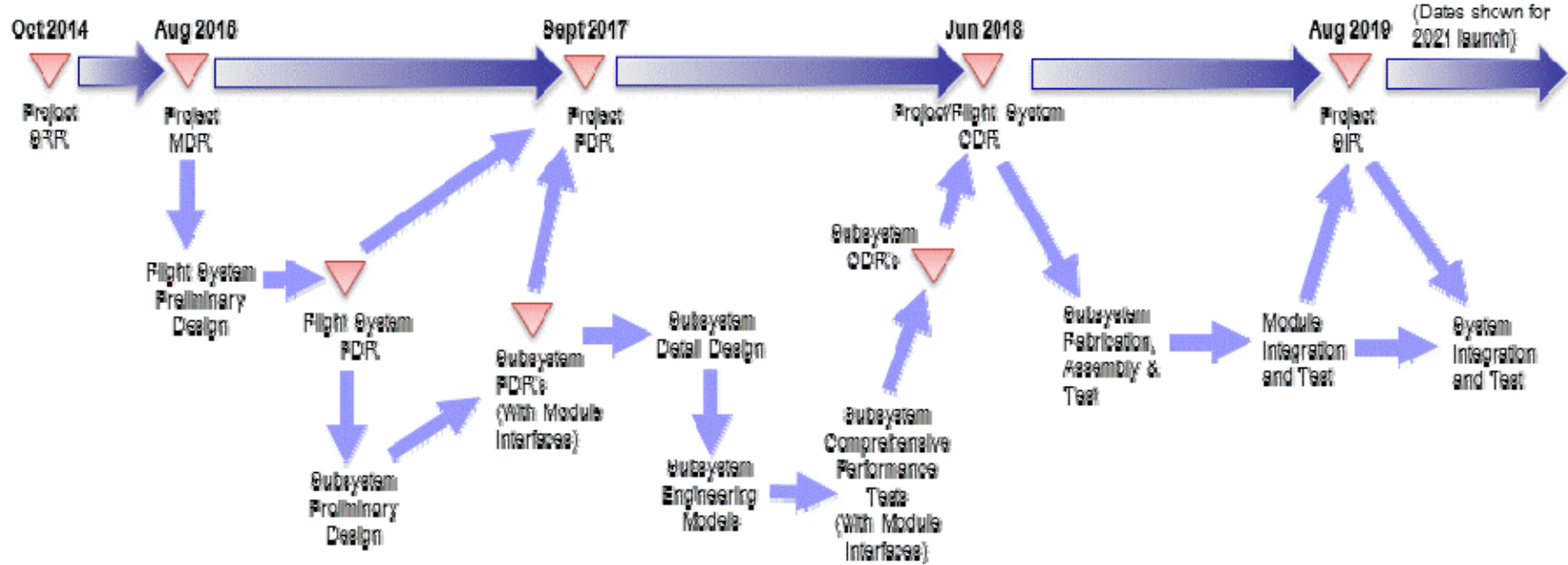


Figure C.3.3-1. Project implementation flow.

During Phase B it is anticipated that there will be a review of the detailed implementation approach, including any major outstanding issues related to mission design, flight system design, or operations concepts. This review might ultimately be combined with the Project PDR if it is effective to do so.

C.3.3.4 Phases C–D

The length of phases C and D (27 months for C, 22 months for D) is primarily driven by the schedule to bring the flight system to launch readiness. Phase C is longer than typical due to the added time required to implement the radiation and planetary-protection aspects of the design. The long Phase C also allows for a lower staff-level profile, which keeps the mission cost profile flatter. Phase D was developed using the Cassini model of ATLO and includes 1.5 months to perform the system-level DHMR.

A trailblazer activity is scheduled to occur at the launch facility in Phase D to ensure that the spacecraft design is compatible with the launch vehicle and facility limitations at the launch site for transporting and loading of the ASRGs. This activity starts at a very low level in Phase B and continues with increasing activity until the approach to ASRG installation is validated in Phase D. The trailblazer activity is also be used to dry-run the system-level DHMR activities that will take place in a thermal-vacuum chamber at KSC.

C.3.3.5 Phases E–F

Phase E (9.5 years) is driven by the interplanetary trajectory and science requirements at Europa. Phase F (6 months) is structured to carry out the end-of-mission disposal scenario and to complete data analysis and archiving.

C.3.4 Risk and Mitigation Plan

The main risks and their mitigation approaches are understood.

The primary challenges of a mission to Europa are Jupiter's radiation environment, planetary protection, trajectory management for numer-

ous consecutive flybys, and the large distance from the Sun and Earth. Driving technical risks are

1. Advanced Stirling radioisotope generator (ASRG) development
2. Performance in a radiation environment
3. Instrument development
4. Planetary protection

C.3.4.1 ASRG

NASA is developing the ASRG as the long-term solution for reducing the plutonium requirements for future planetary missions. Any problems with the development and validation of the ASRG could have a serious impact on the Europa Multiple-Flyby Mission, since it is baselining a radioisotope power system.

ASRG development and qualification risks have high consequences and are outside the control of the Europa Multiple-Flyby Mission project. The ASRGs are a new development, and the likelihood of problems is not known; however, successful development of new radioisotope thermoelectric generators can be difficult. Risks to the mission associated with this development can be mitigated if well-defined and stable ASRG characteristics are known early in Phase A to allow the system designers to adequately incorporate them into the spacecraft system. However, if these characteristics are not known and stable early in Phase A, late design changes and impacts on mass, power, cost, and schedule are likely. The Europa Power Source Module concept allows for later ASRG delivery, thereby diminishing some of the development risk, as does the Europa Study Team's close work with NASA to clearly delineate the mission requirements on the ASRGs. Mitigation of these risks also requires that the project work closely with the Program Executive at NASA Headquarters for the ASRG Development Program to ensure that the technology is flight-qualified with completed life tests, no later than Phase B. A robust ground-test program is essential to migrating the ASRG risks. The NASA ASRG

development efforts are currently underway (see Section C.2.4.6).

C.3.4.2 Performance in a radiation environment

The radiation environment to which the Europa Multiple-Flyby Mission hardware would be exposed, and its accumulated effects by end of mission are significant. Radiation effects expected in the mission are TID effects and SEE in electronic components, displacement damage (DD) effects in components and materials, noise effects in detectors, and surface and internal charging (IC). The primary risk considered here is the likelihood that premature component failure or compromised performance could have a serious impact on spacecraft functionality if the radiation problem is not addressed appropriately. Sensors for instruments used for pointing and navigation and in science instruments are particularly sensitive to radiation effects, primarily due to noise and displacement effects. Test techniques used to verify component suitability might over-predict component hardness due to inadequate accounting for radiation rate or source type effects that are negligible at lower doses. Also, unanticipated failure mechanisms might be present or might become important at high doses or at high DD levels that are not of concern for missions conducted at nominal total-dose exposures. The measures described here reduce both the likelihood and the consequences of such impacts, with designs for this radiation environment robust beyond the level normally accomplished for spaceflight design. The Europa Multiple-Flyby Mission design concept uses an approach similar to that taken by Juno, using an electronics vault to shield the electronic components to a mission dose of 150 krad, thereby reducing the likelihood of radiation-related problems while increasing the likelihood of parts availability. There has been significant effort exerted by experts to mitigate this risk over the past decade. In 2007, the Europa Study Team convened several review teams to assess the particular risks in each ar-

ea. The results of the reviews were presented in Appendix C of the 2007 Europa Explorer Mission Study report (Clark et al. 2007). As a result of those reviews, a Risk Mitigation Plan: Radiation and Planetary Protection (Yan 2007, outlined in Clark et al. 2007) was further developed and executed to make strategic investments related to reducing even further the likelihood of component failure and degradation, and the related radiation risk. Results of this work were reported in the 2008 JEO final report (Clark et al. 2008). An expanded systems engineering approach focuses on graceful degradation and reduces the consequences of any component failures in electronic parts.

C.3.4.3 Instrument Development

Instrument development and delivery will undoubtedly be on the critical path, as has historically been the case. Only four instruments are needed to fulfill the Europa Multiple-Flyby Mission science requirements. An Approved Parts and Materials List (APML), addressing planetary protection and radiation constraints, will be available in time for the instrument AO. In addition, design guidelines will be incorporated into the AO. This facilitates maturation of instrument concepts prior to selection. The instruments in the model payload are all based on mature technologies, and if deployed on a mission in the inner solar system, would represent low risk. For a Europa mission though, radiation can be expected to have a detrimental impact on instrument performance. If such problems cannot be resolved satisfactorily, the science objectives of the mission would not be met. Therefore, instruments will be selected as early as possible in Phase A, and early funding will be made available in order to alleviate development risks. In addition, the project will assign instrument interface engineers to work with each instrument provider to ensure that the instrument meets interface requirements and the spacecraft accommodates specific instrument needs.

To reduce the likelihood that the instruments fall short of their desired specifications or run into resource and schedule problems due to radiation issues, typical interface engineering support will be augmented for each instrument with personnel experienced in the area of radiation design. Design guidelines will be generated for the instrument teams to describe radiation constraints and to provide recommendations for design issues, and for parts and material selection. Development of a knowledge base for potential instrument providers has already begun. Four instrument workshops were held to engage the instrument provider community in a dialogue on needs and potential driving requirements for a mission to Europa. Information regarding radiation and planetary protection requirements was disseminated. The Europa Multiple-Flyby Mission development schedule provides abundant time plus reserves after selection for instrument developers and the project to work through and understand the particular design implications for each instrument of radiation and planetary protection. The project schedule also allows ample time for the instruments to be developed and delivered to system test. In addition, the modular spacecraft approach, early local testing with spacecraft emulators, and a straightforward instrument interface allow instruments to be integrated last in the ATLO integration process, if necessary.

C.3.4.4 Planetary Protection

The planetary protection requirements for a mission to Europa are significant and can drive mission design, schedule, and cost. The final fate of the Europa Multiple-Flyby Mission, impacting on the Ganymede surface, means that the mission will be classified as Category III under current Committee on Space Research (COSPAR) and NASA policy (COSPAR 2002). If prelaunch cleanliness levels are not met, expenditure of cost and schedule reserves might be required to address contamination problems late in the process to prevent contamination of Europa. This risk is cross-

cutting and is mitigated in part by a review added in Phase B to confirm the approach and assess implementation. This risk is also mitigated by the previous Europa Study activities. The approach to planetary protection compliance for the Europa Multiple-Flyby Mission concept, at this time is 1) prelaunch DHMR to control bioburden for those areas not irradiated in-flight and 2) in-flight microbial reduction via radiation prior to the first Europa flybys. The prelaunch method is to perform a full system DHMR as one of the last steps in the ATLO process at KSC. A chamber has been identified at KSC that is capable of performing DHMR, though specific details will need to be worked during Phase A. A pathfinder activity is planned as a dress rehearsal to resolve any procedural challenges. Compilation of the Europa Multiple-Flyby Mission APMML will address compliance of materials with the DHMR process.

C.3.5 Cost

The Flyby Mission cost is well-understood and thoroughly validated.

C.3.5.1 Cost Summary

The Total Mission Cost for the Europa Multiple-Flyby Mission concept is estimated at \$1.9B to \$2.0B FY15, *excluding the launch vehicle, which is costed separately*. The mission baseline comprises a flyby spacecraft carrying four instruments—Ice-Penetrating Radar (IPR), Shortwave Infrared Spectrometer (SWIRS), Ion And Neutral Mass Spectrometer (INMS), and Topographical Imager (TI)—that would spend 18 months taking remote measurements of Europa via multiple flybys. The Europa Multiple-Flyby Mission enables investigators to understand the chemistry of this moon and investigate its habitability for life.

Table C.3.5-1 summarizes the mission cost estimate at WBS level 2.

The total mission cost is broken down into \$1.6 to \$1.7B for the Phase-A through -D development period and \$0.3B for operations during Phases E and F. The Europa Multiple-

Table C.3.5-1. Europa Multiple-Flyby Mission cost summary by WBS (FY15 \$M).

WBS Element	PRICE-H	SEER
01 Proj Mgmt	62	60
02 Project System Engineering	52	50
03 Safety & Mission Assurance	57	55
04 Science	71	71
05 Payload System	262	262
06 Spacecraft System	489	468
ASRG	200	200
07 Mission Operations System	171	171
08 Launch System	—	—
09 Ground Data System	39	39
10 Proj Sys I&T	48	42
11 Education & Public Outreach	13	12
12 Mission Design	25	24
Subtotal (FY15\$M)	1,489	1,456
Reserves	467	454
Total (FY15\$M)	1,956	1,911

Flyby Mission holds 37% in cost reserves that is broken down into 40% for Phases A, B, C, and D, and 20% for Phases E and F.

The estimated cost is based on the implementation approach described in Section C.2, which includes the following key features in the baseline plan:

- Redundant flight system with selected cross-strapping
- No new technologies requiring extraordinary development
- Simple, repeated, algorithm-driven observations capable of achieving all of the science goals
- Experienced providers of key systems and subsystems

C.3.5.2 Cost Estimating Methodology

To estimate the cost for the Europa Multiple-Flyby Mission concept, JPL used their institutional cost-estimation process applicable for the design maturity of a concept study in early formulation. This process focuses on using parametric cost models, analogies, and other non-grassroots estimating techniques, which provide the following advantages:

- Provide rapid turnaround of extensive trade studies

- Enable design-to-cost to narrow the trade space and define a baseline concept
- Establish reasonable upper and lower bounds around a point estimate

A cost-estimation process begins with the Europa Study Team developing a Technical Data Package (TDP) that describes the science requirements, technical design, mission architecture, and project schedule. Next, all work is organized, defined, and estimated according to the NASA standard WBS. The Europa Study Team then tailors the WBS as needed for cost estimation and planning.

The institutional business organization uses the TDP and WBS to develop the cost estimate by applying estimating methods and techniques appropriate for each WBS element, based on the maturity of design and manufacturing requirements, availability of relevant historical information, and degree of similarity to prior missions. For the Europa Multiple-Flyby Mission, the tools and methods used include the following:

- Calibration of commercial, off-the-shelf (COTS) tools PRICE-H and SEER to Juno, the most relevant JPL planetary mission
- Use of the NASA Instrument Cost Model (NICM) for the notional payload, tailored for the Europa environment
- Use of the NASA Space Operations & Cost Model (SOCM) for Phases E and F
- Wrap factors based on analogous historical planetary missions for Project Management, Project Systems Engineering, Safety and Mission Assurance, and Mission Design

The Europa Study Team's estimate is a compilation of these multiple techniques. The Europa Study team then vets the integrated cost rollup and detailed basis of estimate (BOE), and reviews the results for consistency and

reasonableness with the mission design, WBS, and NASA requirements to ensure that technical and schedule characteristics are accurately captured and a consistent cost-risk posture is assumed.

To validate the resulting proposed cost, the Europa Study Team used Team X to independently cost the baseline concept with the JPL Institutional Cost Models (ICMs): 33 integrated, WBS-Level-2 through -4 models built by JPL line organizations to emulate their grassroots approach. The Europa Study Team also contracted with the Aerospace Corporation to perform an Independent Cost Estimate (ICE) and Cost and Technical Evaluation (CATE.) The Team X and Aerospace results are discussed in Section C.3.5.7.

The Europa Study Team then used an S-curve cost risk analysis to validate and bound the cost reserves. The reserves substantiation is discussed in Section C.3.5.8.

C.3.5.3 Basis of Estimate

The integrated Europa Multiple-Flyby Mission cost estimate is based on the science and mission implementation approach described in Section C.2. In addition, the MEL (Section C.4.3) provided the key inputs for mass, quantities, and the quantification of electronics versus structures that are needed to run the parametric tools. The cost estimating methodologies and assumptions used to develop the Europa Multiple-Flyby Mission cost estimate are summarized in Table C.3.5-2.

C.3.5.4 Instrument Cost Estimates

The NASA Instrument Cost Model (NICM) system model with an augmentation to account for radiation and planetary protection was used to estimate instrument costs. Each notional instrument was characterized for performance

establishing instrument type, aggregate power estimates, and subsystem-level mass. Table C.3.5-3 shows the input parameters used for each instrument for the NICM system model.

C.3.5.4.1 NICM Adjustments

NICM outputs at the 70 percentile were reported in FY15\$. This reference cost estimate was then augmented for radiation and planetary protection. The NICM model does not have parameters or characteristics sufficient to model planetary protection requirements or radiation environments. A flat fee for Planetary Protection was added to each instrument, based on instrument complexity. An estimate for the number of electronic boards and detectors was made for each instrument, and an additional fee of \$2M was assessed per detector for radiation redesign costs. The instrument radiation shielding masses were estimated separately in PRICE-H and SEER, and are included in WBS 06 spacecraft costs under Payload Radiation Shielding. Table C.3.5-4 summarizes the instrument cost-estimation process.

C.3.5.4.2 NICM Estimate

Table C.3.5-5 provides the final NICM system cost estimate, including all adjustments for radiation and planetary protection.

C.3.5.5 Spacecraft Hardware Costs

The Europa Multiple-Flyby Mission spacecraft hardware costs were estimated using PRICE-H and SEER, calibrated to Juno. The Flyby spacecraft is most closely analogous to the Juno spacecraft. Configuration, avionics subsystems, radiation environment, mission complexity, and design lifetime match closely to the corresponding aspects of the Juno mission.

Table C.3.5-2. Cost-estimation methodology.

WBS Element	Methodology
01 Project Management	Historical wrap factor based on analogous historical planetary missions. Estimate was augmented by \$15M to account for Nuclear Launch Safety Approval (NLSA) and National Environmental Policy Act (NEPA) costs associated with usage of the advanced Stirling radioisotope generators (ASRGs).
02 Project Systems Engineering	Historical wrap factor based on analogous historical planetary missions.
03 Safety & Mission Assurance	Historical wrap factor based on analogous historical planetary missions.
04 Science	Expert-based estimate from the science team based on mission class, schedule, and the number and complexity of instruments. Cost estimate captures the level of effort for a Project Scientist, two Deputy Project Scientists, the Science Team, and participating scientists, with additional workforce requirements for Phases C and D, based on the size of the team, the number of meetings with the team, and the products required from this group. For Phases E and F, the cost estimate also assumes a science team for each instrument, with the estimated level of effort based on existing instrument teams supporting current mission, and on the number of months in hibernation, cruise, and science operations.
05 Payload System	Historical wrap factor for Payload Management, Systems Engineering, and Product Assurance based on analogous historical planetary missions. Instrument costs developed using the NASA Instrument Cost Model (NICM), Version 5.0. The 70% confidence-level estimate was selected as a conservative point estimate for each notional instrument. Instrument costs are then augmented for radiation shielding, detector radiation redesign, and planetary protection for any DHMR material properties issues. For payload radiation shielding, the cost was estimated separately using PRICE-H and SEER, and the cost is included under WBS 06 Spacecraft System. For planetary protection a flat fee was then added to each instrument, based on instrument complexity. For radiation redesign, an additional fee of \$2M was assessed per detector.
06 Spacecraft System	Historical wrap factor for Flight System Management, Systems Engineering, and Product Assurance based on analogous historical planetary missions. Spacecraft hardware costs estimated using PRICE-H and SEER calibrated to Juno at the subsystem level. Juno selected as an analogous mission for the calibration due to the operation of the flight system in a comparable radiation environment. Software costs estimated using a wrap factor of 10% on the hardware cost. ASRG cost provided by NASA Headquarters in the Europa Study Statement of Work, dated October 4, 2011 (NASA 2011). Estimate includes four ASRGs at \$50M each (FY15\$).
07 Mission Operations System	Team X estimate based on historical data for a Class A mission for Phases A-D; SOCM estimate for Phases E-F
08 Launch System	Launch Vehicle costs, including nuclear processing costs, are not included and will be provided by NASA Headquarters as directed in the Europa Study Statement of Work.
09 Ground Data System	Team X estimate based on historical data for a Class A mission for Phases A-D; SOCM estimate for Phases E-F
10 Project Systems I&T	PRICE-H and SEER estimate calibrated to Juno.
11 Education & Public Outreach	1.0% wrap factor on the total mission cost excluding the launch system (WBS 08), ASRG, and DSN tracking costs. Based on the percentage prescribed in the recent AOs for Discovery 2010 and New Frontiers 2009 (NASA 2010a, 2009c).
12 Mission Design	Historical wrap factor based on analogous historical planetary missions.
Reserves	40% for Phases A–D and 20% for Phases E–F on the total mission cost excluding the launch system (WBS 08), ASRG, and DSN tracking costs. These percentages were based on historical experience with recent planetary missions.

Table C.3.5-3. Inputs for NICM cost estimation.

Instrument Name	Ice-Penetrating Radar (IPR)	Shortwave Infrared Spectrometer (SWIRS)	Ion and Neutral Mass Spectrometer (INMS)	Topographic Imager (TI)
Remote Sensing or In-Situ?	Remote Sensing	Remote Sensing	Remote Sensing	Remote Sensing
Remote Sensing Instrument Type	Active	Optical	Particles	Optical
Mission Destination	Planetary	Planetary	Planetary	Planetary
Total Mass (kg)	28	12	14	3
Max Power (W)	55	19	33	6
Design Life (months)	108	108	108	108
Max Data Rate (kbps)	300	N/A	N/A	N/A
TRL	5	N/A	N/A	N/A
Number of Detectors	0	1	0	1

Table C.3.5-4. Instrument cost-estimation process.

Master Instrument Costing Matrix	Instrument Cost (Excluding Radiation Shielding) (A)	Detector Radiation Design Costs (B)	Planetary Protection Fee (C)	TOTAL INSTRUMENT COST	Radiation Shielding Cost—Included in WBS 06
Instrument X	NICM 70th percentile estimate	\$2M per detector	Based on complexity	A+B+C	Estimated in PRICE-H/SEER

Table C.3.5-5. Instrument cost-estimation details (FY15\$M).

Instrument	Acronym	NICM 70% Cost	Detector Radiation Design Costs	Planetary Protection Fee	TOTAL INSTRUMENT COST
Ice-Penetrating Radar	IPR	109.9	0.0	3.3	113.2
Shortwave Infrared Spectrometer	SWIRS	43.8	2.0	4.4	50.2
Topographic Imager	TI	14.3	2.0	0.7	17.0
Ion and Neutral Mass Spectrometer	INMS	47.9	0.0	1.4	49.4
TOTAL		216.0	4.0	9.8	229.9

PRICE-H and SEER Cost Estimates

The Spacecraft System costs generated for PRICE-H and SEER are shown in Table C.3.5-6. The Spacecraft System comprises the Carrier System and the Lander System in WBS 06. The Payload Radiation Shielding is captured as part of the Lander System and the costs are bookkept under WBS 06B.07. The RPS was estimated at a cost of \$50M per ASRG unit as directed by NASA HQ, and included in WBS 06, separate from the Carrier System and Lander System costs. The I&T costs are kept in WBS 10. Spacecraft flight software was estimated as a 10% wrap factor based on hardware cost, which is a high-level rule of thumb derived from JPL's historical software cost data.

Table C.3.5-6. PRICE-H and SEER cost estimates for the Europa Multiple-Flyby Mission. (FY15\$M)

Spacecraft System	PRICE-H	SEER
06 Spacecraft System		
06.04 Spacecraft Power SS	50	68
06.05 Spacecraft C&DH SS	37	27
06.06 Spacecraft Telecom SS	83	48
06.07 Spacecraft Mechanical SS	52	44
06.07a Radiation Shielding	11	11
06.07b Payload Radiation Shielding	3	2
06.08 Spacecraft Thermal SS	10	10
06.09 Spacecraft Propulsion SS	38	54
06.10 Spacecraft GN&C SS	51	56
06.11 Spacecraft Harness SS	6	6
06.12 Spacecraft Flight SW	34	33
06C RPS System	200	200
10 I&T	48	42

Table C.3.5-7. Phase E and F cost estimate for the Europa Multiple-Flyby Mission (FY15\$M).

WBS Element	Phase E & F Costs
01 Project Management	7
02 Project Systems Engineering	7
03 Safety & Mission Assurance	7
04 Science	46
05 Payload	0
06 Spacecraft	0
07 Mission Operations	124
08 Launch System	0
09 Ground Data Systems	12
10 Project System Integration & Test	0
11 Education & Public Outreach	2
SUBTOTAL	204
DSN Tracking	19
20% Reserves (excluding DSN)	41
TOTAL	264

C.3.5.6 Phase E and F Cost Estimates

The NASA Space Operations Cost Model (SOCM) was used to estimate operations costs in Phases E and F. The Europa Study science team provided an expert-based estimate for WBS 04 Science based on schedule and the number and complexity of instruments. The Europa Multiple-Flyby Mission Phase E and F cost estimate is shown in Table C.3.5-7.

C.3.5.7 Estimate Reasonableness (Validation)

A JPL Team X cost session was used to assess the reasonableness of the parametrically derived PRICE-H and SEER-based Flight System (WBS 06) and Project Systems I&T (WBS 10) estimates and associated wraps. In addition, Aerospace Corporation independently ran an Independent Cost Estimate (ICE) and Cost and Technical Evaluation (CATE). The results of the Team X cost session and Aerospace Corporation analysis are presented in Table C.3.5-8 along with the PRICE- and SEER-based project estimates for comparison.

C.3.5.8 Cost-Risk Assessment and

Table C.3.5-8. Comparison of Europa Study cost estimates with Team X and Aerospace Corporation cost estimates..

WBS Element	PRICE	SEER	Team X	Aerospace ICE	Aerospace CATE
Total (FY15\$B)	2.0	1.9	1.7	2.1	2.1

Reserve Strategy

The Europa Study Team conservatively applied project-level reserves of 40% for Phases A–D and 20% for Phases E and F on all elements except for Launch Services, ASRGs, and DSN tracking. These reserve levels are more conservative than the reserve guidelines set forward in JPL Flight Project Practices, Rev. 8 (JPL 2010b).

The Europa Multiple-Flyby Mission cost risk and uncertainty assessment is a natural extension of the cost modeling discussed in Section C.3.5.1, and is consistent with standard practice at NASA and JPL. This assessment considers the wide band of uncertainty that typically accompanies missions at early phases of development, as well as the technical risk and uncertainties of the Europa Lander Mission as understood at this time and as experienced on prior competed and directed missions (e.g., Juno, MRO, MSL).

The primary technique used for this assessment is an S-Curve. This provides a statistical-based distribution of total project cost around the project's point estimate based on the cost models used in this analysis and the historical JPL data to which they are calibrated. Equivalently, this technique provides a probabilistic estimate of total project cost based on variability and uncertainties in the model-based estimates. An S-curve analysis was performed on the study cost estimate, and demonstrated a 70th-percentile cost estimate of \$1.98B (\$FY15, excluding launch vehicle) (Figure C.3.5-1). Comparing the Europa Study Team estimate (including cost reserves) to the S-Curve indicates that the Europa Study Team estimate of \$1.9B to \$2.0B is at approximately the 68th-percentile. To be at 70th-percentile, the Europa Study Team would need to increase reserves by ~\$25M to ~\$70M, resulting in a

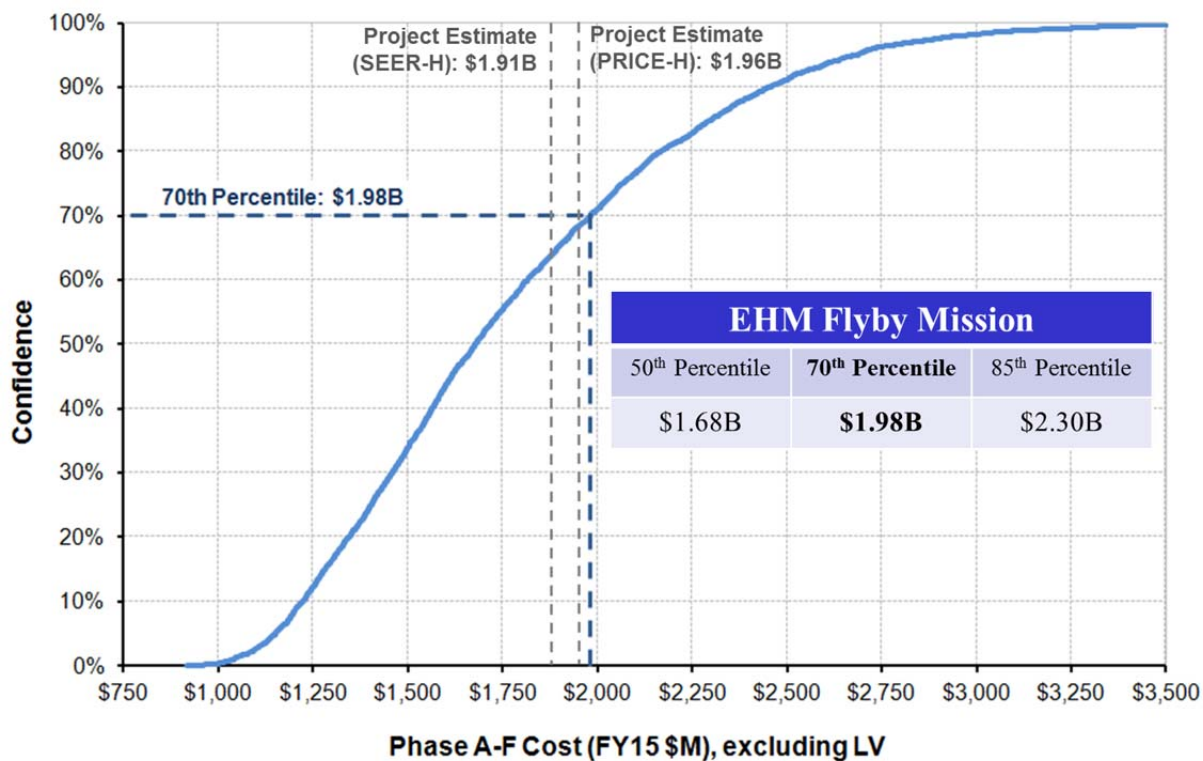


Figure C.3.5-1. Europa Multiple-Flyby Mission cost estimate S-curve analysis.

reserve position of 40% overall (Phases A–F).

C.4 Multiple-Flyby Mission Appendices

C.4.1 References

- Alexander, C., Carlson, R., Consolmagno, G., Greeley, R., Morrison, D. 2009. The exploration history of Europa. In: Pappalardo, R.T., McKinnon, W.B., Khurana, K.K. (Eds.), *Europa*, U. Arizona Press, Tucson, 3–26.
- American National Standards Institute, 1992. ANSI/AIAA Guide G-020-1992, Estimating and Budgeting Weight and Power Contingencies for Spacecraft Systems. American Institute of Aeronautics and Astronautics, Washington, DC.
- Bell, J.F., 1992. Charge-coupled device imaging spectroscopy of Mars 2: Results and implications for Martian ferric mineralogy. *Icarus* 100, 575–597.
- Bibring, J., Langevin, Y., Gendrin, A., Gondet, B., Poulet, F., Berthe, M., Soufflot, A., Arvidson, R., Mangold, N., Mustard, J., et al., 2005. Mars surface diversity as revealed by the OMEGA/Mars express observations. *Science* 307, 1576–1581.
- Bierhaus, E.B., Zahnle, K., Chapman, C.R., 2009. Europa's crater distributions and surface ages. In: Pappalardo, R.T., McKinnon, W.B., Khurana, K.K. (Eds.), *Europa*, U. Arizona Press, Tucson, 161–180.
- Billings, S.E., Kattenhorn, S.A., 2005. The great thickness debate: Ice shell thickness models for Europa and comparisons with estimates based on flexure at ridges. *Icarus* 177, 397–412.
- Boldt, J., et al., 2008. Assessment of radiation effects on detectors and key optical components. JPL D-48256.
- Brown, M.E., 2001. Potassium in Europa's atmosphere. *Icarus* 151, 190–195.
- Brown, M.E., Hill, R.E., 1996. Discovery of an extended sodium atmosphere around Europa. *Nature* 380, 229–231.
- Brunetto, R., et al., 2005. Reflectance and transmittance spectra (2.2–2.4 μm) of ion irradiated frozen methanol. *Icarus* 175, 226–232.
- Carlson, R.W., 1999. A tenuous carbon dioxide atmosphere on Jupiter's moon Callisto. *Science* 283, 820–821.
- Carlson, R.W., 2001. Spatial distribution of carbon dioxide, hydrogen peroxide, and sulfuric acid on Europa. *Bull. Am. Astron. Soc.* 33, 1125.
- Carlson, R.W., et al., 1999a. Hydrogen peroxide on the surface of Europa. *Science* 283, 2062–2064.
- Carlson, R.W., Johnson, R.E., Anderson, M.S., 1999b. Sulfuric acid on Europa and the radiolytic sulfur cycle. *Science* 286, 97–99.
- Carlson, R.W., et al., 2002. Sulfuric acid production on Europa: The radiolysis of sulfur in water ice. *Icarus* 157, 456–463.
- Carlson, R.W., et al., 2005. Distribution of hydrated sulfuric acid on Europa. *Icarus* 177, 461–471.
- Carr, M.H., Belton, M.J.S., Chapman, C.R., Davies, M.E., Geissler, R., Greenberg, R., McEwen, A.S., Tufts, B.R., Greeley, R., Sullivan, R., Head, J.W., Pappalardo, R.T., Klaasen, K.P., Johnson, T.V., Kaufman, J., Senske, D., Moore, J., Neukum, G., Schubert, G., Burns, J.A., Thomas, P., Veverka, J., 1998. Evidence for a subsurface ocean on Europa. *Nature* 391, 363–365.
- Cassidy, T., Johnson, R., Geissler, P., Leblanc, F., 2008. Simulation of Na D emission near Europa during eclipse. *J. Geophys. Res.* 113, doi: 10.1029/2007JE002955.
- Cassidy, T.A., Johnson, R.E., Tucker, O.J., 2009. Trace constituents of Europa's atmosphere. *Icarus* 201, 182–190.

- Cheng, K.S., et al., 1986. Energetic radiation from rapidly spinning pulsars: 1. Outer magnetosphere gaps. *Astrophys. J.* 300, 500–521.
- Christensen, P.R., et al., 2001. Mars Global Surveyor thermal emission spectrometer experiment: Investigation description and surface science results. *J. Geophys. Res.* 106, 23,823–23,871.
- Chyba, C.F., Ostro, S.J., Edwards, B.C., 1998. Radar detectability of a subsurface ocean on Europa. *Icarus* 134, 292–302.
- Clark, K., et al., 2007. Europa Explorer Mission Study: Final Report, JPL D-41283.
- Clark, K., et al., 2008. Jupiter Europa Orbiter Mission Study 2008 Final Report, JPL D-48279.
- Clark, R.N., McCord, T.B., 1980. The Galilean satellites: New near-infrared spectral reflectance measurements (0.65–25 μm) and a 0.325–5 μm summary. *Icarus* 41, 323–339.
- Clark, R.N., Fanale, F., Zent, A., 1983. Frost grain size metamorphism: Implications for remote sensing of planetary surfaces. *Icarus* 56, 233–245.
- Clark, R.N., et al., 2005. Compositional maps of Saturn's moon Phoebe from imaging spectroscopy. *Nature* 435, 66–69.
- Collins, G., Nimmo, F., 2009. Chaotic terrain on Europa. In: Pappalardo, R.T., McKinnon, W.B., Khurana, K.K. (Eds.), *Europa*, U. Arizona Press, Tucson, 259–282.
- Cooper, J.F., et al., 2001. Energetic ion and electron irradiation of the icy Galilean satellites. *Icarus* 149, 133–159.
- Committee on Space Research, 2002. COSPAR Planetary Protection Policy, as amended March 2005). <<http://www.cosparhq.org/scistr/PPPoly icy.htm>>.
- Crowley, J.K., 1991. Visible and near-infrared (0.4–2.5 μm) reflectance spectra of playa evaporite minerals. *J. Geophys. Res.* 96, 16,231–16,240.
- Cruikshank, D.P., et al., 2007. Surface composition of Hyperion. *Nature* 448, 54–56.
- Dalton, J.B., 2000. Constraints on the surface composition of Jupiter's moon Europa based on laboratory and spacecraft data. Ph.D. dissertation, Univ. of Colorado, Boulder.
- Dalton, J.B., 2007a. Linear mixture modeling of Europa's non-ice material using cryogenic laboratory spectroscopy. *Geophys. Res. Lett.* 34, 21,205.
- Dalton, J.B., 2007b. Modeling Europa's surface composition with cryogenic sulfate hydrates. *LPI Contributions* 1357, 36–37.
- Dalton, J.B., Clark, R.N., 1998. Laboratory spectra of Europa candidate materials at cryogenic temperatures. *Bull. Am. Astron. Soc.* 30, 1081.
- Dalton, J.B., Clark, R.N., 1999. Observational constraints on Europa's surface composition from Galileo NIMS data. *Proc. Lunar Planet. Sci. Conf.* XXX, 2064.
- Dalton, J.B., Mogul, R., Kagawa, H., Chan, S., Jamieson, C., 2003. Near-infrared detection of potential evidence for microscopic organisms on Europa. *Astrobiology* 3, 505–529.
- Dalton, J.B., et al., 2005. Spectral comparison of heavily hydrated salts to disrupted terrains on Europa. *Icarus* 177, 472–490.
- Dawson, S., 1999, Office of Space Science Risk Communication Plan for Planetary and Deep Space Missions, JPL D-16993.
- Delitsky, M.L., Lane, A.L., 1997. Chemical schemes for surface modification of icy satellites: A road map. *J. Geophys. Res.* 102, 16,385–16,390.

- Delitsky, M.L., Lane, A.L., 1998. Ice chemistry on the Galilean satellites. *J. Geophys. Res.* 103, 31,391–31,403.
- Doggett, T., Greeley, R., Figueredo, P., Tanaka, K., Weiser, S., 2009. Geologic stratigraphy and evolution of Europa's surface. In: Pappalardo, R.T., McKinnon, W.B., Khurana, K.K. (Eds.), *Europa*, U. Arizona Press, Tucson, 137–160.
- Ehlmann, B., Mustard, J., Fassett, C., Schon, S., Head, J. III, Des Marais, D., Grant, J., Murchie, S., 2008. Clay minerals in delta deposits and organic preservation potential on Mars. *Nature Geoscience* 1, 355.
- Eluszkiewicz, J., 2004. Dim prospects for radar detection of Europa's ocean. *Icarus* 170, 234–236.
- Fanale, F.P., et al., 1999. Galileo's multi-instrument spectral view of Europa's surface composition. *Icarus* 139, 179–188.
- Figueredo, P.H., Greeley, R., 2004. Resurfacing history of Europa from pole-to-pole geological mapping. *Icarus* 167, 287–312.
- Figueredo, P.H., Greeley, R., 2004. Resurfacing history of Europa from pole-to-pole geological mapping. *Icarus* 167, 287–312.
- Gaidos, E., Nimmo, F., 2000. Tectonics and water on Europa. *Nature* 405, 637.
- Geissler, P.E., Greenberg, R., Hoppa, G., McEwen, A., Tufts, R., Phillips, C., Clark, B., Ockert-Bell, M., Helfenstein, P., Burns, J., Veverka, J., Sullivan, R., Greeley, R., Pappalardo, R. T., Head, J. W., Belton, M. J. S., Denk, T., 1998. Evolution of lineaments on Europa: Clues from Galileo multispectral imaging observations. *Icarus* 135, 107–126, doi: 10.1006/icar.1998.5980.
- Greeley, R., Chyba, C.F., Head, J.W. III, McCord, T.B., McKinnon, W.B., Pappalardo, R.T., Figueredo, P., 2004. Geology of Europa. In: Bagenal, F., Dowling, T.E., McKinnon, W.B. (Eds.), *Jupiter: The Planet, Satellites, and Magnetosphere*, Cambridge U. Press, Cambridge, U.K., 329–362.
- Greenberg, R., G.V. Hoppa, B.R. Tufts, P. Geissler, J. Riley, and S. Kadel, 1999. Chaos on Europa. *Icarus* 141, 263–286.
- Grundy, W., Buratti, B., Cheng, A., Emery, J., Lunsford, A., McKinnon, W., Moore, J., Newman, S., Olkin, C., Reuter, D., et al., 2007. New horizons mapping of Europa and Ganymede. *Science* 318, 234.
- Hairston, A., Stobie, J., Tinkler, R., 2006. Advanced readout integrated circuit signal processing, *Infrared Technology and Applications XXXII. Proc. SPIE.* 6206, Part 2: 62062Z.
- Hall, D.T., Strobel, D.F., Feldman, P.D., McGrath, M.A., Weaver, H.A., 1995. Detection of an oxygen atmosphere on Jupiter's moon Europa. *Nature* 373, 677–679.
- Hall, D.T., Feldman, P.D., McGrath, M.A., Strobel, D.F., 1998. The far-ultraviolet oxygen airglow of Europa and Ganymede. *Astrophys. J.* 499, 475–481.
- Hand, K.P., 2007. On the physics and chemistry of the ice shell and sub-surface ocean of Europa. Ph.D. dissertation, Stanford U.
- Hansen, G., McCord, T.B., 2004. Amorphous and crystalline ice on the Galilean satellites: A balance between thermal and radiolytic processes. *J. Geophys. Res.* 109, doi: 10.1029/2003JE002149.
- Hansen, G., McCord, T.B., 2008. Widespread CO₂ and other non-ice compounds on the anti-Jovian and trailing sides of Europa from Galileo/NIMS observations. *Geophys. Res. Lett.* 35, L01202.

- Head, J.W., Pappalardo, R.T., 1999. Brine mobilization during lithospheric heating on Europa: Implications for formation of chaos terrain, lenticula texture, and color variations. *J. Geophys. Res.*, Planets 104, 27143–27155.
- Hoppa, G.V., et al. 1999. Formation of cycloidal features on Europa. *Science* 285, 1899–1902.
- Hunt, G.R., Salisbury, J.W., Lenhoff, C.J., 1971a. Visible and near-infrared spectra of minerals and rocks. III. Oxides and hydroxides. *Mod. Geol.* 2, 195–205.
- Hunt, G.R., Salisbury, J.W., Lenhoff, C.J., 1971b. Visible and near-infrared spectra of minerals and rocks. IV. Sulphides and sulphates. *Mod. Geol.* 3, 1–14.
- Hussman, H., Spohn, T., 2004. Thermal-orbital evolution of Io and Europa. *Icarus* 171, 391–410.
- Janesick, J., Elliott, T., Tower, J., 2008. CMOS detectors: Scientific monolithic CMOS imagers come of age. *Laser Focus World* 44:7, 68.
<http://www.laserfocusworld.com/display_article/332970/12/none/none/Feat/CMOS-Detectors:-Scientificmonolithic-CMOS-imagers-come-of-ag>
- Johnson, R.E., Quickenden, T.I., 1997. Radiolysis and photolysis of low-temperature ice. *J. Geophys. Res.* 102, 10,985–10,996.
- Johnson, R.E., Killen, R.M., Waite, J.H., Lewis, W.S., 1998. Europa's surface composition and sputter-produced ionosphere. *Geophys. Res. Lett.* 25, 3257–3260.
- Johnson, R.E., Leblanc, F., Yakshinskiy, B.V., Madey, T.E., 2002. Energy distributions for desorption of sodium and potassium from ice: The Na/K ratio at Europa. *Icarus* 156, 136–142.
- Johnson, R.E., R.W. Carlson, J.F. Cooper, C. Paranicas, M.H. Moore, and M. Wong 2004. Radiation effects on the surfaces of the galilean satellites. In: Bagenal, F., Dowling, T.E., McKinnon, W.B. (Eds.), *Jupiter: The Planet, Satellites, and Magnetosphere*, Cambridge U. Press, Cambridge, U.K., 485–512.
- Jet Propulsion Laboratory, 2005. Risk Communication Plan for Planetary and Deep Space Missions, Rev. 2, JPL Rules! DocID 61272, August 30, 2005.
- Jet Propulsion Laboratory, 2009. JPL Standard Flight Project Work Breakdown Structure Template, Rev. 5, JPL Rules! DocID 59533, March 18, 2009.
- Jet Propulsion Laboratory, 2010a. Design, Verification/Validation and Ops Principles for Flight Systems (Design Principles), Rev. 4, JPL Rules! DocID 43913, September 20, 2010.
- Jet Propulsion Laboratory, 2010b. Flight Project Practices, Rev. 8, JPL Rules! DocID 58032, October 6, 2010.
- Jet Propulsion Laboratory, 2010c. Software Development (Requirement), Rev. 8, JPL Rules! DocID 23713, September 20, 2010.
- Kargel, J., et al., 2000. Europa's Crust and Ocean: Origin, Composition, and the Prospects for Life, *Icarus* 148, no. 1: 226–265.
- Kattenhorn, S.A., Hurford, T., 2009. Tectonics of Europa. In: Pappalardo, R.T., McKinnon, W.B., Khurana, K.K. (Eds.), *Europa*, U. Arizona Press, Tucson, 199–236.
- Khurana, K.K., et al., 1998. Induced magnetic fields as evidence for subsurface oceans in Europa and Callisto. *Nature* 395, 777–780.

- Klaasen, K., Clary, M., Janesick, J., 1984. Charge-coupled device television camera for NASA's Galileo mission to Jupiter. *Optical Engineering* 23, 334–342.
- Kuiper, G.P., 1957. Infrared observations of planets and satellites. *Astro. J.* 62, 295.
- Kwok, J., Prockter, L., Senske, D., Jones, C., 2007. Jupiter System Observer Mission Study: Final Report, JPL D-41284.
- Lane, A.L., et al., 1981. Evidence for sulphur implantation in Europa's UV absorption band. *Nature* 292, 38–39.
- Leblanc, F., Johnson, R.E., Brown, M.E., 2002. Europa's sodium atmosphere: An ocean source? *Icarus* 159, 132–144.
- Leblanc, F., et al., 2005. Origins of Europa Na cloud and torus. *Icarus* 178, 367–385.
- Lee, S., Pappalardo, R.T., Makris, N.C., 2005. Mechanics of tidally driven fractures in Europa's ice shell. *Icarus* 177, 367–379.
- Lock, R., 2008. EJSM Europa Orbiter Science Scenarios (presentation slides). Outer Planets Flagship Mission Instrument Workshop, June 3, 2008.
- Lock, R., 2010. Concept of Operations (presentation slides), Jupiter Europa Orbiter Internal Mission Concept Review, June 7–9, 2010.
- Lockheed Martin, 2011. ASRG User Interface Control Document. Lockheed Martin Contract No. DE-AC07-00SF22191, Specification #912IC002085, Rev. A, June 2011.
- Ludwinski, J., 1997. Galileo Mission Planning Office Closeout (Lessons Learned), JPL IOM 311.1/98/01, January 19, 1997.
- Ludwinski, J., 1997. Galileo Mission Planning Office Closeout (Lessons Learned), JPL IOM 311.1/98/01, January 19, 1997.
- McCord, T.B., 2000. Surface composition reveals icy Galilean satellites' past. *Eos Trans. Am. Geophys. Union* 81, 209.
- McCord, T.B., et al., 1997. Organics and other molecules in the surfaces of Callisto and Ganymede. *Science* 278, 271–275.
- McCord, T.B., et al., 1998a. Salts on Europa's surface detected by Galileo's near-infrared mapping spectrometer. *Science* 280, 1242.
- McCord, T.B., et al., 1998b. Non-water-ice constituents in the surface material of the icy Galilean satellites from the Galileo near-infrared mapping spectrometer investigation. *J. Geophys. Res.* 103, 8603–8626.
- McCord, T.B., et al., 1999. Hydrated salt minerals on Europa's surface from the Galileo near-infrared mapping spectrometer (NIMS) investigation. *J. Geophys. Res.* 104, 11,827–11,851.
- McCord, T.B., Hansen, G.B., Hibbitts, C.A., 2001a. Hydrated salt minerals on Ganymede's surface: Evidence of an ocean below. *Science* 292, 1523–1525.
- McCord, T.B., et al., 2001b. Thermal and radiation stability of the hydrated salt minerals epsomite, mirabilite, and natron under Europa environmental conditions. *J. Geophys. Res.* 106, 3311–3320.
- McCord, T.B., et al., 2002. Brines exposed to Europa surface conditions. *J. Geophys. Res.* 107, 4-1–4-6.
- McKinnon, W.B., 2005. Radar sounding of convecting ice shells in the presence of convection: Application to Europa, Ganymede, and Callisto. LPI Workshop on Radar Investigations of Planetary and Terrestrial Environments, Feb. 7–10, 2005, Houston, Texas, abstract no. 6039.
- McKinnon, W.B., Zolensky, M.E., 2003. Sulfate content of Europa's ocean and shell: Evolutionary considerations and some geological and astrobiological implications. *Astrobiology* 3, 879–897.

- Moersch, J., Bell, J. III, Carter, L., Hayward, T., Nicholson, P., Squyres, S., Van Cleve, J., 1997. What happened to Cerberus? Telescopically observed thermophysical properties of the Martian surface. Mars Telescopic Observations Workshop II, Lunar and Planetary Science Technical Report 97-03, 26.
- Moore, J.M., 2000. Models of radar absorption in European ice. *Icarus* 147, 292–300.
- Moore, J.M., et al. 2001. Impact features on Europa: Results of the Galileo Europa Mission (GEM). *Icarus* 151, 93–111.
- Moore, J.M., Black, G., Buratti, B., Phillips, C.B., Spencer, J., Sullivan, R., 2009. Surface properties, regolith, and landscape degradation. In: Pappalardo, R.T., McKinnon, W.B., Khurana, K.K. (Eds.), *Europa*, U. Arizona Press, Tucson, 329–352.
- Moore, M.H., 1984. Studies of proton-irradiated SO₂ at low-temperatures—Implications for Io. *Icarus* 59, 114–128.
- Moore, M.H., Hudson, R. L., 1998. Infrared study of ion-irradiated water-ice mixtures with hydrocarbons relevant to comets. *Icarus* 135, 518–527.
- Moore, M.H., Hudson, R.L., Ferrante, R.F., 2003. Radiation products in processed ices relevant to Edgeworth-Kuiper-belt objects. *Earth Moon Planets* 92, 291–306.
- Moore, W.B., Hussmann, H., 2009. Thermal evolution of Europa’s silicate interior. In: Pappalardo, R.T., McKinnon, W.B., Khurana, K.K. (Eds.), *Europa*, U. Arizona Press, Tucson, 369–380.
- Moroz, V.I., 1965. Infrared spectrophotometry of the Moon and the Galilean satellites of Jupiter. *Soviet Astro.* 9, 999.
- Mustard, J., Murchie, S. Pelkey, S. Ehlmann, B. Milliken, R. Grant, J. Bibring, J. Poulet, F. Bishop, J. Dobreá, E., et al., 2008. Hydrated silicate minerals on Mars observed by the Mars Reconnaissance Orbiter CRISM instrument. *Nature* 454, 305.
- NASA, 2005. Planetary Protection Provisions for Robotic Extraterrestrial Missions. NASA Procedural Requirements (NPR) 8020.12C. NASA, Washington, DC.
- NASA, 2007. NASA Program and Project Management Processes and Requirements, NASA Procedural Requirements (NPR) 7120.5D, March 6, 2007. NASA, Washington, DC.
- NASA, 2009a. NASA Emergency Preparedness Plan Procedural Requirement, NPR 8715.2, January 9, 2009. NASA, Washington, DC.
- NASA, 2009b. NASA Software Engineering Requirements, NPR 7150.2, November 19, 2009. NASA, Washington, DC.
- NASA, 2009c. New Frontiers 2009 Announcement of Opportunity, NNH09ZDA0070, April 20, 2009.
- NASA, 2010a. Discovery 2010 Announcement of Opportunity, NNH10ZDA0070, June 7, 2010.
- NASA, 2010b. NASA Emergency Preparedness Plan Procedural Requirement, NPR 8715.3, December 16, 2010. NASA, Washington, DC.
- NASA, 2011. Europa Study Statement of Work, October 4, 2011. NASA, Washington, DC.
- NASA, 2012. NASA Program and Project Management Processes and Requirements, NPR 7120.5E, (anticipated) June 2012. NASA, Washington, DC.
- Nimmo, F., Giese, B., Pappalardo, R.T., 2003. Estimates of Europa’s ice shell thickness from elastically supported topography. *Geophys. Res. Lett.* 30, 1233.

- Noll, K.S., Weaver, H.A., Gonnella, A.M., 1995. The albedo spectrum of Europa from 2200 to 3300. *J. Geophys. Res.* 100, 19,057–19,060.
- Orlando, T.M., et al., 2005. The chemical nature of Europa surface material and the relation to a sub-surface ocean. *Icarus* 177, 528–533.
- Paczkowski, B., et al., 2008. Outer Planets Flagship Mission Science Operations Concept Study Report, JPL D–46870. June 2008.
- Pappalardo, R.T., Barr, A.C., 2004. Origin of domes on Europa: The role of thermally induced compositional buoyancy. *Geophys. Res. Lett.* 31, L01701.
- Pappalardo, R.T., et al. 1998. Geological evidence for solid-state convection in Europa's ice shell. *Nature* 391, 365.
- Pappalardo, R.T., et al. 1999. Does Europa have a subsurface ocean? Evaluation of the geological evidence. *J. Geophys. Res.* 104, 24,015–24,056.
- Paranicas, C., Mauk, B., Ratliff, J., Cohen, C., Johnson, R., 2002. The ion environment near Europa and its role in surface energetics. *Geophys. Res. Lett.* 29, 18–1.
- Paranicas, C., Cooper, J.F., Garrett, H.B., Johnson, R.E., Sturmer, S.J., 2009. Europa's radiation environment and its effects on the surface. In: Pappalardo, R.T., McKinnon, W.B., Khurana, K.K. (Eds.), *Europa*, U. Arizona Press, Tucson, 529–544.
- Parish, A., 1989. Development of algorithms for on-focal plane gamma circumvention and time delay integration. Twenty-Third Asilomar Conference on Signals, Systems, and Computers.
- Park, R.S., et al., 2011. Detecting tides and gravity at Europa from multiple close flybys. *Geophys. Res. Lett.* 38, L24202.
- Pilcher, C.B., Ridgway, S.T., McCord, T.B., 1972. Galilean satellites. *J. Geophys. Res.* 103, 31,391–31,403.
- Presidential Directive/National Security Council Memorandum #25 (PD/NSC-25), Scientific or Technological Experiments with Possible Large-Scale Adverse Environmental Effects and Launch of Nuclear Systems into Space, December 14, 1977.
- Prockter, L.M., Pappalardo, R.J., 2000. Folds on Europa: Implications for crustal cycling and accommodation of extension. *Science* 289, 941–943.
- Prockter, L.M., Schenk, P., 2005. Origin and evolution of Castalia Macula, an anomalous young depression on Europa, *Icarus*, 177, no. 2: 305–326
- Prockter, L.M., Patterson, G.W., 2009. Morphology and evolution of Europa's ridges and bands. In: Pappalardo, R.T., McKinnon, W.B., Khurana, K.K. (Eds.), *Europa*, U. Arizona Press, Tucson, 237–258.
- Prockter, L.M., Head, J.W., Pappalardo, R.T., Sullivan, R.J., Clifton, A.E., Giese, B., Wagner, R., Neukum, G., 2002. Morphology of European bands at high resolution: A mid-ocean ridge-type rift mechanism, *J. Geophys. Res.* 107, 4-1–4-28. doi:10.1029/2000JE001458.
- Rasmussen, R., 2009. System architecture for JEO (presentation slides), EJSI Instrument Workshop, July 15–17, 2009.
- Riley, J., Hoppa, G.V., Greenberg, R. Tufts, B.R., Geissler, P., 2000. Distribution of chaotic terrain on Europa. *J. Geophys. Res.* 105, 22,599–22,616.
- Sarid, A.R., Greenberg, R., Hoppa, G.V., Hurford, T.A., Tufts, B.R., Geissler, P., 2002. Polar wander and surface convergence of Europa's ice shell: Evidence from a survey of strike-slip displacement. *Icarus* 158, 24–41.

- Schenk, P., Pappalardo, R., 2004. Topographic variations in chaos on Europa: Implications for diapiric formation. *Geophys. Res. Lett.* 31, L16703 1–5.
- Schenk, P.M., Turtle, E.P., 2009. Europa's impact craters: Probes of the icy shell. In: Pappalardo, R.T., McKinnon, W.B., Khurana, K.K. (Eds.), *Europa*, U. Arizona Press, Tucson, 181–198.
- Schenk, P.M., Chapman, C.R., Zahnle, K., Moore, J.M., 2004. Ages and interiors: The cratering record of the Galilean satellites. In: Bagenal, F., Dowling, T.E., McKinnon, W.B. (Eds.), *Jupiter: The Planet, Satellites, and Magnetosphere*, Cambridge U. Press, Cambridge, U.K., 427–457.
- Schmidt, B.E., Blankenship, D.D., Patterson, G.W., Schenk, P.M., 2011. Active formation of “chaos terrain” over shallow subsurface water on Europa. *Nature* 479, 502–505.
- Shirley, J.H., Dalton, J.B. III, Prockter, L.M., Kamp, L.W., 2010. Europa's ridged plains and smooth low albedo plains: Distinctive compositions and compositional gradients at the leading side–trailing side boundary. *Icarus* 210, 358–384.
- Smyth, W.H., Marconi, M.L., 2006. Europa's atmosphere, gas tori, and magnetospheric implications. *Icarus* 181, 510–526.
- Smythe, W.D., et al. 1998. Galileo NIMS measurements of the absorption bands at 4.03 and 4.25 microns in distant observations of Europa. *Amer. Astronom. Soc.* 30, 1448.
- Space Studies Board, 2000. *Preventing the Forward-Contamination of Europa*. National Academy Press, Washington, DC.
- Space Studies Board, 2003. *New Frontiers in the Solar System: An Integrated Exploration Strategy 2003–2013*. The National Academies Press, Washington, DC.
- Space Studies Board, 2011. *Visions and Voyages for Planetary Science in the Decade 2013–2022*. The National Academies Press, Washington, DC.
- Spaun, N.A., Head, J.W., Collins, G.C., Prockter, L.M., Pappalardo, R. T., 1998. Conamara Chaos Region, Europa: Reconstruction of mobile polygonal ice blocks. *Geophys. Res. Lett.* 25, 4277–4280.
- Spencer, J.R., Calvin, W.M., 2002. Condensed O₂ on Europa and Callisto. *Astron. J.* 124, 3400–3403.
- Spencer, J.R., et al., 2005. Mid-infrared detection of large longitudinal asymmetries in Io's SO₂ atmosphere. *Icarus* 176, 283–304.
- Spencer, J.R., Pearl, J.C., Segura, M., Flasar, F.M., Mamoutkine, A., Romani, P., Buratti, B.J., Hendrix, A.R., Spilker, L.J., Lopes, R.M.C., 2006. Cassini encounters Enceladus: Background and the discovery of a south polar hot spot. *Science* 311, 1401–1405.
- Sullivan, R., Greeley, R., Homan, K., Klemaszewski, J., Belton, M.J.S, Carr, M.H., Chapman, C.R., Tufts, R., Head, J.W. III, Pappalardo, R., Moore, J., Thomas, P., and the Galileo Imaging Team, 1998. Episodic plate separation and fracture infill on the surface of Europa. *Nature* 391, 371–373.
- Sullivan, R., Moore, J., Pappalardo, R., 1999. Mass-wasting and slope evolution on Europa, Lunar Planet. Sci. 30, Abstract #1747, Lunar and Planetary Institute, Houston (CD-ROM).
- Tufts, B.R., Greenberg, R., Hoppa, G., Geisler, P., 2000. Lithospheric dilation on Europa. *Icarus* 146, 75–97.

- Volwerk, M., et al. 2001. Wave activity in Europa's wake: Implications for ion pickup. *J. Geophys. Res.* 106, 26,033–26,048.
- Willis, P.B., 2011. Materials Survivability and Selection for Nuclear Powered Missions. JPL D-34098.
- Yan, T.-Y., 2007. Risk Mitigation Plan: Radiation and Planetary Protection. JPL D-47928.
- Zahnle, K., Dones, L., Levison, H.F., 1998. Cratering rates in the Galilean satellites. *Icarus* 136, 202–222.
- Zahnle, K., Schenk, P., Levison, H., Dones, L., 2003. Cratering rates in the outer solar system. *Icarus* 163, 263–289.
- Zolotov, M.Y., Kargel, J.S., 2009. On the chemical composition of Europa's icy shell, ocean, and underlying rocks. In: Pappalardo, R.T., McKinnon, W.B., Khurana, K.K. (Eds.), *Europa*, U. Arizona Press, Tucson, 431–458.
- Zombeck, M.V, 1982. *Handbook of Space Astronomy and Astrophysics*. Cambridge U. Press, Cambridge, U.K.

C.4.2 Acronyms and Abbreviations

ΔV	delta velocity, delta-V	BTE	bench-test equipment
3D	three-dimensional	C&DH	Command and Data Handling Subsystem
A	ampere		
A	approach	C_3	injection energy per unit mass (V_{∞}^2), km ² /s ² (also C_3)
A/D	analog to digital		
ABSL	ABSL Power Solutions Ltd. used to be AEA Battery Systems, Ltd., where AEA stood for Atomic Energy Authority (a privatized branch of the U.K. AEA)	CAD	computer-aided design
		CADRe	Cost Analysis Data Requirement
		CATE	Cost and Technical Evaluation
AC	alternating current	CBE	current best estimate
ACS	Attitude Control Subsystem	CCD	charge-coupled device
ACU	ASRG controller unit	CCSDS	Consultative Committee for Space Data Systems
ADC	analog-to-digital converter		
AFT	allowable flight temperature	CDR	Critical Design Review
Ah	ampere-hour	CEM	channel electron multiplier
AO	Announcement of Opportunity	CFDP	CCSDS File Delivery Protocol
APL	Applied Physics Laboratory	CG	center of gravity
APML	Approved Parts and Materials List	CM	center of mass
		CMMI	Capability Maturity Model Integration
APS	active pixel sensor	CMOS	complementary metal-oxide semiconductor
ASC	Advanced Stirling converter		
ASIC	application-specific integrated circuit	COSPAR	Committee on Space Research
ASRG	Advanced Stirling Radioisotope Generator	COT	crank over the top
		CPT	comprehensive performance test
ATK/PSI			
ATLO	assembly, test, and launch operations	CRAM	chalcogenide random-access memory
B	baseline	CRISM	Compact Reconnaissance Imaging Spectrometer for Mars
BIU	bus interface unit		
BOM	beginning of mission	CU	cleanup

DC	direct current	ETL	Export Technical Liaison
DC/DC	direct current to direct current	EVEE	Earth-Venus-Earth-Earth
DD	displacement damage	FMECA	failure modes, effects, and criticality analysis
DDD	displacement damage dose	FO	Foldout
DHMR	dry-heat microbial reduction	FOV	field of view
DOD	depth of discharge	FPPs	Flight Project Practices
DOE	Department of Energy	FS	flight system
DPs	Design Principles	FSW	flight software
DSM	deep-space maneuver	FSWTB	flight software testbed
DSN	Deep Space Network	FWHM	full width at half maximum
DTM	developmental test model	G/T	gain to equivalent noise temperature
DWG	Detector Working Group	GDS	Ground Data System
EEE	electrical, electronic, and electromechanical	GHA	generator housing assembly
EFM	Europa Multiple-Flyby Mission	GM	product of gravitational constant and mass
EGA	Earth gravity assist	GN&C	guidance, navigation, and control
EHS	electrical heater source	GPHS	General-Purpose Heat Source
EIRP	effective isotropic radiated power	GRAIL	Gravity Recovery and Interior Laboratory
EIS	Environmental Impact Statement	GSE	ground-support equipment
EJSM	Europa Jupiter System Mission	H/W	hardware
ELDRS	enhanced low-dose-rate sensitivity	HCIPE	High-Capability Instrument for Planetary Exploration
EM	engineering model	HEPA	high-efficiency particulate air
EMI	electromagnetic interference	HGA	high-gain antenna
EOI	Europa Orbit Insertion	HQ	NASA Headquarters
EOM	end of mission	HY	RF hybrid
ES	Europa Study	I&T	integration and test
ESA	European Space Agency	I/O	input/output
ESD	electrostatic discharge	IC	internal charging

ICD	Interface Control Document	MARSIS	Mars Advanced Radar for Subsurface and Ionosphere Sounding
ICE	Independent Cost Estimate		
ICM	Institutional Cost Model	MCP	microchannel plate
ID	identification/identifier	MCR	Mission Concept Review
ID	inner diameter	MDIS	Mercury Dual Imaging System
IFOV	instantaneous field of view		
IMU	inertial measurement unit	MDR	Mission Definition Review
INMS	Ion and Neutral Mass Spectrometer	MEL	Master Equipment List
IOM	interoffice memorandum	MER	Mars Exploration Rover
IPR	Ice-Penetrating Radar	MESSENGER	Mercury Surface, Space Environment, Geochemistry, and Ranging
IR	infrared		
ITAR	International Traffic in Arms Regulations	MEV	maximum expected value
I-V	current-voltage	MGA	medium-gain antenna
JEO	Jupiter Europa Orbiter	MLI	multilayer insulation
JOI	Jupiter Orbit Insertion	MMM	Moon Mineralogy Mapper
JPL	Jet Propulsion Laboratory	MMRTG	multimission radioisotope thermoelectric generator
K&D	key and driving	MOLA	Mars Orbiter Laser Altimeter
KSC	Kennedy Space Center	MPSS	multimission power switch slice
L1, L2	Level-1, Level-2, etc.	MRO	Mars Reconnaissance Orbiter
LAEP	Launch Approval Engineering Plan	MSL	Mars Science Laboratory
LAT	limited angle torque	MSTB	Mission System Testbed
LCE	launch control equipment	MTIB	minimum torque impulse bit
LEV	lowest expected value	MVIC	Multispectral Visible Imaging Camera
LGA	low-gain antenna	NASA	National Aeronautics and Space Administration
LORRI	Long-Range Reconnaissance Imager	NEPA	National Environmental Policy Act
LST	local solar time	NICM	NASA Instrument Cost Model
LVA	launch vehicle adapter		
M3	Moon Mineralogy Mapper	NIMS	Near-Infrared Mapping Spectrometer
MARCI	Mars Color Imager		

NLS	NASA Launch Services	PoL	point of load
NLSA	Nuclear Launch Safety Approval	PRA	probabilistic risk assessment
NR	nonresonant, nonres	PRA	Project Resource Analyst
NSI	NASA Standard Initiator	PRICE-H	Parametric Review of Information for Costing and Evaluation—Hardware
NTO	nitrogen tetroxide	PSA	Project Schedule Analyst
O&C	operations and checkout	RAD750	radiation-hardened microprocessor
OD	orbit determination	RAM	random-access memory
OPAG	Outer Planets Assessment Group	RCS	Reaction-Control Subsystem
ORT	operations readiness test	RDE	Real-Time Development Environment
OSTP	Office of Science and Technology Policy	RDF	radiation design factor
OTS	off the shelf	RF	radio frequency
P	preliminary	RHU	radioisotope heater unit
P/L	payload	R _J	Jovian radii
P/N	part number	ROD	Record of Decision
PBC	power bus controller	ROIC	readout integrated circuit
PCA	pressurant-control assembly	ROSINA	Rosetta Orbiter Spectrometer for Ion and Neutral Analysis
PCU	power converter unit	RS	Radio Subsystem
PDE	propulsion drive electronics	RTG	radioisotope thermoelectric generator
PDR	Preliminary Design Review	RTOF	reflectron time-of-flight
PEL	Power Equipment List	RWA	reaction wheel assembly (wheel and housing)
PFC	pyro-firing card	RWE	reaction wheel electronics (same as WDE)
PHSF	Payload Hazardous Service Facility	S/N	signal-to-noise ratio
PI	Principal Investigator	S/S	steady state
PIA	propellant-isolation assembly	SAF	Spacecraft Assembly Facility
PIP	Project Information Package	SAR	Safety Analysis Report
PJR	perijove raise maneuver	SDS	shunt driver slice
PMD	propellant-management device	SDST	small deep-space transponder
PMSR	Project Mission System Review		

SDT	Science Definition Team	TCM	trajectory correction maneuver
SDU	shunt dissipater unit		
SEE	single-event effect	TDP	Technical Data Package
SEER	System Evaluation and Estimation of Resources	TI	Topographical Imager
SEL	single-event latchup	TID	total ionizing dose
SEMP	Systems Engineering Management Plan	TOF	time of flight
SER	Safety Evaluation Report	TRL	technology readiness level
set point		TVC	thrust vector control
SEU	single-event upset	TWTA	traveling-wave tube amplifier
SHARAD	Shallow Radar	U	update
SMAP	Soil Moisture Active Passive	UES	Upper Equipment Section
SNR	signal-to-noise ratio	V	volt, velocity, vector
SQRT	mean radiation signal per pixel	V&V	verification and validation
SRAM	static random-access memory	VEE	Venus-Earth-Earth
SRR	System Requirements Review	VEEGA	Venus-Earth-Earth gravity assist
SRU	stellar reference unit	VIMS	Visual and Infrared Mapping Spectrometer
SS	subsystem	VRHU	variable radioisotope heating unit
SSE	spacecraft support equipment	W	watts
SSI	solid-state imager	W_e	watts electrical
SSPA	solid-state power amplifier	W_t	watts thermal
SSR	solid-state recorder	WBS	work breakdown structure
STV	solar thermal-vacuum	WDE	Wheel drive electronics (same as RWE)
SWIRS	Shortwave Infrared Spectrometer	WSTS	workstation testset
SysML	Systems Modeling Language	WTS	waveguide transfer switch
TAYF	test as you fly		
TB	testbed		
TCA	thruster cluster assembly		

C.4.3 Master Equipment List

Master Equipment List (MEL) removed for compliance with export-control (ITAR) regulations. Available upon request.

C.4.4 Aerospace Corporation Independent Cost EstimateAEROSPACE REPORT NO.
ATR-2012(5583)-4**Europa Habitability Mission: Flyby Concept
CATE: Cost and Technical Evaluation**

April 24, 2012

Randy Persinger¹, Robert Kellogg², Mark Barrera³¹Advanced Studies and Analysis Directorate, NASA Programs Division²Space Architecture Department, Systems Engineering Division³Vehicle Concepts Department, Systems Engineering Division

Prepared for:

Jet Propulsion Laboratory
4800 Oak Grove Drive
Pasadena, CA 91109

Contract No. 1393581

Authorized by: Civil and Commercial Operations

PUBLIC RELEASE IS AUTHORIZED.

AEROSPACE REPORT NO.
ATR-2012(5583)-4

Europa Habitability Mission: Flyby Concept CATE: Cost and Technical Evaluation

April 24, 2012

Randy Persinger¹, Robert Kellogg², Mark Barrera³

¹Advanced Studies and Analysis Directorate, NASA Programs Division

²Space Architecture Department, Systems Engineering Division

³Vehicle Concepts Department, Systems Engineering Division

Prepared for:

Jet Propulsion Laboratory
4800 Oak Grove Drive
Pasadena, CA 91109

Contract No. 1393581

Authorized by: Civil and Commercial Operations

PUBLIC RELEASE IS AUTHORIZED.

AEROSPACE REPORT NO.
ATR-2012(5583)-4

Europa Habitability Mission: Flyby Concept CATE: Cost and Technical Evaluation

April 24, 2012

Randy Persinger¹, Robert Kellogg², Mark Barrera³

¹Advanced Studies and Analysis Directorate, NASA Programs Division

²Space Architecture Department, Systems Engineering Division

³Vehicle Concepts Department, Systems Engineering Division

Prepared for:

Jet Propulsion Laboratory
4800 Oak Grove Drive
Pasadena, CA 91109

Contract No. 1393581

Authorized by: Civil and Commercial Operations

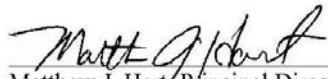
PUBLIC RELEASE IS AUTHORIZED.



AEROSPACE REPORT NO.
ATR-2012(5583)-4

Europa Habitability Mission: Flyby Concept CATE: Cost and Technical Evaluation

Approved by:



Matthew J. Hart, Principal Director
Advanced Studies and Analysis Directorate
Ground Enterprise
NASA Programs Division
Civil and Commercial Operations

© The Aerospace Corporation, 2012.

SL0084(1, 4320, 31, GN)

Acknowledgments

The following individuals are recognized for their contributions as authors, reviewers, and editors of the Cost and Technical Evaluation (CATE) for the Europa Habitability Mission: Flyby concept.

David Bearden
Ray Nakagawa
Anh Tu
Mark Cowdin
Gary North

Contents

1. Purpose	1
2. Executive Summary.....	3
3. CATE Background	5
4. Technical Evaluation	7
5. Cost and Schedule Evaluation	11

Figures

Figure 1.	EHM Flyby Mission Concept Overview.....	1
Figure 2.	Europa Flyby Cost Estimates	3
Figure 3.	EHM Flyby Mission Concept Features	7
Figure 4.	EHM Flyby Launch Mass Margin.....	8
Figure 5.	EHM Flyby Power Margin.....	9
Figure 6.	CATE Cost Estimating Process.....	11
Figure 7.	Analogy-based Estimating Process	12
Figure 8.	Flyby Bus Cost Estimates.....	12
Figure 9.	Flyby INMS Cost Estimates.....	13
Figure 10.	Flyby IPR Cost Estimates.....	13
Figure 11.	Flyby SWIRS Cost Estimates	14
Figure 12.	Flyby TI Cost Estimates.....	14
Figure 13.	Total Payload Cost Comparison	15
Figure 14.	Europa Flyby Planned Development Schedule.....	16
Figure 15.	Cost Reserve Estimate Process Overview	17
Figure 16.	Contingency Values Used for Threat Estimates.....	18
Figure 17.	Independent Schedule Estimate Process Overview	19
Figure 18.	Analogous Mission Development Time Comparison.....	20
Figure 19.	Europa Flyby ISE S-curve	20
Figure 20.	Europa Flyby Analogous Mission Phase Comparison.....	21
Figure 21.	Europa Flyby Key Cost Element Comparison.....	22
Figure 22.	Europa Flyby Cost Estimates.....	22
Figure 23.	Complexity-Based Risk Assessment Cost Analysis	23
Figure 24.	Complexity-Based Risk Assessment Schedule Analysis.....	23

Tables

Table 1.	Europa Flyby Mass Properties	18
Table 2.	Europa Flyby Cost Estimate Comparison (FY15\$M).....	21

1. Purpose

The Aerospace Corporation was tasked in November 2011 to participate as an independent party to review three separate, but related, Europa Habitability Mission (EHM) concepts under study by the Jet Propulsion Laboratory (JPL) to visit Europa in the continuing search for life in our solar system. The three concepts were being studied by JPL in the context of guidance provided by the National Research Council (NRC) Planetary Decadal Survey report released to the public in March 2011. In this report, a mission to the Jupiter/Europa system was rated very high with regard to science importance to the United States in the next decade. However, based on the expected high cost of the baseline reference mission evaluated by the NRC Planetary Decadal Steering Committee, the guidance was to descope the reference mission and significantly reduce mission cost while providing sufficient scientific investigation capability considered to be of paramount importance over the next decade. Aerospace, having participated as the NRC Cost and Technical Evaluation (CATE) contractor in the cost, technical, and schedule risk assessment of the planetary concepts evaluated by the Planetary Steering Committee, was a logical choice to independently evaluate the three updated EHM concepts with the same CATE techniques and processes. The three separate EHM mission concepts evaluated were: Orbiter, Flyby, and Lander. This report presents the cost, technical, and schedule risk assessment for the **EHM Flyby Mission** using the CATE process originally established by the NRC.

The key parameters of the EHM Flyby Mission can be found in Figure 1.



Figure 1. EHM Flyby Mission Concept Overview

2. Executive Summary

The EHM Flyby concept was found to have a Medium-Low technical risk and is well designed for a flyby mission to Europa. Mass and power margins are robust, and the design incorporates modularity with well-defined interfaces. Technology development is mainly related to engineering implementation; however, concern does exist with the technology development of the radioisotope power source (ASRGs) currently under development by NASA. The impact of radiation for this mission is also a concern but has been mitigated by compartmentalization and modular design as well as the mission design.

The CATE cost estimate for the EHM Flyby concept is \$2.1B in FY15 dollars excluding launch services. The EHM Flyby CATE, excluding launch services, is compared to the Project’s cost estimate in Figure 2. Including a launch service cost of \$272M, consistent with CATE estimates for the Planetary Decadal Survey Steering Committee, the CATE estimate including launch services is \$2.4B. The cost estimate for four ASRGs is assumed to be \$200M based on guidance provided by NASA. The cost risk associated with the ASRG technology development required for the EHM mission concepts has not been included in the CATE cost estimate, nor have the associated schedule risk to the project and technical risk to the flight system.

The project schedule of 73 months is considered to be realistic, with the independent estimate being 75 months. The concept’s use of modularity provides the opportunity to focus and minimize risk through parallel development paths.

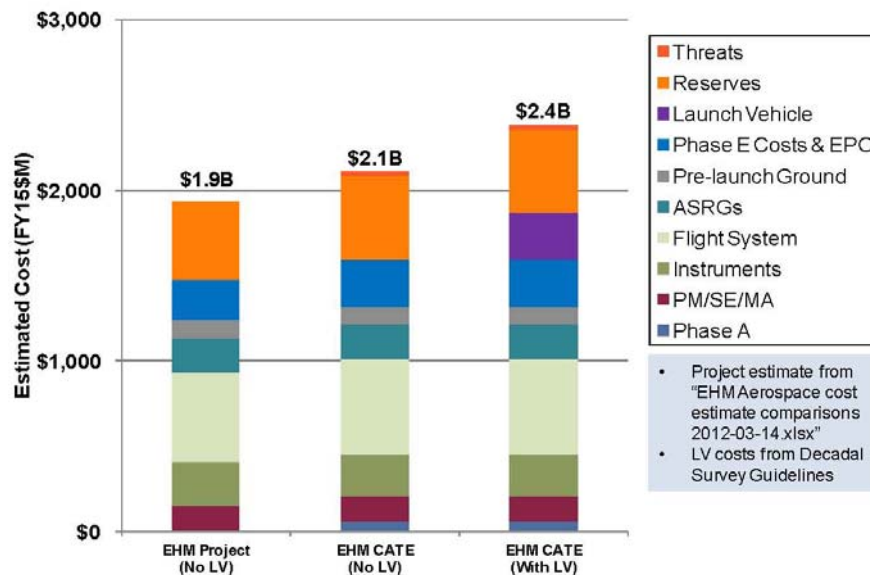


Figure 2. Europa Flyby Cost Estimates

3. CATE Background

The NRC Astro2010 Decadal Survey Steering Committee established the CATE process in June 2009. The CATE process was then used for three NRC Decadal Surveys: Astro2010, Planetary, and Heliophysics. Previous NRC Decadal Surveys had underestimated the costs associated with the recommended science priorities. The NRC and others recognized that mission costs were being underestimated, so the U.S. Congress mandated that an independent contractor be utilized to provide more realistic cost, technical, and schedule risk assessment directly to the decadal steering committees for consideration and evaluation in executing their charter. Select portions of the Planetary Decadal report, *Vision and Voyages*, from Appendix C are provided below to summarize the CATE process. It is important to note that the CATE process is intended to inform future NASA Science Mission Directorate (SMD) budget decisions, not to decide if a specific concept meets a cost target or to decide if a specific mission concept should be selected for flight versus another mission. Because the CATE process is used for future budgetary decisions, it incorporates potential cost threats that may occur in the future based on concept maturity at the time of evaluation.

The CATE process focuses on cost and schedule risk assessment, but limited technical evaluation is also required to categorize concept maturity, technology development, and the potential impact that insufficient margins and contingency (mass and power) may have on schedule or cost.

***Vision and Voyages, Planetary Decadal Report, Appendix C:** The objective of the CATE process is to perform a cost and technical risk analysis for a set of concepts that may have a broad range of maturity, and to ensure that the analysis is consistent, fair, and informed by historical data. Typically, a concept evaluated using the CATE process is early in its life cycle and therefore likely to undergo significant subsequent design changes. Historically, such changes have resulted in cost growth. Therefore, a robust process is required that fairly treats a concept of low maturity relative to one that has undergone several iterations and review. CATEs take into account several components of risk assessment.*

The primary goal of the CATE cost appraisal is to provide independent estimates (in fiscal year [FY] 2015 dollars) that can be used to prioritize various concepts within the context of the expected NASA budgetary constraints for the coming decade. ... To be consistent for all concepts, the CATE cost process allows an increase in cost resulting from increased contingency mass and power, increased schedule, increased required launch vehicle capability, and other cost threats depending on the concept maturity and specific risk assessment of a particular concept. ... All cost appraisals for the CATE process are probabilistic in nature and are based on the NASA historical record and documented project life-cycle growth studies.

The evaluation of technical risk and maturity in the CATE process focuses on the identification of the technical risks most important to achieving the required mission performance and stated science objectives. The assessment is limited to top-level technical maturity and risk discussions. Deviations from the current state of the art as well as system complexity, operational complexity, and integration concerns associated with the use of heritage components are identified. Technical maturity and the need for specific technology development, including readiness levels of key technologies and hardware, are evaluated. ... The CATE technical evaluation is limited to high-level technical risks that potentially impact schedule and cost. The CATE process places no cost cap on mission concepts, and hence risk as a function of cost is not considered. Concept maturity and technical risk are evaluated in terms of the ability of a concept to meet performance goals within proposed launch dates with adequate mass, power, and performance margins.

To aid in the assessment of concept risk, independent schedule estimates are incorporated as part of the CATE cost estimate.

4. Technical Evaluation

The EHM Flyby technical risk rating is Medium-Low. The mission will require medium new development, mostly in the engineering implementation. Radioisotope, or ASRG, power source qualification, radiation mitigation for external hardware, and software fault management will be some of the key challenges associated with this mission. Mass margins are high, with an average mass contingency of 63% for the bus and 88% for the instruments. Power margins and battery depth of discharge are adequate assuming four ASRGs. The concept design is within the capability of the Atlas V 551, 541, and 531 launch vehicles with greater than 10% launch mass margin. The radiation environment contributes to Medium-Low operational risk. The proposed “fail operational” approach to fault management of radiation upsets also contributes to this risk, although adequate time is available to address faults between flybys.

The top technical risks associated with the EHM Flyby Mission are:

1. **Mission Requirements Growth** to utilize additional capacity
2. **Advanced Stirling Radioisotope Generator (ASRGs)** development impact
3. Survival of flight system in **Radiation Environment**

These top risks are discussed below. Figure 3 illustrates some key aspects of the EHM Flyby concept.

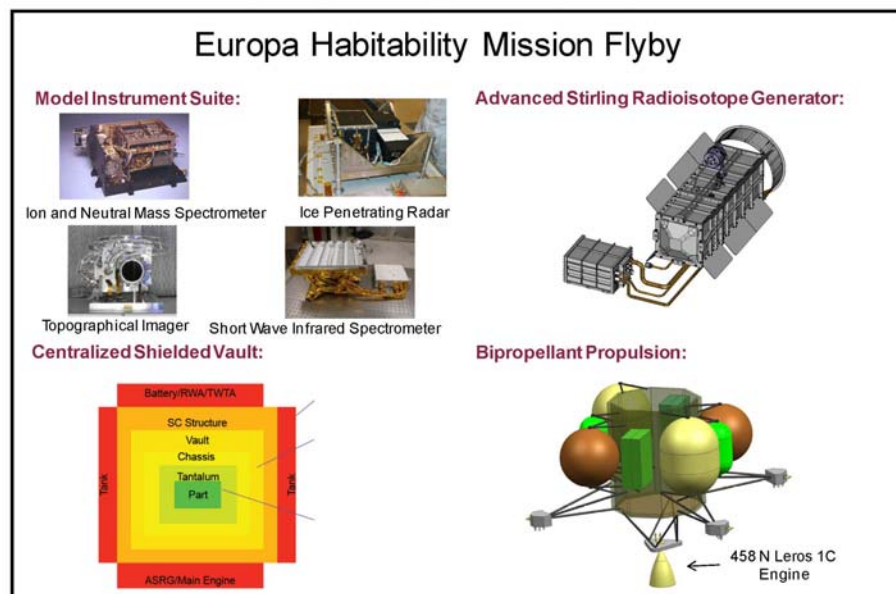


Figure 3. EHM Flyby Mission Concept Features

Mission Requirements Growth

The anticipated high mass margins for the EHM Flyby mission have the benefit of mitigating the risk of unplanned mass growth however, they also offer a temptation to increase the science payload from the current focused concept, which may impact the overall complexity and cost of the mission. As

illustrated in Figure 4, the proposed concept has a launch mass margin of greater than 10% on Atlas V 531 and above. This margin already considers the best-estimate mass as well as an average 63% mass growth contingency for the bus and 88% mass growth contingency for the instruments. Since the mass margins are high, there is a concern that instrument providers may wish to utilize excess capacity. There is a concern that competitively chosen instruments may have higher mass or complexity than the model instruments for the EHM concept. Also, there is a concern that instrument types from the EHM Orbiter concept may be added to the Flyby mission. Neither of these potential scenarios were included in the CATE cost estimate.

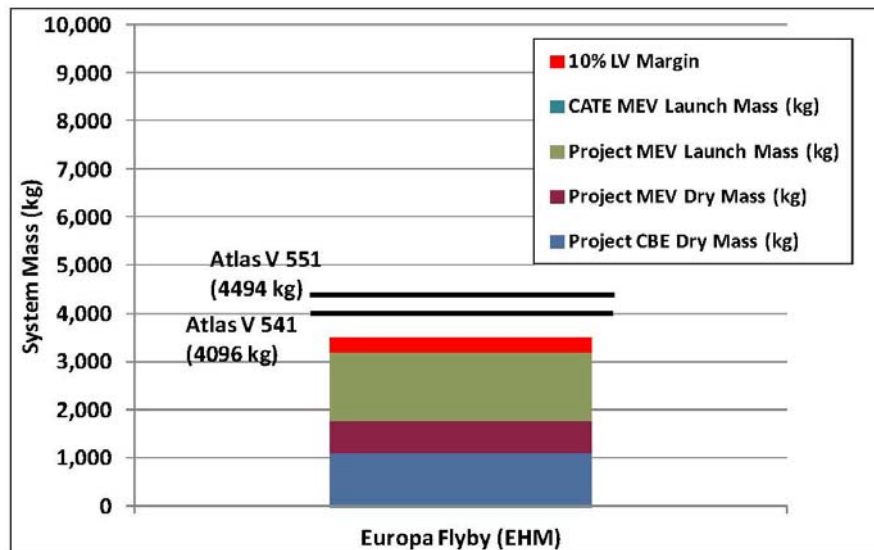


Figure 4. EHM Flyby Launch Mass Margin

Power margins during normal operations are acceptable assuming 4 ASRG power, as shown in Figure 5. There are small differences in the expected maximum battery depth of discharge due to differences in power growth allowances in CATE estimates versus project estimates; however, all estimated power margins are within acceptable limits. Battery depth-of-discharge is held to 35% or lower in the worst case (at Jupiter orbit insertion) and is much lower during the remaining mission phases.

Advanced Stirling Radioisotope Generator (ASRGs)

Uncertainty associated with technology development for the ASRGs contributes to risk of design changes and schedule delays for the project. The ASRG is currently estimated at TRL 5 and is part of an ongoing development effort. Results from the ground based testing program may possibly lead to changes in the ASRG interface to the spacecraft. Items that are of particular concern include the contribution of jitter from the ASRGs to the Topographic Imager and SWIR Spectrometer as well as the impact of electromagnetic interference (EMI). Also, there is concern that the ASRG may not provide the expected power for the mission environment. If the ASRGs provide less power than expected, then either a fifth ASRG may need to be considered or a modification to mission operations may be necessary. No additions to the CATE cost or schedule estimates were made based on possible delays in ASRG development.

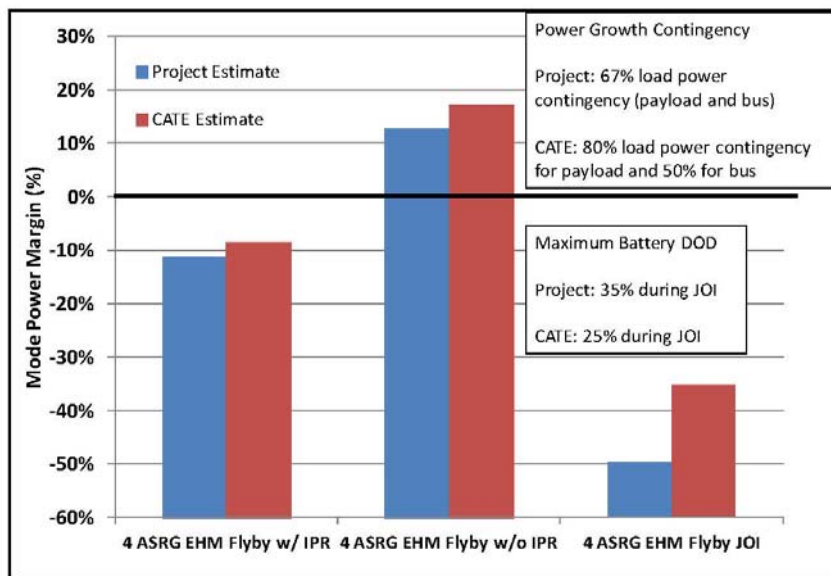


Figure 5. EHM Flyby Power Margin

Radiation Environment

The radiation environment for the EHM Flyby mission contributes to uncertainty in mass, cost, and schedule. Hardware that is external to the radiation vault, particularly exposed sensor heads, will require qualification for the mission radiation environment. Delays in radiation qualification of sensor detectors or optics may adversely impact project cost and schedule. Hardware that is internal to the radiation vault may need to be assessed for compatibility (EMI and thermal) within the common enclosure. Additional systems engineering effort is anticipated for successful integration of electronics within the common radiation vault. In order to maintain operations through radiation upsets, the EHM Flyby mission proposes a “fail operational” software fault management approach. While this approach may help to maintain operations pacing, it will require a more complete understanding of hardware failure modes than a “fail safe” approach. Some delays in fault management software are anticipated as the hardware implementation matures. The impact to the CATE cost estimate was considered by using the Juno mission as a cost analogy and adding a 5% multiplier to the bus and camera estimates for radiation issues.

Technology Development

Technology development items for the EHM Flyby mission include development of the ASRG and radiation-hardened detectors for the Europa mission environment. The ASRG is currently estimated at TRL 5 based on DoE engineering unit testing, with further testing by NASA Glenn Research Center. Further life testing is anticipated as well as a modified housing design. Additional development of radiation-hardened detectors is anticipated to advance beyond TRL 5-6. The current level of maturity depends on the selected manufacturers and their proposed manufacturing techniques for hardening of CCD and CMOS type detectors.

5. Cost and Schedule Evaluation

Figure 6 illustrates the CATE cost estimating approach in the form of a flow diagram. The initial focus is to estimate, with multiple analogies and cost models, the concept hardware such as instruments and spacecraft bus. Following the estimation of other cost elements based on historical data, a probabilistic cost-risk analysis is employed to estimate appropriate cost reserves. To ensure consistency for all concepts, the cost estimates are updated with information from the technical team with regard to mass and power contingencies, and potentially required additional launch vehicle capacity. Using independent schedule estimates, costs are adjusted using appropriate burn rates to properly reflect the impact of schedule delays or multiple work shifts to ensure meeting a launch date. Finally, the results are integrated, cross-checked with other independent cost and schedule estimating capabilities, and verified for consistency.

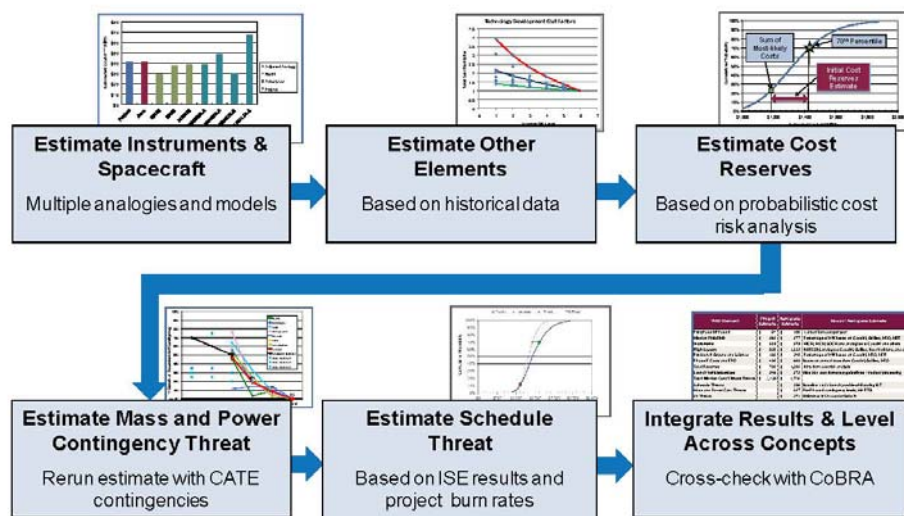


Figure 6. CATE Cost Estimating Process

Hardware Cost Estimates

The hardware cost elements estimated for the Europa Flyby concept are the spacecraft bus and the four instruments. Multiple estimates are developed for each of these elements. Both parametric cost models and analogy-based estimates are used. Figure 7 illustrates the analogy-based estimating process, which uses a cost estimating relationship (CER) to adjust the actual costs of past missions. By using the actual costs of past missions, unique attributes of those missions or performing organizations, which are similar to the mission being estimated, can be captured. This can provide insight that is different from most parametric cost models, which are based more on an “industry average” approach.

For the spacecraft bus, a total of five estimates were developed using the NASA and Air Force Cost Model (NAFCOM), the PRICE-H cost model and analogy-based estimates using Juno, Cassini, and Mars Reconnaissance Orbiter (MRO). The final CATE estimate is an average of these five estimates. The results of these estimates are depicted in Figure 8. The cost estimates shown include the spacecraft hardware, Project Management and Systems Engineering at the bus level, as well as bus

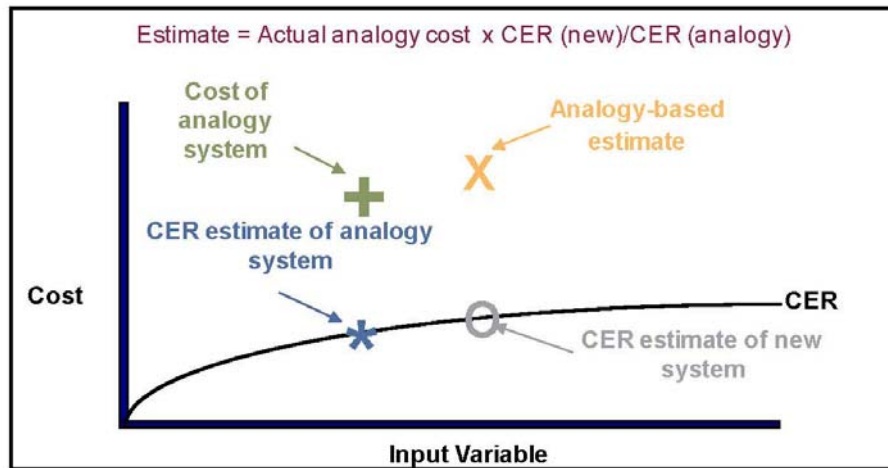


Figure 7. Analogy-based Estimating Process

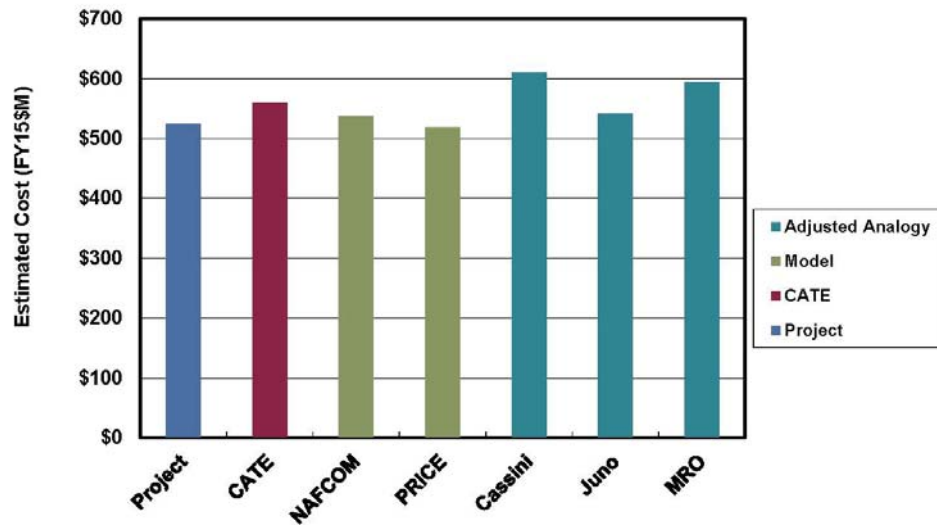


Figure 8. Flyby Bus Cost Estimates

and system-level integration and test. ASRG costs are not included in these estimates. As can be seen, there is good agreement between the CATE (\$560M) and Project (\$524M) cost estimate for the spacecraft bus or flight system.

For the Flyby instruments, the cost estimates are based on either two or three parametric cost models and either two or three analogy-based estimates. The parametric models used for the Flyby

instruments include the NASA Instrument Cost Model (NICM), The Multivariate Instrument Cost Model (MICM), and the Space-based Optical System Cost Model (SOSCM). The results for the instruments are depicted in Figures 9 to 12. In addition to the individual instrument estimates, the total payload estimates include an estimate of the payload-level Project Management and Systems Engineering. For the total payload, there is good agreement between the CATE (\$248M) and Project (\$262M) cost estimates, as shown in Figure 13.

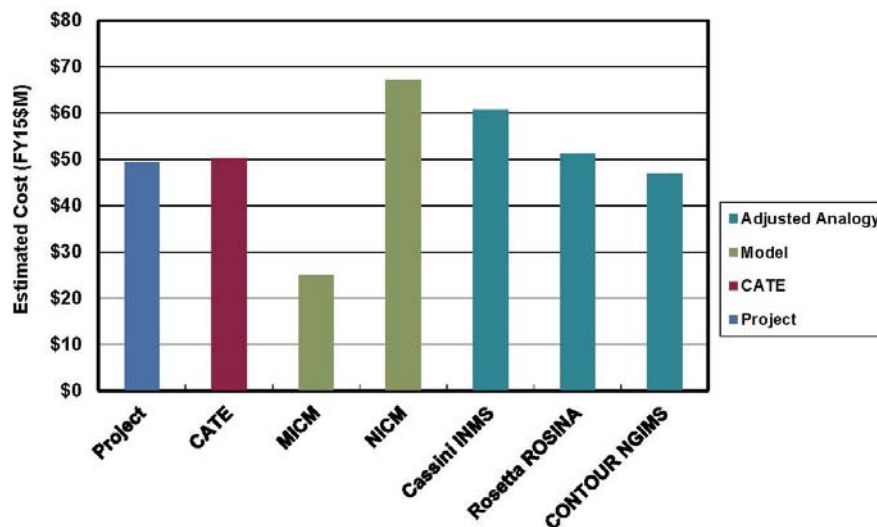


Figure 9. Flyby INMS Cost Estimates

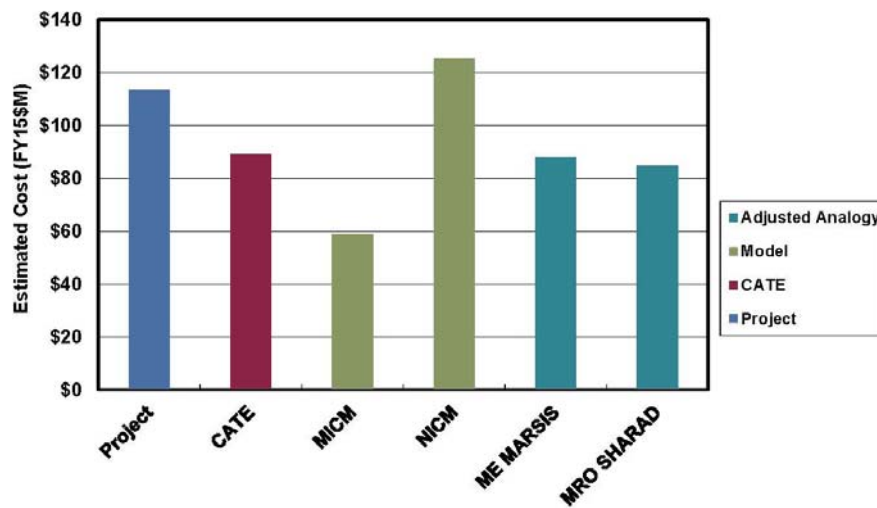


Figure 10. Flyby IPR Cost Estimates

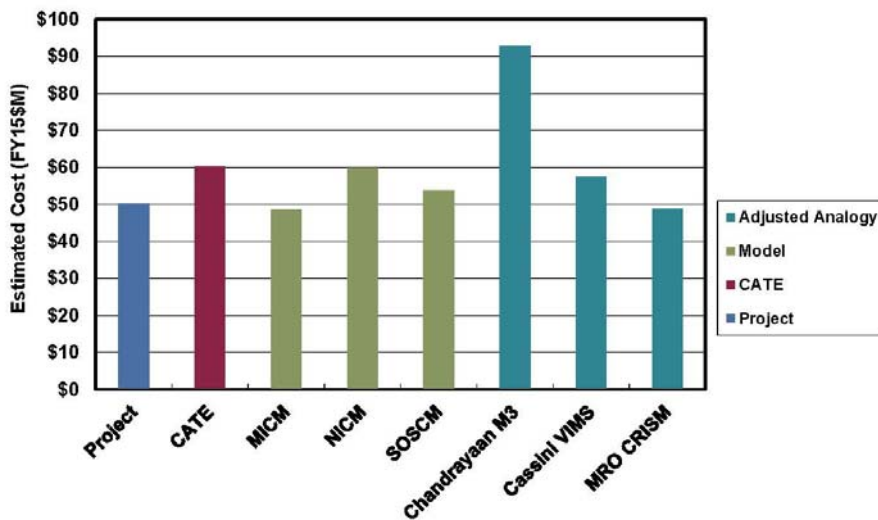


Figure 11. Flyby SWIRS Cost Estimates

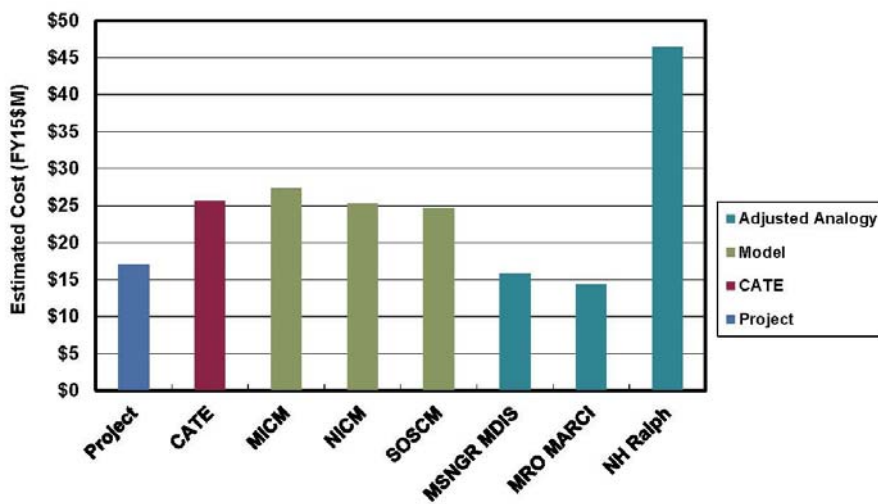


Figure 12. Flyby TI Cost Estimates

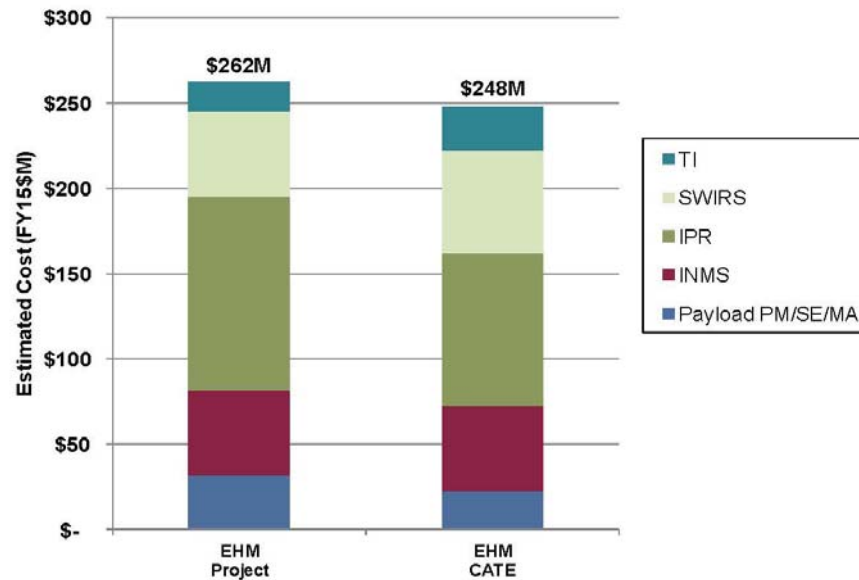


Figure 13. Total Payload Cost Comparison

Other Cost Elements

Other cost elements estimated for the EHM Flyby concept include project-level Project Management, Systems Engineering, and Mission Assurance, pre-launch Science and Ground System Development, Pre-Phase A/Phase A, Phase E, and Education and Public Outreach (EPO). Other cost elements included in the total cost estimate, but not independently estimated, are the ASRGs and launch vehicle.

Project Management, Systems Engineering, and Mission Assurance were estimated as a single total (PM/SE/MA) using “wrap factors” based on similar historical projects. The historical missions used for the Flyby PM/SE/MA estimate are Cassini, Juno, Mars Exploration Rover (MER), and MRO. The “wrap factors” are calculated as a percentage of hardware costs for the historical missions. These percentages are then applied to the estimated hardware cost of the Flyby concept. Specifically, the average percentage wrap factor is applied to the total of the average estimate for each hardware element.

Pre-launch Science and Ground System Development estimate is similarly developed using wrap factors based on historical missions. The historical missions used are Cassini, Juno, MER, and MRO.

Pre-Phase A/Phase A costs are estimated using a rule of thumb of 1.5% of the Phase B-D development costs per year of Pre-Phase A/Phase A. For the EHM Flyby concept, the total duration used was 40 months starting in June 2012 and ending in October 2015. This is actually earlier than the Phase A end date shown on the project schedule (Figure 14). However, significant activities are planned to start in October 2015. These activities have historically been a part of Phase B, so an adjusted Phase B start date is used for all schedule-related analyses.

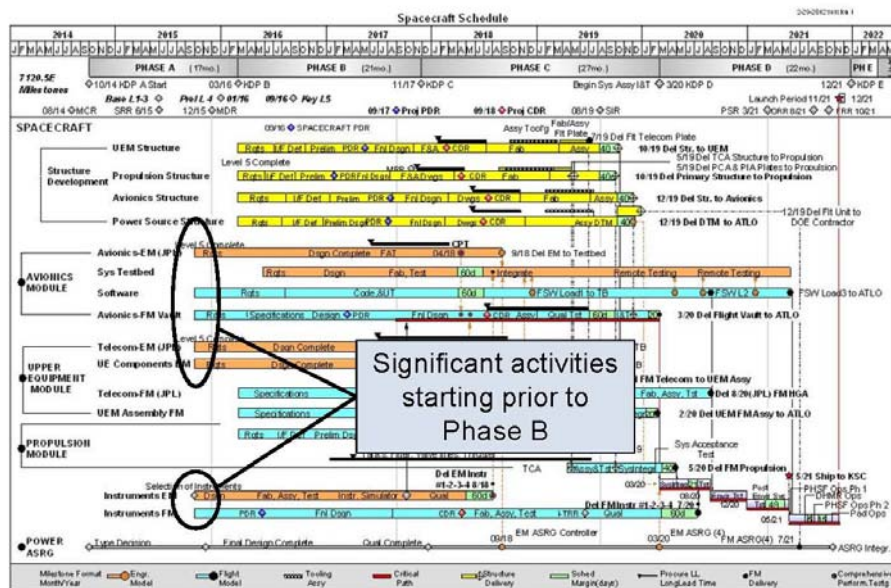


Figure 14. Europa Flyby Planned Development Schedule

Phase E costs were estimated using annual spend rates from similar historical projects. Because of the potentially different staffing required during cruise and encounter, these phases were estimated separately using historical rates appropriate for the respective phase. For the cruise phase, annual rates from MESSENGER, Juno, and New Horizons cruise phases were used. For the encounter phase, annual rates from MRO and the predicted annual rate from Juno encounter phases were used.

EPO costs were estimated as 1% of total project costs excluding launch vehicle.

For the ASRGs, the project estimate of \$50M each, supplied by NASA HQ, was used in the CATE estimate. For the Atlas V 551 launch vehicle, a \$272M estimate from the Planetary Decadal Survey was assumed for consistency.

Cost Reserves

Cost reserves are estimated using a process illustrated in Figure 15. For each Work Breakdown Structure (WBS) element, a triangular distribution of possible costs is developed. The cost values for the triangle are derived from the range of cost estimates as illustrated in the bus and instrument figures above. The lowest of the multiple estimates is used as the low value of the triangular distribution. The average of the multiple estimates is used as the mode or most-likely value of the triangular distribution. The high value of the triangular distribution starts with the highest of the multiple estimates but then adds an additional Design Maturity Factor (DMF). The DMF is a multiplier based on the maturity of the proposed design and the experience of the team. This factor helps ensure that the high value of the distribution truly represents a worst case.

Once the triangular distributions are developed for each WBS element, they are statistically combined to produce a total cost probability distribution. This distribution is typically plotted as a cumulative

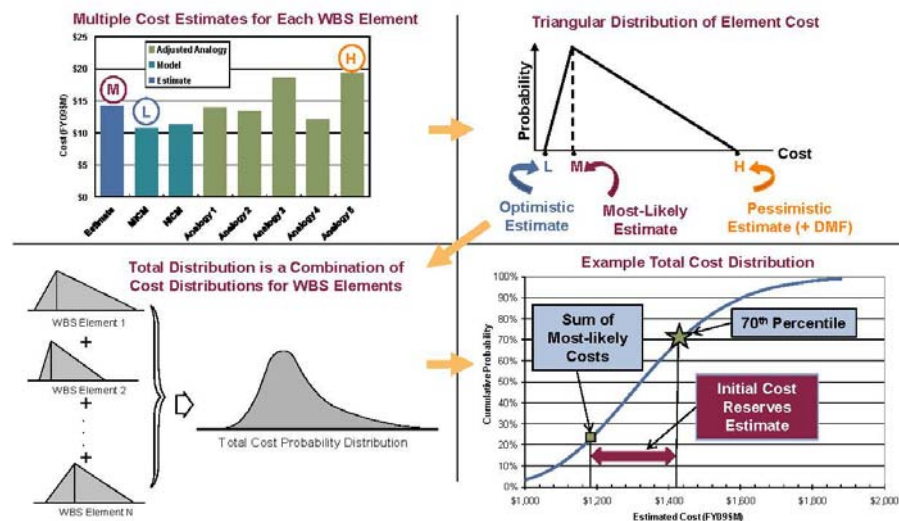


Figure 15. Cost Reserve Estimate Process Overview

distribution, which takes the familiar “S-curve” shape. The difference between the 70th percentile value from this curve and the sum of the most-likely estimates is the cost reserves estimate.

Mass and Power Contingency Threat

The mass and power contingency threat is a concept that was developed to support the CATE estimates, initially for the Astro2010 Decadal Survey, then later applied to the Planetary Science and Heliophysics Decadal Surveys. The motivation was to provide a methodology to account for the design evolution that has historically occurred from early conceptual design through development and launch. In order to assign a cost to these design changes, historical mass and power growth data was examined. This data showed values that were well above the typical guidelines of roughly 30% at Phase B start. Because data prior to Phase B start was sparse, the available data was extrapolated back to early conceptual phases.

Figure 16 shows an example of the data used for the mass and power contingency threats. This plot shows payload mass growth data for seven historical planetary missions. The red line is the average of this historical mission data. The black line is the CATE contingency that is used for the threat calculation.

To estimate the threat cost, the project-proposed mass and power contingencies (used in the hardware estimates described above) are replaced with the CATE contingencies. The estimates, including reserves, are then recalculated and the difference between this result and the result using project contingencies is recorded as the mass and power contingency threat.

For most projects, the CATE contingencies are well above the contingency values assumed in the proposed concept. However, the Europa Flyby concept already carried significant contingencies, so the estimated contingency threat was insignificant (\$9M). Table 1 is a summary of the mass properties provided for the CATE assessment.

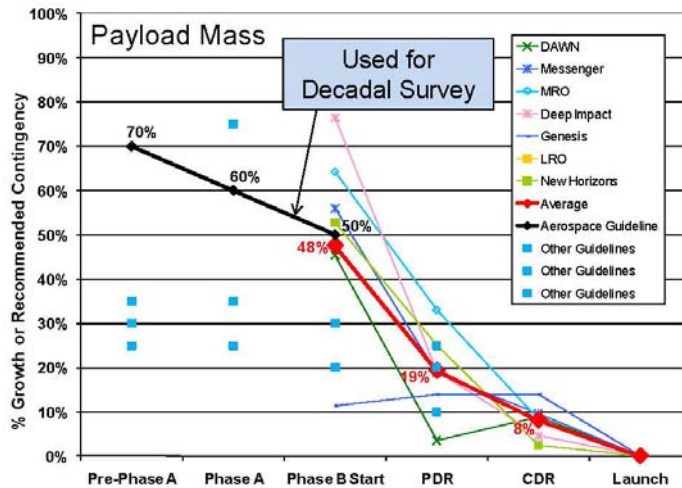


Figure 16. Contingency Values Used for Threat Estimates

Table 1. Europa Flyby Mass Properties

	Project CBE (kg)	Project Cont. (%)	Project MEV (kg)	CATE Cont. (%)	CATE MEV (kg)
Flyby Flight System Total	1079.9	65%	1778.1	52%	1636.9
Flyby Payload Total	85.3	82%	155.6	70%	145.0
Instrument Chassis	2.0	63%	3.3	70%	3.4
INMS	11.2	88%	21.0	70%	19.0
IPR	22.4	88%	42.0	70%	38.1
SWRS	9.3	88%	17.4	70%	15.8
TI	1.9	88%	3.5	70%	3.2
Payload Shielding	38.5	77%	68.4	70%	65.5
Flyby Bus Total	994.6	63%	1622.5	50%	1491.9
C&DH	12.0	63%	19.5	50%	18.0
GN&C	29.4	54%	45.2	50%	44.1
Harness	56.0	88%	105.0	50%	84.0
Mechanical	423.3	59%	673.4	50%	634.9
Power (w/o ASRGs)	41.5	34%	55.4	50%	62.2
ASRGs (4)	102.4	88%	192.0	50%	153.6
Propulsion	136.4	61%	219.2	50%	204.6
Telecom	63.8	63%	103.8	50%	95.8
Thermal	35.0	63%	56.9	50%	52.5
Bus Shielding	94.8	60%	152.1	50%	142.3

Schedule Threat

The base cost estimate described above uses the project-proposed development schedule. Historically, project schedule estimates have proven to be optimistic. As part of the CATE process, a probabilistic Independent Schedule Estimate (ISE) is developed. If the 70th percentile duration from the ISE is longer than project schedule, then a schedule threat is added.

Figure 17 illustrates the ISE process. The ISE is based on actual schedule durations from similar, historical missions. The duration of each schedule phase is treated as a triangular distribution, which

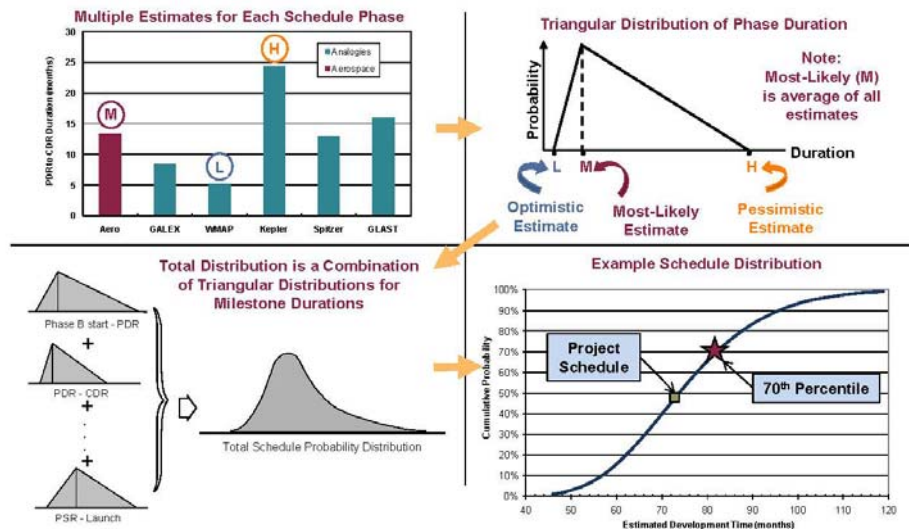


Figure 17. Independent Schedule Estimate Process Overview

can be statistically combined to yield a probability distribution of total project development time. The triangular distribution of durations for each phase is derived from the actual phase durations from the historical missions. The lowest duration is used as the low end of the triangular distribution, the average duration is used as the mode or most-likely value, and the highest historical value is used as the high value of the triangular distribution.

Figure 18 compares the actual Phase B-D duration of the four analogous missions used in the ISE with the proposed Europa Flyby Phase B-D duration. Figure 19 shows the results of the ISE as a cumulative probability distribution or S-curve. The 70th percentile ISE value is 75 months while the Europa Flyby proposed value is 73 months (after adjusting the effective Phase B start date as described above). Figure 20 is a breakdown of the results by project phase. While the overall durations agree quite well, the 70th percentile historical duration for the CDR to start of spacecraft I&T phase is significantly longer than the project value. Although this difference does not contribute to the CATE cost estimate, the plan for this phase should be examined to ensure its adequacy.

The difference between the 70th percentile value and the proposed project duration is then converted to a cost threat using a burn rate based on the project budget without reserves or launch vehicle. For Europa Flyby, the roughly two months' difference is multiplied by a burn rate of roughly \$7M per month to yield a schedule threat of \$17M.

Results

Table 2 presents the final CATE cost results compared to the current Europa team cost estimate. The agreement between the two estimates is quite close in all WBS elements. Figures 21 and 22 present the same data in graphical form.

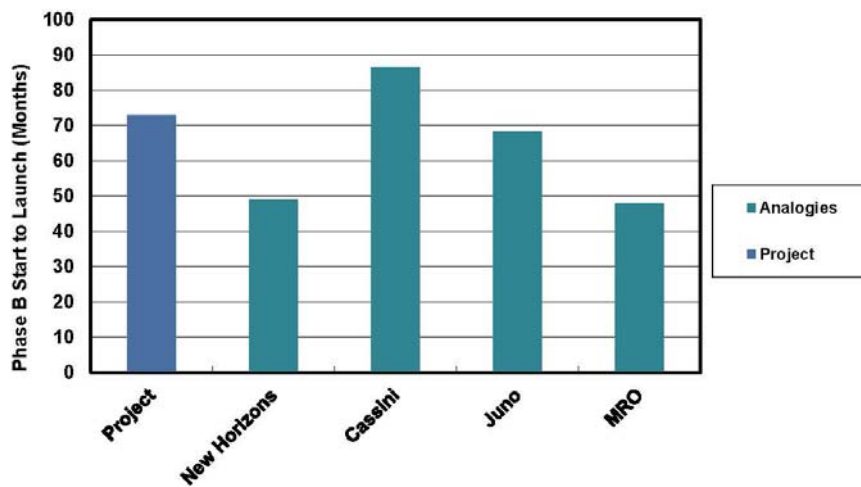


Figure 18. Analogous Mission Development Time Comparison

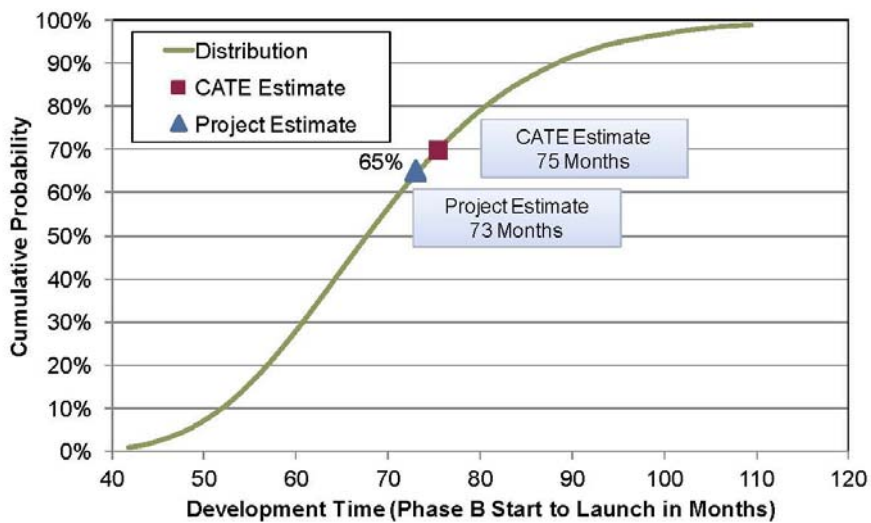


Figure 19. Europa Flyby ISE S-curve

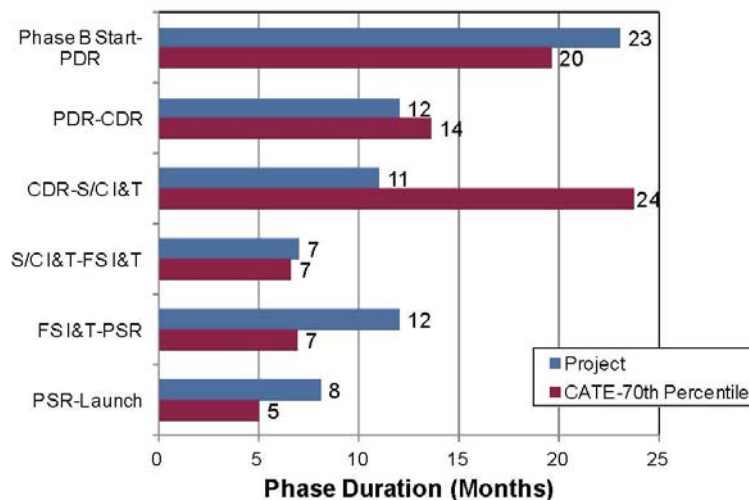


Figure 20. Europa Flyby Analogous Mission Phase Comparison

Table 2. Europa Flyby Cost Estimate Comparison (FY15\$M)

WBS Element	Project Estimate	CATE Estimate	Basis of Aerospace Estimate
Pre-Phase A, Phase A	incl. below	\$ 63	1.5% of Dev cost per year for 40 months
Mission PM/SEMA	\$ 148	\$ 143	Percentage of HW based on Cassini, Juno, MRO, MER + NEPA
Instruments	\$ 262	\$ 248	MICM, NICM, SOCM and analogies to planetary instruments
Flight System	\$ 524	\$ 560	NAFCOM11, PRICE, Juno, MRO, Cassini
ASRGs	\$ 200	\$ 200	Project Value for 4 ASRGs
Pre-launch Ground and Science	\$ 105	\$ 103	Percentage of HW based on Cassini, Juno, MRO, MER
Phase E and EPO	\$ 234	\$ 280	Based on annual rates from MESSENGER, NH, Juno, MRO
Total Reserves	\$ 461	\$ 488	70% from cost risk analysis
Mission Cost Before Threats	\$ 1,934	\$ 2,085	
Schedule Threats		\$ 17	2 months at Phase D burn rate (\$7M/month scaled from JEO)
Mass and Power Contingency Threats		\$ 9	Based on 2/14 MEL
LV Threats		\$ -	Adequate margins on Atlas V 551
Mission Cost With Threats	\$ 1,934	\$ 2,111	
Launch Vehicle/Services	\$ 272	\$ 272	Atlas V 551 cost from DS guidelines + nuclear processing
Total Mission Cost With Threats	\$ 2,206	\$ 2,383	

Complexity-Based Risk Assessment (CoBRA)

As a cross-check of the CATE results, the Complexity-Based Risk Assessment (CoBRA) process was also applied to the Europa Flyby concept. The CoBRA process uses technical and programmatic parameters from the conceptual design to calculate a complexity value for the design. This is done by ranking each of the individual parameters against a database of historical space missions. The calculated complexity values for the historical missions are plotted against development cost and schedule. The missions are classified as successful, partially successful, failed, or yet to be determined. A best fit line is drawn through the successful missions, and the estimated cost and schedule of the Europa Flyby concept can be compared to missions of similar complexity. Figures 23 and 24 show the CoBRA cost and schedule analysis results. Both the project and CATE cost estimates are slightly above the green trend line, which is in family with successful past missions of this complexity. Both the project and CATE schedule estimates are below the green trend line but above the blue trend line, which is drawn through successful missions that had a planetary launch window constraint. Again, this result adds confidence that the Europa Flyby schedule estimates are in family with comparable successful missions.

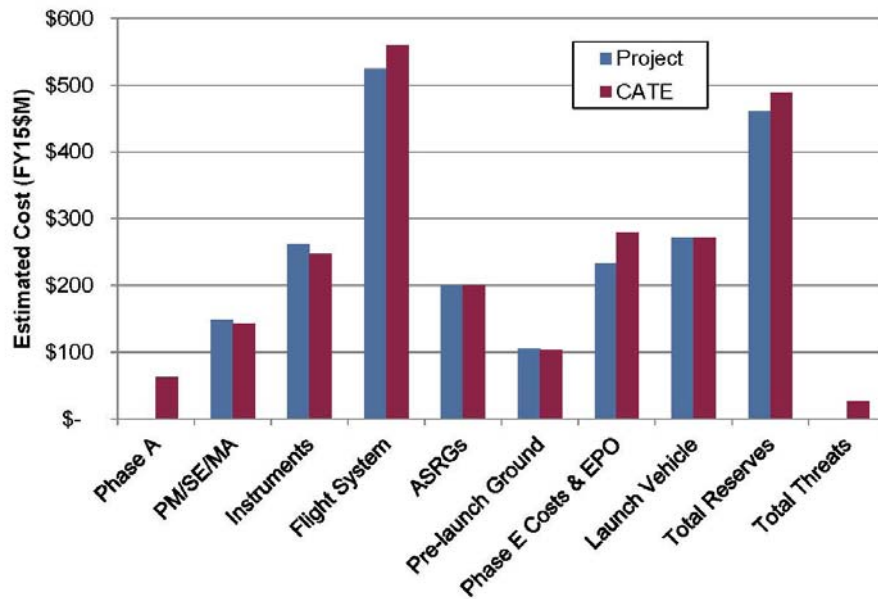


Figure 21. Europa Flyby Key Cost Element Comparison

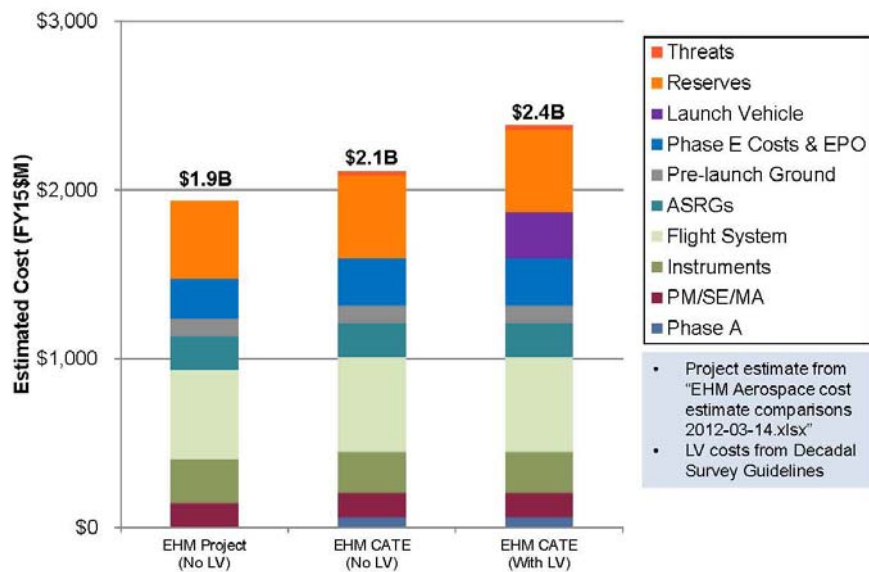


Figure 22. Europa Flyby Cost Estimates

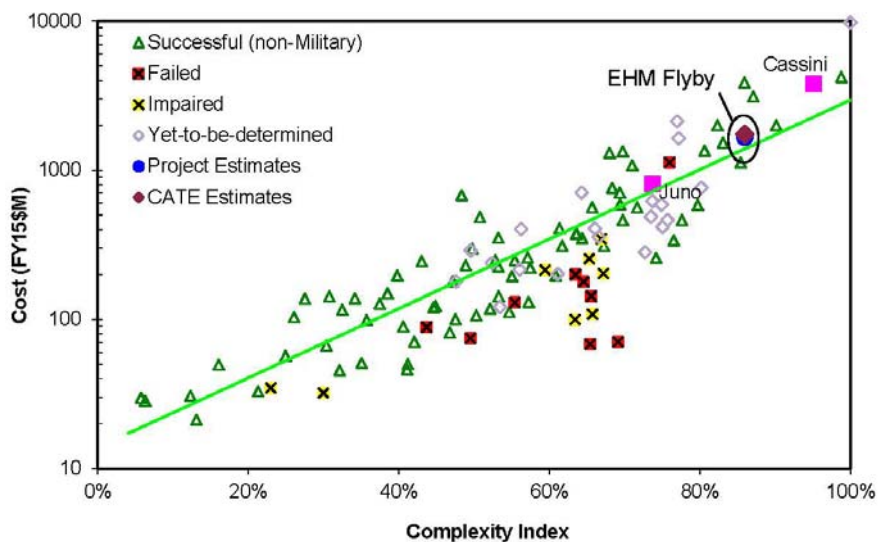


Figure 23. Complexity-Based Risk Assessment Cost Analysis

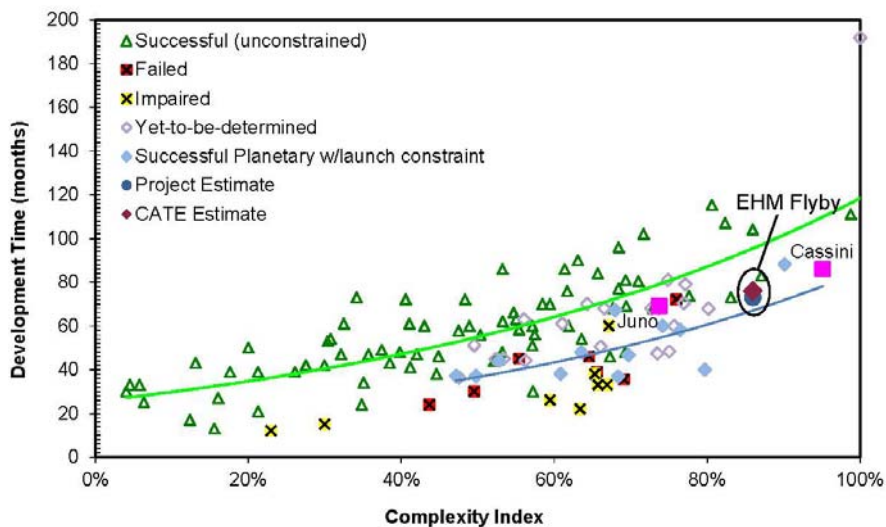


Figure 24. Complexity-Based Risk Assessment Schedule Analysis

C.4.5 NASA Review Board Report

DURAND BUILDING, 496 LOMITA MALL
 STANFORD, CA 94305-4035
<http://aa.stanford.edu>
 (650) 723-3317, fax: (650) 723-0279

Dr. Firouz Naderi
 Solar System Exploration Directorate
 JPL
 Pasadena, CA

December 1, 2011

Dear Dr. Naderi

The recent Planetary Decadal Survey determined that the Europa Jupiter Science Mission (EJSM) had compelling science but was not affordable based on an independent cost estimate of \$4.8B provided to the National Research Council by The Aerospace Corporation. The Decadal Survey recommended that the mission be descope to significantly reduce cost. In response, the Europa Jupiter System Mission (EJSM) was separated into two elements (i.e., Orbiter and Flyby) and focused solely on Europa science. Subsequently, NASA directed that a soft lander be added to the options under consideration.

As requested by JPL and consistent with the direction from NASA HQs, a Review Board was created to assess the viability of the three mission options to be provided to NASA HQ. These options were to focus on Europa only and develop Orbiter, Flyby (multiple) and Lander concepts, identifying the lowest achievable cost with a target value of \approx \$1.5B for each concept, not including launch vehicle. It was recognized by the Board that at a \approx 70% reduction in cost from the original EJSM concept any new mission design and corresponding science content would be dramatically different and go far beyond the usual meaning of a simple "descope".

In the charge to the Board, it was emphasized that the Board's responsibility was to conduct an "existence proof" evaluation of a pre-pre Phase A concept. In addition, each project was to be evaluated independently, not as one element of a program series.

The Board listed below was assembled and on November 15, convened at JPL to review the Orbiter and Flyby mission designs.

Scott Hubbard	Chair – NASA Ret.
Orlando Figeroa	NASA Ret. (via telephone)
Mark Saunders	NASA Ret.
Dave Nichols	JPL Div. 31
Jeff Srinivasan	JPL Div. 33
Barry Goldstein	JPL Div. 34
Cindy Kahn	JPL Div. 35
Rosalyn Lopes	JPL Div. 32

Gentry Lee	JPL 4X Chief Engineer
Will Devereux	APL
Douglas Eng	APL

To assist the Board in assessing the concepts, members of the JPL staff provided presentations and responded to many questions. This entire effort was applauded by all of the members of the Board and contributed to a most successful meeting.

The high level Europa Review Board conclusions can be summarized in a few statements:

- The overall approach to spacecraft modularity and radiation shielding was unanimously lauded as a creative approach to reducing technical risk and cost. No engineering “showstoppers” were identified.
- Both the Orbiter and Flyby mission concepts satisfied the “existence proof” test as missions that met Europa science requirements, could be conducted within the cost constraints provided and have substantial margins.
 - o However, several Board members expressed a strong opinion that a “science per dollar” criterion such as applied by the Decadal Survey would find the Flyby mission to yield much greater benefits than the Orbiter Project.
- The Board was unanimous in identifying two technical risks that impact both mission concepts:
 - o The Advanced Stirling Radioisotope Generator (ASRG) has been selected as a critical enabling technology. The Board recommends that the study teams thoroughly familiarize themselves with the development status, schedule and performance of the current version of the ASRG and identify any potential modifications from the Discovery version for Europa. In addition, availability of ²³⁸Pu stock and ASRG performance elicited concerns from the Board. In particular, there was a recommendation that much more data be collected on ASRG response to the space mission environment, *e.g.*, microphonics and performance under loads.
 - o While the “nested” approach to radiation shielding clearly mitigated the risk to the spacecraft and instrument electronics, the detectors will be exposed to the space environment. The Board found that early assessment and investment must be provided to ensure proper sensor performance.
- Consistent with the above statement, a Board consensus emerged that if either of these mission concepts moves ahead, particular attention must be paid to the Announcement of Opportunity (AO) for the science investigations so that the AO enables a simple approach and clearly specifies the PI-mission interface in critical areas such as total detector dose.

Detailed Considerations:

In the charter distributed to the Board prior to the review, we were asked to consider the following criteria:

- Ability of the mission to satisfy the Science Objectives
- Mission design approach
- Robustness of the mission and system architectures

- Robustness of mission and system margins; compliance with JPL design principles.
- Proposed scope, including available options, is consistent with funding target value to complete the mission
- Cost risk Project planning risks, including design, environment mitigation plans, integration and test plans, schedule and margins.

Within this overall review framework the following more specific comments were noted where at least two or more Board members addressed similar issues:

Science and Mission Design:

- During the science presentations, there were numerous questions about the changes from the original EJSM instrument suite and experiment goals. Following a request from the Board, Dr. Pappalardo gave a summary of science traceability. A number of the Board members suggested that more work be done by the SDT to clearly define the relationship of a given mission concept to the Decadal Survey.
- The Orbiter mission is challenging in that the science campaign occurs in the last 30 days of the mission and after significant radiation exposure. The Flyby mission has a much slower accumulation of total dose. This distinction needs to be sharpened.

Robustness and Margins:

- Systems margins presented for power, mass, and data were substantial, and of course have implications for launch vehicle requirements and cost. There was considerable discussion and some disagreement about whether maintaining such large technical margins may inappropriately drive the costs at this stage of maturity. A majority of the Board concluded that a conservative approach was appropriate at this point in the life cycle, particularly with the uncertainty in the launch vehicle capabilities a decade or more away from now.

Cost and Cost Risk:

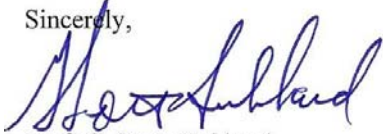
- A majority of the Board appeared satisfied that the two study teams had produced credible cost estimates using a variety of tools and approaches. While the Flyby mission was slightly higher than the \$1.5B FY15 target, both projects were deemed to be “in the ballpark”. There was a minority opinion that expressed concern over an inconsistency in trends between two parametric tools. Clearly, ongoing cost evaluation and the Aerospace CATE are needed to track these concepts.

Schedule:

- The Study leader (Gavin) noted at the beginning of the review that detailed schedules would not be available. While the Board accepted this limitation as a necessary element of an “existence proof” review, there was clear concern about whether the schedule supported the hardware development as proposed. At subsequent reviews more explicit schedule data is required in order to understand the risks involved.

On behalf of the entire Board, I wish to express again our congratulations to the JPL team in the high quality of the studies. We look forward to the Lander review early in 2012.

Sincerely,



Prof. G. Scott Hubbard
Chair, Europa Mission Review Board
Cc: Board members, Tom Gavin

Gentry Lee	JPL 4X Chief Engineer
Will Devereux	APL
Douglas Eng	APL

To assist the Board in assessing the concepts, members of the JPL staff provided presentations and responded to many questions. This entire effort was applauded by all of the members of the Board and contributed to a most successful meeting.

The high level Europa Review Board conclusions can be summarized in a few statements:

- The overall approach to spacecraft modularity and radiation shielding was unanimously lauded as a creative approach to reducing technical risk and cost. No engineering “showstoppers” were identified.
- Both the Orbiter and Flyby mission concepts satisfied the “existence proof” test as missions that met Europa science requirements, could be conducted within the cost constraints provided and have substantial margins.
 - o However, several Board members expressed a strong opinion that a “science per dollar” criterion such as applied by the Decadal Survey would find the Flyby mission to yield much greater benefits than the Orbiter Project.
- The Board was unanimous in identifying two technical risks that impact both mission concepts:
 - o The Advanced Stirling Radioisotope Generator (ASRG) has been selected as a critical enabling technology. The Board recommends that the study teams thoroughly familiarize themselves with the development status, schedule and performance of the current version of the ASRG and identify any potential modifications from the Discovery version for Europa. In addition, availability of ²³⁸Pu stock and ASRG performance elicited concerns from the Board. In particular, there was a recommendation that much more data be collected on ASRG response to the space mission environment, *e.g.*, microphonics and performance under loads.
 - o While the “nested” approach to radiation shielding clearly mitigated the risk to the spacecraft and instrument electronics, the detectors will be exposed to the space environment. The Board found that early assessment and investment must be provided to ensure proper sensor performance.
- Consistent with the above statement, a Board consensus emerged that if either of these mission concepts moves ahead, particular attention must be paid to the Announcement of Opportunity (AO) for the science investigations so that the AO enables a simple approach and clearly specifies the PI-mission interface in critical areas such as total detector dose.

Detailed Considerations:

In the charter distributed to the Board prior to the review, we were asked to consider the following criteria:

- Ability of the mission to satisfy the Science Objectives
- Mission design approach
- Robustness of the mission and system architectures

- Robustness of mission and system margins; compliance with JPL design principles.
- Proposed scope, including available options, is consistent with funding target value to complete the mission
- Cost risk Project planning risks, including design, environment mitigation plans, integration and test plans, schedule and margins.

Within this overall review framework the following more specific comments were noted where at least two or more Board members addressed similar issues:

Science and Mission Design:

- During the science presentations, there were numerous questions about the changes from the original EJSM instrument suite and experiment goals. Following a request from the Board, Dr. Pappalardo gave a summary of science traceability. A number of the Board members suggested that more work be done by the SDT to clearly define the relationship of a given mission concept to the Decadal Survey.
- The Orbiter mission is challenging in that the science campaign occurs in the last 30 days of the mission and after significant radiation exposure. The Flyby mission has a much slower accumulation of total dose. This distinction needs to be sharpened.

Robustness and Margins:

- Systems margins presented for power, mass, and data were substantial, and of course have implications for launch vehicle requirements and cost. There was considerable discussion and some disagreement about whether maintaining such large technical margins may inappropriately drive the costs at this stage of maturity. A majority of the Board concluded that a conservative approach was appropriate at this point in the life cycle, particularly with the uncertainty in the launch vehicle capabilities a decade or more away from now.

Cost and Cost Risk:

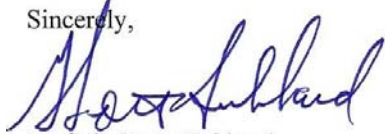
- A majority of the Board appeared satisfied that the two study teams had produced credible cost estimates using a variety of tools and approaches. While the Flyby mission was slightly higher than the \$1.5B FY15 target, both projects were deemed to be “in the ballpark”. There was a minority opinion that expressed concern over an inconsistency in trends between two parametric tools. Clearly, ongoing cost evaluation and the Aerospace CATE are needed to track these concepts.

Schedule:

- The Study leader (Gavin) noted at the beginning of the review that detailed schedules would not be available. While the Board accepted this limitation as a necessary element of an “existence proof” review, there was clear concern about whether the schedule supported the hardware development as proposed. At subsequent reviews more explicit schedule data is required in order to understand the risks involved.

On behalf of the entire Board, I wish to express again our congratulations to the JPL team in the high quality of the studies. We look forward to the Lander review early in 2012.

Sincerely,



Prof. G. Scott Hubbard
Chair, Europa Mission Review Board
Cc: Board members, Tom Gavin